



THE UNIVERSITY *of* EDINBURGH

This thesis has been submitted in fulfilment of the requirements for a postgraduate degree (e.g. PhD, MPhil, DClinPsychol) at the University of Edinburgh. Please note the following terms and conditions of use:

This work is protected by copyright and other intellectual property rights, which are retained by the thesis author, unless otherwise stated.

A copy can be downloaded for personal non-commercial research or study, without prior permission or charge.

This thesis cannot be reproduced or quoted extensively from without first obtaining permission in writing from the author.

The content must not be changed in any way or sold commercially in any format or medium without the formal permission of the author.

When referring to this work, full bibliographic details including the author, title, awarding institution and date of the thesis must be given.

UNIVERSITY OF EDINBURGH

ANDREA BONICELLI

**POTENTIAL OF MECHANICAL AND
PHYSICOCHEMICAL ANALYSIS OF HUMAN
CORTICAL BONE FOR FORENSIC AGE
ESTIMATION**

SCHOOL OF HISTORY, CLASSICS AND
ARCHAEOLOGY

Academic Year: 2019-2020

Supervisors: Dr Catriona Pickard, Dr Elena Kranioti, Prof
Peter Zioupos
2020

UNIVERSITY OF EDINBURGH

SCHOOL OF HISTORY, CLASSICS AND
ARCHAEOLOGY

Academic Year: 2019-2020

ANDREA BONICELLI

**Potential of Mechanical and Physicochemical Analysis of
Human Cortical Bone for Forensic Age Estimation**

Supervisors: Dr Catriona Pickard, Dr Elena Kranioti, Prof
Peter Zioupos
2020

© University of Edinburgh 2020. All rights reserved. No part
of this publication may be reproduced without the written
permission of the copyright owner.

ABSTRACT

Age estimation remains one of the most challenging tasks for forensic practitioners when establishing the biological profile of unknown skeletonised remains. Morphological methods based on developmental markers of bones can provide accurate age estimates. Yet, these methods tend to be unreliable when the individuals are over 35 years of age as all the key developmental markers gradually disappear. Current methods are also highly population- and sex-specific, and individual differences must be considered when interpreting the results. Aspartic acid racemisation, radiocarbon dating and DNA-methylation have all shown to be accurate to only a margin of ± 5 years. A recent method using quantification of biomechanical properties in conjunction with bone microstructure for the mid-femur cortical bone has shown potential and a better accuracy. In the present research, analyses of samples from the 4th rib are detailed and a methodology for estimation of age of individuals is presented. The physical characteristics of ribs are less influenced by mechanical stress compared to weight bearing bones and ribs are relatively accessible from the thoracic cage during autopsy, which increases the applicability of any such rib-based method.

This study exploits the changes in the biomechanical properties of bone tissue and matrix. These properties continue to change with age even after skeletal maturity and they are valuable for age estimation. The relationship of 28 variables at the macroscopic, microscopic and structural/compositional level were investigated in 113 ribs retrieved during autopsies. The experimental design comprehensively documents the changes in mineral size and composition, organic matrix quality and their combined effect on mechanical properties. The powder x-ray diffraction (XRD) method is applied to measure the crystal size and strain, and lattice parameters. Further, Fourier-transform infrared (FTIR) spectroscopy is used to investigate the changes in carbonate substitution and crystallinity. This examination allows a dependable evaluation of the increase in mineral to matrix ratio and therefore, the increase in collagen. Subsequent analysis of combined mineral and organic changes with age was done through thermal analysis. The physicochemical characterisa-

tion was compared to functional mechanical properties. The study showed that, in contrast to other bones, skeletal maturity for the rib cortical bone is reached between 40 and 50 years of age.

The study revealed that with age, there is an increase in crystal size and mineral content that is combined with the decrease in organic matrix amount and quality. It was also possible to confirm the importance of standardisation of the procedures. It was found out that a simple defatting procedure based on consecutive baths of chloroform, methanol and ethanol affects the evaluation of crystal size, which in turn affects the age estimation when using the powder XRD method. The 28 parameters measured using standard biomechanical (nanoindentation and microindentation), physical (DSC/TGA, FTIR and XRD) and histomorphometry (porosity-ImageJ) procedures were used to obtain an age-at-death estimation for unknown skeletal remains. Stepwise regression was employed to develop relations that would produce the best 'estimates of age-at-death' vs real age of the cadavers. Seven relationships were proposed: the relationship of primary importance containing 13 parameters and resulting in an $R^2 = 0.873$ with a mean absolute error of ± 4.47 . The relationship that performs poorly utilised only five parameters and resulted in an $R^2 = 0.840$, with an average error estimate of ± 4.96 years.

To conclude, physicochemical and mechanical characterisation of bone cortical bone shows good potential in accurate age-at-death estimation. Furthermore, the multi-factorial approach allows the combination of different methods to reach the best performance. A further employment of this method may involve histomorphometry and macroscopic examination of the age related degeneration if the sternal rib end, still largely used in forensic anthropology.

DECLARATION OF OWN WORK

I hereby declare that this thesis has been composed by me; the work presented here is my own and has not been submitted for any other degree or any professional qualification except as specified. Any previous own publication relevant to this work has been referenced in this work when appropriate.

Signed

.....

ACKNOWLEDGEMENTS

I would like to thank all the people that one way or another went through this years with me but another 300 pages thesis would not be sufficient.

First and foremost, I would like to thank my two supervisors, Elena Kranioti and Peter Zioupos that equally contributed not only in this project but taught me how to solve all problems that could arise and not only in the academic world. With your Mediterranean enthusiasm supported me during these long years of jumping around. I feel like with you I started the never ending curve of learning and improving. Thanks also for your personal touch, as a Mediterranean I could not have gone through all this without it. Elena you really were the first to introduce in this world and you taught me how to love it and Peter, although sometimes I still struggle to follow you (your thinking is too quick for us common mortals), I could not find anybody with a broader scientific wisdom. I hope this is going to be the beginning of a long collaboration.

A special thanks to Catriona Pickard for stepping in when most needed and for the very thorough review of this thesis. I would like also to thank all the lab technicians and, in particular, Adrian Mustay for answering millions of questions. I would like to thank Kath McSweeney and Linda Fibiger for the help given during my first teaching experience.

Julieta Gomez Garcia-Donas and Mara Karrel, it has been amazing to be first one of your students than your fellow and, I hope, finally your friend. We went through much more than a PhD together and we had quite a lot of fun. I could not ask for more.

Thanks to all the Edinburgh (non-Italian) people who witnessed every stage of Italian happiness and madness. Thanks for never complain about me and July being excessively laud. Between all of you I would like to pick Gram as the flag of the group: We'll make it out of that place together. Now the HCA Italian colony, you are really too many to mention all, but I would to thank particularly Vincenzo, Martina, Lucia (also for killing all my dreams of greatness). You were always there for me these years.

Thanks to all the Swindonians I had the pleasure to meet these years. Thanks Alejandro Dena and Akhil Koothrappali for the IT support, discussing basically all my research and

for the beers. I would have never imagined I could have missed that place but, thanks to you, now I am.

Impossibile sarebbe ringraziare a sufficienza la mia famiglia per il supporto. Grazie a voi non ho mollato la prima volta che ho deciso di trasferirmi all'estero ed ora si conclude un percorso che rifarei ad occhi chiusi. Dire che sarebbe stato impossibile senza di voi sarebbe banale. Non penso sarei nemmeno riuscito ad immaginare quello che abbiamo fatto insieme e l'abbiamo fatto come piace a noi: con passione e non senza tentativi sbagliati. Spero che questo sia il più bel libro della tua libreria Paps. Madre non so proprio da dove cominciare quindi non comincio nemmeno: spero di riuscire a renderti sempre fiera.

Un grazie speciale a Marco Veronese perchè a tutti serve un amico con cui non ci si azzecca per nulla per capire la fortuna di avere un amico. Grazie Cimo, Giappo e Viane le uniche anime pie che son venute a trovarmi in quella topaia e che mi hanno aiutato mille volte con le loro doti grafiche.

Last but not least, grazie Francesca che, nonostante tu sia arrivata alla fine di un lungo percorso, hai deciso di restare nonostante vedessi la tempesta in arrivo. Mi hai aiutato molto più di quello che pensi e spero di poter fare lo stesso per te. Speriamo pure che la tempesta sia passata.

And this would be it!

LIST OF CONTRIBUTIONS

Journal Articles

- Bonicelli A, Xhemali B, Kranioti EF, Zioupos P (2017). *Rib biomechanical properties exhibit diagnostic potential for accurate ageing in forensic investigations*. PloS One, 12(5): e017678r5. <https://doi.org/10.1371/journal.pone.0176785>.
- Bonczarowska J, Bonicelli A, Papadomanolakis A, Kranioti EF (2019). *The posterior portion of the ilium as a sex indicator: a validation study*. Forensic Science International, 249: 216.e1-216.e6. <https://doi.org/10.1016/j.forsciint.2018.10.031>.
- Kranioti EF, Bonicelli A, García-Donas JG (2019). *Bone-mineral density: clinical significance, methods of quantification and forensic applications*. Research and Reports in Forensic Medical Science. 9: 9-21. 10.2147/RRFMS.S164933.
- Kranioti EF, Michopoulou E, Tsiminikaki, K, Bonicelli A, Xhemali B, Paine RR, Garcia-Donas JG. *Bone histomorphometry of the clavicle in a forensic sample from Albania*. Forensic Science International. In press.

Conference Oral Presentation

- Bonicelli A, Zioupos P, Xhemali B, Kranioti EF. *Determining ‘age-at-death’: A New Multidisciplinary Laboratory method based on ribs*. 22nd Congress of the European Society of Biomechanics, Lyon, 10 July 2016.
- Bonicelli A, Zioupos P, Papadomanolakis A, Kranioti EF. *Case study: Age estimation using Structural, Chemical and Biomechanical data of modern rib retrieved from the seashore*. Anthropology and Migration, FASE one-day Symposium, Milan, 16 September 2017.
- Bonicelli A, Karell MA, Kranioti, EF. *Sexual dimorphism of the clavicle in modern Cretan population – A CT imaging methodology*. 4th SSFRS, Dundee, 28 March 2018.

- Bonicelli A, Zioupos P, Xhemali B, Kranioti EF. *Bone matrix analysis and its potential for accurate age estimation*. X Reuniòn Científica AEOF, Palma de Mallorca, 25 November 2018.
- Bonicelli A, Zioupos P, Xhemali B, Kranioti EF. *Collagen and mineral interaction in human cortical bone in ontogeny*. 25th Congress of the European Society of Biomechanics, Vienna, 10 July 2019.

Conference Poster Presentation

- Bonicelli A, Karell, MA, Garcia Donas, JG, McWhirter, Z, Kranioti, EF. *The Clavicle in two Modern Mediterranean Populations – A sexual dimorphism and Ancestry study based on CT Imaging*. FASE Symposium, Marseille, 22 September 2018.
- Bonicelli A, Zioupos P, Xhemali B, Kranioti EF. *Collagen and mineral interaction in human cortical bone in ontogeny*. BRS and BORS annual meeting, Cardiff, UK, September 4-6, 2019.

TABLE OF CONTENTS

ABSTRACT	i
ACKNOWLEDGEMENTS	v
LIST OF CONTRIBUTIONS	vii
TABLE OF CONTENTS	ix
LIST OF FIGURES	xiii
LIST OF TABLES	xxi
ABBREVIATIONS	xxv
SYMBOLS, UNITS AND NAMES	xxix
1 INTRODUCTION	1
1.1 Conceptual Overview and Scope	3
1.2 Research Questions	4
1.3 Thesis Structure	4
2 CURRENT APPROACHES TO AGE-AT-DEATH	7
2.1 Age-at-death — Juveniles	9
2.2 Age-at-death – Adults	10
2.3 Laboratory Based Methods	17
2.3.1 Aspartic Acid Racemization	18
2.3.2 Collagen Cross-links	21
2.3.3 Advanced Glycation End-products (AGEs)	22
2.3.4 Molecular Methods	23
2.3.5 Histological Analysis	28
2.4 Concluding Remarks	31
3 BONE BIOLOGY	33
3.1 Bone composition and nano-structure	35
3.1.1 Mineral Matrix	36

3.1.2	Collagen Matrix	37
3.1.3	Mineralisation	39
3.2	Non-collagenous Proteins (NCPs)	42
3.3	Sub-micro and Microstructure	44
3.3.1	Primary bone	45
3.3.2	Secondary Bone	48
3.4	Macrostructure: Cortical vs. Cancellous bone	49
3.5	Brief Description of Rib Anatomy and Breathing Mechanics	50
3.6	Bone Cells	52
3.6.1	Osteoclast	52
3.6.2	Osteoblast	55
3.6.3	Osteocyte	56
3.6.4	Bone Lining Cells	58
3.7	Intramembranous Ossification	59
3.8	Endochondral Ossification	59
3.9	Bone Modelling	61
3.10	Bone Remodelling	62
3.11	Theories of Bone Turnover	63
3.12	Concluding Remarks	66
4	BONE AGEING AND MECHANICAL PROPERTIES	67
4.1	Mineral Crystals and Ion Substitution	68
4.2	Mineral Content	70
4.3	Collagen Ageing	71
4.4	Bone Mass Changes with Age	73
4.5	Bone Mechanics	74
4.5.1	Mechanical Testing and Influencing Factors	75
4.5.2	Structural Mechanical Properties	77
4.5.3	Material Mechanical Properties	78
4.5.4	Anisotropy and Viscoelasticity	79
4.5.5	Elastic Properties	80
4.5.6	Toughness	81
4.5.7	Strength	82
4.6	Concluding Remarks	83
5	MATERIALS AND METHODS	85
5.1	Study Sample	88
5.1.1	Ethical Approval	88
5.2	Sample Preparation	88
5.3	Image Analysis	91
5.4	Thermal Analysis	93
5.5	Powder X-ray Diffraction	96
5.6	Fourier Transform Infrared Spectroscopy	101

5.7	Mechanical Analysis	105
5.8	Statistical Analysis	111
5.8.1	Chloroform-methanol Defatting Procedure	112
5.8.2	Sex differences and General Variable Correlation	112
5.8.3	Age estimation	113
5.8.4	Regression Diagnostic	115
5.8.5	Cross-validation (CV)	118
5.9	Concluding Remarks	119
6	RESULTS	121
6.1	Chloroform-methanol Preparation	122
6.2	Variables Distribution	123
6.3	Sex Differences	127
6.4	Age Related Changes	130
6.4.1	Optical porosity	130
6.4.2	Thermal Analysis	131
6.4.3	Powder X-ray Diffraction and Fourier Transform Infrared Spectroscopy	133
6.4.4	Mechanical Analysis	135
6.5	Bone Matrix Compositions: Reciprocal changes in mineral and organic	140
6.5.1	Stepwise Regression Relationship - Collagen vs. Mineral	143
6.6	Matrix Composition and Mechanical Properties	144
6.6.1	Stepwise Regression Relationship - Mechanical Properties vs. Composition	152
6.7	Skeletal Maturity	154
6.8	Age estimation - Unrestricted Parameter Selection	161
6.9	Age estimation - Restricted Parameter Selection	167
6.10	Age Determination - Sex Specific Regression Formulas	170
6.11	Cross-validation	172
7	DISCUSSION	175
7.1	Chloroform-methanol Preparation	176
7.2	Age- and Sex-related Variation of the Bone Matrix	180
7.2.1	Mineral Content	180
7.2.2	Organic Matrix	182
7.2.3	Carbonate Substitution and Crystallinity	185
7.2.4	Crystal Geometry	187
7.3	Mechanical, Physicochemical Properties and Heterogeneity of Human Cortical Bone	189
7.3.1	Osteon vs. Interstitial Bone	189
7.3.2	Tissue Mechanical Properties: Effect of Crystal Modifications	191
7.3.3	Tissue Mechanical Properties: Mineral and Organic Matrix	193
7.3.4	Stepwise Regression – Mechanics vs. Physicochemical Properties	195

7.4	Mineral and Organic Matrix Interaction	196
7.4.1	Stepwise Regression – Mineral vs. Organic	199
7.5	Cortical Bone Maturity: the Rib Example	201
7.6	Age-at-death Estimation	205
7.6.1	Unrestricted Parameter Selection	206
7.6.2	Restricted Parameter Selection	208
7.6.3	Sex Specific Formulas	209
7.7	Comparison with Other Age Estimation Methods	210
7.8	Research Limitations	215
8	CONCLUSIONS	219
8.1	Chloroform-methanol Procedure	219
8.2	Structural Relationship between Collagen and Mineral	220
8.3	Age Related Changes and Comparison of Mechanical and Physicochemical Parameters	220
8.4	Skeletal Maturity	221
8.5	Age-at-death Estimation	221
8.6	Future Work	222
8.7	Summary	225
	BIBLIOGRAPHY	226
	APPENDICES	267
	APPENDIX A ETHICAL APPROVAL	269
	APPENDIX B PARAMETERS	275
	APPENDIX C REGRESSION DIAGNOSTIC	277
	APPENDIX D SEX SPECIFIC REGRESSION FORMULAS	283
	APPENDIX E SAMPLE DEMOGRAPHICS	293

LIST OF FIGURES

1.1	Histological surface of rib cortical bone (20X under reflected light) shows the presence of concentric structures called osteons, that indicates that remodelling has replaced old with newly form one to allow bone to better support bone.	2
2.1	Measurement of translucency of the apical area of the dental root used in the Lamendin method combined with periodontosis to assess age-at-death. The increase in translucency and the area of the root affected by periodontosis increases with age Reprinted with permission from [John Wiley and Sons] (Lamendin et al., 1992).	12
2.2	Locations on the ectocranial surface for the assessment of suture closure. The neurocranium is the most durable part of the cranium and therefore more likely to be retrieved intact in archaeological contexts (1 = Midlambdoid; 2 = Lambda; 3 = Obelion; 4 = Anterior Sagittal; 5 = Bregma; 6 = Midcoronal; 7 = Pterion; 8 = Sphenofrontal Inferior; 9 = Sphenotemporal Superior; 10 =Sphenotemporal Inferior). Reprinted with permission from [John Wiley and Sons] (Meindl and Lovejoy, 1985).	13
2.3	Example of the rib sternal end metamorphosis showing the increase in pit depth and appearance as well as rim and wall configurations. Reprinted with permission from [John Wiley and Sons] (Adserias-Garriga and Wilson-Taylor, 2019)	16
2.4	Flow chart describing the steps generally adopted for aspartic acid racemization. Reprinted and adapted with permission from [John Wiley and Sons] (Waite et al., 1999).	19
2.5	Methylation occurs when the methyl group is attached to the 5 th carbon of the cytosine by means of an enzyme called DNA methyltransferases. The results is a 5-methylcytosine (Nevin and Carroll, 2015).	24
2.6	Extension of telomere length. Telomerase binds to 3' flanking end of telomere that is complementary to telomerase RNA. Telomerase adds bases using RNA as template. Finally, DNA polymerase complements the lagging strand. Reprinted with permission from [Elsevier] (Zapico and Ubelaker, 2013).	26

2.7	Human lymphocyte chromosomes visualised by means of FISH procedure. In blue is possible to see DNA of chromosomes while in yellow telomers. Reprinted with permission from [Bentham Science Publishers](Aubert and Lansdorp, 2008).	28
2.8	Packing effect: relation between osteon area and number of osteons that can accumulate on a given cortical area. Grey shapes represent fragmentary osteons (Gómez García-Donas, 2018).	30
3.1	Hierarchical structural organisation of bone. Reprinted with permission from [Elsevier] (Rho et al., 1998).	34
3.2	Diagram showing the combined variation of bone constituents and the distribution in different animal species and human femur. The arrow shows the increase in mineralisation and, consequently, the decrease in the remaining components. Reprinted with permission from [Elsevier] (Zioupos, 2005).	35
3.3	Representation of HAp mineral lattice structure (Beckett, 2009)	36
3.4	Mineral and collagen spatial organisation. Reprinted with permission from [Elsevier] (Rho et al., 1998).	38
3.5	Schematic representation of fibrillar mineralisation via fluid precursor: (a) beginning of the adsorption of the liquid-liquid precursor in the collagenous matrix due to critical ion concentration, (b) complete permeation of the fluid in the fibrillar structure and (c) mineralisation of the precursor occurs. Reprinted with permission from [Elsevier] (Olszta et al., 2007).	41
3.6	SEM images of trabecular (a) and cortical (b) bone. Cortical bone shows the circular osteons, formed by concentric lamellae around the vascular canals, and interstitial non-remodelled bone. Darker grey areas represent lesser mineralised bone in both images. For cortical bone (b), these are the newly remodelled osteons (given by Prof Peter Zioupos).	44
3.7	Types of primary and secondary bone in human rib cross-section photomicrographs. (A) the black circle shows primary lamellar bone formed by parallel laminar sheets and the arrow points at trabecular bone (40x). (B) plexiform bone form by the typical brick-like structure. (C) cortical bone formed by interstitial bone and osteons under semi-polarised (100x). (D) osteon showing the central vascular canal (black small arrow), cement line (arrow and black outline), osteocytes (white arrows) at 100x magnification (Gómez García-Donas, 2018).	48
3.8	Influence of architecture and mass in mechanical properties of bone. Well connected bone with high Tb.N, BV/TV and low Tb.Sp is capable of support more stress. <i>Vice versa</i> , bone that is normally subject to stress maintains better structural properties. Reprinted with permission from [Elsevier] (Burr and Akkus, 2013).	50

3.9	Differentiation between osteoclasts in motile and resorptive phase. After polarisation it is possible to see the four domain involved in demineralisation of the bone matrix. Reprinted with permission from [Landes Bioscience] (Itzstein et al., 2011).	54
3.10	Schematic representation of the network of osteocytes (elliptical shapes) in bone matrix. When this cells record an increase in strain or the network breakage due to microdamage accumulation the BMU is recruited to begin remodelling. Reprinted with permission from [Elsevier] (Martin, 2000). .	58
3.11	Different stages of development of bone during endochondral ossification. Reprinted and adapted with permission from [Elsevier] (Allen and Burr, 2013).	61
3.12	Remodelling cycle showing the different stages of the process. it starts with (A) activation followed by (B) resorption, (C) reversal and (D) formation. After new bone s formed, the cycle enters the (E) quiescence phase. Reprinted and adapted with permission from [Elsevier] (Allen and Burr, 2013).	63
3.13	Flowchart of the Mechanostat theory. The variation in bone mass is mainly drive by mechanical stimuli but there are other factor that can influence this process. Adapted from Frost (1987a)	65
3.14	Anabolic treatment given to rats (solid line), followed by withdrawal (dashed line). After this protocol, bone mass is at 50% higher than control levels (dotted line). The red line shows the increase of bone mass after treatment withdrawal. Reprinted and adapted with permission from [Springer Nature] (Turner, 1999).	66
4.1	Solid-liquid interface that induces ion exchanges. The main substitution that occurs in the hydrated layer is carbonate that normally induces and increase in crystal size. Reprinted with permission from [Elsevier] (Rey et al., 2007).	69
4.2	Representation of crystal growth. 'a' and 'b' axis are assumed to be equivalent while 'c' axis represents the length of the crystal and it is aligned with the major axis of collagen fibres. (Boivin, 2007)	70
4.3	μ CT scans of trabecular bone showing a sample with high density (right) and one with low density (left). Decrease in density and consequent increase in porosity is a characteristic effect of bone ageing and it impairs mechanical behaviour. Reprinted with permission from [Elsevier] (Qin et al., 2013).	74
4.4	Different types of mechanical testing. Arrows show where the force is applied. Reprinted and adapted with permission from [Elsevier] (Wallace, 2013).	76
4.5	Characteristic force-displacement curve showing the elastic phase of the deformation until the yield point and the following plastic until failure. Reprinted and adapted with permission from [Elsevier] (Wallace, 2013). .	77

5.1	Flow chart of preparation and experimental procedures.	87
5.2	Schematic representation of the sampling area in the proximity of the sternal rib end. The white area shows where thick section is sampled for nanindentation while the remaining bone away from the cartilage was used to obtain bone powder to be physically and chemically tested.	89
5.3	Metallographically polished resin used for supporting bone during mechanical testing. On the surface is possible to see two fragments of bone embedded. This is used to support the specimen during indentation and to acquire pictures for histomorphometry.	90
5.4	Transformation of images for porosity estimation. The black areas in the picture (b) are the bone surfaces while the white represents areas of porosity.	92
5.5	Schematic representation of DSC equipment, the sample and the reference pan are heated simultaneously in order to record heat flow variations for the sample only.	93
5.6	Example of TGA/DSC 3+ curve. Above (A) the TGA curve showing the two main weight loss characterising dehydration ($W_{\%}$) and organic combustion ($Or_{\%}$). At the end only mineral content is left ($Ash_{\%}$) that accounts for mineral content. In the DSC curve (B), in red sample dehydration and collagen degeneration, responsible for the breakdown of hydrogen bonds that confer the triple helix conformation to collagen fibres ($L\Delta H$), and in blue the combustion of the organic matrix peak ($C\Delta H$).	96
5.7	Application of the Bragg's law that shows the diffraction pattern for different crystallographic planes. Reprinted with permission from [John Wiley and Sons](Jenkins and Snider, 1997).	97
5.8	Example of XRD profile at 10-80 angular range indicating the main peaks under investigation with coherence length.	101
5.9	Schematic representation of refraction pattern of infrared light in a spectrometer in ATR mode.	102
5.10	FTIR spectrum of human rib cortical bone.	103
5.11	calculation of total work from the two portions of the indentation curve. The point G is where hardness is calculated and it is the point where load is maximum. After this point the unloading phase of the indentation curve starts and a tangent function is used to calculate elastic modulus.	106
5.12	Indentation creep calculation from the time vs depth curve. h_1 is the indentation depth at time t_1 when maximum load is reached. h_2 is the indentation depth after t_2 when force is held constant.	108
5.13	Nanoindentation impression on osteon (O) and interstitial bone (I). The small black triangle are the indentation impressions.	109
5.14	Schematic representation of a single osteon. The dashed grey lines represent the concentric lamellae while the solid black line the cement line. Nanoindentation(triangle) and microindentation (rhombus) location are shown.	111
5.15	Example of best fit line and errors in dashed lines for each sample (x_1 = real values, y_1 = predicted values).	114

5.16	Graphic representation of R^2 calculation (www.machinelearningplus.com).	116
5.17	Diagnostic plots for regression analysis.	118
6.1	Effect of treatment on coherence length at 002, 004 and 210 peaks.	122
6.2	Box plots of the variables that show significant difference according to sex.	127
6.3	Scatter plot of the increase in Po.Ar% with ageing. It can be seen that there is a decrease in correlation with the increase of age.	130
6.4	Variation of thermal analysis parameters at different ages. With age there is a general increment in mineral content (e) combined with the degeneration of collagen quality and content.	131
6.5	Logarithmic scale for the examination of matrix composition variation with age suggests a non linear behaviour of mineral (a), organic (b) and water phase (c).	133
6.6	Variation of FTIR and XRD parameters with age. There is an overall increase in size of the crystals (c, d) and shrinkage of crystal lattice (a). This is associated with the increase in carbonation of the matrix (b).	134
6.7	Variation of mechanical parameter between osteonal and interstitial bone. All mechanical properties are higher for osteons except for indentation creep.	135
6.8	Behaviour of mechanical properties with age. Elastic modulus (c), and indentation creep (d) is seen to decrease with age. In contrast, microhardness (b) and indentation work ratio (e) increase significantly with age. The only variable not significant with age is nanohardness (a).	137
6.9	Correlation between crystal geometry and collagen degradation. Young collagen, characterised by high thermal stability, is associated with small crystals (b). In contrast, lattice parameters is positively correlated with collagen thermal stability (a and c).	140
6.10	Collagen thermal stability is related to the amount of structural water (a) that allows the creation of hydrogen bonds that keeps the triple-helix configuration intact. The increase in collagen thermal stability is also associated with increased collagen content (b).	142
6.11	Influence of mineral content on mean tissue mechanical properties. The only property negatively affected by mineral content is indentation creep (d).	146
6.12	Influence of coherence length at 002 peak on mechanical properties of the entire tissue. It is possible to see the predominant role of crystals' modification in the elastic behaviour of bone.	148
6.13	Relationship between carbonate substitution and mechanical properties. It almost equally affect plastic and elastic deformation of bone.	150
6.14	Behaviour mechanical properties with age explain by loess curve shows a peak in mechanical properties at ~40 years of age.	155
6.15	Behaviour of collagen and mineral related physicochemical parameters acquired by thermal analysis show an increase in mineral content and a decrease in organic and water phase.	157

6.16	mineral crystal length reaches its maximum at 40 years. The first increase in associated with carbonate substitution (Figure 6.17c/d) and followed by crystal size reduction.	158
6.17	Infrared spectroscopy shows that the majority of this variation occurs until the age of 30 years. However, no clear trends are shown by mineral to matrix ration and crystallinity index.	159
6.18	thermal stability and 'a' axis decrease until 50 years of age compared to what shown for the other physicochemical parameters. It is interesting to note that the behaviour of the lattice parameter is opposite compared to the crystallite size ones but, the lack of clear correlations does not allow confident speculations.	160
6.19	Visual diagnostic for backward selection of the full model (PR1).	163
6.20	Visual diagnostic for forward selection of the full model (PR2).	165
6.21	Visual diagnostic for forward selection of the full model (PR3).	167
7.1	Schematic representation of two collagen molecules. The hydrogen bonds (black dashed line) maintain the triple helix configuration of the collagen fibres.	182
7.2	Coherence length shows a very specific pattern that can be explained by a steep increase before maturity to then decrease at a much lower pace. . . .	188
7.3	Loess curves show how mechanical properties change with age and the different behaviour between them. The blue squares approximately between 30 and 50 years show how the combination of all the physicochemical changes reaching maturity at different ages affect the transition between increase and degeneration of mechanical properties.	201
7.4	The sketch represents the issue with age estimation. The increase in age drastically reduces the accuracy of the majority of the methods as shown by the area between the green lines.	206
A.1	Ethical approval from the Directorate of Investigation Control and Penal Proceeding.	269
A.2	NHS Lothian Tissue Governance audit.	270
C.1	Diagnostic plot for PR4.	278
C.2	Diagnostic plot for PR5.	279
C.3	Diagnostic plot for PR6.	280
C.4	Diagnostic plot for PR7.	281
C.5	Real age vs Predicted age for (a) PR1, (b) PR2, (c) PR3, (d) PR4, (e) PR5, (f) PR6 and (g) PR7. It is possible to note the decrease in accuracy from the first to the last model as variables are taken out from the models. . . .	282
D.1	Diagnostic plot for PR1 - Male.	284
D.2	Diagnostic plot for PR1 - Female.	285
D.3	Diagnostic plot for PR2 - Male.	287

D.4	Diagnostic plot for PR2 - Female.	288
D.5	Diagnostic plot for PR3 - Male.	290
D.6	Diagnostic plot for PR3 - Female.	291

LIST OF TABLES

2.1	Original table containing the seven phases used to estimate age from the auricular surfaces of the ilium. It is interesting to note the decrease in accuracy with the increase of age. Reprinted with permission from [John Wiley and Sons] (Buckberry and Chamberlain, 2009).	15
3.1	Non-collagenous proteins in bone and related functions in bone metabolism.	43
5.1	Combination of experimental procedures and target of the investigation related to them.	85
5.2	Sample demographics (SE = standard error of the mean).	88
5.3	FTIR Variables (A = area of the peak, I = intensity of the peak). Baseline was set for all the different peaks separately.	105
6.1	Results for S-W test shows violation of normal distribution for certain variables due to the large sample size (*: $p \leq 0.05$).	124
6.2	Descriptive statistic for mechanical parameters (SD = standard deviation; Min = minimum; Max = maximum; Se = standard error; Mad = mode). . .	125
6.3	Descriptive statistic for physicochemical parameters (SD = standard deviation; Min = minimum; Max = maximum; Se = standard error; Mad = mode).	126
6.4	Mean values and standard deviation for the sample split between male and female for mechanical parameters. Results for t-test and ANOVA (SD = standard deviation; *: $p \leq 0.05$).	128
6.5	Mean values and standard deviation for the sample split between male and female for physicochemical parameters. Results for t-test and ANOVA (SD = standard deviation; *: $p \leq 0.05$).	129
6.6	Mean values and standard deviation for the sample split between osteon and interstitial area for mechanical parameters. Results for t-test and ANOVA (SD = standard deviation; *: $p \leq 0.05$).	136
6.7	Pearson's correlation between age and mechanical properties for interstitial and osteonal bone (^a : $p \leq 0.5$; ^b : $p \leq 0.01$; ^c : $p \leq 0.001$).	139
6.8	Stepwise regression analysis of CI vs Compositional parameters of the organic matrix, $R^2 = 0.36$ (SE: standard error; *: $p \leq 0.05$; **: $p \leq 0.01$; ***: $p \leq 0.001$).	143

6.9	Stepwise regression analysis of CP vs Compositional parameters of the organic matrix with $R^2 = 0.34$ (SE: standard error; *: $p \leq 0.05$; **: $p \leq 0.01$; ***: $p \leq 0.001$).	143
6.10	Stepwise regression analysis of 'c' axis vs Compositional parameters of the organic matrix with $R^2 = 0.33$ (SE: standard error; *: $p \leq 0.05$; **: $p \leq 0.01$; ***: $p \leq 0.001$).	144
6.11	Correlation Matrix of mechanical properties for interstitial bone and coherence length for the 004 and 030 peak (a : $p \leq 0.05$; b : $p \leq 0.01$; c : $p \leq 0.001$).	147
6.12	Correlation Matrix of mechanical properties for osteonal bone and coherence length at 004 and 003 (a : $p \leq 0.05$; b : $p \leq 0.01$; c : $p \leq 0.001$).	149
6.13	Correlation Matrix of mechanical properties for interstitial bone and coherence length at 004 and 003 (a : $p \leq 0.05$; b : $p \leq 0.01$; c : $p \leq 0.001$).	149
6.14	Correlation Matrix of mechanical properties for interstitial bone and physicochemical changes (a : $p \leq 0.05$; b : $p \leq 0.01$; c : $p \leq 0.001$).	151
6.15	Effect of compositional parameters on nanohardness (SE: standard error; *: $p \leq 0.05$; **: $p \leq 0.01$; ***: $p \leq 0.001$).	152
6.16	Effect of compositional parameters on elastic properties. It is possible to see how the parameters related to mineral modifications have increased in the attempt of explaining the behaviour of elastic properties (SE: standard error; *: $p \leq 0.05$; **: $p \leq 0.01$; ***: $p \leq 0.001$).	153
6.17	Effect of compositional parameters on microhardness (SE: standard error; *: $p \leq 0.05$; **: $p \leq 0.01$; ***: $p \leq 0.001$).	154
6.18	Parameter selection based on the entire set of parameters (*: $p \leq 0.05$; **: $p \leq 0.01$; ***: $p \leq 0.001$).	161
6.19	(RSE: residual standard error; *: $p \leq 0.05$; **: $p \leq 0.01$; ***: $p \leq 0.001$; (R^2 : coefficient of estimation; RSE: residual standard error; AIC: Aikake information criterion; BIC: Bayesian information criterion)).	162
6.20	Linear model assumption with global test based on 4 degree of freedom for PR1.	163
6.21	Linear model assumption with global test based on 4 degree of freedom for PR2.	164
6.22	Linear model assumption with global test based on 4 degree of freedom for PR3.	166
6.23	Comparison between models created with backward selection for the entire sample and split between male and female.	170
6.24	Comparison between models created with forward selection for the entire sample and split between male and female.	171
6.25	Comparison between models created with backward selection for the entire sample and split between male and female.	172
6.26	Comparison between original results and cross-validated for the unrestricted parameter selection (MAE = mean absolute error; CV: cross-validated).	173

7.1	Table summarising results for all the models developed showing the effectiveness of the multifactorial approach: reducing the number of factors obtained with different experimental procedures there is a decrease in the inaccuracy of the prediction. PR1, developed with backward stepwise regression, is the best performing model in terms of accuracy and statistical robusticity (R^2 : coefficient of determination; RSE: residual standard error; AIC: Aikake information criterion; BIC: Bayesian information criterion).	209
7.2	Main laboratory methods applied in forensic anthropology for age-at-death estimation (R^2 : coefficient of determination; RSE: residual standard error; SDE: standard deviation of residual standard error).	214
B.1	Description of the parameters involved in the investigation.	275
D.1	Comparison between models created with backward selection for the entire sample and split between male and female (*: $p < 0.05$; **: $p < 0.01$; ***: $p < 0.001$).	283
D.2	Comparison between models created with forward selection for the entire sample and split between male and female (*: $p < 0.05$; **: $p < 0.01$; ***: $p < 0.001$).	286
D.3	Comparison between models created with BIC selection for the entire sample and split between male and female (*: $p < 0.05$; **: $p < 0.01$; ***: $p < 0.001$).	289
E.1	Demographics and cause of death for the entire sample and predicted age for the stepwise based models (GSW: gunshot wound).	293

ABBREVIATIONS

Å	Ångstroms
AAD	Age-at-death
AAR	Aspartic acid racemization
AGEs	Advanced glycation end products
AIC	Akaike information criterion
ALP	Alkaline phosphatase
ANCOVA	Analysis of covariance
ANOVA	Analysis of variance
ATR	Attenuated total reflectance mode
BIC	Bayesian information criterion
BMD	Bone mineral density
BMU	Bone multicellular unit
BPS	Bone sialoprotein
Ca	Calcium
CL	Coherence length
CO ₃	Carbonate
CT	Computed tomography
CV	Cross validation
DNA	Deoxyribonucleic acid
DPD	Deoxypyridinoline
DSC	Differential scanning calorimeter
DVI	Disaster victim identification
D-W	Durbin-Watson test
DXA	Dual energy X-ray absorptiometry

FWHM	Full width at half maximum
FTIR	Fourier transform infrared spectroscopy
Gly	Glycine
H	Hydrogen
H ₂ O	Water
HAp	Calcium hydroxyapatite
HCl	Hydrochloric acid
<i>It</i>	Interstitial bone: non remodelled hypermineralised bone
Loess	Locally estimated scatterplot smoothing
M-W	Mann–Whitney U test
MES	Minimum effective strain
NCPs	Non-collagenous proteins
NMR	Nuclear magnetic resonance
O ₂	Oxygen
<i>On</i>	Osteonal bone: newly remodelled bone resulting in Haversian system
OPD	Osteon population density
P	Phosphorus
PCR	Polymerase chain reaction
PILP	Polymer-induced liquid precursor
PMI	Post-mortem interval
PO ₄	Phosphate
PYD	Pyridinoline
pXRD	Powder x-ray diffraction
QCT	Quantitative computed tomography
RANKL	NF-kB ligand
RSE	Residual standard error

SE	Standard error
SEM	Scanning electron microscope
S-W	Shapiro-Wilk Test
Tb.Conn	Trabecular connectivity
Tb.N	Trabecular number
Tb.Sp	Trabecular spacing
Tb.Th	Trabecular thickness
TCR	T-cell receptor
TEM	Transmission electron microscopy
TRF	Terminal restriction fragment
TMD	Tissue mineral density
TGA	Thermogravimetric analysis
TRAP	Tartrate-resistant acid phosphatase
W-H	Williamson-Hall
wt%	Percentage weight
XRD	X-ray diffraction
Yrs	Years

SYMBOLS, UNITS AND NAMES

Symbol	Unit	Name
'a' axis	Å	Length of lattice cell along 'a' axis
Ash%	%	Mineral content
'c' axis	Å	Length of lattice cell along 'c' axis
BV/TV	%	Bone volume fraction
CL002	nm	Coherence length of 002 peak reflection
CL004	nm	Coherence length of 004 peak reflection
CL030	nm	Coherence length of 030 peak reflection
CL210	nm	Coherence length of 210 peak reflection
CC	Ratio	Amount of collagen in the sample
CI	Ratio	Mineral crystallinity Index
CP	Ratio	Carbon substitution
CΔH	Wg ⁻¹	Enthalpy value of the exothermic episode
G _c	F/area	Release rate
^{It} E	GPa	Indentation modulus for interstitial bone
^{It} C _{IT}	%	Indentation creep at hold for interstitial bone
^{It} H	Vickers	Indentation nanohardness for interstitial bone
^{It} HV	Kg/mm ²	Indentation microhardness for interstitial bone
^{It} η _{IT}	%	Elastic work over the total for interstitial bone
LΔH	Wg ⁻¹	Enthalpy value of the endothermic episode
^{On} E	GPa	Indentation modulus for osteons
^{On} C _{IT}	%	Indentation creep at hold for osteons
^{On} H	Vickers	Indentation nanohardness for osteons

$O_n HV$	Kg/mm^2	Indentation microhardness for osteons
$O_n \eta_{IT}$	%	Elastic work over the total for osteons
$O_r\%$	%	Weight loss for organic fraction
MO	Ratio	mineral to matrix matrix ratio
K_{Ic}	$Pa \cdot m^{1/2}$	Intensity factor
$Po.Ar\%$	%	Optical porosity
Size	nm	Mineral size
Strain	%	Lattice strain
U_{ult}	N/mm^2	Yield force
W_f	KJ/mm^2	Work of fracture
$W\%$	%	Weight loss for water fraction
ν_s	Ratio	Poisson's ratio ($\nu = 0.3$)

CHAPTER 1

INTRODUCTION

Forensic anthropology includes, amongst other applications, the positive identification of unknown human skeletal remains. The first step in this process consists of the assessment of the biological profile, which includes establishing sex, age, stature and ancestry. These physical characteristics facilitate the exclusion of individuals from a larger pool of missing persons in order to narrow down the focus of the investigation. More specifically, correct age estimation is of importance for administrative and ethical reasons (Ritz-Timme et al., 2000). In forensic contexts, age represents one of the main challenges in the process of identification. Inaccurate assessment of this demographic feature can potentially rule out the actual match from the potential candidates of the missing person's archive, compromising the investigation of the case. Recently, researchers have been trying to improve accuracy and consistency of the estimation by applying experimental procedures from different fields (e.g. material engineering, molecular biology, biomedical sciences) in order to meet requirements for whiteness admissibility in the forensic setting. The present study investigates the potential of biomechanics and physicochemical analysis of bone nanostructure in order to develop an observer independent and highly replicable method for age estimation based on rib cortical bone that could be accessible by personnel not specifically trained in anthropology.

Developments in biomedical engineering have led to a greater understanding in the dynamics of bone degeneration and an increased risk of a fracture. The high incidence of age related conditions such as osteoporosis and osteoarthritis and the cost connected with treatment and hospitalisation that are connected with skeletal injuries have lead to an implementation of analytical methods employed to study changes in bone, such as the development of microscopy and physical methods (e.g. spectroscopy and diffraction). This has allowed penetration of the bone surface and therefore, an in depth understanding of struc-

tural organisation behind what the naked-eye examination can provide. This structural analysis has proven to be extremely useful in order to explain the mechanical behaviour of bone. Likewise, composition was found to also play a central role in the determination of mechanical behaviour (Ziopoulos, 2001). The investigation of this has allowed the unveiling of the three components that compose bone matrix (i.e. mineral, organic and water) and their variation according to age and pathological conditions (Ziopoulos, 2005; Greenwood et al., 2016). The main challenge of this research is to apply effectively the approach of biomedical sciences to forensic anthropology in order to fit the requirements of this field.

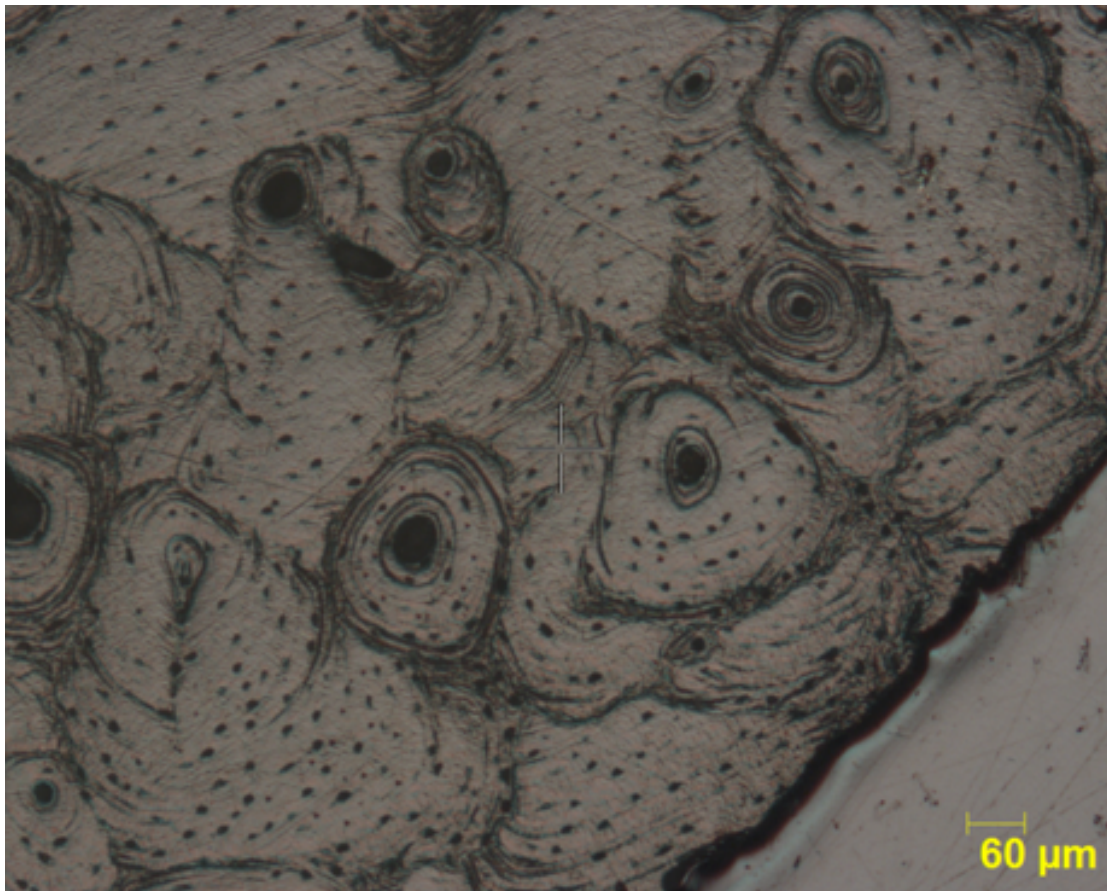


Figure 1.1: *Histological surface of rib cortical bone (20X under reflected light) shows the presence of concentric structures called osteons, that indicates that remodelling has replaced old with newly form one to allow bone to better support bone.*

1.1 Conceptual Overview and Scope

As bone is well known to be a composite material, a multifactorial approach was chosen in order to achieve a comprehensive understanding of age related changes of bone matrix chemical, mechanical and structural properties. The different aspects under examination should reflect the behaviour of bone in a certain interval so that the combination of multiple properties could improve age estimation along the entire age range.

The need for accurately estimating biological age in humans was raised for the first time in 1963 during the meeting of the European Bureau of the World Health Organization in Kiev without attracting much attention (Ries and Pöthig, 1984). Since that moment the interest has grown and this can be seen by the large number of different approaches in literature and part of them are described in detail in this thesis. In order to fully understand the difficulties related to age estimation it is necessary to first introduce the difference between chronological and biological age. Chronological age refers to the amount of time elapsed since birth and counted in days and years. Biological age, in contrast, describes the general condition of an organism at a given time of the chronological age. This condition can be defined in various ways by physical, psychical, and social characteristics (Ries and Pöthig, 1984). The main focus of this thesis would be to find appropriate biomarkers that can be measured and represent accurately the biological age of the bone. Between these biomarkers the ones for which biological age matches the best chronological age will be the one selected to produce estimation models.

In practice, to investigate the mineral phase XRD is an excellent tool that provides an indication of crystal size and strain as well as lattice measures. The variation of these parameters are affected by ion substitution evaluated by means of FTIR. This procedure also allows the investigation of crystallinity that is negatively correlated to size. Thermogravimetric analysis is employed in order to obtain percentage weight fraction for mineral, collagen and water content. Collagen thermal stability and organic content is further investigated by differential scanning calorimeter. These results are further confirmed by FTIR. Finally, porosity is evaluated by histomorphometry (Figure 1.1). To conclude, all these

compositional parameters are compared with functional data obtained by indentation to gain a comprehensive understanding of the structure-function relationship in ontogeny. This way mineral, organic and water phase will be fully analysed.

1.2 Research Questions

The primary goal of this study is to evaluate the potential of mechanical and physico-chemical properties of human rib cortical bone for forensic age-at-death estimation. Furthermore, this study intends to improve the understanding of age related changes in bone mineral and organic matrix and the effect that these have on the mechanical behaviour of bone. The research questions investigated and answered in this thesis are listed below.

1. What is the impact of chloroform-methanol degreasing procedure on the quantification the physicochemical properties of human rib cortical bone?
2. What is the effect of age on nanomechanical properties and physicochemical composition of rib bone matrix?
3. What is the structural relationship between collagen and mineral and how is this affected by age?
4. How changes in matrix composition affect mechanical behavior at different ages?
5. At what age does rib cortical bone reach skeletal maturity and, considering different compositional properties, is maturity reached at the same age for all of them?

1.3 Thesis Structure

This thesis brings together the knowledge of different fields in order to fully understand the potential of bone analysis for forensic anthropology. Chapter 2 presents the current approaches used in anthropology for age-at-death estimation. It starts with visual methods for juvenile and adults then switches to a thorough analysis of laboratory methods to provide the reader with an understanding of the advantages offered by this approach. This chapter offers the starting point to build a comparison between the method developed in

this thesis and current approaches. Chapter 3 will provide all the information regarding bone biology that is essential in order to understand age related changes of cortical bone matrix. The literature review concludes with chapter four that presents previous studies regarding bone structural, compositional and functional degeneration. This provides a first comparison term to then discuss results produced in this research with previous findings.

In Chapter 5 materials and methods are presented. First, all the methods are discussed in order to briefly explain the principle upon what they are based, the rationale behind the choice of the specific procedure and the main applications that are present in literature. The novel data will be presented in Chapter 6: first the behaviour of all the variables with age will be discussed. This will be followed by the results explaining the interaction between different components of bone matrix and then the interaction of them with mechanical properties. The chapter ends with the presentation of age predictive regression formula to assess age at death. The same topic, in the very same order will be further discussed in Chapter 7. A final section (Chapter 8) sums up results of the research, highlighting limitations and suggesting future directions this approach should take.

CHAPTER 2

CURRENT APPROACHES TO AGE-AT-DEATH

In order to understand the concepts that facilitate age-at-death estimation, this chapter will draw attention to the current research and recent developments in the field. The sections are divided conceptually, so as to bring together the various approaches that represent a starting point for the development of the new methodology in this thesis.

In cases where the remains are well preserved, visual traits can be assessed in order to obtain information about age. A large number of methods have shown that age can be accurately estimated for juveniles based on developmental traits of the human skeleton. Examination of bone length and shape is the first step in the ageing process. A number of features can be subsequently used to approximate juvenile individuals: tooth calcification and eruption, presence of centres of ossification and degree of fusion of epiphyseal areas (Ubelaker, 1987; Pfau and Sciulli, 1994; Panchbhai, 2011). In adulthood, and in particular after 30-35 years of age (Zioupos, 2001), the skeleton reaches maturity and age is determined through the analysis of physiological degeneration. Tooth wear remains a good target for age assessment (Kvaal et al., 1995). Degeneration can be quantified for various articular surfaces such as pubic symphyses and auricular surfaces (Brooks, 1955; Lovejoy, 1985; Villa et al., 2013). Although these methods can be conducted in the field without requiring preparation or equipment, they can be affected by endogenous and exogenous factors such as pathological conditions, diet and occupational markers (Simmons, 1985; Richardson, 2003; Cooper et al., 2007). Additionally, they are sex- and population-specific, and care must be taken when designing the investigation approach to each case (Kranioti et al., 2009; Franklin, 2010).

Recently established admissibility criteria are forcing researchers towards standardisation of methodological procedures (Baccino et al., 1999; Ritz-Timme et al., 2000; Garvin and Passalacqua, 2012). Despite these changes, experience plays a central role in anthro-

pological examinations. Garvin and Passalacqua (2012) compared three commonly used morphological age estimations methods and analysed the effect of experience of different operators. Results showed that inter-observer bias in the methods of choice and ,as a result, age estimation are unpredictable. This makes the application of such methods in a forensic situation problematic. In order to avoid this issue, as suggested by Ritz-Timme et al. (2000), age estimation procedures (1) must be presented to the scientific community and published in peer reviewed-journals, (2) must be accurately explained in terms of procedure and (3) must present clear information about accuracy of the estimation and error. Finally, in treating living individuals, methods such as low intensity X-ray images and high intensity CT imaging have been employed (Ritz-Timme et al., 2000; Schmeling et al., 2007; Franklin, 2010; Zapico and Ubelaker, 2013).

In order to fulfil all these requirements, a large number of methods based on physiological processes that causes biochemical changes in various tissue structures at the molecular level has been developed (Franklin, 2010; Zapico and Ubelaker, 2013). They examine a wide range of modifications such as DNA-methylation and telomere shortening, racemization of proteins, stable isotopes analysis and mechanical integrity of the bone structure (Ritz-Timme et al., 2000; Schmeling et al., 2007; Franklin, 2010; Zapico and Ubelaker, 2013). These procedures are laboratory-based and require trained personnel but not necessarily a forensic anthropologist. Consequently, the burden of experience when establishing a biological profile can be significantly reduced. The necessity, therefore, is to accomplish consistency and reliability by standardisation of the preparation procedure. This would make the methodology reproducible in any laboratory facilities, which in turn meets the necessary requirements for medico-legal applications (Waite et al., 1999). With this motivation in mind, the literature surveyed here focuses on age-at-death estimation for juveniles and adults. Thereafter, the sections present discussions regarding laboratory-based methods.

2.1 Age-at-death — Juveniles

Age estimation in juvenile individuals for the most part relies on skeletal growth, maturation traits and dental eruption. Dental eruption has proven to be the most effective trait in terms of correlation between chronological and biological age rather than skeletal traits. This is attributed to the lower degree of individual variation and environmental influences (Ritz-Timme et al., 2000; Scheuer, 2002; Lewis and Nyman, 2008; Franklin, 2010).

Deciduous dentition starts mineralising around the 15th embryonal week and ends approximately around three years of age, while the formation and eruption of permanent dentition occurs between birth and 14 years of age, with a highly variable eruption of the third molar around the 17th year (Scheuer, 2000). For this reason, it does not represent a reliable age indicator. Sexual dimorphism influences tooth eruption with a delay of one to six months in males in comparison to females and variation for individual teeth as well (Rösing et al., 2007). For instance, the eruption of the first six permanent teeth can vary up to 0.98 years for the maxillary lateral incisor, making it an accurate age indicator (Hurme, 1948). The consistent degree of genetic variation in the population can affect the estimation. This has resulted in a large body of research and associated literature around the ageing approach (Lewis and Nyman, 2008; Moze and Roberts, 2012; Karkhanis et al., 2015). One of the first methods was developed by Schour and Massler (1941). It was based on both deciduous and permanent tooth formation and eruption from five months *in utero* until 35 years with completion. This method was later improved by Ubelaker (1989) who presented a more accurate study providing standard deviations for each age range for both prenatal and postnatal teeth formation and eruption. The method, although developed on the native American population, it stands out as a reference method for osteological analysis worldwide (Hillson and Bond, 1997).

In order to perform age estimation in the absence of dentition, analysis of bone development and maturation are employed. This relies mostly on the appearance and fusion of secondary sites of ossification with diaphysis and diaphyseal length evaluation (Scheuer, 2002; Lewis, 2007). Between birth and 2.5 years of age, measurements of long bone can

be used for the assessment with a certain degree of accuracy (Scheuer, 2000, 2002). However, diaphyseal length is heavily affected by malnutrition and pathology. Consequently, this method is better suited to understanding environmental-related modification rather than chronological age (Lewis, 2007). More accurate results can be obtained by the examination of epiphyseal fusion, which starts between 11 and 12 years of age with the mineralisation of cartilage in the elbow and roughly ends at the age of 30 years with the medial clavicular epiphyses fusion, although genetic variations are frequently reported (Lewis, 2007). In dry bone, what can be observed of this phenomenon is the presence of separated bone ossicles in early stages of fusion or grooves between diaphysis and epiphysis when the stage of ossification is more advanced (Buikstra and Ubelaker, 1994; Scheuer, 2002). A sample size must be reasonably large and the reference population must be taken into consideration when choosing the most suitable approach for the case. Finally, this principle for age estimation can be applied to living individuals or non-skeletonised remains with the employment of new medical imaging technologies (Schmeling et al., 2004; Eki-zoglu et al., 2015; Lefèvre et al., 2016).

2.2 Age-at-death – Adults

In comparison, the age-at-death estimation for adult bones involves a few additional considerations. The absence of developmental markers in adult skeletons motivated researchers to develop methods based on bone degeneration for age estimation. A large number of non-invasive procedure was based on the visual assessment of degenerative processes developed on different bones. The main difficulties in this task are related to inter-individual variations in the degeneration pattern and intra-/inter-observer variation that can affect the age estimation (Baccino et al., 1999; Garvin and Passalacqua, 2012). Within the scope of the literature analysed for this thesis, visual assessment is still at the base of the identification process although it does not fulfil all the requirements of being applicable in a forensic scenario previously presented.

The analysis of teeth has also been employed for age estimation in adulthood. The most simple and straightforward approach is the visual examination of dental wear. This is

based on the correlation between the amount of enamel removed and of dentine exposed, and age according to the principle that more wear relates to an older individual (Scott, 1979; Smith, 1984; Lovejoy, 1985). The method is simpler to apply and is suitable in the forensic context. It is, however, unreliable due to the variations in wear related to jaw and teeth morphology that can affect contact points representing an issue in standardising the evaluation (Cunha et al., 2009). Similarly, the type of diet plays a central role in the determining the extent of wear (Franklin, 2010). It was pointed out by Garvin and Passalacqua (2012) in a study surveying methodological preference of 145 forensic anthropologists that tooth wear analysis is the least preferred on the visual age assessment based on skeletal degeneration. For this reason Lamendin et al. (1992) developed a two-step method for age estimation based on the combination of periodontosis and root transparency. The first is the progressive degeneration of the soft tissue from the neck to the apex of the tooth. The second one, shown in Figure 2.1 is based on the principle that the dental root placed on a negatoscope would be transparent only on the apex area and the maximum height of the transparent area is consistently correlated with age. This technique has the potential to assess age with an error of 8.9 ± 2.2 years. The main limitation is that the accuracy is lost for individuals <40 years of age (Lamendin et al., 1992). Although efficient and accurate within its scope, the Lamendin method has been unsuitable for population different from the reference (Prince and Ubelaker, 2002; Schmitt et al., 2010) and therefore discretion and caution are necessary when using this method.



Figure 2.1: *Measurement of translucency of the apical area of the dental root used in the Lamendin method combined with periodontosis to assess age-at-death. The increase in translucency and the area of the root affected by periodontosis increases with age Reprinted with permission from [John Wiley and Sons] (Lamendin et al., 1992).*

The fibrous joints of the skull, known as sutures (Meindl and Lovejoy, 1985), are good indicators as their progressive fusion shows a consistent relationship with age. A series of specific sites (Figure 2.2) on the ectocranial surface of the skull are observed and scored 0 to 3 based on the degree of fusion. The different sites give an indication of age ranges. A composite score is then calculated summing up the scores from each site and correlated to age. For their study, a total of 236 crania from the Hamann-Todd Collection were analysed. Of the 17 sites included initially in the estimation, only 10 (Figure 2.2) were not affected by poor interpretability, asymmetry or closure at highly variable ages (Meindl and Lovejoy, 1985). Considering these features separately, the pterion was found to be the most accurate in age estimation for samples from individuals beyond the age of 40, while the Obelion is an early point of obliteration useful as an early life change indicator. Results show a very large interval that may not be useful for age estimation in forensic settings (Meindl and Lovejoy, 1985). Although this is a very simple method, it provides a very broad indication of age range and cannot be used for remains in cases of poor preservation. Furthermore, high inter-population and sex-related variation was detected (Cunha et al., 2009). Overall, it has been seen that this approach can be used to have

a rough orientation during the age estimation process that can, however, to an incorrect assessment in certain situations (Rösing et al., 2007). For all these reasons, Garvin and Passalacqua (2012) in their study showed that cranial suture closure for age estimations is the least preferred methodology between the ones evaluated.

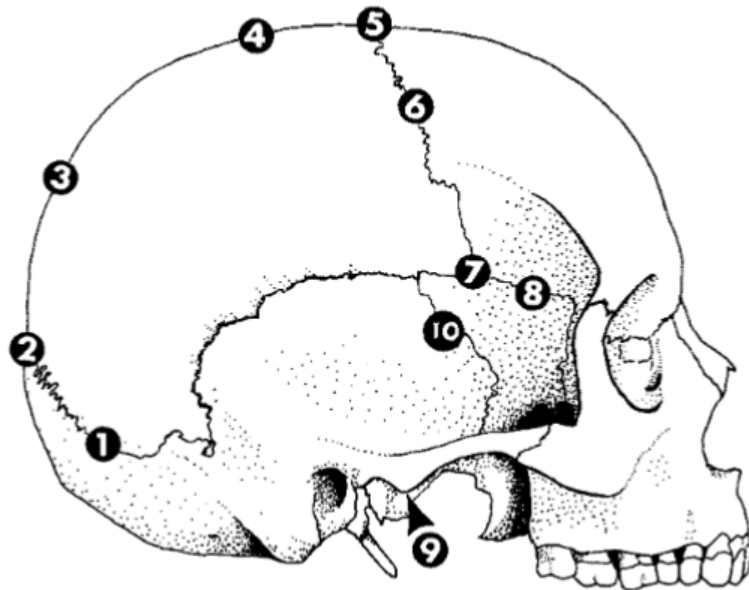


Figure 2.2: *Locations on the ectocranial surface for the assessment of suture closure. The neurocranium is the most durable part of the cranium and therefore more likely to be retrieved intact in archaeological contexts (1 = Midlambdoid; 2 = Lambda; 3 = Obelion; 4 = Anterior Sagittal; 5 = Bregma; 6 = Midcoronal; 7 = Pterion; 8 = Sphenofrontal Inferior; 9 = Sphenotemporal Superior; 10 = Sphenotemporal Inferior). Reprinted with permission from [John Wiley and Sons] (Meindl and Lovejoy, 1985).*

Pubic symphysis analysis remains one of the most utilised articular areas to be employed for age estimation. This is due to the greater reliability compared to other morphological methods for age estimation (e.g. cranial suture) (Meinl and Lovejoy, 1989). This joint is located on the anterior area of the pubis and it is the direct junction between the two os coxae. For the first time, Todd (1920) established that there was a good correlation between morphological modifications of the articular surface and age when visually examined. In a subsequent study, different methodologies for females and black populations were presented (Todd, 1921). The main limitation of this method is the high

inter-individual variation in the degeneration pattern of the articular surface. The potential of this indicator for age estimation was later confirmed by testing the methodology on two different collections for a total of 5070 specimens that showed good performance for age estimation (Brooks, 1955). Meindl et al. (1985) highlighted the advantage of morphological characterisation over numerical classification due to the fact that describing a physiological and non-homogeneous degeneration process is easier in comparison to quantification to reduce errors induced by inter-individual variations in shape and size. More recently, Suchey and Brooks (1990) adapted the original Todd's methodology to create a new procedure based on six phases according to the degree of morphological changes of the articular surface. This technique is extremely simple and the operator compares morphology of the specimens to a written description or a cast in order to assign the specimen to one of six phases. The examination of 1225 corpses with known age during autopsies is found to accurately estimating age valid for 95% of population. Additionally, this technique is sex-specific: sex can be estimated by the pubic symphysis if preservation allows it (Márquez-Grant, 2015). However, fragmentation and incompleteness of the skeletal remains can represent a limitation in the application of the method. Overall, the revised method based on a large modern population is the ultimate effort to meet all the standard requirements given by the legal system to the practice of forensic anthropology for age-at-death estimation. Garvin and Passalacqua (2012), who collected data with a questionnaire regarding preference in methodological choice of 145 forensic scientists, proved that the analysis of the os pubis represents the ideal methodology for age estimation based on morphological examination despite the level of experience or background (>95% of the operators utilise it regularly) of the examiner and did not show significant inter-observer error.

Another target for age estimation based on articular surface degeneration are the auricular surfaces of the ilium, connecting the two os coxae to the sacrum. Lovejoy et al. (1985) showed that the main advantage is the high probability of recovering intact surfaces. The method consists of the analysis of several morphological features (e.g. granularity and density, microporosity, billowing, striation, apical activity, retroauricular area

and transverse organisation) for the entire surface in order to classify the specimen in eight phases. Each phase accounts for a five year interval, from 20 to 60+ years (Lovejoy et al., 1985). Although the examination is proved to be accurate in mature individuals, the region does not present the same extent of chronological modification shown by the anterior portion of the pubis and interpretation of these results are difficult in fragmented or heavily weathered scenarios (Lovejoy et al., 1985). Buckberry and Chamberlain (2009) aimed to simplify and reduce the number of morphological elements considered in the estimation to reduce observer bias. This was achieved by scoring transverse organisation, texture, micro- and macro-porosity and apical changes separately in order to produce a composite score that could lead to one of the seven stages of degeneration shown in Table 2.1.

Table 2.1: *Original table containing the seven phases used to estimate age from the auricular surfaces of the ilium. It is interesting to note the decrease in accuracy with the increase of age. Reprinted with permission from [John Wiley and Sons] (Buckberry and Chamberlain, 2009).*

score	Stage	No.	Mean age	SD	Median age	range
5-6	I	3	17.33	1.53	17	16-19
7-8	II	6	29.33	6.71	27	21-38
9-10	III	22	37.86	13.08	37	16-65
11-12	IV	32	51.41	14.47	52	29-81
13-14	V	64	59.94	12.95	62	29-88
15-16	VI	41	66.71	11.88	66	39-91
17-19	VII	12	72.25	12.73	73	53-92

The main advantage of this approach is the absence of differences between sexes, allowing estimates age for individuals of unknown sex (Buckberry and Chamberlain, 2009). A number of tests were carried out to understand the potential application of this methodology to different reference populations. They showed a reduction in accuracy when estimating the age-at-death, which further highlighted the necessity of developing population specific procedures and relationships (Mulhern and Jones, 2005; Moraitis et al.,

2014). Changes in size and shape of the areas targeted for the assessment as well as inter-individual variation represent factors that could induce error in the estimation.

An additional fundamental method for age estimation based on degenerative bone patterns was developed by Işcan et al. (1984). This involves the visual evaluation of structural changes of the right 4th sternal rib end. It focuses especially on the evaluation of rim morphology and pit formation of this articular surface. Sternal rib ends are typically characterised by a uniform and rounded rim, and a flat surface in younger individuals. This area becomes more irregular and the bone texture is less visible with the increase of age. Finally, morphology of ribs from individual of older age are characterised by projections due to osteophytes formation and ossification of the costal cartilage. More specifically, the method is based on a nine-phase scoring pattern that allows accurate estimation of age. The method can estimate age with an accuracy of ± 2 years in the 2nd and ± 5 years in the 5th decade (Işcan et al., 1984). It has also been suggested that, despite developed on the 4th rib, the methodology can be applied to the 3rd and 5th ribs without compromising the significance of results (Nikita, 2013).



Figure 2.3: Example of the rib sternal end metamorphosis showing the increase in pit depth and appearance as well as rim and wall configurations. Reprinted with permission from [John Wiley and Sons] (Adserias-Garriga and Wilson-Taylor, 2019)

In general, the main drawback is the difficulty in identifying the 4th rib in disarticulated situations. Therefore, it is suggested to isolate the appropriate specimen on site and store it separately (Márquez-Grant, 2015; Adserias-Garriga and Wilson-Taylor, 2019). Furthermore, the pattern of the degeneration is observed to be highly affected by activity,

resulting in a less accurate estimation potential (Rösing et al., 2007). Despite the fact that the method is considered one of the most popular for age estimation based on morphological examination of bone changes, the correlation between structural changes and chronological age is not always ideal (Nikita, 2013). Further research is necessary to evaluate effectiveness of this approach in a forensic setting.

Finally, what was recently analysed is the potential of the analysis of the clavicle sternal epiphysis after complete fusion. Results reported by Falys and Prangle (2015) show that surface topography, porosity and osteophyte formation on the clavicular surface could represent a good age indicator when analysed in an ordinal scoring system. The method (Falys and Prangle, 2015), which relies on a similar degeneration process seen for pubic symphyses and auricular surfaces, does not provide the minimum accuracy for the forensic setting, although it is still a pilot study and with larger sample representing individuals a broader age range. It could represent an additional morphological method for age assessment in individuals under 30 years of age (Scheuer, 2000; Falys and Prangle, 2015).

These methods are a few of the many examples of age estimation by means of visual assessment of developmental or degenerative traits of bone gross anatomy. Accuracy of these approaches heavily relies on qualification and experience of the observer. This factor does not allow these methods to be universally suitable for forensic age estimation.

2.3 Laboratory Based Methods

Advances in medical sciences and biomedical engineering have led to the development of several quantitative methodologies in order to investigate physiological processes related to ageing and pathological conditions. Having considered the different methods of visual examination, this section will discuss the laboratory methods employed for age-at-death estimation. The main advantages offered by these approaches is that they are independent of experience and should provide a highly standardised experimental procedure, easy to replicate in order to test results or to apply the method in other contexts. Furthermore, the statistical approach that is involved in the development of the age estimation give the

possibility to provide error and reliability of the formulas.

2.3.1 Aspartic Acid Racemization

Aspartic acid racemization (AAR) is based on the conversion of optically active amino acids into racemic compounds. All amino acids, with the exception of glycine, have the ability to rotate the plane of plane-polarised light. These optic isomers are known as L-enantiomers (levorotary) and D-enantiomers (dextrorotary). The change in the ratio of these two isomers, quantified by gas chromatography or high performance liquid chromatography (HPLC) is related to the natural ageing process with an increase in D-amino acid. Aspartic acid is affected by a very high rate of turnover due to its tendency of bonding with acidic residues, resulting in a quick accumulation of D-Asp over L-Asp making a suitable target in clinical and forensic settings (McCudden and Kraus, 2006; Meissner and Ritz-Timme, 2010; Zapico and Ubelaker, 2013).

There have been many attempts to quantify this process in order to understand the potential for age estimation. Ritz et al. (1994) tested non-collagenous bone proteins (osteocalcin) extracted from the skull in order to predict age-at-death, reporting good performance for individuals under 60 years of age. Results for this age range were promising, with a correlation with age of $R = 0.99$. Due to the limited number of specimens ($N = 10$) employed in this study, the test was repeated with a sample size of 53 individuals. This study showed similar results to the previous study with a standard error of age estimation of 2.8 years (Ritz et al., 1996). These results were further reaffirmed by Pfeiffer et al. (1995b) and this proved the effectiveness of AAR analysis extracted from cortical bone from the frontal bone. This new work showed good correlation with chronological age for acid-soluble peptide fraction ($R = 0.72$) and acid-insoluble collagen-rich fractions ($R = 0.84$) with an estimated error of ~ 15 years. The main advantage of the application of AAR analysis of bone is the possibility to retrieve the material in forensic and archaeological cases (Pfeiffer et al., 1995b). The application of this type of analysis on soft tissue has also been considered. Pfeiffer et al. (1995a) sampled rib cartilage from 24 individuals showing the possibility of predicting age with acid-insoluble and acid-soluble collagen-

rich fraction respectively with $R = 0.91$ and $R = 0.97$ (standard error of estimation 7.07 years). Different tissues have also been considered as a target for AAR analysis. Racemization of elastin from arteries also showed good correlation with age providing another sampling possibility for age estimation (Dobberstein et al., 2010). Recently, a new regression method was developed for epiglottis cartilage elastin confirming the potential that this protein offers for assessing AAD (Matzenauer et al., 2013). Purification of elastin remains a sophisticated and complex procedure, prone to contribute to the inaccuracy of age estimation (Meissner and Ritz-Timme, 2010).

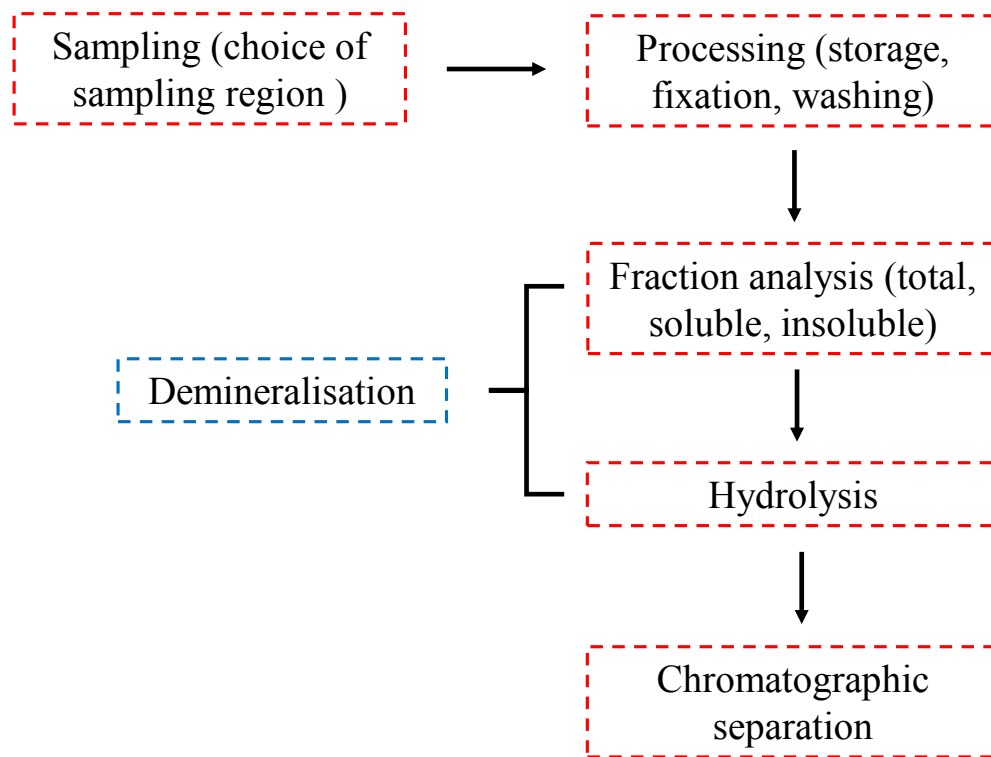


Figure 2.4: Flow chart describing the steps generally adopted for aspartic acid racemization. Reprinted and adapted with permission from [John Wiley and Sons] (Waite et al., 1999).

Teeth have been identified as the most suitable skeletal element for AAR analysis. Both dentin and enamel proteins have a lower turnover rate compared to bone and it is easy

to isolate pathological specimens (e.g. caries) to obtain the best age estimation possible. Caries have been seen to promote the accumulation of D-aspartic acid resulting in an over estimation of the sample (McCudden and Kraus, 2006; Sirin et al., 2018a,b). Ohtani (1995b) tested the methodology on longitudinal sections of dentin to obtain promising results with a variability of ± 3 years. In a different study, the method showed that similar results could be obtained by testing tooth cementum and enamel. The comparison between the three tissues shows that dentin remains the most accurate for ageing skeletal remains (Ohtani, 1995c). A further improvement was shown by Sakuma et al. (2012) using the whole tooth longitudinal section. In addition to improving the overall accuracy for the methodology, the protocol was also made easier and the sampling area more consistent. This approach allows accurate age estimation with a very low standard deviation and the potential to standardise the protocol. Although the effect of taphonomic processes is not yet fully understood, a large number of biases related to the procedure has been addressed by standardising the sampling and laboratory protocol (Meissner and Ritz-Timme, 2010). Care must be taken on the target of the examination. Racemization is highly dependent on the type of tooth chosen. Considering molar teeth, this is due to the fact that dentin forms earlier on the first molar and later in the second and therefore in middle age individuals the degree of racemization is higher for the first molar. However, for older individuals, the amount of racemization favours the second due to the ambient temperature that is higher in the deeper area of the oral cavity (Ohtani et al., 2003).

Overall, the intrinsic issue related to ARR for age estimation is the unstable ratio of the two isomers in the root tend to be lower than the one found in the crown. This trend changes from the age of 30 years when the ratio becomes higher than the one for the crown. Furthermore, temperature is normally stable at $\sim 37^{\circ}\text{C}$ in the human body. After death/deposition, variations in the environmental temperature could speed up or slow down the racemization process (Ritz et al., 1993). Dobberstein et al. (2008) reported an increase of 45 to 50% in the D/L ratio after 20 days at 90°C for AAR in total non-collagenous and collagenous proteins in dentin. A slower but consistent increase in the ratio is also seen in natural ageing, suggesting the accumulation of AAR is affected also by postmortem

interval (PMI) (Dobberstein et al., 2008). Environmental pH also plays a central biasing role in the application of this method. Similar results were also reported previously by Ohtani (1995a), who reported a linear increase of the D/L with the increment of temperature. This increase is also seen to be favoured by alkaline environment (pH 9) due to the higher concentration of OH^- . These two aspects must be taken into consideration when applying this technique with specific attention paid to the season and the geographic area where the remains were found.

The development of protocols based on AAR (Figure 2.4) is an example of the application of physiological processes to age estimation. The trend explained in this section shows that the final aim of forensic anthropology is to develop a highly repeatable and standardised procedure that can provide the most accurate results reducing the possible sources of error. In the case of ARR, the choice of the most appropriate tooth and the portion of it to be sampled (e.g. dentin, enamel, root or crown) is of importance in order to standardise the technique and allow applicability in the forensic setting.

2.3.2 Collagen Cross-links

As will be further explained in Section 3.1.2, collagen molecules are stabilised by means of water mediated covalent cross-links. All the fibril-forming collagen types in higher vertebrates (types I, II, III, V and XI) are cross-linked through a mechanism based on the reactions of aldehydes generated enzymically from lysine (or hydroxylysine) side-chains by lysyl oxidase. This process has been investigated due to the role played by inter-molecular cross-linking in mechanical behaviour of bone (Zioupos and Currey, 1998; Wang et al., 2001, 2002b; Garnero et al., 2006). Martin-De Las Heras et al. (1999) analysed molar dentin in order to evaluate the potential of cross-links quantification for age estimation. Specifically, they extracted and quantified total and percentage deoxypyridinoline (a non-reducible trifunctional cross-links) amount before and after demineralisation by means of EDTA using enzyme immunoassay. The ratio is calculated and correlated with age. This gives the procedure consistency and reproducibility. Although results did not show the same degree of accuracy of AAR, the model developed from human molars of 22 individ-

uals was able to predict age with 65% confidence level and mean error of ± 14.9 years. This could represent a complementary methodology to apply on teeth and/or an advantageous asset when developing multi-factorial approaches for age estimation Martin-De Las Heras et al. (1999). One main advantage of this method is the fact that it is completely non-invasive and therefore highly repeatable. However, the laborious preparation, the small sample size tested to date and the low accuracy obtained with this method, make it an example of a process that cannot be employed in forensic anthropology for age estimation.

2.3.3 Advanced Glycation End-products (AGEs)

Another post-translational modification of collagen are AGEs, which are related to the normal ageing process, oxidative stress or hyperglycaemia (Stock, 2015; Barthelat et al., 2016; Willett et al., 2019). Regarding the forensic application of this process, Pilin et al. (2007) analysed the variation in colour, from yellow to brown with the increase in AGEs, of cartilage from intervertebral disks, Achilles tendons and ribs with a postmortem interval less than three days. RGB colour channels were analysed in order to obtain mean values for different colours and results showed good correlation between rib cartilage and age, while no good correlations were found for the rest of the sites sampled. The authors also reported that the potential application of this methodology is limited only to individuals < 45 years of age (Pilin et al., 2007). Visual estimation of colour changes in teeth was also applied to a collection of 1000 specimens proving a progressive "yellowing" with age. This method does not reflect the essential need of reproducibility, introducing inter-observer bias that is not acceptable in forensic setting. The same study showed also the potential of determining age from tissue density using a transmission densiometer (Ten Cate et al., 1977). Martin-De Las Heras et al. (2003) presented results for the analysis of chromaticity coordinates, luminance and whiteness and yellowness index obtained by means of spectroradiometry for dental roots. Multiple regression analysis showed a 70% confidence interval with 13.7 years of mean error of the estimation (Martin-De Las Heras et al., 2003). These results are not comparable with the potential shown by AAR but the

application of this methodology could represent an effective complementary technique due to the very low level of complexity in the procedure. Furthermore, Meissner and Ritz-Timme (2010) pointed out that fluorescence could be generated by other reactions (e.g. lipid peroxidation products, proteins and amino acids oxidation) without reflecting the real concentration of AGEs. Finally, individuals suffering from diabetes or bodies that have been exposed to prolonged heat will show higher values in ages, introducing bias in the age estimation that would tend to an overestimation (Meissner and Ritz-Timme, 2010). As for the application of cross-links to age estimation, this physiological principle does not show the necessary degree of accuracy accepted in forensic anthropology. However, this method again could be a complementary test when choosing the multi-factorial approach.

2.3.4 Molecular Methods

Epigenetic modification of DNA that causes phenotypical expression modifications not related to genetic coding have been seen to be accurate biomarkers for age estimation (Kader and Ghai, 2015; Zampieri et al., 2015). One of these processes is DNA methylation. It consists of the addition of a methyl group to the 5' position of cytosine bases present within a CpG dinucleotide (Figure 2.5). Demethylation is the oxidation of the 5'-methyl-cytosine. Hypermethylation and hypomethylation both result in modification in the control of gene expression. This is one of the most accessible epigenetic modifications of DNA and for this reason largely employed in forensic anthropology in order to assess age, sex, ancestry, biological fluids and tissue association with disease (Kader and Ghai, 2015; Zampieri et al., 2015; Meissner and Ritz-Timme, 2010). The method usually employs a very small quantity of biological material (e.g. bone, tooth, saliva, blood, semen/vaginal fluids) in order to actuate a minimally destructive procedure. The advantage is that this method is applicable when the sample is scarce and forensic scientists intend to avoid loss of crucial evidence of crime scenes (Kader and Ghai, 2015). The assessment is done by means of regression equations previously developed on known age samples. The laboratory procedure is based on a highly standardised protocol that avoids the introduction of intra-/inter-observer error and makes it accessible to researchers/technicians with no

previous knowledge in forensic anthropology (Kader and Ghai, 2015). Epigenetic modifications are heavily affected by environmental factors such as pathological conditions, dietary habits and lifestyle choice as noted in studies on monozygotic twins (Fraga et al., 2005; Poulsen and Simonsen, 2007; Kader and Ghai, 2015; Zampieri et al., 2015). For this reason, it is of paramount importance to gain a comprehensive understanding of the effect of this factors on the age assessment based on different type of tissue (Kader and Ghai, 2015; Bocklandt et al., 2011).

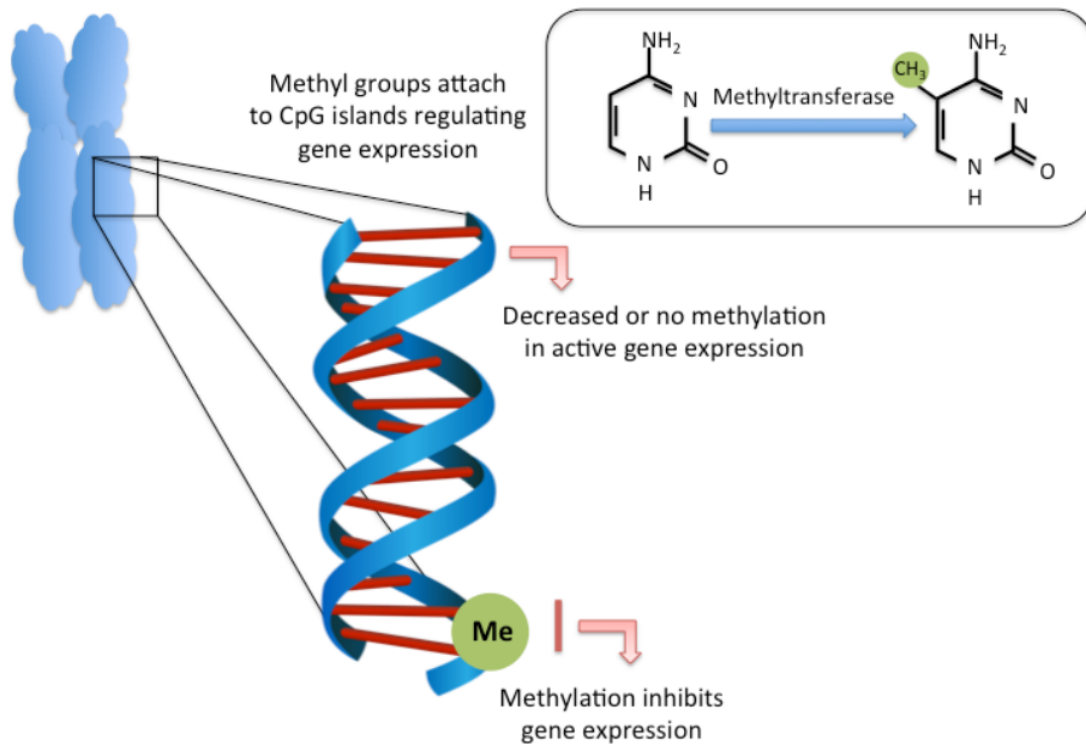


Figure 2.5: Methylation occurs when the methyl group is attached to the 5th carbon of the cytosine by means of an enzyme called DNA methyltransferases. The results is a 5-methylcytosine (Nevin and Carroll, 2015).

Zubakov et al. (2010) developed an AAD method employing T-Cell DNA extracted from blood stains of a sample of 195 individuals. T lymphocytes employ T-cell receptors (TCRs) to identify antigens. Signal joint TCR excision circles (sjTRECs) is the intervening DNA sequences in the TCR loci are deleted and circularised into episomal DNA molecules and has been seen to start soon after birth sjTREC shows a log-linear decline

with age. The study, therefore, aims on one side to reduce the degree of invasive nature of the procedure. This limits the sampling of bone and teeth and to find an accurate and reliable marker to correlate with age. Results showed $R = 0.836$ with $SE = 8.9$ years after 10 000 iterations of cross-validation and a 95% of accuracy. The method tested the same samples after 1.5 year without highlighting any significant differences, suggesting the potential of the procedure even in case of long interval between death and analysis (Zubakov et al., 2010). Overall, the procedure appears to be extremely efficient in forensic scenarios and it could have useful application in DVI. Furthermore, it gives information on the immunological age in relation with the chronological age. Recently, Huang et al. (2015) developed a method based on blood stains analysed immediately and after four months from extraction. Multiple regression analysis displays 82% accuracy of the age assessment and mean square error ± 8.055 years for the whole sample, without significant variations between age ranges and genders. Inconclusive remain results for understanding how time from extraction and conservation modality influences the age assessment (Huang et al., 2015). Independence from postmortem interval and time from the tissue extraction are confirmed from a large number of tests (Zubakov et al., 2016; Hamano et al., 2016; Freire-Aradas et al., 2016). These methods demonstrate good accuracy and versatility. More than one demographic feature can be assessed through DNA analysis without any previous experience in forensic anthropology (Zubakov et al., 2016; Hamano et al., 2016). Although it is said that no specific training is required, availability of facilities can be a limitation in the application of this assessment.

Another examination that has been largely applied to age estimation is the telomere length quantification. Telomeres are the terminal parts of DNA, composed by around 15 000 - 20 000 bases repeating sequence of base pairs $(TTAGGG/CCCTAA)_n$. The main function of these portions is to stabilise chromosomes. It plays a central role to maintaining replicability of somatic cells. Although the telomerase enzymes (Figure 2.6) are responsible for adding repeat sequences, they are affected by different factors such as oxidative stress and processing of telomere sequence in cell duplication that result in the shortening of the telomeres (Meissner and Ritz-Timme, 2010). Consequently, with age,

DNA polymerase and the absence of telomerase enzyme results in the reduction of the telomere length sequence and this modification can be assessed by different methods.

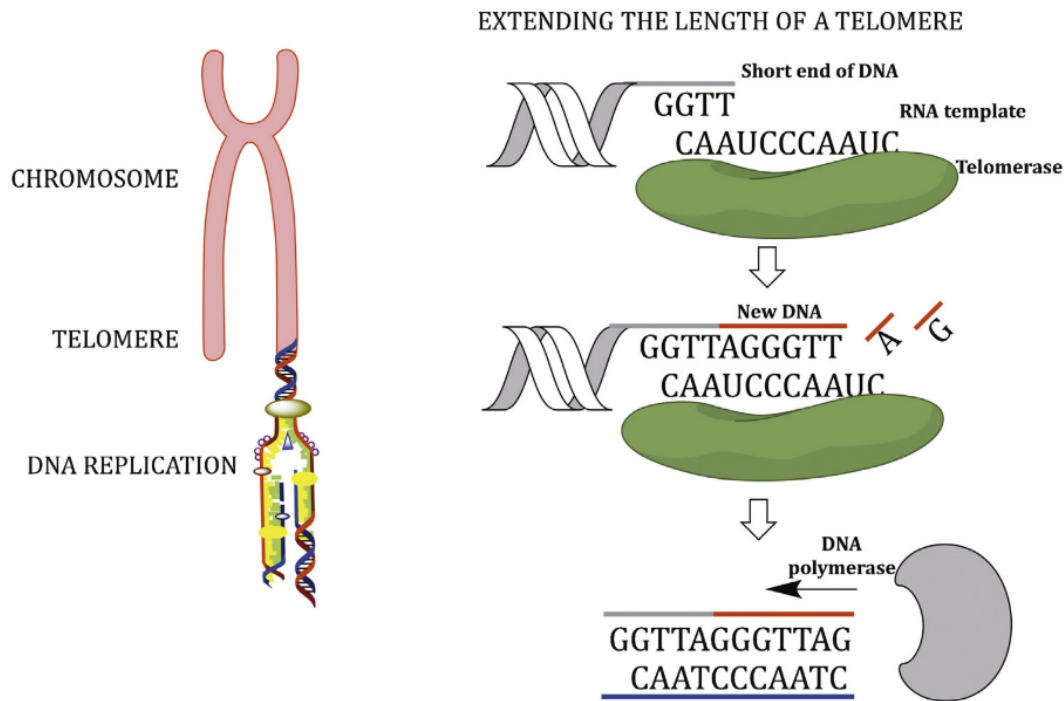


Figure 2.6: Extension of telomere length. Telomerase binds to 3' flanking end of telomere that is complementary to telomerase RNA. Telomerase adds bases using RNA as template. Finally, DNA polymerase complements the lagging strand. Reprinted with permission from [Elsevier] (Zapico and Ubelaker, 2013).

The most common technique used to detect a specific DNA sequence is Southern Blotting, the transfer of DNA sections from the electrophoresis gel to a membrane in order to immobilise the fragment, that has become a golden standard in telomere length analysis. It consists of cutting DNA using specific enzymes, separating it and arranging it on a membrane by means of electrophoresis. A telomere-specific probe is used to visualise different length that characterised telomere areas at various ages. The two main drawbacks are the amount of DNA necessary for this analysis ($\sim 10 \mu\text{g}$) and the large sample size necessary to obtain comprehensive results (Svenson and Roos, 2009). Another variation of this approach involves evaluation of mean terminal restriction fragment (TRF) that is reduced by 20-60 bp per year. This, combined with real-time PCR, have shown limited potential of

the application of this genetic bio-marker to assess age-at-death (Karlsson et al., 2008). This procedure is not fundamentally different from the previous one as it still employs the Southern Blotting procedure. An example of the application of this method was done by Tsuji et al. (2002). They tested bloodstains from 60 individuals (0-85 years) and correlated TFR with age obtaining a method that showed $R = 0.832$ with an estimation error of 7.037 years. Results proved to be less accurate when analysing dental pulp DNA. Takasaki et al. (2003) show a correlation $R = 0.749$ and a slightly higher error of the estimation (± 7.52 years). The authors also highlighted a the loss of 0–952 bp after one year of storage that must be taken into consideration as it could affect the age assessment (Takasaki et al., 2003).

Another common technique employed to evaluate telomeres' length are Q-FISH and Flow-FISH, quantitative fluorescence *in situ* hybridisation. These procedures employ fluorescence labelling of $(CCCTAA)_3$ peptide nucleic acid probes (Figure 2.7). However, it is extremely difficult to perform and slow, and can be applied on telomere sequences containing a limited range of primers. The fluorescence signal is then calculated and compared with reference standard telomere length in metaphase. Although they are extremely laborious and time consuming, these approaches are the best choice for TRF specific subsets of blood cells (Meissner and Ritz-Timme, 2010).

A certain correlation between age and telomere shortening has been found. Accuracy and methodological procedure are not suitable for forensic investigation due to excessive individual and inter-genic variation and for the large influence of pathological and environmental factors that make the phenomenon difficult to correlate consistently with age (Hewakapuge et al., 2008; Karlsson et al., 2008; Meissner and Ritz-Timme, 2010). One example is given by the difference between male and female. Samples from female individuals show a loss of 16 bp/year in comparison to 25 bp/year of male individuals, as estrogen have been suggested to promote catalysis of hTERT, subunit of telomerase (Hewakapuge et al., 2008). It also indicates towards a certain degree of inheritance telomere length pattern, with 78% for twins according to the study carried out by Hewakapuge et al. (2008). In addition, heterogeneity of telomere length is normally dependent on in-

determinable circumstances and changes between 10% and 80% within a population of cells, indicating intra-individual differences not only between different tissues but also in the same tissue (Meissner and Ritz-Timme, 2010). The limited invasiveness and the replicability of these procedures have made them an ideal choice for age estimation. One main limitation remains the risk of sample contamination that can affect these approaches.

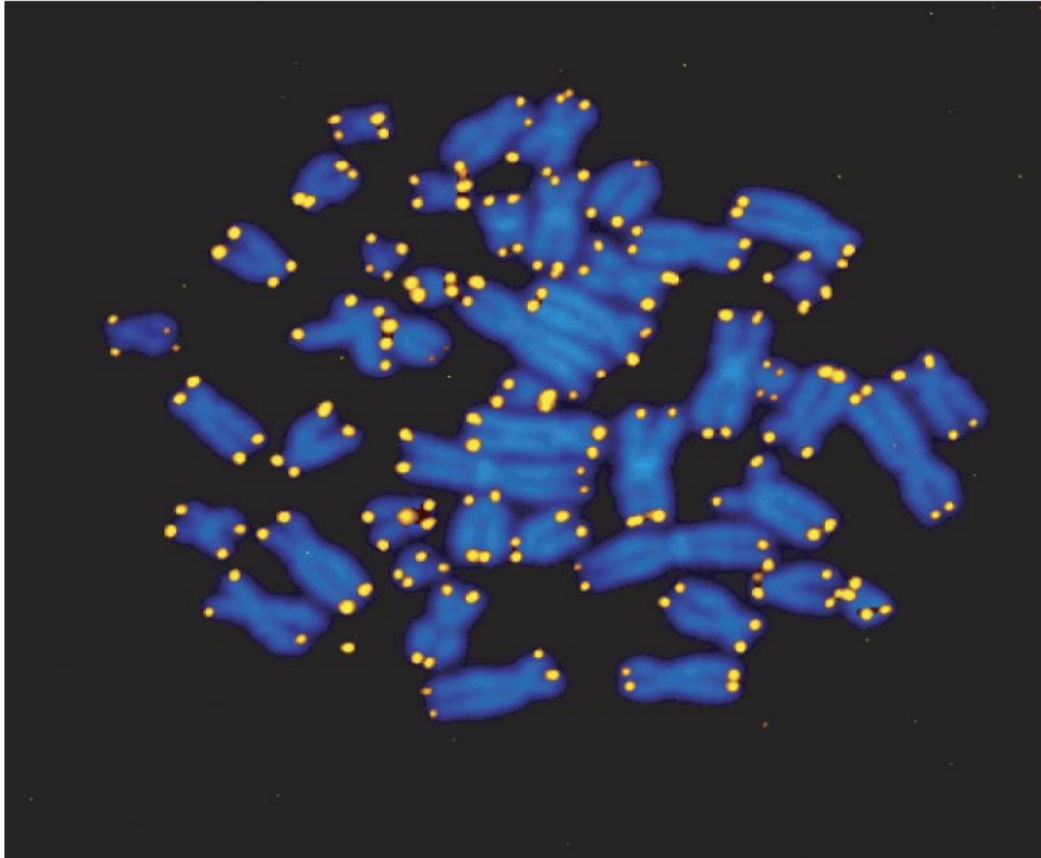


Figure 2.7: *Human lymphocyte chromosomes visualised by means of FISH procedure. In blue is possible to see DNA of chromosomes while in yellow telomers. Reprinted with permission from [Bentham Science Publishers](Aubert and Lansdorp, 2008).*

2.3.5 Histological Analysis

Microscopic analysis of bone matrix has been largely applied to evaluate age in human populations. The process involves the quantitative evaluation of a number of histomorphometric features of the bone cortical area. The process quantifies secondary remodelling

that determines the accumulation of secondary osteons on cortical bone. In fact, osteon density (OPD) has been seen to increase consistently with age, although it presents a high regional variability (Mcfarlin et al., 2008). Accuracy of histological age assessment is also affected by population specific variation: a large number of studies have been developed for different populations and this has to be taken into consideration when methodological selection is made (Cho et al., 2002).

An early study by Kerley (1965) quantified the number of intact osteons, osteon fragments, non-Haversian canals and the percentage of lamellar bone in four areas of the femur, tibia and fibula cortical bone analysed at 100x magnification. Results of the four areas were then averaged and regression analysis was applied to create age predicting relationships. The best prediction was for fibular fragments and presented 97.4% of accuracy with ± 5.27 years of mean deviation from the chronological age of the donors. This research highlighted the high degree of accuracy of the estimation for older individuals due to the larger discrepancy between biological and chronological age for this age range (Kerley, 1965). This is due to the fact that between 50 and 60 years of age, the bone is completely remodelled and new osteons replace the preexisting osteons. The consequence is that the remodelled bone portion does not increase the number of osteons, decreasing the accuracy of the estimation: after the age of 60 years, therefore, it would not be possible to appreciate any age variation (Frost, 1987b,a). This is called the packing effect (Figure 2.8). It has been suggested that the femur, due to its larger cortical, should provide enough space to avoid osteons overlapping (Stout and Paine, 1992). This represents the physiological explanation of the inaccuracy for any individual over 50 years of age.

Later studies such as Kerley and Ubelaker (1978) review this technique and found inconsistencies in the calculation of field view by Kerley (1965). The author found a general underestimation of the entire sample due to the fact that they assumed a 1.25 mm field of view in the study while the microscope set up may have been greater (Kerley and Ubelaker, 1978). The final diameter used in the study was found to be 1.62 mm and, therefore, all the variables, except from lamellar bone, have to be adjusted to 2.06 mm² field of view in order to obtain the correct surface density (Kerley and Ubelaker, 1978).

After correction, the new regression formulas showed a higher degree of accuracy with a lower mean standard deviation. Furthermore, this exercise proved how the methodological procedure influences the estimation and more studies have been carried out to evaluate the extent of this problem.

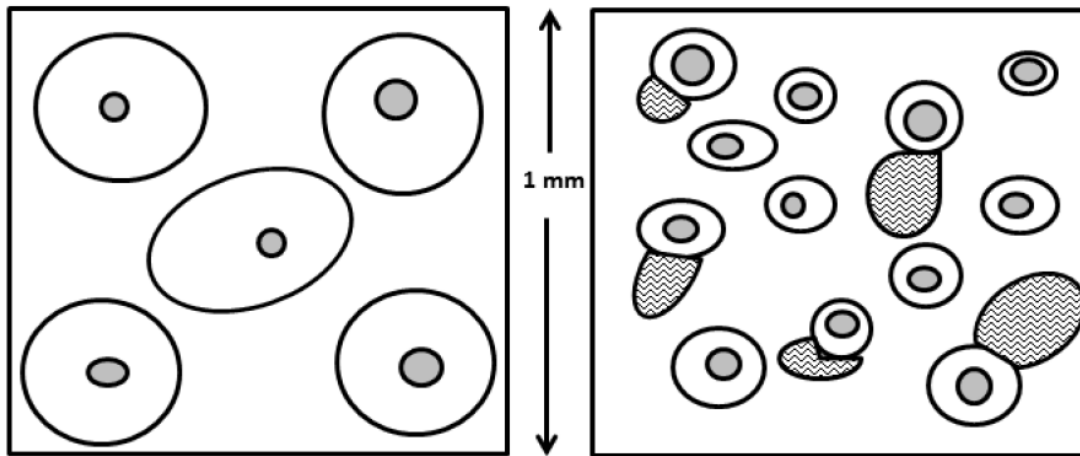


Figure 2.8: *Packing effect: relation between osteon area and number of osteons that can accumulate on a given cortical area. Grey shapes represent fragmentary osteons (Gómez García-Donas, 2018).*

In order to reduce invasiveness of the technique, Thompson (1979) developed an innovative method for age assessment based on histology consisting in drilling bone cores of 0.4 mm of diameter at different areas of femur, tibia and fibula. With this technique, destruction of the entire bone was avoided. A large number of variables were tested and new microscopy techniques to optimise the efficiency of methodology were presented. Furthermore, a complete and clear analysis of sex and side influence on the estimation was proposed. This procedure attempted to investigate different problems related to the characterisation of various histological features, the preparation technique of the slides, sampling of the area observed when counting each feature and type of microscopy that better suits the aim (Thompson, 1979).

As the majority of age estimation methods, the histological approach is heavily affected by inter-population variation. To this point, the research is scarce and the influence of different populations is not quantified. However, the study of Cho et al. (2002) showed

the differences between African-American and European-American population. It was proved that there are significant differences in OPD, osteon area and relative cortical area. Furthermore, the rate at which osteons accumulate in males and females is different after bone reaches maturity and this must be taken into consideration when developing a new methodology. Considering all these factors the aforementioned authors developed new regression formula for remains of unknown ethnicity that showed a lower accuracy and a higher mean standard deviation as predictable (Cho et al., 2002). Finally, pathological conditions can severely affect the age estimation due to alterations to the normal bone turnover and for this reason the selection of reference samples for all these methods always includes healthy individuals as control samples. Although it is a destructive method and its accuracy decrease sensibly for individual over 50 years of age they can be used as a valuable tool for the establishment of a correct biological profile, a necessary step in the process of identification.

2.4 Concluding Remarks

This chapter has introduced the most common approaches in forensic anthropology for age estimation. The advantages offered by macroscopic estimation of age rely on the fact that they do not require any particular equipment to be carried out but they heavily rely on observer experience, which affects replicability. Furthermore, it has been shown that they lose accuracy when applied to individuals with advanced age. The need to meet necessary requirements for a method to be accepted in court during trial have stimulated the development of laboratory based, highly repeatable and accurate methods. These are taken from different discipline and adapted to the field of anthropology to address the complex task of age estimation. The large number of methods presented in this chapter aims to provide the reader with a comprehensive view of the trends in the field and to show advantages and disadvantages that will be used to evaluate the effectiveness of the method that will be developed and presented in this thesis.

CHAPTER 3

BONE BIOLOGY

Bone is three-phase composite material comprising mineral, water and collagen. The physics and chemistry of bone and its composition are optimised so as to resist fracture and maintain the optimal balance between stiffness (resistance to deformation), strength (maximum stress to failure) and toughness (ability to absorb energy) (Boskey and Coleman, 2010). A comprehensive understanding of bone biology helps both a better choice of methods to be applied and drawing inferences from the final results. The understanding requires a multidisciplinary approach spanning across medical and dental sciences, branches of engineering and physical anthropology. These allow to better understand the spatial arrangement at different scales that work jointly in order to fulfil specific mechanical, biological and chemical functions (Rho et al., 1998; Burr and Akkus, 2013). Structural relationship between the different components can be seen in Figure 3.1 and confers the tissue its heterogeneous and anisotropic nature (Rho et al., 1998). Bone structure is generally divided into the following categories:

- macrostructure: trabecular and cortical bone;
- microstructure (10-500 μm): Haversian systems, osteons, single trabeculae;
- sub-microstructure (1–10 μm): lamellae;
- nanostructure (from a few hundred nm to 1 μm): fibrillar collagen and embedded mineral
- sub-nanostructure (< 200 nm): molecular structure of constituent elements.

In terms of function, mechanical support remains the most studied and well understood aspect (Rho et al., 1998). Cortical bone supports most of the load due to the higher bone mass while trabecular bone redirects the stress to compact bone. Bone also provides

protection to internal organs and serves as support for muscle attachment that allows body movement (Rho et al., 1998; Burr and Akkus, 2013). The trabecular area, also called the marrow cavity, is the site where bone marrow is embedded. Red marrow is responsible for the production of red blood cells and is preponderant in young individuals. With age it is replaced by yellow marrow that originates from osteoblasts precursors and regulates the production of triglycerides as well as being stored in marrow adipose tissue (Rho et al., 1998; Burr and Akkus, 2013). Another key aspect of cancellous bone is the rapid turnover that reacts to hormonal and mechanical induced stimuli and this allows the rapid exchange of calcium, phosphate and carbonate ions that regulates enzymatic reactions, blood clotting and muscle contraction. This mineral storage and ion-releasing process involve both cortical and trabecular bone at a very slow rate quantifiable in days to weeks and corresponding to bone remodelling, that replace old bone with new one. Bone also plays a role in the production of fibroblast growth factor 23 (FGF-23) and osteocalcin, hormones essential for the functioning of bone marrow, brain, kidneys and intestine (Rho et al., 1998; Burr and Akkus, 2013).

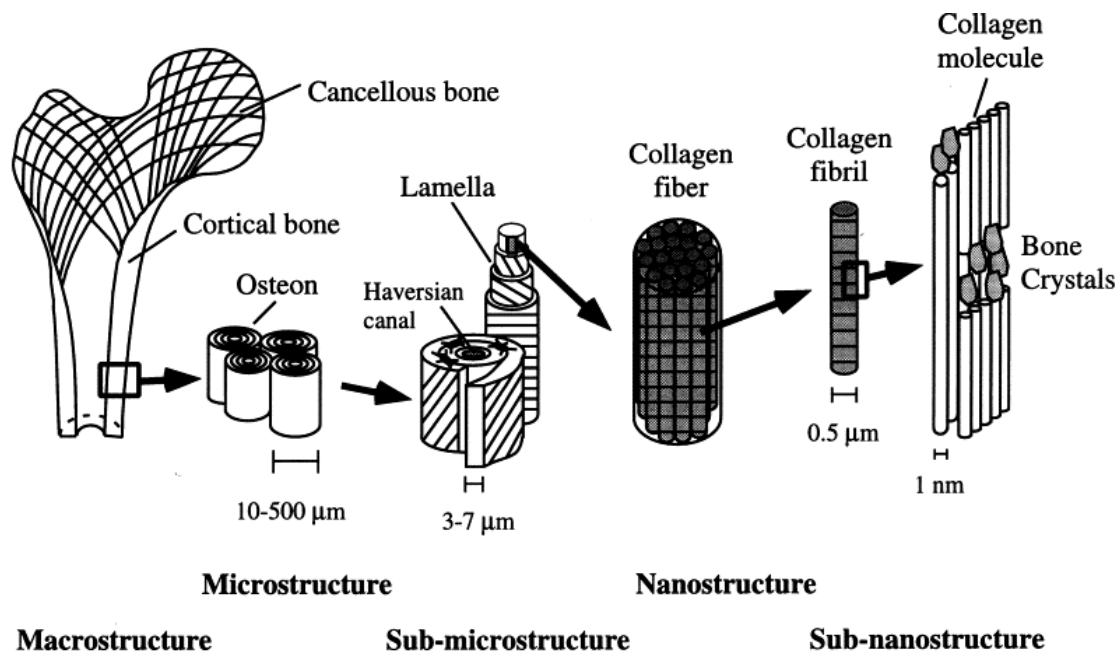


Figure 3.1: Hierarchical structural organisation of bone. Reprinted with permission from [Elsevier] (Rho et al., 1998).

3.1 Bone composition and nano-structure

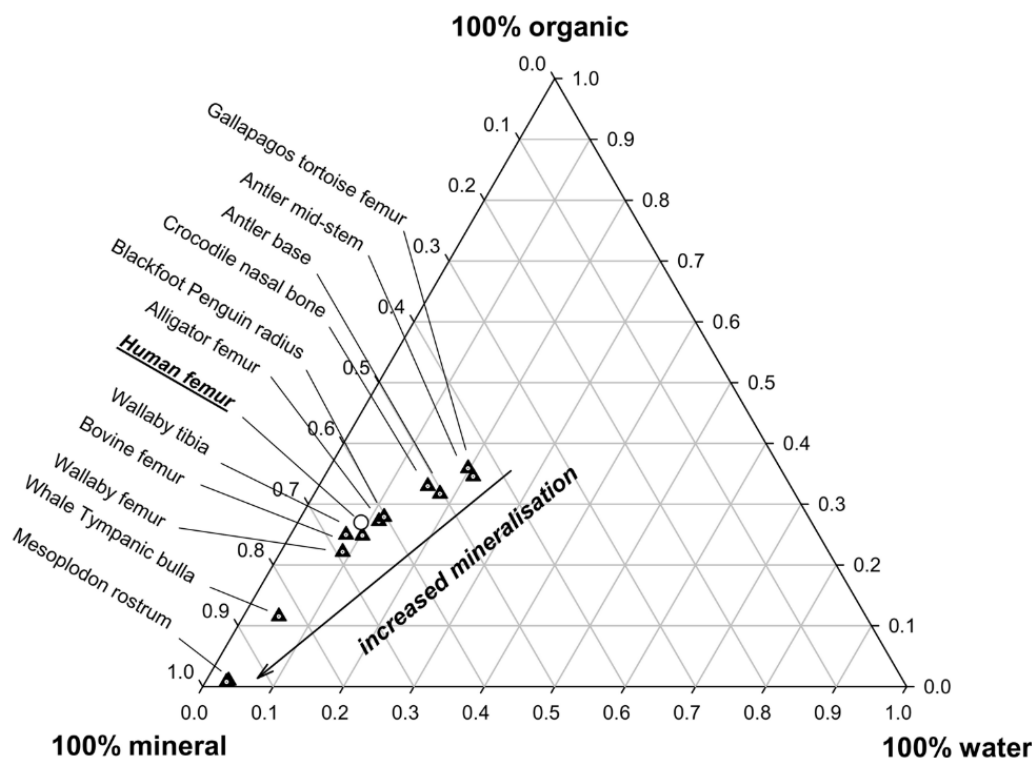


Figure 3.2: Diagram showing the combined variation of bone constituents and the distribution in different animal species and human femur. The arrow shows the increase in mineralisation and, consequently, the decrease in the remaining components. Reprinted with permission from [Elsevier] (Zioupos, 2005).

Considering the different components present in bone, carbonated apatite accounts for approximately 65% of bone mass and the organic collagenous and non-collagenous matrix for 20-25% of the total dry weight (Burr and Akkus, 2013). Of this organic portion almost 90% is type I collagen, with traces of type III and V, while the remaining 10% accounts for non-collagenous proteins (NCPs), responsible for formation of the collagen fibrils, mineralisation, and cell regulation (Burr and Akkus, 2013). The remaining approximately 10% of the total weight is water, which, in part, binds the organic and mineral compound. Some of this water is also unbound and its amount keeps the mineral content stable, controlling mineralisation of the tissue. Variation in the ratio of these different compounds determine

the changes in the mechanical properties of bone as shown in Figure 3.2 (Zioupos, 2005). An increase of mineral content, and consequent decrease in organic and water content, results in a stiffer structure that, due to the more brittle nature, which is more prone to fracture (Clarke, 2008).

3.1.1 Mineral Matrix

Calcium hydroxyapatite is present in bone, teeth and calculi as an impure and poorly crystalline form of carbonated apatite that consists of phosphate PO_4^{3-} , calcium Ca^{2+} and hydroxyl OH^{1-} ions. It has the general unit formula $\text{Ca}_5(\text{PO}_4)_3(\text{OH})$ presenting a Ca/P ratio of approximately 1.66 with a small quantity of water and CO_3^{2-} . Calcium apatite is also represented normally in nature as $\text{Ca}_5^{2+}(\text{PO}_4^{3-})_3(\text{OH}^{1-})_2$, but this indicates only the most common references as apatite's biological composition is highly inconsistent (Olszta et al., 2007). Crystal size is highly variable but can be between 30-50 nm in length, 15-39 nm in width and 2-10 nm in thickness. The variability can be due to sample preparation and type of bone (Figure 3.3) (Olszta et al., 2007).

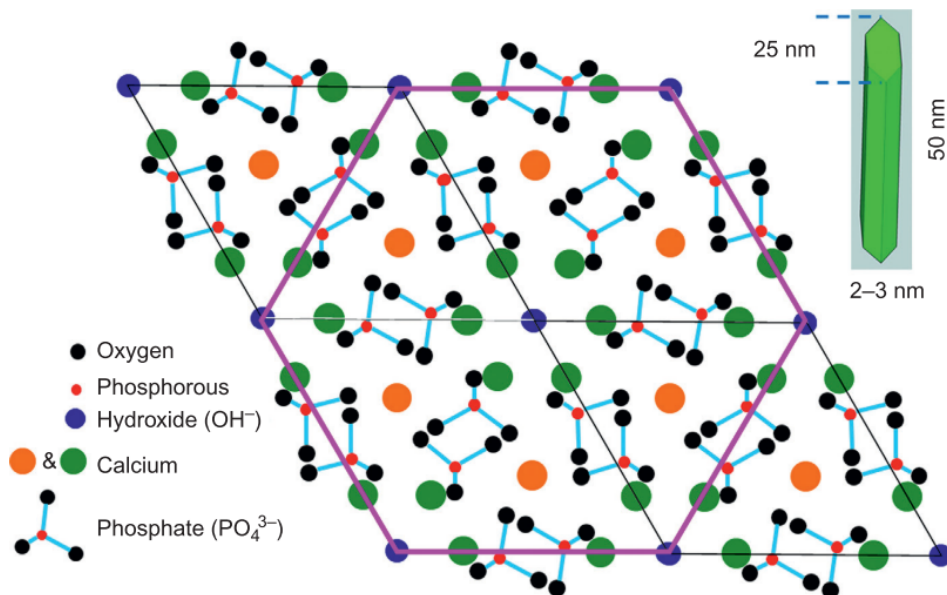


Figure 3.3: Representation of HAP mineral lattice structure (Beckett, 2009)

With age, the crystals increase in size and become more crystalline following a process of ion substitution and mineral stoichiometry. This increase in crystallinity reflects crystal size and strain ratio and the degree of order of the ions' distribution in the unit cells (Farlay et al., 2010). PO_4^{3-} ions dominate the crystal lattice such that they occupy tetrahedral sites and each ion is in 4-fold coordination with the OH^{1-} ions. This structure reveals octahedral interstices of different sizes that run vertically to each other. The larger ones can accommodate the Ca^{2+} ions (Gross and Berndt, 2002; Rey et al., 2007, 2009; Greenwood et al., 2012). Due to the large area/volume ratio and the hydrated surface, which contains a number of mineral ions on charged organic compounds that envelopes the apatite crystals, the structure is subject to ion migration (Cazalbou et al., 2005; Rey et al., 2007, 2009). This phenomenon, which fulfils the requirement of neutral charge in the molecules accounts for the number of modifications in the cell structure and crystallinity of the apatite and transform the apatite into a more non-stoichiometric compound (Betts et al., 1981; Cazalbou et al., 2005; Rey et al., 2007, 2009). Further discussion regarding the mechanism of crystal modification with age is present in Section 4.1.

3.1.2 Collagen Matrix

At the molecular level collagen is constituted by three chains of about 1000 amino acids, periodically repeating the $-(\text{Gly} - \text{X} - \text{Y})_n-$ triplet unit, where X represents proline amino acid residues and Y any amino acid residue but primarily hydroxyproline. Of the three chains, two of them are $\alpha 1$ and one $\alpha 2$. In mammalian organisms, type one is the collagen organised in a triple helix structure: this molecule is called tropocollagen. Stability of this configuration is given by the hydrogen covalent bonds created between the hydroxyl groups of Y and H_2O . During the registration process of the three chains, at the end of the molecule, the interaction N-propeptide and C-propeptide in sulphur bonds secures the procollagen structure and prevents the premature formation of collagen fibres within cells (Burr and Akkus, 2013; Stock, 2015; Burr, 2019). These telopeptide regions are then enzymatically removed to ensure the right configuration of collagen and formation of fibres once outside the cell. Five molecules of tropocollagen are assembled into a

semi hexagonal spatial arrangement to form microfibrils. These are usually of 10 μm in length and 150 nm in diameter. A number of studies have shown, with the aid of electron microscopy, that the overlapping of adjacent collagen fibres leaves a gap of 67 nm for the embedding of mineral nanocrystal (Miles and Bailey, 1999; Wang et al., 2001; Burr, 2019; Fratzi P et al., 2004). This model, shown in Figure 3.4, has been proven to vary according to different factors (such as age and pathological conditions) and the sites of the gaps for mineral embedding can change, resulting in a non-homogeneous structure (Olszta et al., 2007).

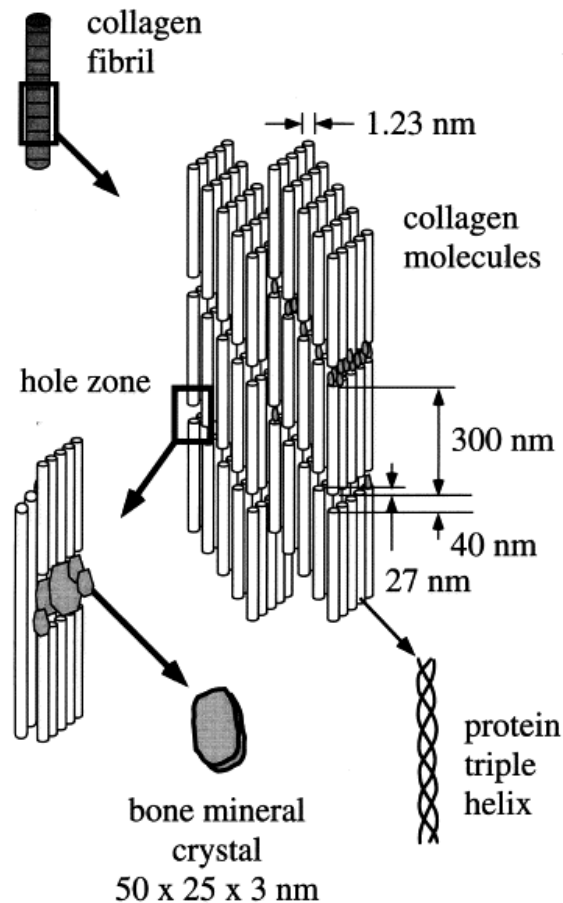


Figure 3.4: Mineral and collagen spatial organisation. Reprinted with permission from [Elsevier] (Rho et al., 1998).

A number of different cross-links are present in collagen fibrils that result in different mechanical properties of bone. These differences are the result of two main processes:

enzymatically mediated and non-enzymatically mediated collagen cross-linking. For the first type, divalent immature cross-links undergo post-translational modification by means of lysyl oxidase, that induces the maturation of the telopeptide area in pyridinoline (PYD) and deoxypyridinoline (DPD) with the two hydroxylysyl groups. As a result, this divalent cross-link becomes trivalent. The process normally takes few weeks after collagen deposition. The overall mature/immature cross-links tends to increase after the age of 15 years. The higher PYD/DPD ratio indicates a more mature and stable collagen. The main effect of the presence of these kinds of bonds is the increase of compressing strength and stiffness (Wang et al., 2001; Paschalis et al., 2003; Stock, 2015). Overall, enzymatic cross-links play a advantageous role in bone toughness (Burr, 2019).

In contrast, cross-links can be produced by non-enzymatic glycation, involving the condensation of arginine, lysine and free sugars. This process produces intra-molecular bonds called advanced glycation end-products (AGEs) (Burr, 2019). Pentosidine is the smallest component of these AGEs and it is normally used for accurate quantification of this phenomenon by means of gas chromatography, although the same method gives good indication of PYD and DPD (Viguet-Carrin et al., 2009). The amount of AGE increases significantly with advanced age reducing the diameter of collagen fibres, resulting in an increased bone fragility and a reduced thermal stability (Gelse et al., 2003; Saito and Marumo, 2010). The formation of these links is usually associated with sugar and therefore they accumulate individuals with diabetes mellitus (Burr, 2019). As the presence of AGEs can impair osteoblast and osteoclast activity, osteocalcin secretion and cell adhesion it can result in bone mass variations. This, coupled with the fact that AGEs make bone more brittle, increases significantly the risk fracture (Wang et al., 2001, 2002b; Stock, 2015).

3.1.3 Mineralisation

Bone mineralisation consists of the embedding of apatite crystal in the organic matrix, with a respective ratio 75% to 25%. The first attempt to explain bone mineralisation process was made by Posner et al. (1965) but still highly debated. According to their two

stages theory, first the dissolution of a non-crystalline calcium phosphate precursor leads to the formation of colloidal apatite via diffusion in a rapid process that produces crystals of roughly constant size. Later, the crystals consolidate into larger-sized structures (that can involve the fusion of more than one crystal) with a consequent reduction in the crystal number and increase in crystal size and homogenisation of average size (that will be referred in this thesis as crystal size homogeneity). This phenomenon is called secondary mineralisation. This theory revealed to be extremely useful in explaining the main differences between precursor and mature crystallised apatite structural units (Weiner, 2006; Olszta et al., 2007; Grynypas and Omelon, 2007). Other hypotheses include the possibility that a number of proteins can be responsible for the nucleation in the bone mineralisation process, although there is no general agreement on the role of calcium and phosphate binding proteins. Yang et al. (2010) investigated the role of bone sialoproteins (BPS, highly phosphorylated acidic proteins) using molecular dynamic simulation. BPSs have the function of distributing calcium and phosphate ions in solution and the increase in concentration will initiate mineralisation of collagen fibres. Results showed that, independently of the peptide conformation (helical or unstructured), BPSs help nucleation of the amorphous calcium phosphate precursor that will convert to crystalline hydroxyapatite with age. By contrast, a number of studies have proposed that in the formation of apatite, proteins may inhibit nucleation and growth of crystal (Boskey et al., 2002; Shapses et al., 2003). Despite the controversy related to apatite formation process, the structural relation between mineral and collagen in bone is fundamentally accepted. A clear explanation of interfibrillar mineralisation was given by Landis et al. (1996) observing mineralising turkey tendon via TEM and CT imaging. According to their theory apatite crystals impregnate the interstices left between collagen fibrils. With time, crystal growth leads to the formation of poorly mineralised sheets between the fibres (Landis, 1995; Landis et al., 1996; Olszta et al., 2007; Yang et al., 2010).

An alternative model was suggested in order to explain mineralisation of collagen fibres. According to Olszta et al. (2007), mineralised fibres do not originate from the nucleation of crystals in the interstices but a fluid precursor (PILP) of mineral would be soaked

in the collagen fibres and diffused via capillarity, as shown in Figure 3.5. The crystallisation process would eliminate the water and the structure would achieve the thermodynamic stability typical of mature bone.

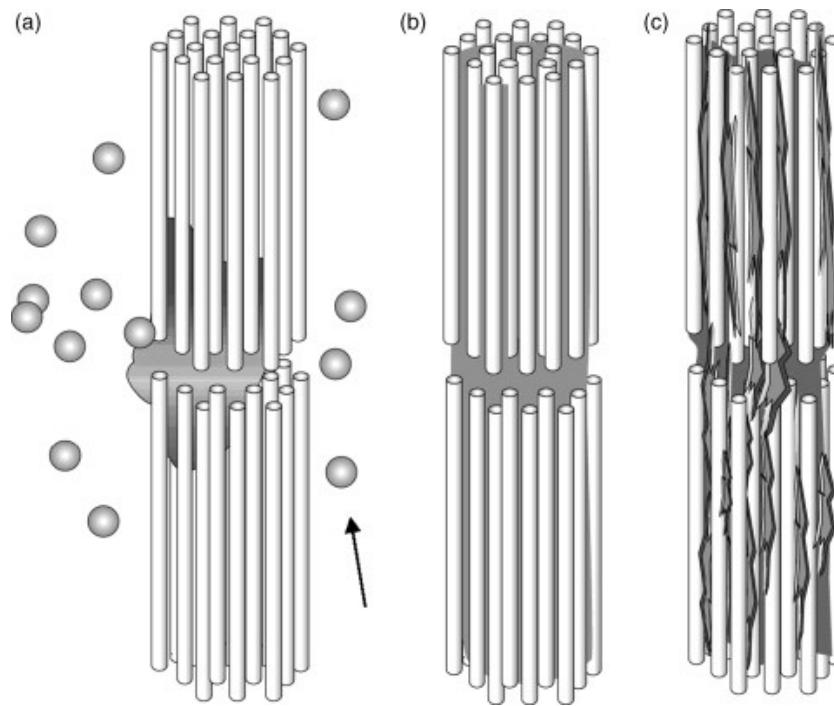


Figure 3.5: Schematic representation of fibrillar mineralisation via fluid precursor: (a) beginning of the adsorption of the liquid-liquid precursor in the collagenous matrix due to critical ion concentration, (b) complete permeation of the fluid in the fibrillar structure and (c) mineralisation of the precursor occurs. Reprinted with permission from [Elsevier] (Olszta et al., 2007).

Despite the strong experimental data supporting the explanation of this process, the mineralisation process is still unclear and widely debated. Most of the models that have been presented agree on the function of collagen fibrils as a template for the mineral deposition with mediation from non-collagenous proteins (NCPs) (Landis, 1995; Landis et al., 1996; Olszta et al., 2007; Silver and Landis, 2011; Wang et al., 2018). Within this model, nucleation normally occurs in the gap zones as previously described or on the collagen fibrils themselves. Intrafibrillar mineralization involves nucleation of crystallites, followed by crystal growth along the long axis of collagen on the preferential $\langle 00\ell \rangle$ (Posner et al.,

1965). The growth occurs first in length and width while the growth in thickness involves the fusion of contiguous crystal (Posner et al., 1965; Landis, 1995; Landis et al., 1996). Another similar theory states that in the extracellular matrix, NCPs control nucleation and growth of the crystals (Boskey, 2003; Chen et al., 2015). This mechanism is still not definitive and there is evidence that collagen could initiate mineralisation without the mediation of proteins. Wang et al. (2012) compared biological apatite from sheep bone and an *in vitro* model based on continuous injection of carbonated apatite in the collagenous matrix, showing that, although NCPs may play a central role, collagen is able not only to offer a structural template but also control the process of mineralisation and crystal growth due to the superficial charge. Despite this model suggesting that collagen initiate mineralisation without the action of NCPs support from other studies (Nassif et al., 2010; Nudelman et al., 2010, 2013), the debate around the molecular mechanism that drives mineralisation of biogenic apatite is still open (Boskey, 1998, 2003). Several studies have shown that biomimetic HAp can be synthesised in the absence of both collagen and NCPs (Wei et al., 2003; Penel et al., 1998), showing that both collagen and NCPs may play only a marginal role in the mineralisation.

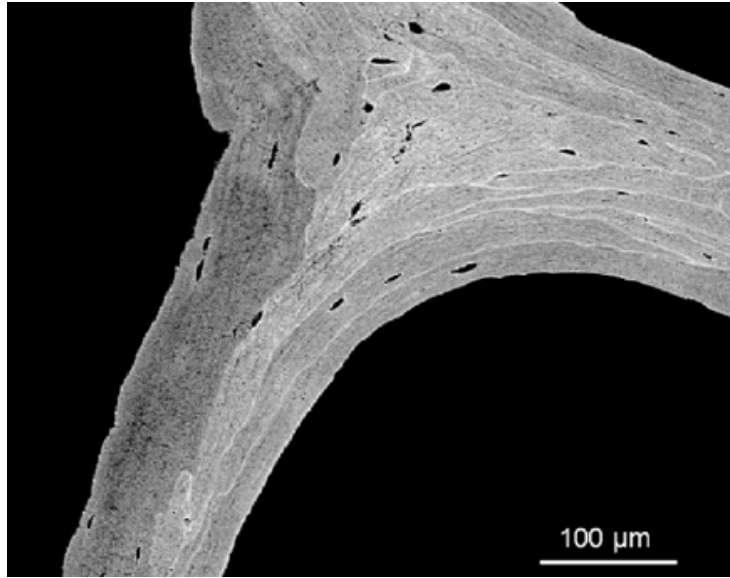
3.2 Non-collagenous Proteins (NCPs)

NCPs comprise 2% of bone weight. They play central roles in bone formation and maintenance: mineral nucleation and growth, formation of collagen fibres and cellular signalling and regulation (Burr and Akkus, 2013). Although essential for bone metabolism, they are not the central topic of this thesis and Table 3.1 aims to report the main groups of proteins and their primary functions (Bellido and Hill Gallant, 2013; Bellido et al., 2014).

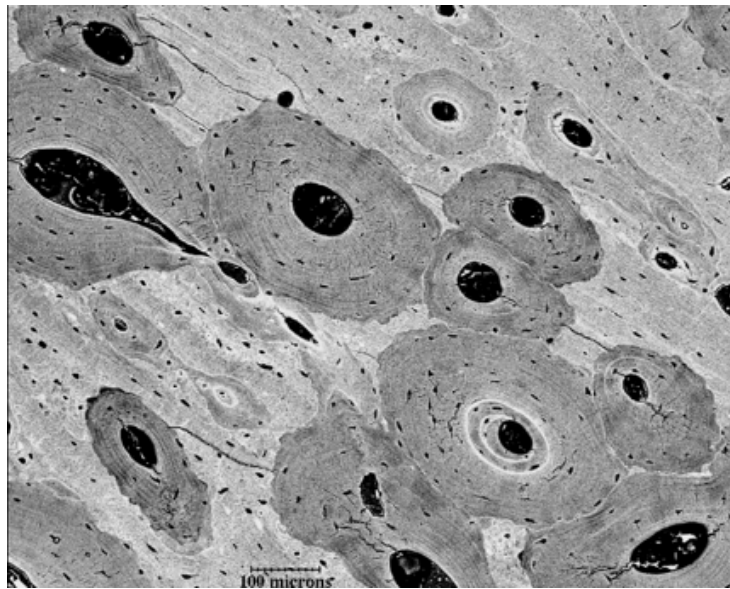
Table 3.1: *Non-collagenous proteins in bone and related functions in bone metabolism.*

Proteoglycans and Glycosaminoglycans	
Heparan sulfate	Control cell to cell interaction
Hyaluronan	Active during bone development
Small leucine-rich proteoglycans	Structural organization of bone
Versican	Localisation of sites for mineralisation
Glycoproteins	
Alkaline phosphatase	Inhibitor of mineral deposition
Fibronectin	Involved in bone cells proliferation
Thrombospondin	Regulates bone development and have anti-angiogenic function
Vitronectin	Responsible for cells attachments and proliferation
SIBLING Proteins	
Bone sialoprotein	Regulates mineralisation
Dentin, matrix acidic phosphoprotein 1	Regulates mineralisation
Matrix extracellular phosphoglycoprotein	Regulates mineralization and inhibits osteoclast activity
Osteopontin	Controls chrystal growth by inhibition
Others	
Osteocalcin	Controls mineral deposition, bone remodelling marker
Osteonectin	Binds collagen - HAp and interact with osteoblast proliferation

3.3 Sub-micro and Microstructure



(a) *Trabecular bone*



(b) *Cortical Bone*

Figure 3.6: SEM images of trabecular (a) and cortical (b) bone. Cortical bone shows the circular osteons, formed by concentric lamellae around the vascular canals, and interstitial non-remodelled bone. Darker grey areas represent lesser mineralised bone in both images. For cortical bone (b), these are the newly remodelled osteons (given by Prof Peter Zioupos).

At a sub-microscopic level, bone shows different spatial organisation for which collagen is mainly responsible and this results in different types of bone and related functions. Highly oriented mineralised collagen sheets of 3-7 μm of thickness are the basic structural unit and they are called lamellae. This oriented structure shows an increase in stiffness of between 20-50% compared to the inter-lamellar space. Cancellous bone is formed by concentric lamellae forming rod-like structure of 150-300 μm in diameter called trabecula, that creates an internal framework that helps in dissipating stress and hosts bone marrow (Olszta et al., 2007). The interconnection could assume one of the following configurations: rod-rod, rod-plate or plate-plate (Rho et al., 1998). At the microscopic level, apart from the distinction between cortical and trabecular bone (Figure 3.6), it is possible to identify other types of bone according primarily with collagen spatial orientation (Currey, 2003b).

3.3.1 Primary bone

Morphologically, it is possible to identify three types of primary bone that are structured to fulfil specific and different functions. The common characteristic is that they are all laid down *ex novo* on pre-existent substrate. Figure 3.7 shows different types of bone and the main features of it from photomicrographs of human rib cross-section.

1. **Woven bone** displays randomly oriented collagen fibres. It is normally deposited *ex novo* and, although the tissue is highly mineralised, the mineralisation pattern is not regular (Burr and Akkus, 2013). However, the presence of this type of bone is also characteristic of the callus formed during fracture healing in order to give immediate stability to the bone. It is also typical of certain pathological conditions such as osteosarcoma (Martin and Burr, 1989). For this reason it is produced quickly (4 $\mu\text{m}/\text{day}$) due to the large cell/bone ratio and it is characteristic of foetal growth. Following the normal ageing process, it disappears by the age of four. It can be found in area where there is unusual stress applied and fast material deposition is required to increase the mass of the structure. It provides a template for lamellar

bone to be deposited and provides temporary strength due to the high degree of mineralisation (Martin and Burr, 1989).

2. **Plexiform bone** is as rapidly deposited as woven bone but has a higher degree of strength. It is characteristic of rapidly growing animals and is deposited on a persistent surface as lamellar bone, with highly oriented trabeculae that in the endosteal and periosteal surface became cortical bone by apposition. It is often found in certain pathological conditions (e.g. fibrohistiocytic tumor) in order to face not only the needs of better mechanical support but also to enhance the haematopoietic and homeostatic process (Martin and Burr, 1989).
3. **Primary lamellar** bone collagen fibres are highly oriented and organised in sheets (lamellae) of fibrils (2-3 μm in diameter) that lie within the same plane. Deposition occurs at a much slower rate compared to woven bone ($<1 \mu\text{m}/\text{day}$) and the degree of mineralisation is lower. Osteocyte lacunae identifiable on the cross-sectional surface of bone due to the characteristic ogive shape with the short axis always oriented in the direction of the thickness of the lamella (Currey, 2003a). It was observed by Martin and Burr (1989) that lamellae thickness varies between 3-7 μm and in the bone structure, it is possible to identify, using SEM, the alternation between a thick and a thin structures. Two main models were developed in order to explain patterns between consecutive lamellae. The first suggests that the concentric layers have the same parallel orientation of collagen fibres while the angle that is formed with the vascular canals changes. The second only explains the alternation of a dense and a loose fibril (Pazzaglia et al., 2013). These two situations are equally possible as it has been shown by Pazzaglia et al. (2012) that thickness of the walls, shape and size of the vascular canal and number of the lamellae is strongly correlated to osteocyte lacunae density that controls thickness of the thick lamellae ($\sim 5 \mu\text{m}$) and the crystals are oriented in only one direction, along the major axis of the bone. In contrast, thin lamellae are 1 μm in thickness and show crystals oriented towards the circumferential plane of the bone (Martin and Burr, 1989; Weiner et al., 1999).

Further analysis of two contiguous lamellae have shown discontinuity of the angles in the crystals arrangement (Martin and Burr, 1989; Weiner et al., 1999). Although this model represents the general structure of the bone, many different arrangements and orientations of both crystals and collagen fibrils are present in order to adapt to different mechanical stimuli in terms of intension and direction of the stress applied (Martin and Burr, 1989; Weiner et al., 1999). Furthermore, primary osteons in cortical bone are systems composed of three to eight concentric lamellae arranged around a vascular canal. This structure is also called the Haversian system and runs longitudinally on the direction of the main axis of the bone. These structures are the results of remodelling processes, which replace damaged bone or increase the mass of certain areas that are affected by unusual strain. Primary osteons are around 50 to 100 μm in diameter and the presence of these structures is related to fast growth (Martin and Burr, 1989).

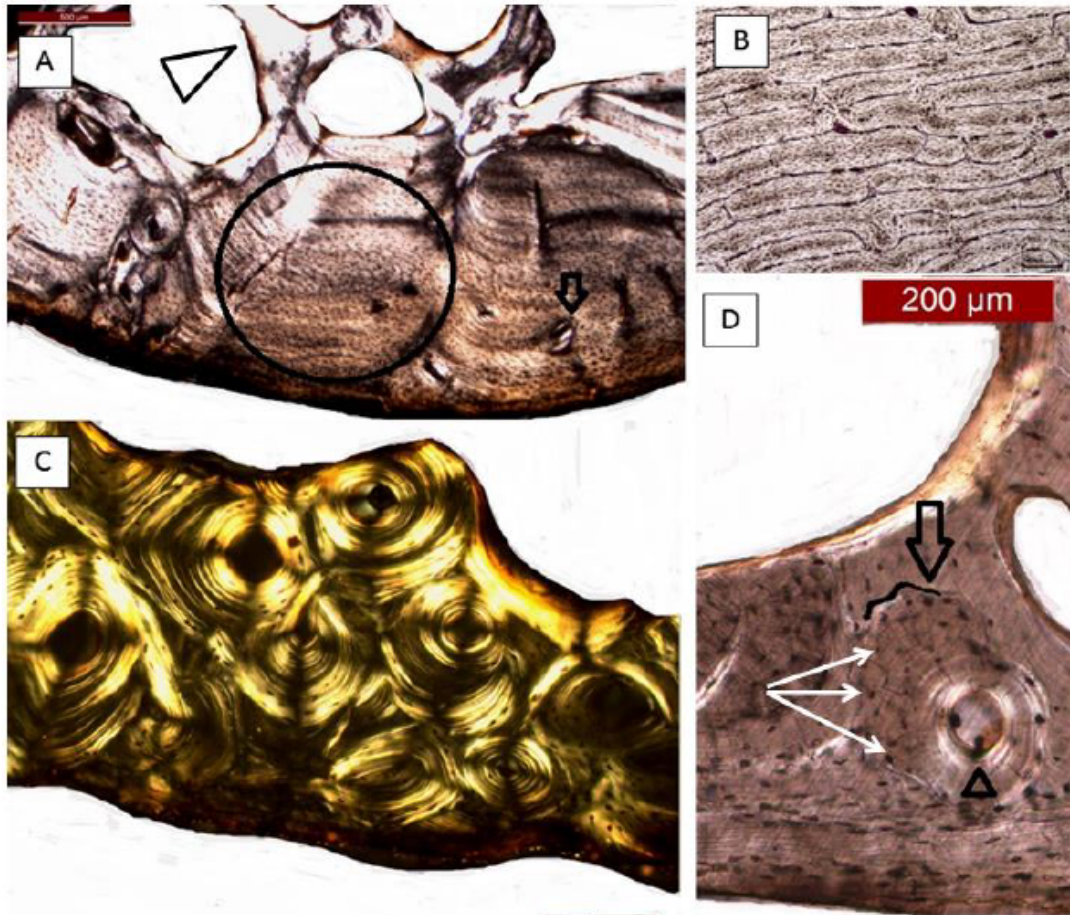


Figure 3.7: *Types of primary and secondary bone in human rib cross-section photomicrographs. (A) the black circle shows primary lamellar bone formed by parallel laminar sheets and the arrow points at trabecular bone (40x). (B) plexiform bone form by the typical brick-like structure. (C) cortical bone formed by interstitial bone and osteons under semi-polarised (100x). (D) osteon showing the central vascular canal (black small arrow), cement line (arrow and black outline), osteocytes (white arrows) at 100x magnification (Gómez García-Donas, 2018).*

3.3.2 Secondary Bone

Secondary bone results from the resorption-deposition process (e.g. remodelling). It is the only mechanism for repairing damaged bone and maintain mechanical integrity, preventing from the risk of fracture. Secondary osteons form through this process and they can be distinguished from primary ones by the increase in diameter (100-250 μm) that accounts for approximately 20 or 25 lamellae and the presence of highly mineralised con-

tours known as cement lines that physically divide this structure from the rest of interstitial lamellae. They normally run around an irregularly shaped vascular canal. These Haversian systems are connected to each other transversely by Volkmann canals, that connect Haversian systems in a vascular plexus (Burr and Akkus, 2013). All around these structures are interstitial bone, formed by incomplete parallel lamellae without any direction pattern. This structure are characterised by lower mineral content because the hypermineralised areas are replaced via remodelling (Martin and Burr, 1989). Another aspect that differentiate primary from secondary osteons is the presence of hyper-mineralised cement lines that enclose the structure (Martin and Burr, 1989).

3.4 Macrostructure: Cortical vs. Cancellous bone

When looking at the macroscopic cross-section of the bone, it appears obvious that the structure is composed of an outer dense shell, called cortical bone, and a porous core known as trabecular bone. While the chemical composition of both components is similar, the architectural organisation of the mineral and organic matrix is substantially different (Martin and Burr, 1989; Currey, 2003a; Burr and Akkus, 2013). Cortical bone is a dense structure with only $\sim 5\%$ porosity, accounting osteocyte lacunae, canaliculi and Haversian canals for blood vessels. Porosity value increases with age with the formation of erosion cavities, in a process characteristic of the physiological ageing and accentuated in certain pathological conditions (e.g. osteoporosis) (Martin and Burr, 1989; Currey, 2003b; Burr and Akkus, 2013).

In contrast, trabecular bone is composed by plates and rods ($\sim 200 \mu\text{m}$ in thickness) of bone and is extremely porous ($>50\%$), although variations are present according with mechanical usage and location of the measurement (e.g. denser in weight bearing bones, Figure 3.8). It is formed at a very fast rate and only occasionally are present osteon-like structures called hemiosteons. This hemiosteons are characterised by lower diameter and elongated shape. This structure provides essential mechanical support without increasing the weight of the whole structure and accommodates the bone marrow (Martin and Burr, 1989; Burr and Akkus, 2013). In terms of mechanical performance, trabecular bone de-

rives its properties from the architectural organisation. The first function is to displace the stress on the compact and more rigid cortical bone. For this reason the more connected the structure the better the bone will support stress. Trabecular bone architecture is normally evaluated according to trabecular number (Tb.N), thickness (Tb.Th) and separation (Tb.Sp). With age and certain pathological conditions (e.g. osteoporosis) there is a decrease in trabecular volume, resulting in a weaker structure. Coupled with the decrement in connectivity (Tb.Conn) and volume (BV/TV) there is also a decrease in strength and stiffness not only of the trabecular component but for the entire bone (Burr and Akkus, 2013).

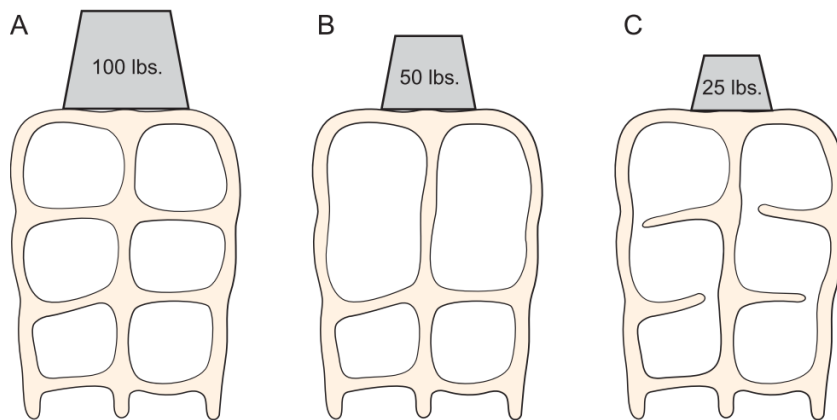


Figure 3.8: *Influence of architecture and mass in mechanical properties of bone. Well connected bone with high Tb.N, BV/TV and low Tb.Sp is capable of support more stress. Vice versa, bone that is normally subject to stress maintains better structural properties. Reprinted with permission from [Elsevier] (Burr and Akkus, 2013).*

3.5 Brief Description of Rib Anatomy and Breathing Mechanics

Despite the functions previously described, ribs are also involved in lungs ventilation that allows gas exchanges in order to maintain the optimal O₂ saturation level in the blood. Understanding how the rib cage is involved in this process is also useful in order to comprehend the stress that the bones in the rib cage undergo throughout life.

The rib cage is organised in 12 pairs of ribs, 12 vertebrae (thoracic) and the sternum. A normal rib is composed by the head characterised by demi-facets that provides articulation

with the vertebral body at the level of the costovertebral joint. The joint is encapsulated and stabilised by the interosseus ligament and radiate ligament that reduce the mobility of 2nd to 9th ribs. The remaining ribs only have one proximal articular facet. The interosseus ligament is also absent in the remaining ribs to allow more movement. Moving towards the opposite end (sternum), there is the neck. The tubercle, a small round articular surface, is located at the end of the neck and allows the articulation of the rib with the vertebral transverse process at the costotransverse joint. This articulation is present from the 1st to the 10th rib. From this point, the rib curves in the area known as angle, that connects the neck with the shaft. The shaft is the flat elongated portion of the rib and has an anterior inferior curvature. Distally, the 1st to 7th ribs articulates directly with the sternum via cartilage at the sternocostal joint. The 8th to 10th ribs articulate between the sternum and the seventh costal cartilage via costochondral joint. The last two ribs do not articulate with the sternum and are noticeably shorter than the others. This structure facilitates the rib cage in protecting the vital organs while also maintaining the necessary degree of movement during breathing (Standring, 2008).

In terms of muscles, the diaphragm accomplishes 70-80% of the dilation and contraction of the rib cage during breathing. The costal portion attaches to the posterior aspect of the xiphoid process and on the posterior inferior of 6th ribs. Additionally, intercostal muscles participate in the ventilation from 1st to 11th ribs. The muscles are divided between internal posterior, when they run between the caudal border of the superior rib the cranial border of the inferior one, compared to the external intercostal muscles. The innermost intercostal muscles insert on the area above the costal groove and attaches on the internal aspect of the shaft. The last group of muscles primarily involved in the ventilation process is the scalenes. Attached on the transverse processes of thoracic vertebra 3 to 7, they descend to the superior aspect of ribs from 1st to 7th, generating more force when the diaphragm is in the inspiration phase (Standring, 2008).

At inspiration, the diaphragm contracts and counteracts the opposing motion *viscera* downwards. The 1st to 10th ribs subsequently elevate and rotate. Transverse dimensions increases due to the movement of 7th to 10th ribs. Upper ribs (2nd to 6th) move in the

anterior direction, which results in an increase in the cage volume. Finally, the lower ribs from 8th to 12th rotate at the costovertebral joint medially. This increases the lateral volume. Intercostal muscles, which are responsible for the elevation of the ribs, assist in this process (Levangie and Norkin, 2005).

The expiration, in contrast, is a passive process that returns the rib cage to its rest position. Pressure level in the pleural surface also returns at rest level. The resting breathing frequency is around 16-20 acts per minute in an average healthy adult individual. With physical activity, frequency can rise by 80% with pressure and volume variation showing clear increases (Bechbache and Duffin, 1977).

It is clear that ribs undergo cyclic loading with a certain degree of stability throughout life. Furthermore, due to the different movement that different ribs have, ageing pattern might vary along the rib cage.

3.6 Bone Cells

Modelling accounts primarily for bone growth, reduction of trabecular porosity in bone metaphyseal growth and achievement of final bone shape and mechanical resistance. It involves the processes of formation and resorption originated from endosteal and periosteal membranes. In contrast, remodelling is the process aimed to maintain structural and functional integrity of the fully matured bone, replacing old bone with new bone by the activation of the bone multicellular unit (BMU). In this section an overview of the cells involved in these processes will be given.

3.6.1 Osteoclast

Osteoclasts are multi-nucleated cells which are the result of the fusion of mono-nuclear precursors of the monocyte/macrophage lineage. The process of osteoclastogenesis transforms monocyte-macrophage precursors stem cells in multi-nucleated giant osteoclast via osteoclast differentiation factor with the main function of bone resorption. The two cytokines involved in formation are RANKL and M-CSF. Osteoclasts exist in both motile and resorptive phases presenting a distinct functional morphology: in the first phase they

migrate towards the resorption sites and in the second phase they perform bone resorption. They are usually located within the osteons and/or beneath the periosteum with a density of $\sim 3/\mu\text{m}^3$ (Kular et al., 2012; Väänänen et al., 2000; Clarke, 2008).

When cells enter the resorptive phase become polarised and a number of cytoskeletal modifications occur and these favour attachment to the bone surface to break down and the release of chemicals that actuate resorption (Figure 3.9). The sealing zones is the area where the osteoclasts is attached to bone matrix by means of podosomes, which show a core of densely packed filaments of F-actin associated with proteins that helps adhesion of the osteoclasts on the bone matrix. The area between these two attachment point is the ruffled border, where the secretion of protons and proteases initiate the matrix demineralisation. The degradation products are transported by endocytosis in the third area, the functional secretory domain, located on the apical end of the cell.

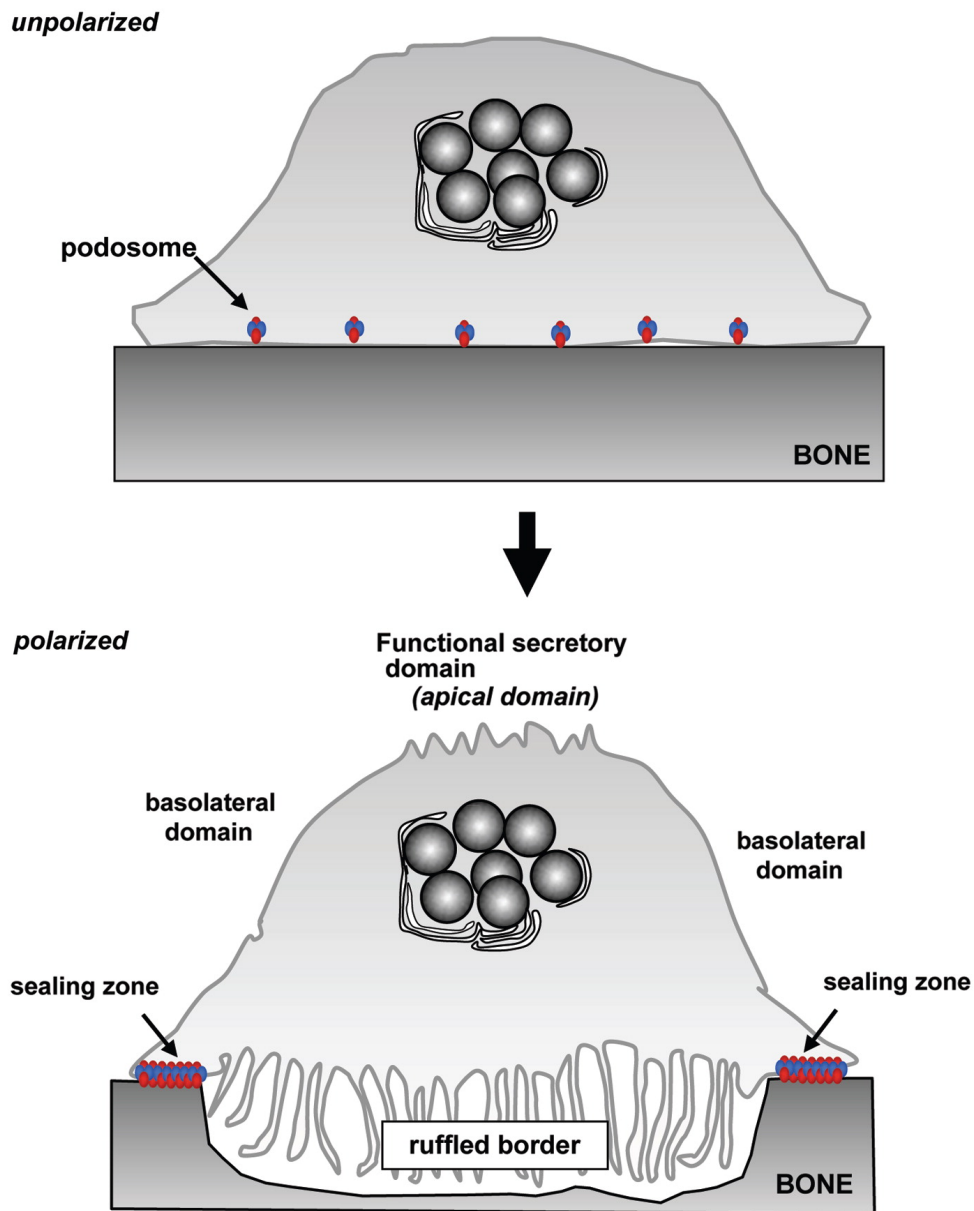


Figure 3.9: Differentiation between osteoclasts in motile and resorptive phase. After polarisation it is possible to see the four domain involved in demineralisation of the bone matrix. Reprinted with permission from [Landes Bioscience] (Itzstein et al., 2011).

The resorption cycle involves a number of stages that will be soon discussed. It starts with the transition of the cells on the resorption sites and the tight attachment with the bone matrix. The precise process it is still in process of elucidation but it is accepted that

integrin plays a central role in the bonding process. Furthermore, it might involve other membranous signalling in order to create the sealing zone before matrix resorption (Blair, 1998; Väänänen et al., 2000). A study of Ilvesaro et al. (1998) proved the possibility of the involvement of cadherin family in an epithelial junction like in the creation of the sealing zone. After the junction is completed the ruffled border starts to form. It is the result of the fusion of acidic vesicles with the plasma membrane in the basolateral area. At this point dissolution occurs by the secretion of HCl in the resorption lacuna from the ruffled border. In the lacuna, the low pH is maintained by H⁺-ATPase pumps combined with Cl⁻ that allows the abundant secretion of HCl in the lacuna allowing Ca²⁺ dissolution from bone matrix. At the same time, bicarbonate is exchanged via the basolateral membrane. The protons are derived from carbonic anhydrase II (Blair, 1998; Väänänen et al., 2000). The organic matrix is later degraded by a number of proteolytic enzymes (Väänänen et al., 2000). The final stage of bone resorption involves transcytotic vesicles that reverse the degraded products of the bone matrix in the extracellular space. It has been proved the presence of tartrate-resistant acid phosphatase (TRAP) in the vesicle operate a further decomposition of the products in this site (Salo et al., 1997, 1999). It is interesting to note that a similar path is followed in antigen-presenting cells, as osteoclasts probably follow a similar differentiation pathway of functional cells. After resorption completion, osteoclasts can undergo cell apoptosis or return to their motile phase with a consequent conformational modification (Väänänen et al., 2000).

3.6.2 Osteoblast

The main role of osteoblasts is bone formation. They are cuboidal cells with multiple nuclei located on the basal membrane, well-developed Golgi apparatus and extensive endoplasmic reticulum to help protein production and secretions. They are characterised by alkaline phosphatase (ALP) and osteocalcin expression and they are responsible for laying down the organic matrix that will be mineralised later. The anchorage of these cells to the bone surface is mediated by cadherins and connection with adjacent cells is provided via gap junction. The process of differentiation can be divided in four steps:

proliferation, extracellular matrix development and maturation, mineralisation and apoptosis. This cell type has been seen to follow a different maturation process presenting a precursor known as preosteoblast and two further stages that transform them into osteocytes and bone-lining cells. 50%-70% of the osteoblast population undergoes apoptosis. Structurally, preosteoblasts are very similar to mature ones but functionally they are unable to deposit bone. They lay down tropocollagen and a number of non-collagenous proteins, including osteocalcins calcium proteins, and alkaline phosphatase essential for mineral nucleation (Clarke, 2008; Kular et al., 2012). Bone formation occurs by two different pathways: intra-membranous ossification and endochondral ossification (Clarke, 2008). The first comprises deposition of type I collagen on a pre-existing fibrous matrix and the calcium phosphate will be later deposited on the structure, this is responsible for the formation of flat bones. Endochondral ossification shapes mesenchyme in a cartilage structure that resembles the bone outline. The cartilage is invaded by blood vessels and osteoblasts and initiates the deposition of collagen that will undergo mineralisation. Additionally, osteoblasts control osteoclast localisation by deposition of osteocalcin and collagen I, two chemo-attractants for the cells deputed to bone resorption. They are also responsible for nuclear RANKL production and deposition, the master cytokine essential for osteoclast differentiation and activation (Kular et al., 2012).

3.6.3 Osteocyte

Osteocytes are derived from osteoblast differentiation of mesenchymal stem cells. They represent approximately 70-90% of bone cells. Their main function is to coordinate osteoclast and osteoblast activity according to mechanical and hormonal stimuli (Bellido et al., 2014). With respect to cell morphology, osteocytes are embedded in the mineralised matrix inside lacunae interconnected by canaliculi in which dendritic processes have the role of establishing communication through gap junction and to transport proteins secreted by the osteocytes and control cell activity. On average each lacuna has 50 radiating protrusions that extend from the periosteal surface to the endocortical one throughout cortical bone. They are also located on the outer layer of trabeculae (Bellido and Hill Gallant,

2013; Bellido et al., 2014).

The main role of osteocytes is to control bone formation. The most widely studied pathway for osteoblast differentiation is Wnt/b-catenin mediated signalling. Osteocytes express inhibitors for this pathway (DKK1, sFRP1 and sclerostin) for negative regulation of bone formation. Sclerostin is only produced by osteocytes and travels through the osteocyte network inhibiting Wnt/b-catenin signalling. Apart from reducing osteoblast proliferation it also has a negative effect on mineralization and increases apoptosis. This results in an increase in bone mass (Poole et al., 2005; Kular et al., 2012; Prideaux et al., 2016).

Additionally, the accumulation of micro-damage can represent a stimulus for targeted remodelling as it interferes with the integrity of the osteocyte network present on the bone matrix (Figure 3.10). Osteocyte apoptosis can directly or indirectly secrete RANKL and osteoprotegerin. The first stimulates osteoblastic differentiation and activation while the second plays an antagonist role in inhibiting differentiation (Hadjidakis and Androulakis, 2006; Bellido and Hill Gallant, 2013; Bellido et al., 2014). Fatigue loading leads to an increase in damage accumulation that increases with porosity. Mori and Burr (1993) applied cyclic loads to dog limbs, this highlighted the clear correspondence between crack accumulation and bone remodelling. Despite cyclic loading and microdamage accumulation are stimuli for the initiation of bone turnover, in the absence of these remodelling is activated by systemic signalling (e.g. hormonal changes, growth factors) (Mori and Burr, 1993). Examples are the increased apoptosis due to increased glucocorticoids and inhibition of osteocyte-derived sclerostin production that limits bone formation due to the increased Parathyroid Hormone concentration (Bellido and Hill Gallant, 2013). These results were supported by Martin (2002) who demonstrated that micro-damage also plays an important role in bone turnover. Overall, there are findings that support the role of remodelling in micro-damage repair and the consequent increase of bone turnover as micro-damage density on cortical area increases and the role of osteocyte apoptosis is central in mediating this phenomenon. More quantitatively, ~30% of total bone remodelling is micro-damage induced, showing the complexity of understanding physiological causes of

bone turnover (Burr, 2019).

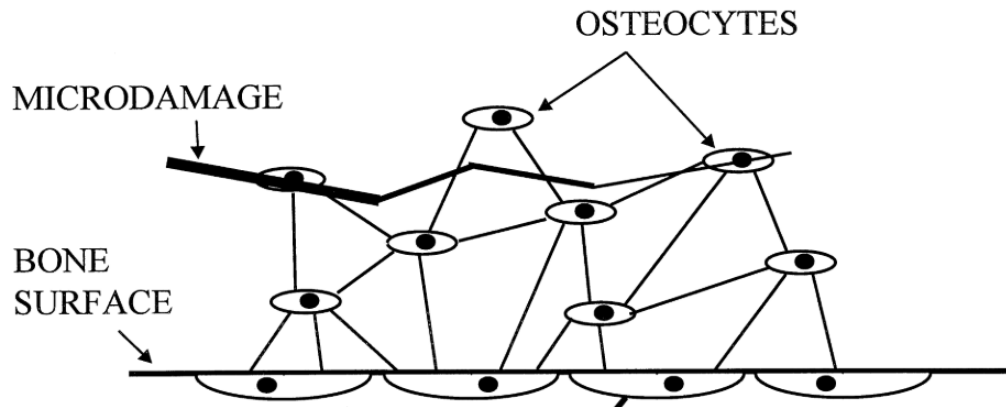


Figure 3.10: Schematic representation of the network of osteocytes (elliptical shapes) in bone matrix. When this cells record an increase in strain or the network breakage due to microdamage accumulation the BMU is recruited to begin remodelling. Reprinted with permission from [Elsevier] (Martin, 2000).

3.6.4 Bone Lining Cells

Osteoblast differentiation results in the formation of bone lining cells, sitting on the majority of bone surfaces which are not remodelled at a given stage. The main role of these cells is to secrete collagenase that digests the outer layer of non-mineralised bone, exposing the location where resorption should start. They also seem to express RANKL, which could explain their role in recruiting and guide osteoblast in resorption of specific sites (Kular et al., 2012; Florencio-silva, R.; Sasso, G.; Sasso-cerri, E.; Simões, M. J. & Cerri, 2015). They also seem to play a central role in mineral exchange between bone and extracellular marrow. This has been suggested by the close relationship between lining cells and osteocytes, connected through gap junction. After bone formation is concluded, they completely cover the entire surface of bone. In extreme cases, they can also recover the ability to produce bone matrix (Bellido and Hill Gallant, 2013; Bellido et al., 2014).

3.7 Intramembranous Ossification

Intramembranous ossification starts with the reorganisation and consolidation of mesenchymal cells into a structure known as blastema, starting to differentiate cells and recruit osteoblasts for bone deposition. These cells are driven by the RUNX2 factor in the deposition sites and start the formation of primary centres of ossification. When the osteoblast is enclosed in the neo-deposited bone matrix it turns into an osteocyte. Woven bone is primarily deposited in this phase and more osteoblasts are recruited and more organized lamellar bone can be deposited. At this stage, osteocyte density is low and cannot provide an adequate connection and blood supply. Therefore, the bone is invaded with vessels that go on to form the marrow cavity (Allen and Burr, 2013).

3.8 Endochondral Ossification

Endochondral ossification involves the deposition of the cartilage template that will be later replaced by mineralised bone tissue. It begins with condensation of mesenchymal cells and differentiation into chondroblasts that produce the cartilage matrix (Allen and Burr, 2013). Some of these cells are enclosed in the connective tissue becoming chondrocytes. The cartilage model is also enveloped into the perichondrium, a fibrous membrane which surrounds the surface of the cartilage template providing cells necessary for the cartilage growth. The differentiation of these cells into active osteoblasts is driven by transcription factor RUNX2 (Allen and Burr, 2013). Mineralisation starts on the periosteal area of the long bone shafts with the creation of a bone collar: this process leads to a reduction in vascularisation that causes death of chondrocytes. This triggers the penetration of the mineralised area with primary blood vessels that allows bone growth and removal in the central area to leave space for the marrow cavity and for the primary centre of ossification. The same process also produces secondary centres of ossification in the epiphyseal areas. At the interface between primary and secondary centres of ossification there is a structure known as the epiphyseal plates, responsible for longitudinal growth as shown in Figure 3.11 (Allen and Burr, 2013).

Histologically, this area can be divided into five zones according to morphology. The most peripheral is the resting zone and it is composed of hyaline cartilage matrix with enclosed chondrocytes. This area undergoes continuous growth, with chondroblasts laying down a cartilaginous template rich in type II collagen. The adjacent area is known as the proliferative zone due to the very active mitotic process where the chondrocytes are involved in cartilage deposition. Cells stack longitudinally and are oriented towards the direction of the growth. The last active region is the hypertrophic zone. Growth of the long bones is driven by cells in the upper regions of this zone. In the lower hypertrophic zone, cells begin to enlarge and die. Thyroxine appears to be the main promoter of chondrocyte hypertrophy, although other factors (e.g. components of the Wnt- β -catenin pathway) also are important for promoting hypertrophy. Another characteristic aspect of this area is that the collagen present is type X, that provides more stiffness and provides an environment for blood vessel penetration. The next region is called calcified cartilage zone. In this area, chondrocytes are subject to apoptosis and release vesicles containing alkaline phosphatase, ATPase and other enzymes in order to increase the mineral concentration and chondroclasts remove the cartilage template. The final area, the zone of ossification, is where the osteoblasts finally perform mineral deposition on the tissue. When the area is completely ossified, the epiphyseal lines are still visible (Allen and Burr, 2013).

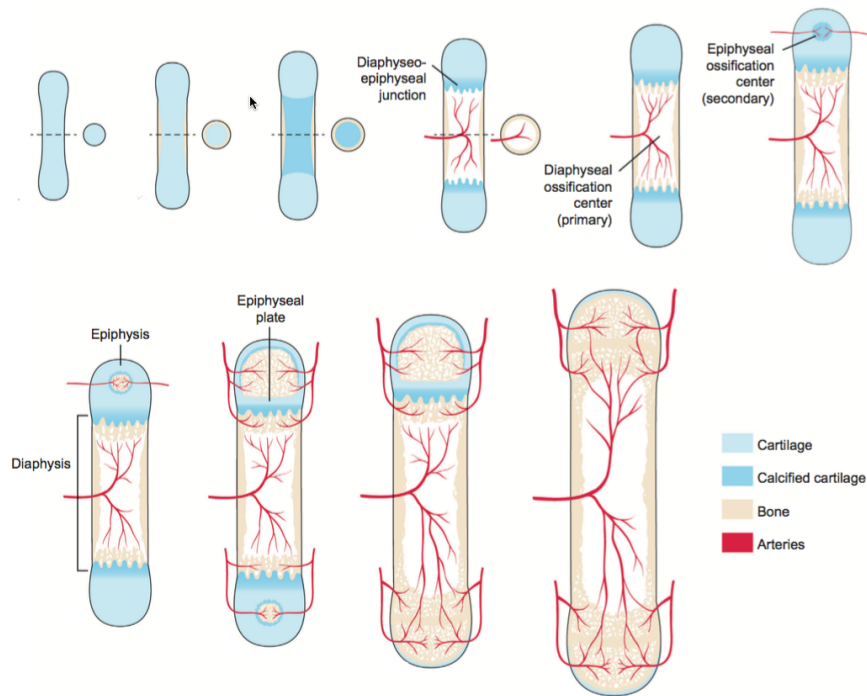


Figure 3.11: *Different stages of development of bone during endochondral ossification. Reprinted and adapted with permission from [Elsevier] (Allen and Burr, 2013).*

3.9 Bone Modelling

This process involves the action of bone resorption via osteoclast and bone deposition via osteoblast activity in specific areas in order to modify shape and size of bone. The main difference to bone remodelling is that the two actions are not coupled and are locally independent. However, the two processes happen simultaneously in order to achieve the shape of the adult bone (Allen and Burr, 2013). Modelling can occur on periosteal, endocortical and trabecular surfaces. It accounts for longitudinal and radial growth and the two modalities involve slightly different processes. In case of longitudinal growth, resorptive modelling is localised on the periosteal surfaces while formation modelling is localised on the endocortical ones. For radial growth the opposite mechanism is triggered and resorption is localised on the endocortical surface while deposition is on the periosteal one. This process is highly sexually dimorphic as it is mainly hormonally driven: on one side, oestrogens inhibit radial growth while growth hormone and testosterone in male in-

dividuals stimulate growth (Weaver and Gallant, 2014). Bone modelling is also influenced by other factors such as mechanical loading and pathological conditions (Robling et al., 2013). One aspect of radial growth that should be mentioned is bone drift. This occurs when bone resorption takes place on one periosteal and one endosteal area and deposition on the opposing endosteal and periosteal surfaces. This is typical of bone subject to specific load application or pathological conditions such as rickets (Allen and Burr, 2013).

3.10 Bone Remodelling

The difference with bone modelling relies on the sequential resorption/deposition on the same surface. As such it has been described as a quantum concept as discrete packages of bone are removed from one site and redeposited by the action of osteoblasts: the final goal is to replace old bone and repair bone micro-damage. The combination of osteoclasts and osteoblasts is known as bone multi-cellular matrix (BMU) and in intracortical remodelling the effect is visible in the accumulation of osteons, cylindrical structures of approximately 2,000 μm in length and 150-200 μm in diameter deposited with a speed of 20-40 $\mu\text{m}/\text{day}$. In targeted remodelling, the most common stimuli for bone turnover are micro-damage accumulation and cell apoptosis; it represents the response to impaired mechanical integrity in bone (Martin and Burr, 1989). By contrast, stochastic remodelling seems to be randomly initiated with the primary role of calcium homeostasis (Mori and Burr, 1993; Allen and Burr, 2013). The process for both alternatives involves different stages (Figure 3.12) and takes 4 to 6 months to be completed: activation, resorption, reversal, formation and quiescence. The activation process involves all the processes previously described that lead to differentiation and maturation of osteoclasts and consequent recruitment in the targeted area (Allen and Burr, 2013). Size and location of resorption sites are highly variable. The process enters the reversal phase when resorption stops and deposition is initiated. The commonly accepted explanation of this phase is the direct interaction between osteoblast and osteoclast. When resorption of the mineral phase is completed, collagen fragments are eliminated by bone-lining cells in order to proceed with deposition. Formation represents the last step of the remodelling process. Osteoid is deposited on the

lacuna. Matrix is composed of demineralised type I collagen that performs the function of a template for the hydroxyapatite crystals. Primary mineralisation accounts for $\sim 70\%$ of the total mineral matrix deposited in around 24 hours (Martin and Burr, 1989; Allen and Burr, 2013). Secondary mineralisation accounts mainly for crystal maturation. Part of the osteoblasts remain as inactive bone lining cells, while the majority undergo apoptosis. The matrix enters at the end of the process, the quiescence phase, during which there is no BMU activity and the surface is covered with bone-lining cells (Martin and Burr, 1989; Allen and Burr, 2013).

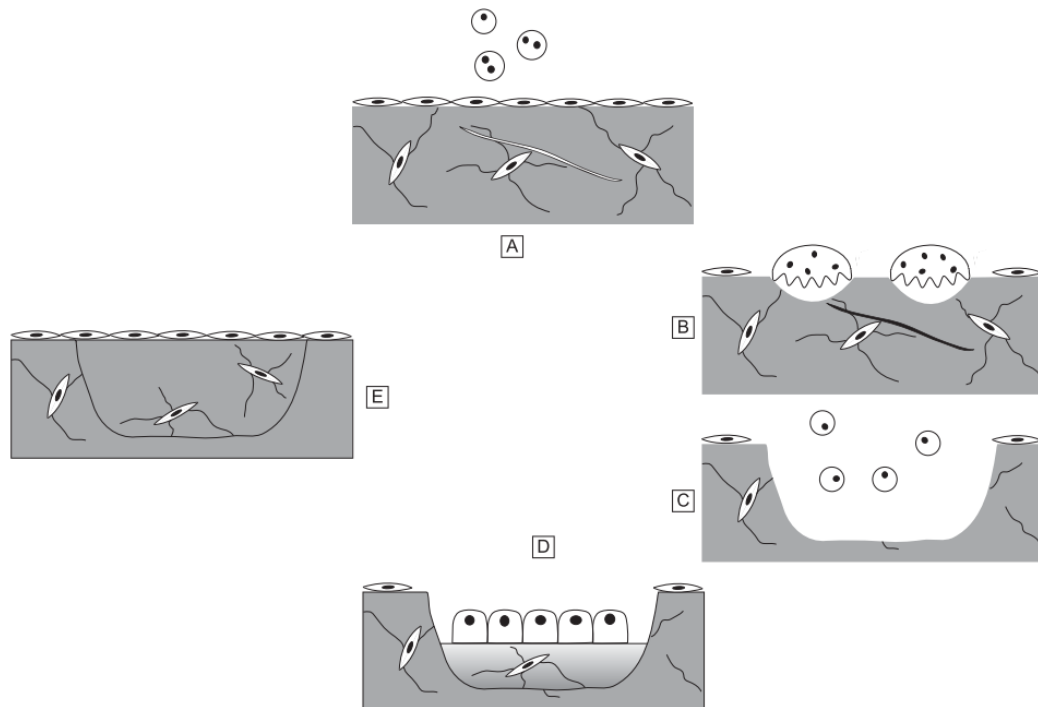


Figure 3.12: Remodelling cycle showing the different stages of the process. it starts with (A) activation followed by (B) resorption, (C) reversal and (D) formation. After new bone is formed, the cycle enters the (E) quiescence phase. Reprinted and adapted with permission from [Elsevier] (Allen and Burr, 2013).

3.11 Theories of Bone Turnover

The mechanostat theory formulated by Frost (1987a) effectively explains the negative feedback mechanism that regulates the activation and deactivation of remodelling. Acti-

vation of bone turnover is triggered when the increase in mechanical load exceed a certain limit, similar to the functioning of a thermostat that switches on after a certain temperature. This limit is set at 1.5-2.5 $\mu\epsilon$ known as minimum effective strain modelling (MESm) point. This leads to the increment in bone mass. In contrast, remodelling minimum effective strain (MESr) is much lower than MESm (50–100 $\mu\epsilon$). Bone remodelling does not necessarily imply an increase in bone mass as the amount of resorption could exceed the deposition (Frost, 1997b). In practice, when strain level is below the MESr, there is an increase in BMU recruitment while when peak strain is above, it is possible to notice a decline in BMU recruitment. In the second case the results would be bone retention. This has been called by Frost (1997a, 2000, 2001) "conservation-mode". In the case in which strain level is below the MESr bone enters the "disuse-mode", during which bone is permanently removed from trabecular and cortical-endosteal areas. This decrease in bone mass has been identified as osteopenia that accounts for an increase in porosity of approximately 40% between the age of 25 and 75 years in healthy individuals (Frost, 2000). Considering now that modelling activation occurs at 2.5 $\mu\epsilon$ and remodelling at 200 $\mu\epsilon$, it is easy to understand that activation of modelling is coupled with the remodelling inhibition maintaining balance in bone mass (Robling et al., 2013). In addition, this theory of mechanical control of bone growth, modelling and remodelling includes also a number of non mechanical factors. It is true that hormones, calcium, vitamin D and genetics assists the turnover control by acting on bone cells and accounts for approximately 10% of postnatal strength (Frost, 2001, 2004; Martin et al., 2015) (Figure 3.13). Finally, the proposal also suggested that the accumulation of microcracks related to *in vivo* fatigue loading turnover by interrupting the canalicular network and initiating cells recruitment (Frost, 1987a).

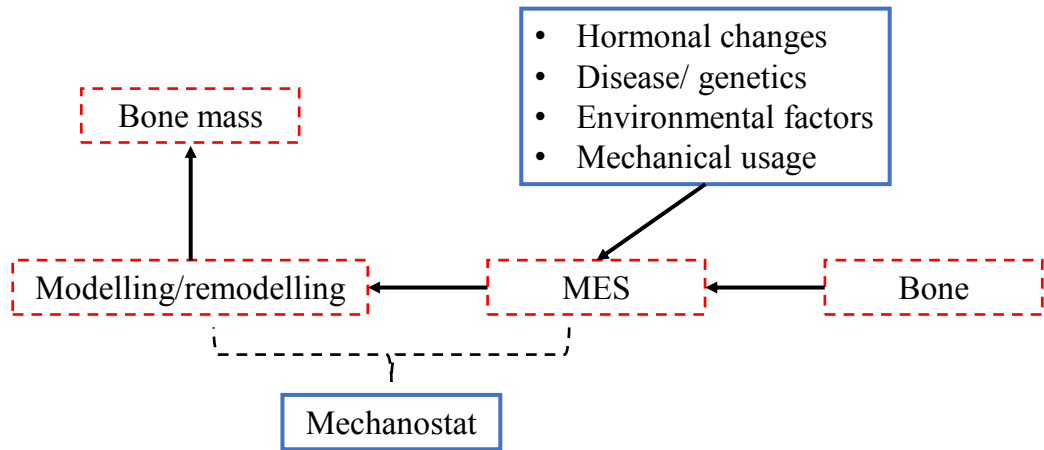


Figure 3.13: *Flowchart of the Mechanostat theory. The variation in bone mass is mainly drive by mechanical stimuli but there are other factor that can influence this process. Adapted from Frost (1987a)*

The following step in explaining bone mass variations was offered by Turner (1999) and it is known as “cellular accommodation theory.” According to this, although the mechanostat could explain response to mechanical stimuli, it does not address how cell signalling induces these changes and, moreover, does not stress enough the deleterious effect of disuse on bone mass. It is suggested that cells react to transients in the environment in order to accommodate the new condition. This, after a first reaction, would bring back environmental conditions and cells would go back to a quiescent mode. However, Turner (1999) suggested that receptor down-regulation or cytoskeletal reorganisation must affect cell sensitivity in order to avoid the turnover process from stopping. This theory was experimentally verified with anabolic treatments. In other words, when an anabolic treatment starts there is an increase in bone mass. Upon withdrawal, there is a quick loss in mass as initial physiological conditions will be reached again. Nonetheless, if cellular accommodation is quick enough bone growth should stop at a point in which mass is greater compared to the initial stage, as can be seen in Figure 3.14 (Jee et al., 1991; Turner, 1999).

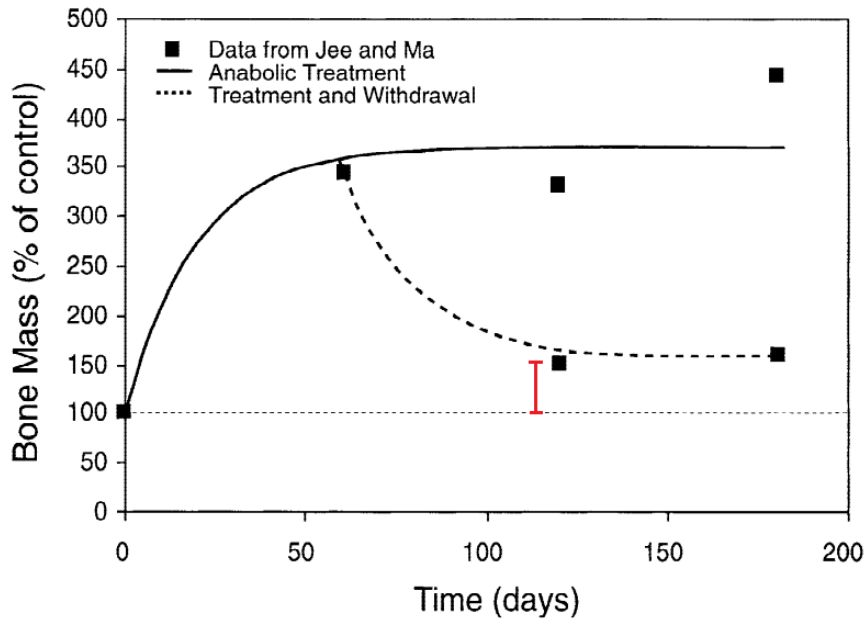


Figure 3.14: Anabolic treatment given to rats (solid line), followed by withdrawal (dashed line). After this protocol, bone mass is at 50% higher than control levels (dotted line). The red line shows the increase of bone mass after treatment withdrawal. Reprinted and adapted with permission from [Springer Nature] (Turner, 1999).

3.12 Concluding Remarks

This section demonstrated the level of structural complexity that bone has at different levels. A description from the nanostructure and compositional level was drawn in which the main focus is on type I collagen and HAp crystal. These are meticulously described as they represent the main focus of the analysis employed in this thesis. Micro-structural level will also be investigated from a structural and mechanical point of view. Features of bone macro-structure were illustrated for completeness although the study in this thesis does not aim to investigate variations at this level. The section concludes with the description of modelling, remodelling and different growth patterns in order to illustrate the complexity of these physiological processes that results in the heterogeneous nature of bone: this is the reason why there are still discussions ongoing towards an agreement concerning the very fundamental aspects of bone structure and behaviour.

CHAPTER 4

BONE AGEING AND MECHANICAL PROPERTIES

Mechanical resistance to fracture relies on the quality of bone and its spatial arrangement (Currey, 2002, 2003b). It is well established that the risk of fracture increases dramatically with age and the causes are largely believed to rely on structural modification, specially in relation to conditions such as menopause and osteoporosis. This, in fact, explains only 75% of the increase in risk of fracture (Burr, 2019). Structural changes cause a considerable decrease in toughness and increase the risk of fracture due to the brittleness (Boskey, 2003). Regarding the other factors affecting mechanical integrity, between 20 and 80 years of age there is a drop of $\sim 80\%$ for bone toughness and ultimate strain that results in a loss of approximately 30-40% of overall strength (Burr, 2019). These modifications are independent of bone architecture and mineral density and can be attributed to physico-chemical changes affecting the bone matrix at the nanoscale level (Burr, 2002, 2019; Boskey, 2003). Bone matrix is composed of mineral, collagen, non-collagenous proteins and water; its quality and spatial organisation explains a portion of the mechanical behaviour of this tissue. The changes that involve one or more of these constituents have an effect on the larger scale. An example is given by the case of osteogenesis imperfecta (a genetic disease affecting collagenous matrix) that induces an excessive production and growth of extrafibrillar crystals coupled with small-sized intrafibrillar crystals. This condition affects bone at the anatomical level increasing brittleness dramatically, additionally due to the increase of turnover in young, and decrease in elderly individuals (Boskey, 2003). To fully understand the consequences of these types of phenomena, it is essential to evaluate the normal physiological changes that occur within the matrix. In the study in this thesis, the interaction between collagen and mineral in human cortical bone will be investigated. The close relationship between crystals and collagen fibres in the bone matrix has been recently presented, thanks to the progress of diffraction and microscopy

techniques (Olszta et al., 2007).

It remains difficult to produce an exhaustive and accurate model as biogenic apatite is highly affected by a large number of factors. Although this represents a problematic aspect, it is appropriate to give a general model of composition and structure of bone matrix. Human bone reaches its skeletal maturity in the third decade of life. This is followed by deterioration due to the impaired response to mechanical stimuli offered by new bone formation (Zioupou, 2001). After maturation, a gradual decrease in fracture resistance and elastic properties has been seen. Explanation for matrix properties can be extended to cortical and trabecular bone as they are both made up of the same tissue material (Zioupou, 2001).

4.1 Mineral Crystals and Ion Substitution

Previously, the nature of biological hydroxyapatite (HAp) as a calcium-deficient poorly crystalline apatite phase similar to that of stoichiometric HAp was discussed. The size of these mineral platelets is highly variable but approximated from 30-200 nm in length, 30 nm in width and 2-10 nm in thickness (Ottani et al., 2002; Olszta et al., 2007; Rey et al., 2007; Stock, 2015). Mineral crystals grow in size in both inter- and intra-fibrillar sites and become more crystalline following a process of ion substitution and mineral stoichiometry. PO_4^{3-} ions dominate the crystal lattice such that they occupy tetrahedral sites and each ion is in 4-fold coordination with the OH^- ions. This structure reveals octahedral interstices of different size that run vertical to each other. The larger of these can accommodate the Ca^{2+} ions (Rey et al., 2007, 2009). Due to the large specific surface area (surface area/volume ratio) and the hydrated surface, which contains a number of mineral ions on charged organic compounds that envelope the apatite crystals, the structure is subject to ion migration (Cazalbou et al., 2005; Rey et al., 2007, 2009). This phenomenon, shown in figure 4.1, fulfils the requirement of neutral charge in the molecules, explains the number of modifications in the cell structure and crystallinity of the apatite and originates a non-stoichiometric compound (Cazalbou et al., 2005; Rey et al., 2007, 2009; Betts et al., 1981). The most significant of substitutions is that of the CO_3^{2-} , with 2-6 wt% within biological

HAp (LeGeros, 1981). It has been observed to increase with the age of the individual (Handschin and Stern, 1995). Many studies have shown that CO_3^{2-} level and site (A-type which substitutes for OH^- ions and B-type which substitutes for PO_4^{3-} ions) alters lattice parameters of the crystallites (LeGeros et al., 1969, 1970; Madupalli et al., 2017). There is a charge differential between both PO_4^{3-} and CO_3^{2-} as well as OH^- and CO_3^{2-} , and as such several mechanisms are available for balancing the charges within the lattice, namely additional substitutions (such as Na^+ for Ca^{2+}) and vacancies (such as the loss of Ca^{2+}) (Rey et al., 2009; Elliott et al., 2002). Figure 4.1 offers a schematic representation of the ion substitution process happening to the bone surface.

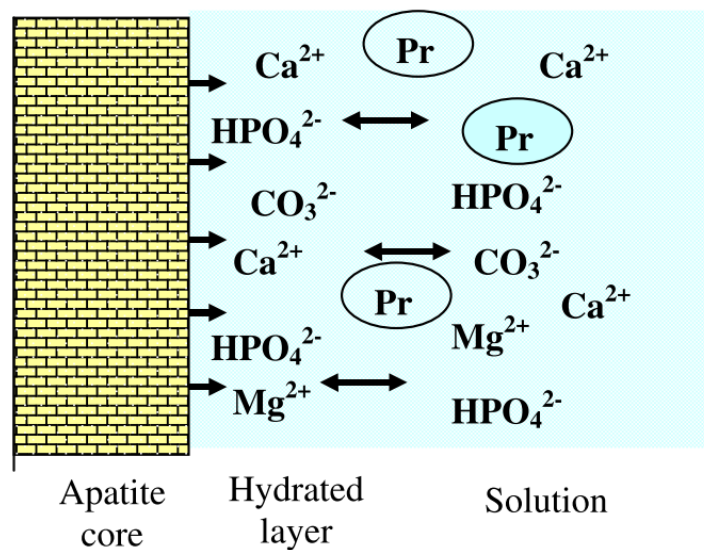


Figure 4.1: Solid-liquid interface that induces ion exchanges. The main substitution that occurs in the hydrated layer is carbonate that normally induces and increase in crystal size. Reprinted with permission from [Elsevier] (Rey et al., 2007).

Changes in mineral crystallinity are interpreted as being related to an imbalance of bone turnover. The relationship between crystallite geometry and age was investigated in human samples dissected from the crista iliaca (age range of 0-90 years). It was found that for individuals who have not yet reached skeletal maturity there is an increase in crystal size along both the 'a' axis and 'c' axis (Figure 4.2), while for reflection of 002 and 300

peaks there is an increment for the entire age range. No variations in crystallite size were found to be significant for the increase of age between 30 and 60 years. Microstrain was also found to increase for skeletally immature individuals and then stabilise for the rest of the sample (Handschin and Stern, 1992, 1995).

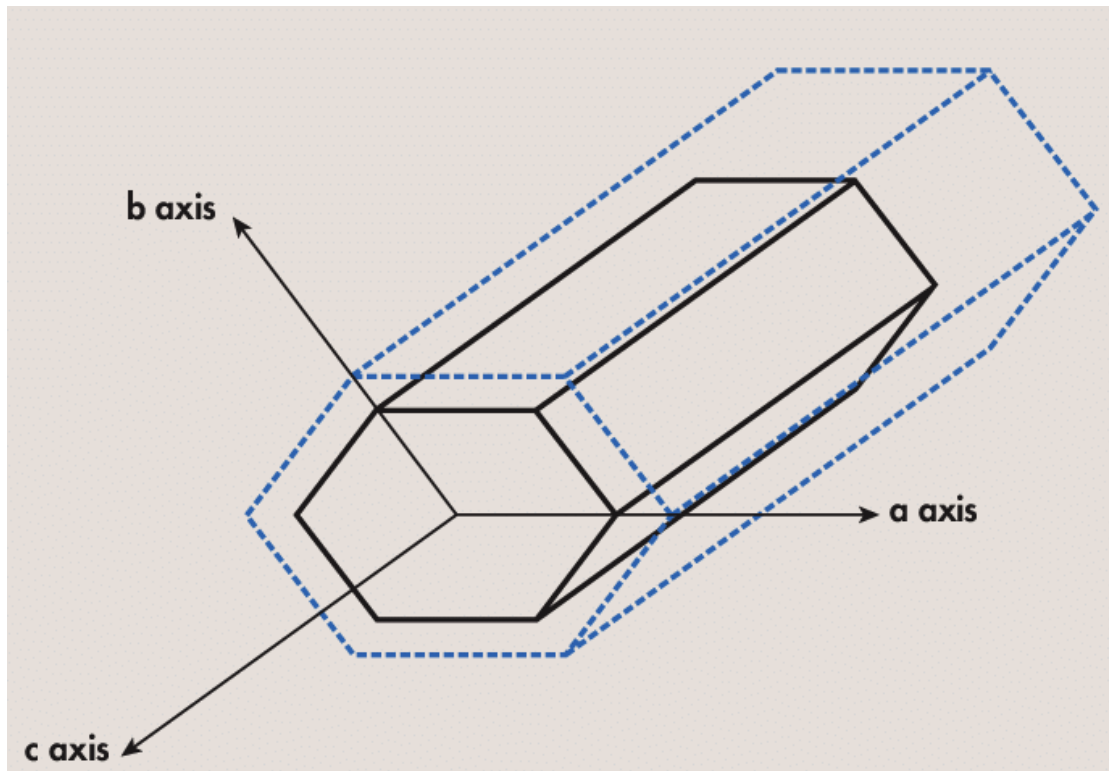


Figure 4.2: Representation of crystal growth. 'a' and 'b' axis are assumed to be equivalent while 'c' axis represents the length of the crystal and it is aligned with the major axis of collagen fibres. (Boivin, 2007)

4.2 Mineral Content

The degree of mineralisation of the bone represents a key aspect in understanding degeneration of biomechanical properties in cortical bone. The increase of mineral size is linked to an increase in crystal size (Boskey, 2003). Tissue mineral density (TMD) quantifies the mineral content per volume of solid tissue, while bone mineral density (BMD) refers to the ratio of mineral content to total area or volume. Simmons et al. (1991) proved that there is an increase in BMD up to the age of 80-85 years in the human femur. After skeletal

maturity is reached, mineral density is ~ 2.0 g/cc that reaches ~ 2.2 g/cc in 80-85 years old individuals. The increase does not follow a regular pattern although it shows strong correlation with ($R = 0.76$) according to Currey et al. (1996). Srinivasan et al. (2012) employed dual energy X-ray absorptiometry (DXA) and quantitative computed tomography (QCT) in order to understand the difference in BMD changes in cross-sectional and longitudinal data between men and women at different ages in total body and different sites (e. g. wrist, humerus, vertebrae) (Kranioti et al., 2019). The study revealed no differences between male and female group. In men, a continuous bone loss was detected with higher value for the forearm due to the higher degree of cortical bone. In contrast, women presented a slight acceleration in the BMD decrease in the postmenopausal phase, especially on the hip bones (Kranioti et al., 2019). The study showed the influence of sex and site on the process of mineral loss in human bone. Furthermore, the process of mineralisation is extremely heterogeneous, to the extent that in osteons the mineral content decreases when moving away from the Haversian canal. This results in a similar pattern of decrease for elastic modulus and hardness (Rho et al., 1999). The heterogeneous distribution of mineral in cortical bone is supported by Akkus et al. (2003) who, by means of Raman spectroscopy, describes how mineral content increases with age until approximately 40 years without showing any major change afterwards. SEM and micro-radiographs showed a general increase and homogenisation of mineral distribution on the bone surface that confers the tissue mechanical strength. Additionally, increased degree of mineralisation leads to increase cortical porosity with a decrease of osteocyte lacunae, that weakens the architecture of bone on one side and reduces the signalling in detecting micro-damage and stimulating remodelling (Milenkovic et al., 2014).

4.3 Collagen Ageing

Bone organic matrix is mainly composed of type I collagen that shows the accumulation of inter-molecular cross-links with age affecting the mechanical efficiency of bone primarily (Stock, 2015). Collagen maturation leads to increased cross-linking concentration, degeneration in the quality of these links and in reduced hydration of the collagen fibres

that account for a general decrease of thermal stability of the tissue (Stock, 2015). The accumulation of these links is a normal process in life and they are later substituted with “mature” links that bond two or three collagen molecules reducing molecular configuration, that results in an increase in toughness. However, this process reduces the capability of binding water molecules due to the increase number of covalent bonds. What is striking in this process is that below a certain level of hydration, the enthalpy of the collagen drops resulting in lower stability and affecting biomechanical properties (Miles et al., 2005). A number of studies employing differential scanning calorimeter (DSC) have shown that human bone undergoes a first dehydration (endothermic) episode between 50 and 90°C, involving mainly water molecules on the surface of the sample. A second exothermic episode is recorded between 345 and 425°C and is associated with cross-link degeneration and collagen combustion, while the rest of the organic matrix continues to burn until 1200°C (Lozano et al., 2003; Miculescu et al., 2011). The interpretation of qualitative and quantitative bone loss was possible through the application of thermo-gravimetric analysis (TGA) that shows a major bone loss of 20-30% of the normalised mass of the sample for the second exothermic peak; this provides an alternative tool to evaluate bone mineral density variation with age (Lozano et al., 2003; Miculescu et al., 2011). Finally, the study of Lozano et al. (2003) debated on the interaction between the COO^- groups of collagen and apatite crystals in thermal stability of bone that influences both elastic behaviour and strength of bone.

Remodelling of compact bone is the main mechanism of maintaining the mechanical integrity of the tissue. However, it has been observed that it triggers a mechanism of degeneration of the structure for a number of reasons: depositing less mineralised bone, increasing cortical porosity and altering collagen fibres orientation and quality. The various works of Ascenzi on single osteons showed a number of interesting mechanical features applying compression, tension and torsion test to a single osteon. First, a very large difference in Young’s modulus, indication of the elastic behaviour of a material (in GPa), gives different results when tested in tension and compression. Furthermore, torsional modulus was found to be much higher compared to the bending one. Finally, bending and torsional

strength are high compared to tension and compression strength (Ascenzi and Bonucci, 1967, 1968; Ascenzi et al., 1990, 1994; Currey, 2002; Martin et al., 2015). Ascenzi et al. (1973) proved that orientation of fibres in relation to two consecutive lamellae can have an effect in the mechanical properties of each osteon. Therefore, they divided osteons into two types, one type in which the fibres created angles of 90° and a second type with practically no angulation. These findings showed that the ultimate compression strength and Young's modulus of compression are greater for the first type of osteons, while in tension values are higher for longitudinally oriented lamellae osteons. This findings were later confirm by Ascenzi et al. (1990), and partially confirmed by Pidaparti and Burr (1992) using a finite element model, showing that collagen orientation plays a central role in determining mechanical properties of cortical bone and in Haversian systems. Bending stiffness is seen not to vary when fibres are oriented at $<60^\circ$ angle. It was, otherwise found, that torsional stiffness is maximised when the angle of collagen fibres is 15° – 30° (Pidaparti and Burr, 1992). To conclude, Ascenzi and Bonucci (1968) divided the osteons sampled from human femora according not only to fibres orientation but also with the degree of mineralisation. It was clear that fully mineralised bone showed better elastic properties and strength. When tested for shear, the entire cohort showed fracture patterns with an angle of 30 – 35° .

4.4 Bone Mass Changes with Age

Loss of bone, seen in Figure 4.3, is the most common result of the ageing process and can also result from certain pathological conditions (e. g. osteoporosis) (Turner, 2002) and this heavily affects biomechanical properties due to the insurgence of hollow areas in the cortical area due to remodelling. Cooper et al. (2007) showed the potential of 3D imaging in assessing porosity changes in samples of different ages and highlighted the difficulties in distinguishing the cause from a range of intrinsic and extrinsic factors, such as sex, body weight, diet, pathological condition and genetic variation. Additionally, they identified a clear increase in cortical porosity until 60 years of age, with a decrease of the phenomenon after this stage, due to the decrease in total mass (Cooper et al., 2007). A

more qualitative examination of the increase in porosity was carried out with NMR T2 relaxation techniques; this showed that the increase in porosity is mainly due to increased resorption in the Haversian canals, while osteocyte related porosity did not prove to be sensitive in the overall increase (Wang and Ni, 2003). Feik et al. (1997) reported an increase in intra-cortical porosity of 4-6% in the 3rd decade and a successive 9% in the 9th decade, with a rapid increase in postmenopausal individuals, although only the difference in the 3rd decade showed significant correlation.

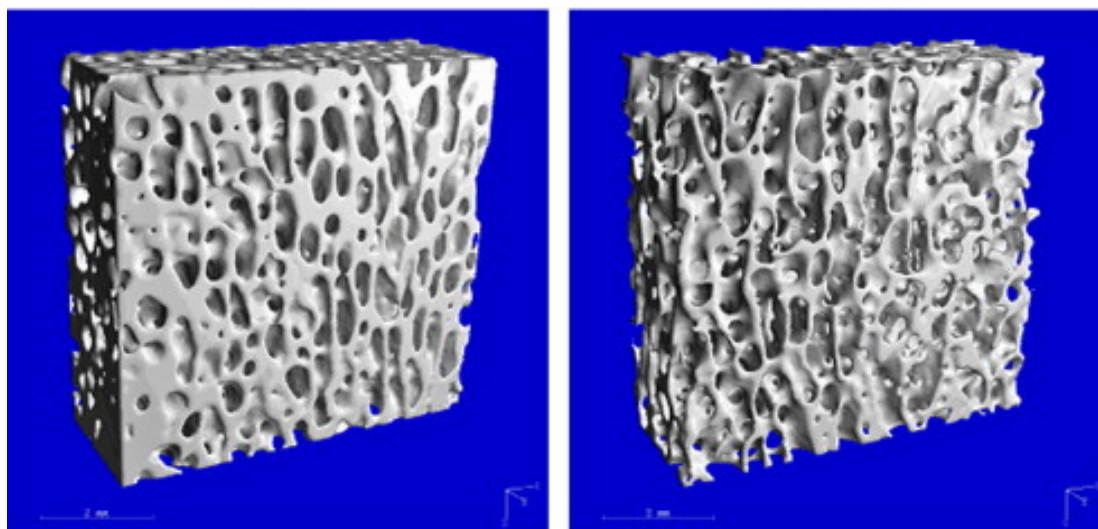


Figure 4.3: μ CT scans of trabecular bone showing a sample with high density (right) and one with low density (left). Decrease in density and consequent increase in porosity is a characteristic effect of bone ageing and it impairs mechanical behaviour. Reprinted with permission from [Elsevier] (Qin et al., 2013).

4.5 Bone Mechanics

The final aim in compositional and structural analysis is to understand, and therefore predict and prevent, the risk of fracture to the bone. A large number of testing techniques have been developed for different purposes. A general understanding on bone mechanical properties is essential even as this thesis focuses solely on indentation methods. The following section introduces the main mechanical parameters and general principles of testing, followed by a focused discussion on the effect of compositional changes on bone

mechanical behaviour.

4.5.1 Mechanical Testing and Influencing Factors

There are several aspects that are essential in the preparation of a mechanical test involving bone. Properties measurement sensibly varies with the type of bone tested (cancellous, cortical, etc.), with age and anatomical location. While this information can be reported, what has to be standardised in a large sample pool is the preservation condition – storage, hydration and temperature (Nazarian et al., 2009). Furthermore, the hydration state positively influences Young's modulus and strength, while it determines a significant decrease in stiffness. To obtain accurate results, it is recommended that the hydration of each bone specimen should be measured. Similarly, temperature influences the mechanical properties. Although, variation is minimal and different protocols involve different testing temperatures, control temperature throughout the entire experiment would ensure consistency of the results (Turner, 1993). Different testing methods can be used according to specimen feature and purpose of the research. Tensile test can be applied to both cancellous, cortical or whole bone with good accuracy. It necessitates large sized samples and strain must occur in the central portion of them. Forces are applied on two ends and direction is diagonally opposed in order to increase length and reduce section of the specimen. This is due to the fact that both in the whole bone and in coupons, the central part is narrower and is where the majority of the strain will occur (Turner and Burr, 1993).

In the case of limited sample size, bending tests are more suitable. It causes tensile stress on one side and compressive stress on the other when the bone is loaded until fracture. As bone is more resistant in compression, the failure mechanism is indicative of the tensile side of the specimen. The two main protocols are three-point and four-point bending. The second is suitable for avoiding shear stress effect. Compressive test models the main tool in cancellous bone mechanical characterisation, because of the employment of small specimens. Figure 4.4 shows where force is applied in different testing protocols.

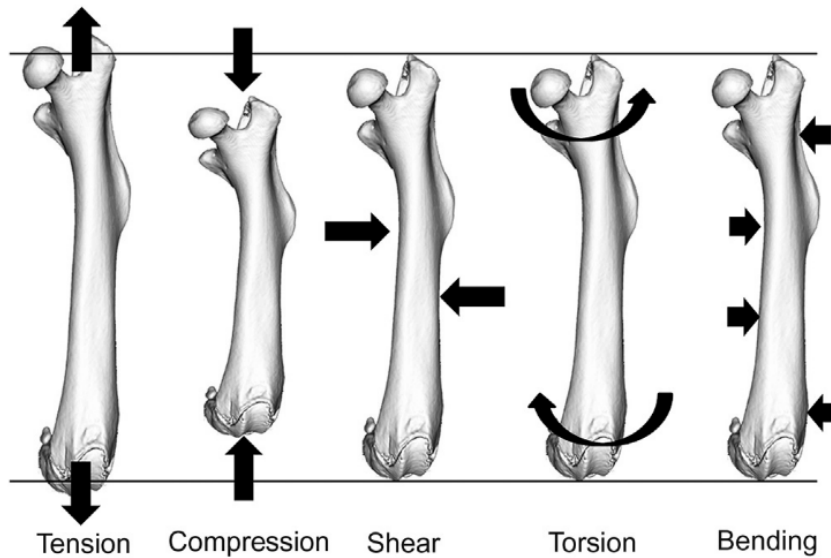


Figure 4.4: *Different types of mechanical testing. Arrows show where the force is applied. Reprinted and adapted with permission from [Elsevier] (Wallace, 2013).*

Indentation is an additional testing protocol, chosen and applied in the study in this thesis. The surface of the bone is pierced by a small tip driven by a static force. The area and depth of the impression are calculated in order to calculate hardness by the ratio of force over area. This simple and consistent technique gives indication of resistance of bone to plastic deformation (Hunt and Donnelly, 2016). Also for indentation protocol dehydration of the sample is related to the increase in hardness (Hunt and Donnelly, 2016). The two main protocols used are micro- and nano-indentation. In the first protocol, load is static and hardness is calculated by force divided by the area of the impression left by the tip of the indenter (Hunt and Donnelly, 2016). Boivin et al. (2008) showed that the increase in mineral content determines an increase in hardness with good correlation ($R = 76-80\%$). This protocol is extremely simple to apply and benefits of good replication of the results (Hunt and Donnelly, 2016). Nano-indentation, in contrast, allows investigation of the tissue's mechanical properties at $1 \mu\text{m}$ of resolution and assumes isotropy of the material analysed. It employs the Oliver-Pharr method from general contact mechanics. The hardness and elastic modulus is calculated from the unloading portion of the force-displacement curve (Figure 5.12) (Wallace, 2013; Hunt and Donnelly, 2016).

The possibility of obtaining two mechanical parameters at tissue level is the main advantage of this protocol. However, for loads >1 mN leads to local yielding and permanent deformation of the indentation area that prevents further investigation for the true elastic properties (Wallace, 2013). The advantages of this methodology rely on the very high resolution that allows to investigate tissue mechanical behaviour and the high consistency of the results that enhance replicability.

4.5.2 Structural Mechanical Properties

Whenever a force is applied to bone, no matter the modality, it induces a deformation in the structure known as displacement. The analysis of load as a function of the deformation is studied in order to understand structural mechanical properties via the force-displacement curve (Wallace, 2013).

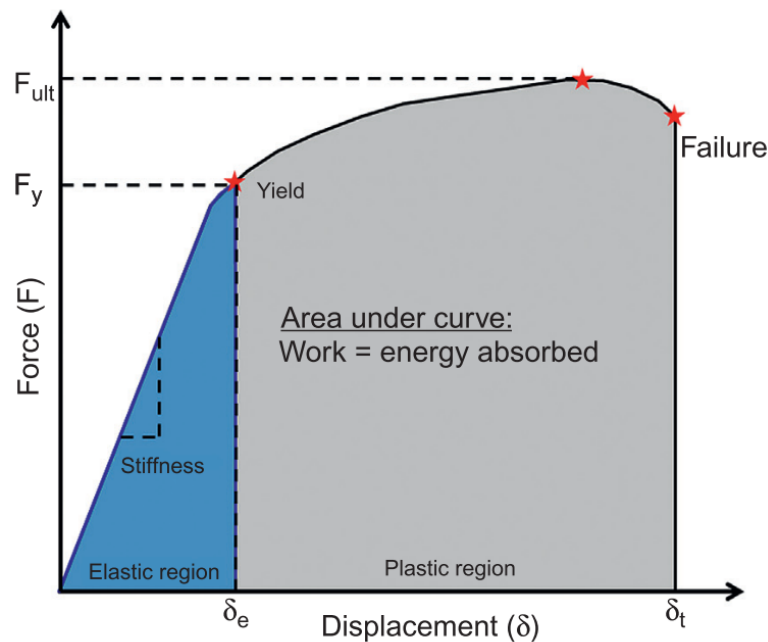


Figure 4.5: Characteristic force-displacement curve showing the elastic phase of the deformation until the yield point and the following plastic until failure. Reprinted and adapted with permission from [Elsevier] (Wallace, 2013).

As seen in Figure 4.5, there are certain peculiar features useful for calculating the struc-

tural mechanical properties. A first, linear increase can be observed, which represents the loading phase, followed by a non linear phase where the maximum force is reached. A final recovery phase is noted when the bone encounters a structural failure and cannot support any further load. The first phase, from the beginning of the loading phase to the yield point is known as elastic phase (Currey, 2002; Wallace, 2013). In this phase, there is no permanent deformation and the slope indicates stiffness (K), which is the capacity of the material to resist deformation under a certain load. Past the yield point, the experiment enters the plastic region, where deformation is permanent and reaches the ultimate force (F_{ult}). The quantification of the displacement for this portion of the curve is an indication of the ductility of the material (amount of post-yield deformation). To conclude, the area under the curve is a measure of the energy absorbed (W_f) during the cycle (Currey, 2002; Wallace, 2013). This curve can accurately describe the deformation to the whole bone under load. The factors affecting this measurement are bone mass, geometry and composition: the material properties. It is essential to normalise these properties related to mechanical behaviour according to bone geometry in order to obtain material properties of the tissue itself (Burr and Martin, 1989; Currey, 2002; Wallace, 2013).

4.5.3 Material Mechanical Properties

Before describing material properties, the concepts of stress and strain must be understood. Strain (ϵ) indicates the physical deformation of the material when a directional force is applied and has no unit, while stress (σ), measured in Pa ($1 \text{ Pa} = 1 \text{ N/m}^2$), is the intensity of the force that is applied to the material also indicated as load per unit area (Burr and Martin, 1989).

$$\epsilon = \frac{\Delta L}{L} \quad (4.1)$$

$$\sigma = \frac{P}{A} \quad (4.2)$$

Where P is the load applied, A is the the unit area and L is the geometry of the specimen.

Stress and strain are used in engineering to normalise the test results to sample geometry, converting a load-displacement curve into stress-strain relationship (Burr and Martin, 1989; Wallace, 2013). When a structure is loaded in tension, there is a clear increase in the length along the direction of the load and a significant reduction in transverse size. The ratio between these two deformations is called Poisson's ratio and is set as less than 0.5 for geometric reasons. For cortical bone, this varies between 0.28 and 0.45. Material mechanical properties, therefore, are not subject to variation in relation to size and architecture. Once the load-displacement curve is converted to a stress-strain curve, it is possible to calculate material properties. Young's modulus, for example, indicates material elasticity and is calculated from the slope of the elastic deformation. In bone, it is usually around 10-20 GPa: the stiffer the material, the steeper is the initial part of the curve. Consequently, intrinsic stiffness (calculated normalising for size) and elastic modulus explain the same behaviour, with minimum variation related to the sample size (Currey, 2002; Wallace, 2013). Bone is a stiff material and most of the strain occurs during the elastic phase of the deformation, while a small variation in stress leads to great post-yield deformation. Furthermore, ultimate strain is calculated by the value of the peak force the material can support before reaching the fracture point. Toughness is the maximum energy required in order to yield or fracture the material (Martin and Burr, 1989; Turner and Burr, 1993; Currey, 2002; Martin et al., 2015).

4.5.4 Anisotropy and Viscoelasticity

Two more aspects considered when describing the mechanical properties of skeletal tissue are anisotropy and viscoelasticity. Bone is an anisotropic material as its properties change if measured in different directions. For this reason, bone, like other anisotropic biological materials has a "grain" or preferred direction of measurement (Burr and Martin, 1989; Currey, 2002). The best approach to mechanical analysis of anisotropic materials would be the experimental evaluation of all the components of each property taken from different planes. This would be an impossible task when the number of directions exceeded three. Besides, bone is assumed to be an orthotropic material and each property is composed

of three mutual components with mutually perpendicular directions, which would require nine different measurements (Currey, 2002). The speed of loading of material during a mechanical test also influences the measurement and as a result Young's modulus is a strain-rate dependent value, where strain-rate refers to the variation of strain divided by the time interval. This effect is given by the viscoelastic properties of bone. Some other effects of interest in this research are stress relaxation and creep. In the first case, when the material is subject to strain and then held at that strain, stress would decrease over time. If the same experiment is repeated with load, the result would be an increase in strain and therefore deformation will increase at a proportional rate, resulting in a process called creep. Finally, if the material is loaded and unloaded, the result would be that the load curve is different from the unloading step for a process called hysteresis, loss of energy during cyclic loading (Currey, 2002; Martin et al., 2015).

4.5.5 Elastic Properties

Due to the orientation of osteons along the length of the shaft, it is possible to assume that elastic properties in cortical bone are transversely isotropic. As a result, Young's modulus values are higher in longitudinal directions than in the transverse direction and a complete characterisation of elastic properties will require more than one test (Ascenzi and Bonucci, 1967, 1968; Ascenzi et al., 1990, 1994; Orías et al., 2009). One of the main properties that correlates with modulus and affects it directly is porosity (defined as the ratio between void volume and bone total volume, measured also in two dimensions) (Martin and Burr, 1989; Zioupos et al., 2008). Elastic modulus dissipation is largely documented and connected to cyclic loading that results in the formation of micro-damage in the bone matrix (Burr, 2003). Mechanically, there is a much higher incidence of linear damage accumulation in compression, while tension creates diffused damage and to different extents, both account for elastic energy release (Reilly and Currey, 1999).

Schaffler and Burr (1988) investigated the relationship between porosity, mineral content and apparent density with elastic properties of compact bone. Results showed a clear decrease in elastic modulus with the physiological increase of porosity. As expected,

apparent density presented the same relation with stiffness, while mineral content was observed to not influence the elastic behaviour of bone significantly. The combined analysis, however, showed that there is a connection between the two architectural properties and mineralisation. This leads to the conclusion that mineralisation itself does not play a role in degeneration of elastic behaviour. Also, it has been observed that porosity accounts for 70% of elastic modulus (Augat and Schorlemmer, 2006). Finally, there is a high level of correlation between structural organisation (density and porosity) and stiffness (Schaffler and Burr, 1988). These results were argued by Hernandez et al. (2001) where the study revealed a strong correlation between ash fraction and elastic properties of bone, supported by the fact that the sample employed in the previous study presented very low porosity and high degree of mineral content. Quantitatively, bone reaches its mechanical maturity around 30-35 years of age and a study on human femora detected a decrease in elastic modulus of 2.3% per decade (Zioupou and Currey, 1998; Zioupou, 2001). Similar data were presented by Augat and Schorlemmer (2006), with a decrease of $\sim 2\%$ per decade in elastic modulus in tension and compression. It is also interesting to note that collagen degeneration does not affect elastic modulus (Zioupou and Currey, 1998).

4.5.6 Toughness

Toughness can be seen as the energy dissipated when a structure reaches its failure point and collapses. Therefore, the accumulation of cracks on bone has been reported to have a toughening effect as the initiation of damage requires energy that retards fracture (Zioupou, 2001). Furthermore, osteon structure, and in particular the presence of the cement lines, tend to stop crack propagation which prevents bone failure (Yeni and Norman, 2000). Bone resists fracture by stopping crack propagation in cortical bone and via the activation of bone remodelling when canalicular network integrity is interrupted by micro-damage (Akkus and Rimnac, 2001).

Currey et al. (1997) irradiated bone samples with ^{60}Co gamma-ray in order to damage collagen quality and found a steep decrease in toughness as well as strength while the elastic modulus remained unaffected. This finding is further confirmed by Wang et al. (2002b)

who compared demineralised and fresh human femoral samples and showed significant correlation between integrity of collagen network and toughness. The extent of degeneration of toughness was quantified by Zioupos and Currey (1998) at 4.1% per decade. Collagen has been seen to significantly correlate with toughness. Particularly, non-enzymatic cross-links play a central role in mechanical integrity of bone structure. A study from Wang et al. (2002b) showed the age-related deterioration of collagen network integrity is correlated to a decrease of toughness. The authors also suggested that glycation plays a central role in decreasing collagen integrity and stability, leading to deterioration of bone mechanical behaviour (Wang et al., 2002b). Furthermore, integrity of matrix is associated with bone remodelling. Therefore, microstructure organisation heavily influences toughness of bone as a higher number of osteon results in increased fracture resistance and prevent micro-damage propagation (Wang and Puram, 2004). Zioupos (2005) proved that micro-cracks originate in interstitial, non-remodelled bone. Cement lines in secondary osteons have the function of blocking propagation of micro damage, which enhances fracture resistance ability of the bone. Finally, the influence of porosity in decreasing toughness is still in debate due to the fact that different testing directions provide contradictory data but it is clear that there is a correlation between the two phenomena (Wang and Puram, 2004; Augat and Schorlemmer, 2006).

4.5.7 Strength

Strength in cortical bone is highly dependent on the orientation of the specimen in relation to the loading direction: as a result, bone has been found to be 50% stronger in compression compared to tension (Wang, 2013). Once again, micro-damage accumulation (derived from cyclic loading) has been observed to affect bone strength as well as elastic properties due to the accumulation of micro-damage (Schaffler et al., 1995; Zioupos et al., 1996).

After bone has reached maturity at approximately 35 years of age, Zioupos and Currey (1998) found that there is an extra 3.7% decrease in strength by testing cortical femoral bone in compression. The same study revealed a great influence of porosity increase in

the loss of fatigue strength that accounts for nearly the 70% of the overall decrease. This strength loss has been correlated mainly with ash fraction as a change in mineral content but only if concomitant degeneration of organic matrix and tropocollagen in the specific, as mineral content does not play a central role when isolated, deproteinised bone is tested (Zioupos and Currey, 1998; Hernandez et al., 2001; Zioupos et al., 2008). Another study on the femur mid-shaft reported a loss in compressive stress and strain of respectively 5% and 9% per decade, showing the same negative trend (McCalden et al., 1997).

4.6 Concluding Remarks

At ~30 years of age skeletal maturity is reached. Until this point, it is possible to notice an increase in matrix quality and mechanical behaviour. Beyond this age, there is an inevitable degeneration that affects different bone components. A series of molecular changes in collagen (enzymatic and non-enzymatic) reduce strength and stability affect primarily plastic deformation. With age, crystals show an increase in size and a higher degree of crystallinity and stoichiometric impurity. This mainly affects the elastic deformation. These changes in crystallite geometry are also related to the increase of mineral content, which affects the mechanical properties in all aspects. Another important variation that has been reported is the decrease in bone mass which is linked to the deleterious increase in fracture risks (i.e. osteoporosis). These age-related changes will be considered and analysed in this study in order to elucidate the behaviour of rib cortical bone.

CHAPTER 5

MATERIALS AND METHODS

In order to investigate bone matrix ageing, a number of experimental procedures were combined in order to obtain information about the mineral, organic and water phase as well as tissue mechanical behaviour (Table 5.1). Appendix E provides demographics for the entire sample.

Table 5.1: *Combination of experimental procedures and target of the investigation related to them.*

Procedure	Mineral	Organic	Water	Mechanics	Histomorphometry
XRD	Yes	No	No	No	No
ATR-FTIR	Yes	Yes	No	No	No
TGA/DSC3+	Yes	Yes	Yes	No	No
Nanindentation	No	No	No	Yes	No
Microindentation	No	No	No	Yes	No
ImageJ RBS	No	No	No	No	Yes

The samples were taken from routine autopsies. Samples were taken from the sternal end of the 4th. One portion was degreased and cast in epoxy resin for indentation protocols while the rest was reduced to powder. The powder was analysed using X-ray diffraction to understand variations in crystal size/strain and lattice parameter. Thermal analysis (TGA/DSC3+) is used to obtain enthalpy values for collagen thermal degeneration and weight loss for organic and water phase, including mineral content. ATR-FTIR bridges these two procedures, allowing investigation of mineral crystallinity and overall matrix composition in terms of organic to mineral ratio. All these physicochemical parameters are then correlated to functional mechanical parameters to obtain a clear understanding of the age-related changes in rib cortical bone. The main objective of this

thesis is, however, to understand the efficiency of these variables for age estimation in forensic settings. For this purpose, stepwise regression is used and the results are systematically reported to quantify the efficiency of the models. The entire analysis was carried out in R, an open source software commonly used for statistical analysis. Using this, further evaluation of the effectiveness of the estimation method was also done. The experimental approach aims to simplify and standardise the procedures in order to respect the previously presented standards that apply to forensic anthropology. Figure 5.1 shows preparation and experimental procedures. For 10 randomly chosen samples a portion was not chemically treated in order to investigate the effect of the defatting procedure on bone matrix properties.

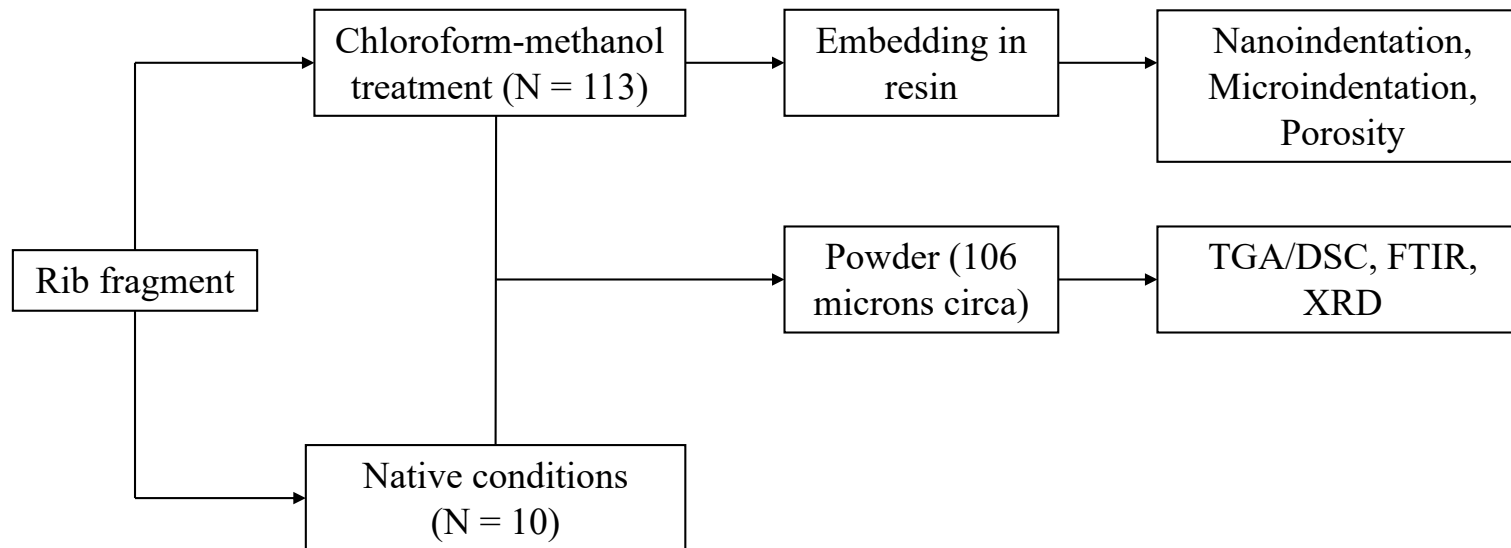


Figure 5.1: *Flow chart of preparation and experimental procedures.*

5.1 Study Sample

The skeletal material employed in this study consists of 113 sternal ends of the fourth right rib, ~5 cm in length collected at the Institute of Forensic Medicine in Tirana, Albania. The first cut was applied two centimeters from the sternal cartilage and the second cut five cm apart towards the spinal direction. This results in a five cm-long segment of bone. After removal, the samples were anonymised and kept in plastic boxes (replaced by airtight plastic bags at Cranfield University) and kept at -20°C. Table 5.2 shows demographics for the skeletal collection.

Table 5.2: *Sample demographics (SE = standard error of the mean).*

Sex	N	Min (yrs)	Max (yrs)	Mean Age (yrs)	SE (yrs)
Males	77	12	84	45.23	16.66
Females	36	19	84	44.57	16.88
Total	113	12	84	46.64	16.33

5.1.1 Ethical Approval

The study protocol was approved by the Ethics Committee of the University of Edinburgh (Ethics Assessment Level 2) and the Institute of Forensic Medicine (Protocol Number 795/3 A. Xh.) in Tirana, Albania. All methods were carried out in accordance with the approved guidelines and the appropriate standards that apply in the medico-legal context. The material was further cleared by the NHS Lothian Tissue Governance (reference number ICA01/17). Documentation is reported in Appendix A.

5.2 Sample Preparation

The autopsy material was collected at the Institute of Forensic Medicine in Tirana, labelled and stored in plastic labeled boxes providing the anonymous code. The specimens were store in Tirana at -20°C. When the number of specimens was sufficient to be shipped (after a maximum of ~ 2 years), it was sent in dry ice with a next day delivery formula. The sample was stored again at -20°C between preparation and experimental procedures. Furthermore, the bone were allowed to dry completely every time it was defrosted in order

to avoid the accumulation of artefactual micro-damage due to the increase of water volume when freezing, which would initiate a toughening process of the bone. Several studies have shown the effect of low temperature preservation on the mechanical properties of bone. It is generally accepted that there is evidence of an increase in strength and stiffness for -20°C (Pelker et al., 1984; Moreno and Forriol, 2002). This phenomenon is clearly related to the physicochemical modification of both mineral and organic components that the bone undergoes in these conditions (Moreno and Forriol, 2002; Andrade et al., 2008). Therefore, the experimental procedure was carried out, ensuring minimal storage time and avoiding repeated freezing and defrosting cycles.

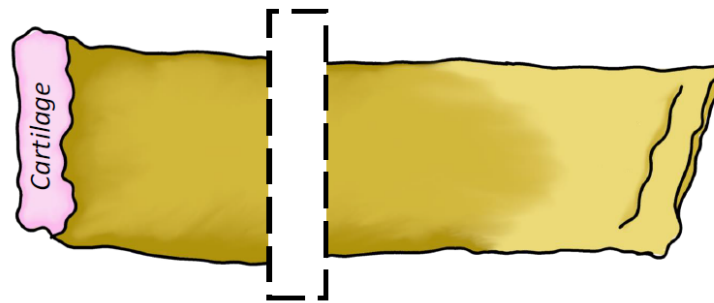


Figure 5.2: *Schematic representation of the sampling area in the proximity of the sternal rib end. The white area shows where thick section is sampled for nanindentation while the remaining bone away from the cartilage was used to obtain bone powder to be physically and chemically tested.*

A Struers[®] Accutom wafering saw equipped with diamond impregnated blade ($300\ \mu\text{m}$) cooled down using deionised water was used to produce two 3 mm thick cross section of the sternal portion of the rib (location is shown in Figure 5.2). The sections were high pressure washed to remove bone marrow and then degreased using a solution of chloroform-methanol in the ratio 1:1 for 36 hours. Subsequently, the samples were immersed in 100% ethanol for 12 hours and left overnight to dry at room temperature. This procedures aims to normalise any bias introduced by the amount of grease. More porotic bone is supposed to be able to store a larger amount of fat and marrow in the voids in the bone. This could influence measurements acquired by means of properties by means of

thermal and spectroscopic analysis. Due to the fact that the precise effect of treatment on mineral, organic and water fractions of bone is unknown ten specimens were tested both before and after the degreasing protocol.

The sections were cast in epoxy resin. After drying for 24 hours at room temperature, the sections were embedded in epoxy resin (Metprep Klear Set Type SSS) and metallographically polished using an automatic Struers RotoPol-15 with 203 mm silicon carbide abrasive disks grinding paper of decreasing grit size (400, 800, 1200, 2500) on a MasterTex cloth with Alumina 3B 6oz. The result is a mirror-like surface that enables magnification x20, as shown in Figure 5.3.

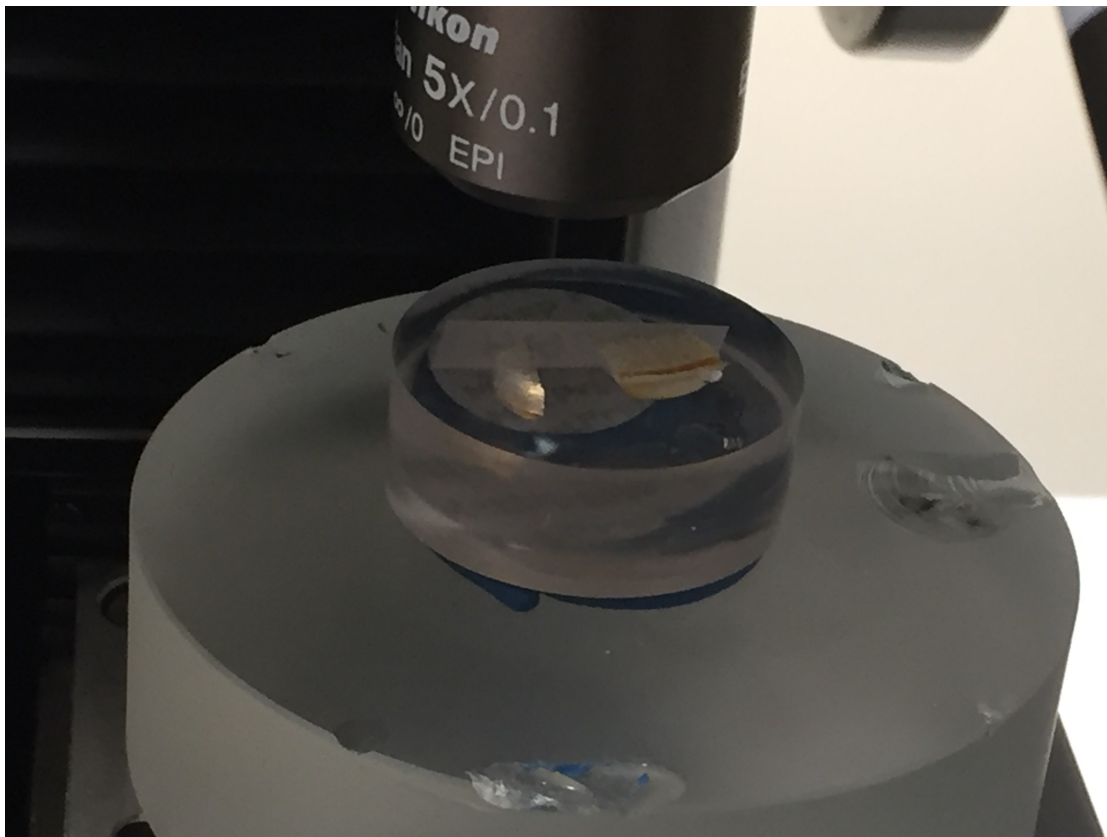


Figure 5.3: *Metallographically polished resin used for supporting bone during mechanical testing. On the surface is possible to see two fragments of bone embedded. This is used to support the specimen during indentation and to acquire pictures for histomorphometry.*

The remaining material was divided in two parts using the wafering saw. Trabecular

bone and periosteum were scraped off using a scalpel. Half of the bone was dried out completely at room temperature and the other half was treated following the chloroform-methanol procedure explained in the above paragraph. In order to obtain the powder, the material was processed using a Retsch Mixer mill 2000 by cycling for 1 minute and at 60 Hz. In between the two different cycles, the powder was filtered using a 106 μm sieve to guarantee particle homogeneity. The powder was left resting at room temperature the night before testing. In order to maintain consistency throughout the study, the same particle size (106 μm) was kept the same for chemical characterisation.

5.3 Image Analysis

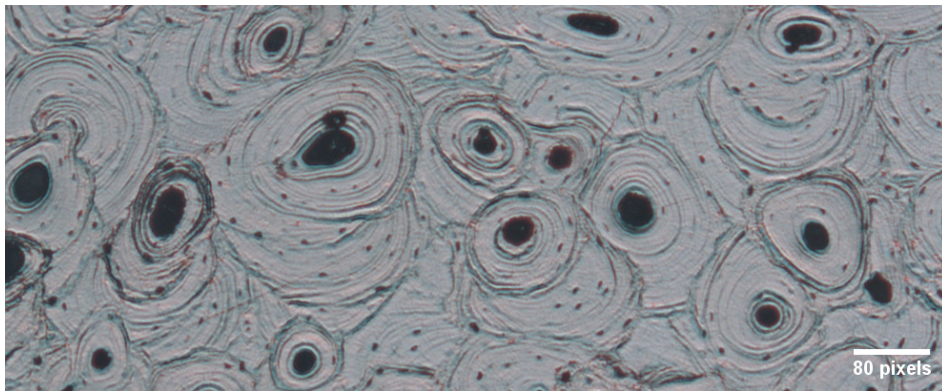
Optical porosity was obtained from four pictures taken for each specimen with a reflected light microscope 20x and the use of ImageJ RBS. Four locations were selected in order to sample the entire cortical area in the four quadrants, two sites on the pleural surface and two from the cutaneous surface. Each picture was cropped to select areas completely occupied by bone and converted into 16-bit images (Image > Type > 16-bit). The plugin BoneJ was employed to calculate automatically area fraction by applying a threshold mask (Plugins > BoneJ > Volume Fraction) (Figure 5.4). When some vascular canal area were not highlighted due to the different color of the background resin, these canals were filled in black using the Paintbrush Tool of ImageJ. This allows to repeat the automatic calculation in more accurate way.

Alternatively, the Polygon tool was used to first draw the contour of the total bone area of the image and measured (Ctrl+M). Further, the same tool was used to calculate the area of all vascular canals. Subtracting Total vascular area (sum of all vascular canal areas) from Total Area it is possible to obtain Bone Area. Bone Area and Total area was used to calculate porosity according to the Equation 5.1.

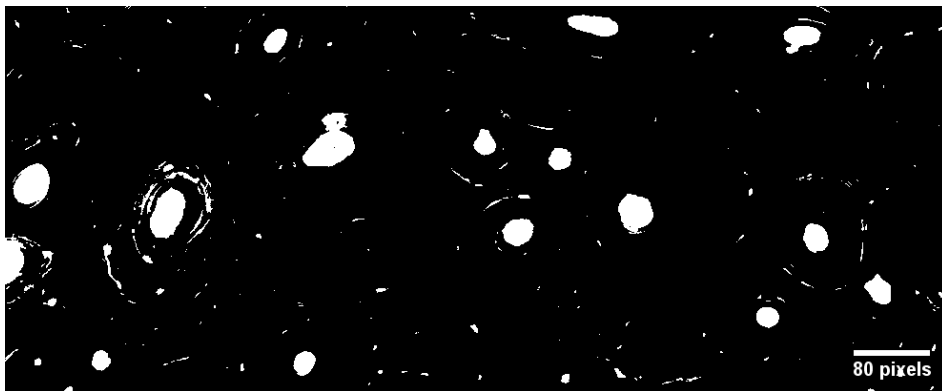
$$Porosity = \frac{BoneArea}{TotalArea} \quad (5.1)$$

Careful polishing of the sample and consistent thickness of the sections would allow

to avoid using the manual protocol. This represent the only technique that involves basic knowledge of bone microanatomy. However, the only features to be known are vascular canals so minimal training is required to carry out the procedure. Finally, the software is open source allowing maximum applicability.



(a) *Original*



(b) *Threshold mask applied*

Figure 5.4: *Transformation of images for porosity estimation. The black areas in the picture (b) are the bone surfaces while the white represents areas of porosity.*

5.4 Thermal Analysis

Differential scanning calorimeter is a simple and powerful instrument used to evaluate thermodynamic properties of biological and non-biological materials. It has been applied to bone to understand the deterioration of the collagenous matrix, effect of heat treatment and diagenetic processes in archaeological remains (Nielsen-Marsh et al., 2000; Lozano et al., 2003; Greenwood et al., 2012). In this study, differential scanning calorimetry will be applied to investigate water loss, collagen combustion and relationship with age. Kerch (2018) explains how water interaction plays a central role in protein conformation. In the specific case of bone, bond water gives collagen the structural stability that, ultimately, confers bone its plasticity. This is explained by the fact that the increase of cross-linking with age (especially non-enzymatic) reduces the amount of hydration sites and therefore the amount of bond water. Furthermore, it allows quantification of the organic fraction in the bone that is known to decrease with age combined with the increase in mineral content (Zioupos, 2001). The direct relationship between the three components is well explained in Figure 3.2 that shows the decrease in water and organic with the increase of mineral content (Zioupos, 2005). Therefore, this instrument is an ideal choice to investigate age related changes of collagen quality.

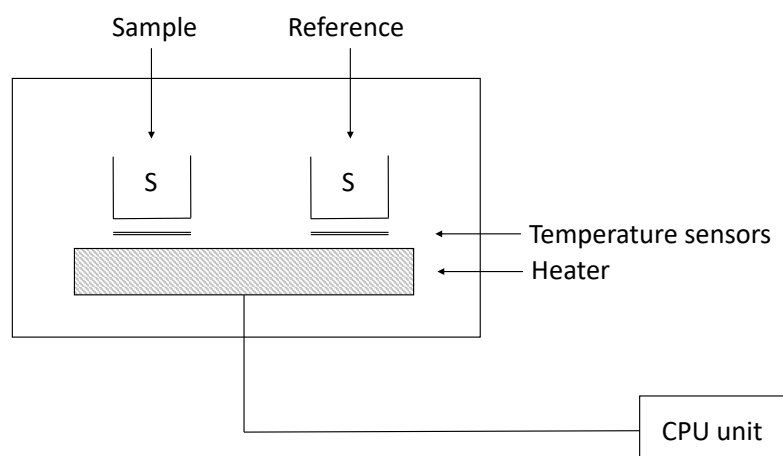


Figure 5.5: Schematic representation of DSC equipment, the sample and the reference pan are heated simultaneously in order to record heat flow variations for the sample only.

The sample and the empty reference were simultaneously heated in a crucible while measuring the heat flow as a function of temperature (Figure 5.5).

In terms of quantification, linear integration is employed to calculate enthalpy values (Jg^{-1}) and peak temperature ($^{\circ}\text{C}$) for the episodes as shown in Equation 5.2, where ΔH is enthalpy variation, R is heating rate, dQ/dt is heat flow changes and dT is temperature variation.

$$\Delta H = \int \frac{1}{R} \frac{dQ}{dt} dT \quad (5.2)$$

Data, normalised by sample size, are reported in a plot with heat flow (Wg^{-1}) and temperature ($^{\circ}\text{C}$) or/and time (min). Any changes inducing an increment in temperature are recorded as exothermic episodes. In Figure 5.6 (Pg. 96), the curve below show the heat flow as a function of temperature. Highlighted in blue is the endothermic peak for cortical bone powder from human ribs according to literature (Lozano et al., 2003; Miculescu et al., 2011). This peak ranging between 50 to 200 $^{\circ}\text{C}$ is representative of sample dehydration and collagen triple helix configuration breakage. As shown in Figure 5.6 with the blue portion of the curve, it corresponds to the negative enthalpy values that represent heat absorption (Miles et al., 2005). Enthalpy value as well as peak temperatures increase with the increasing collagen stability. Decreasing values are normally associated with the increase of age or certain pathological conditions such as osteoporosis (Kopp et al., 1989; Miculescu et al., 2011; Charmas, 2013). In contrast, the red exothermic peak represent the combustion of the organic matrix in bone which has a negative correlation with age (Miculescu et al., 2011; Bonicelli et al., 2017).

Gravimetric analysis is another approach to thermal investigation of bone matrix. The advantage of this procedure is the ability to record weight loss while dynamically heating the sample. This is a complementary method to DSC, employed to understand changes in mass related to the three main components of bone (water, organic and mineral). It is also an essential tool to understand mineral content. With age, a decrease in organic and water fraction is expected, coupled with the relative increase in mineral content (Zioupos, 2001;

Mkukuma et al., 2004). In order to be able to compare results for different specimens, weight loss is normalised by sample weight and reported in function reference temperature or time as can be seen in Figure 5.6 (Coats and Redfern, 1963). As seen for DSC, the crucible containing the sample is heated simultaneously with the reference sample and they are placed in a furnace equipped with a scale that records the weight loss (Coats and Redfern, 1963). Considering Figure 5.6, it is evident that there are two stages of weight loss: the first relative to the dehydration of the sample and collagen thermal denaturation (shown by DSC) and the second representing the loss due to the organic matrix combustion. The final weight indicates the amount of mineral matrix present in the sample (Lozano et al., 2003; Miculescu et al., 2011; Bonicelli et al., 2017). The main applications of TGA for bone material analysis focuses on the understanding of temperature exposure during burning and variation in bone mass according to ageing or pathological conditions (Kopp et al., 1989; Lozano et al., 2003; Mkukuma et al., 2004; Miculescu et al., 2011; Charmas, 2013).

In this thesis, Thermogravimetric analysis and Differential Scanning Calorimetry were performed using a TGA/DSC 3+ (Mettler Toledo[®], Indium calibrated). This increases consistency of the measurements and allows confident comparison between results of the two examinations. An initial increase in temperature between 25°C and 550°C at 10°C/min was followed by an isothermal combustion over 10 min at 550°C to completely eliminate the organic components and obtain ash content. Temperature in the chamber was controlled by a continuous flow of water at room temperature. The powder was tested in air in 20 mL aluminium pans with flat bases filled with ~10 mg of bone powder and the weight was recorded using a microbalance (Sartorius Genius ME235), while an empty crucible was used as a reference. The entire analysis was carried out using StarE V 15.00 software after normalising the results to sample size. Quantitative investigation involved the calculation of the percentage value of the two major weight losses in the TGA curve by linear tangent between temperature thresholds (Kopp et al., 1989; Miculescu et al., 2011): ~50-120°C and ~200-550°C as shown in Figure 5.6. Ash weight was calculated in a spreadsheet by subtracting the two percentage values from 100. The water weight

loss is believed to represent structural/bond water due to the dehydration induced by the chloroform-methanol preparation procedure (Unal et al., 2019). The same temperature intervals were taken as references in order to analyse linear integration values for enthalpy variation. The same limits were used in order to investigate enthalpy variation by means of linear integration of the peak under the curve.

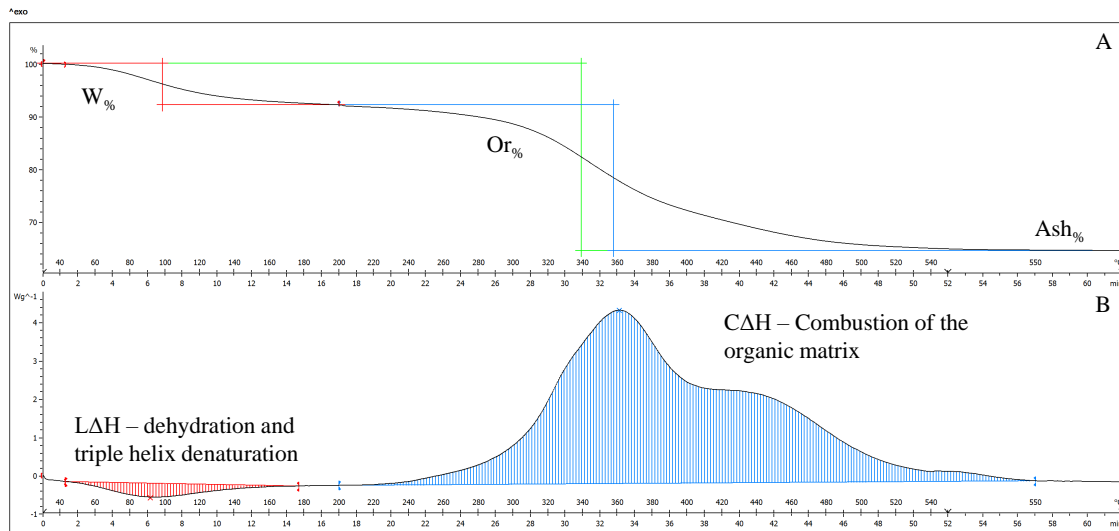


Figure 5.6: Example of TGA/DSC 3+ curve. Above (A) the TGA curve showing the two main weight loss characterising dehydration ($W_{\%}$) and organic combustion ($Or_{\%}$). At the end only mineral content is left ($Ash_{\%}$) that accounts for mineral content. In the DSC curve (B), in red sample dehydration and collagen degeneration, responsible for the breakdown of hydrogen bonds that confer the triple helix conformation to collagen fibres ($L\Delta H$), and in blue the combustion of the organic matrix peak ($C\Delta H$).

5.5 Powder X-ray Diffraction

X-ray diffraction is another powerful tool for apatite characterisation as it is informative of structural parameters of the material, such as strain, size crystallinity and eventual defects in the organisation. Diffraction is the constructive interference at a certain angle also intended as the coherent scatter of radiation. In other words, an x-ray beam is diffracted by a surface and recorded in a spectrum (diffractogram). The peak intensity is dependent on the

position of each atom in the lattice, the crystal unit. If the atoms are arranged periodically, a coherent spectrum in X-ray region will be observed. The angles of diffraction in this situation are therefore predictable and measurable, facilitating the calculation of not only spatial arrangement but also distances in Ångstroms, that will be converted in lattice and crystal size as well as strain values. At the beginning of the 20th century, William Henry and William Lawrence Bragg explained the phenomenon of diffraction as schematised in Figure 5.7 (Jenkins and Snider, 1997).

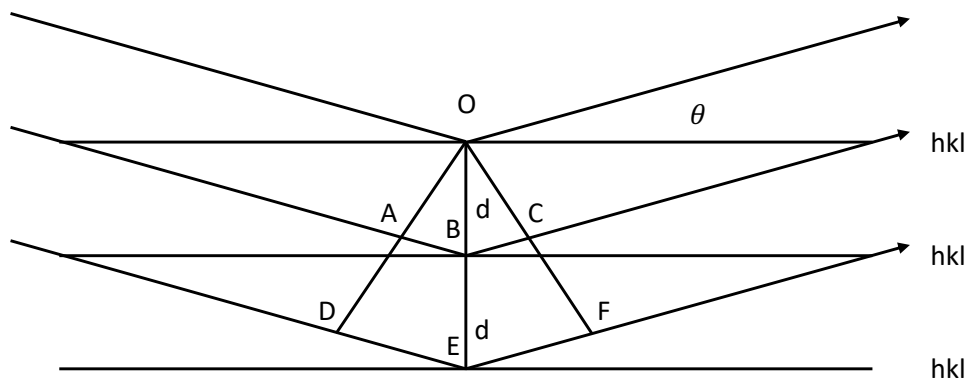


Figure 5.7: Application of the Bragg's law that shows the diffraction pattern for different crystallographic planes. Reprinted with permission from [John Wiley and Sons](Jenkins and Snider, 1997).

This model assumes that if the three beams are in phase then the incidence angle is equal to the reflection angle according to Snell's law. Further, assuming that distance ABC is equal to one wavelength (λ), DEF is considered equal to 2λ resulting in constructive interference. From this, Bragg's equation 5.3 was developed (Jenkins and Snider, 1997).

$$AB = d_{hkl} \sin \theta \quad (5.3)$$

XRD has been used in the analysis of bone mineral phase. The main advantage on analysing powdered material is the possibility to rotate the sample in order to increment the number of lattice plane under analysis. Furthermore, being base on the detection of the

diffraction pattern it is clear that the structure of a solid surface can affect the measurement. Powder analysis allows to avoid any geometry effect and to homogenise the sample to obtain more consistent results. For biological material the most common approach is profile fitting and line-broadening analysis in order to obtain a computation of crystallite size. This variation relates to lattice strain which manifests as peak broadening. Due to the difficulties in separately analysing variation in size and strain, what is normally employed are diffraction broadening methods such as Scherrer Equation 5.4 (Jenkins and Snider, 1997), where τ is the mean coherence length often referenced as crystallite size, K is a dimensionless shape factor ($k= 0.9$), λ is the x-ray wave length, β is the line broadening at half the maximum intensity of the selected peak (FWHM, integral breadth value), and θ is the Bragg angle (Jenkins and Snider, 1997). In biological HAp, the main causes of peak broadening are crystallite dimensions and lattice imperfection. In particular, lattice strain plays a central role in determining peak broadening. However, procedures for separating size and strain of crystallite have been proved to be ineffective and, therefore, coherence length has been largely used to observe this phenomenon (Greenwood et al., 2012, 2016).

$$\tau = \frac{K\lambda}{\beta \cos \theta} \quad (5.4)$$

Williamson and Hall (1953) is also the preferred method for isolated analysis of size and strain. It is based on the premise that size (β_L) and strain broadening (β_e) vary with the Bragg angle (θ). This single line procedure is calculated from convolution of the integral breadths of Lorentzian and Gaussian peak functions and it can be calculated from two reflections in the same crystallographic directions (Williamson and Hall, 1953; Greenwood et al., 2012).

$$\beta_L = \frac{K\lambda}{L \cos \theta} \quad (5.5)$$

$$\beta_e = C_\epsilon \tan \theta \quad (5.6)$$

K is the Scherrer shape constant, λ is wavelength, L crystallite size, θ the Bragg angle and β_e crystallite strain. Total broadening was measured from 002 and 004 peaks. Instrumental broadening was calculated using the Caglioti equation and subtracted from the total broadening (β_{sample}). Plotting this as function of $\beta_{sample}\cos\theta$ and $\sin\theta$, C_e is equivalent to the slope of the linear function and β_L to the intercept (Jenkins and Snider, 1997).

$$\beta_{sample} = \beta_L + \beta_e \quad (5.7)$$

$$\beta_{sample} = \left(\frac{K\lambda}{L\cos\theta}\right) + (4 \times C_e \tan\theta) \quad (5.8)$$

$$\beta_{sample}\cos\theta = \left(\frac{K\lambda}{L}\right) + (4 \times C_e \sin\theta) \quad (5.9)$$

This analytical technique has been employed in many different fields related to bone matrix analysis. A large body of literature is present regarding bone mineralisation/crystallisation and to understand the relationship between bone mineral and bone collagen (Weiner and Traub, 1992; Olszta et al., 2007; Greenwood et al., 2012; Wang et al., 2012) as well as the analysis of the effect of different conditions on mineral phase (Grynopas, 1993; Boskey, 2003; Greenwood et al., 2016). Another field that has largely employed XRD is the analysis of the effect of heat on bone mineral. This represents a crucial aspect in forensic investigation when accidental or voluntary incineration of the remains is involved (Greenwood et al., 2013; Thompson et al., 2013; Piga et al., 2016). Unfortunately, not many researchers have explored the effect of ageing on mineral architecture, leaving this field still open for new research opportunities (Handschin and Stern, 1992, 1995).

This study employs a pXRD sample holder with a glass spacer filled with bone powder for XRD analysis. PANalytical X'Pert PRO Multi-Purpose Diffractometer by means of a Cu K_α radiation was employed for the characterisation. Data collection was carried out across an angular range of 15–80 2θ ($^\circ$) (5.90–1.20 Å) using a PIXcel strip detector at

a count rate of ~ 1 second. Data was also collected for two further stepped scans under the same sample conditions but across an angular range of $23\text{--}27\ 2\theta$ ($^\circ$) ($3.86\text{--}3.30\ \text{\AA}$ d-spacing) and $50\text{--}55\ 2\theta$ ($^\circ$) ($1.82\text{--}1.67\ \text{\AA}$ d-spacing), and with a count time at each step equivalent to ~ 3 s. The two additional stepped scans were collected to provide greater quality data at the 002 and 004 Bragg maxima respectively. Asymmetrical split pseudo-voigt (SPV) peaks were fitted to the 002, 004, 030 and 210 diffraction maxima (as it represents satisfying compromise between intensity, overlapping and differing lattice direction) for all diffraction data. SPV peaks are an approximation to a voigt function which is a combination of Gaussian and Lorentzian peaks. From this data, the full width at half maximum (FWHM) of the 002 and 004 Bragg maxima was calculated. FWHM was also calculated from the $10\text{--}80$ angular range for the 030 and 210 peaks. The FWHM values were to calculate coherence length using the Scherrer equation. Figure 5.8 shows the location of the peaks under analysis in a typical human bone profile. In order to control the instrument resolution factor, a silicon standard (NB1640) was measured weekly and the factor is calculated by means of Caglioti equation.

Bruker Topas software (Version 4.1, 2008) was used for fitting of each diffraction profile. This provided quantitative crystallite size and morphology parameters through calculation of the coherence length and structural parameters of the crystal lattice. Coherence length was calculated for three orthogonal crystallographic directions, $\langle 00\ell \rangle$, $\langle hk0 \rangle$ and $\langle 0k0 \rangle$ using the Scherrer equation, which uses the instrument corrected, FWHM of the desired peak. Asymmetrical split pseudo-voigt (combination of Gaussian and Lorentzian peaks) were used to fit the peaks at 002, 004, 030 and 210 diffraction maxima. FWHM was used to calculate coherence length (CL) at all crystallographic directions under investigation. Coherence length is a calculation of both size and strain of the crystal showing positive relationship with size and negative with strain. Coherence length at 002 and 004 are, therefore, indications of crystal length along its main axis (the same long axis of the collagen fibre) while 210 (perpendicular direction to 002/004) and 030 giving an indication of width and thickness. The lattice parameters were calculated from whole pattern fitting refinement of diffraction profiles to obtain the 2θ peak positions. Considering the

difficulties in analysing peak broadening for biogenic hydroxyapatite, the high intensity peaks 002 and 004 were therefore selected to calculate crystallite size and lattice strain by means of the indirect Williamson-Hall model (Williamson and Hall, 1953; Rogers et al., 2010; Mote et al., 2012). Table B.1 shows the entire set of parameters acquired by means of XRD.

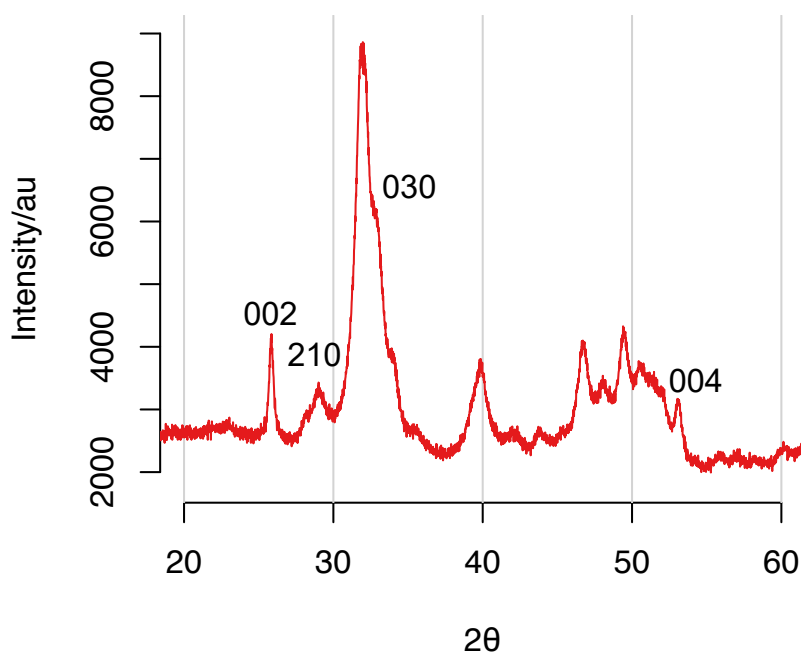


Figure 5.8: Example of XRD profile at 10-80 angular range indicating the main peaks under investigation with coherence length.

5.6 Fourier Transform Infrared Spectroscopy

Spectroscopic analysis is the investigation of the interaction between light and matter. A sample is excited with radiation in the mid-infrared region of the electromagnetic spectrum (between 4000 to 400 cm^{-1} wavelength). The sample absorbs a certain amount of transmitted light at each wavelength that can be measured as follows (Equation 5.10)

$$T = \frac{I_i}{I_0} \quad (5.10)$$

Where T is transmittance, I_i transmitted intensity and I_0 radial intensity. With a simple transformation is possible to convert transmittance in absorbance as shown in Equation 5.11.

$$A = -\log T \quad (5.11)$$

This allows the creation of a spectrum that plots absorbance as a function of wavenumber (cm^{-1}). Peak positions in an infrared spectrum correlate with molecular structure. In practice, when the infrared beam passes through the sample, a certain amount of energy is absorbed by permanent electrical dipoles of covalent bonds that have specific vibration frequencies. The frequency of the absorbed energy is proportional to resonant energy of specific bonds (Smith, 2002, 2011).

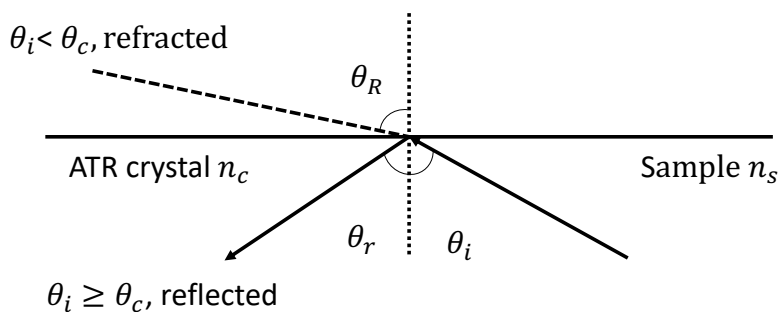


Figure 5.9: Schematic representation of refraction pattern of infrared light in a spectrometer in ATR mode.

Attenuated total reflectance (ATR) was used for this project and it relies on the principle of internal reflectance. In this case, light travels through a crystal of high refractive index (N_c) that meets the edge with a sample at lower refractive index (N_s). θ_i represents the incidence angle of the ray and the dotted line divides the reflection angle in to half angles. With a small incidence angle some of the beam will reflect off the internal surface

of the crystal. θ_R is the angle the refracted beam makes with the surface. The minimum angle of incidence at which total internal reflectance occurs in a material is called its critical angle, θ_c . Total internal reflectance occurs when $N_s < N_c$ and $\theta_i > \theta_c$. This principle allows the analysis of any substances (solids, polymers, and powders) that can be brought in touch with the crystal. Figure 5.9 shows the functioning of the spectrometer in ATR mode (Smith, 2002, 2011). Figure 5.10 shows the complex spectrum of bone powder. In the region $1800\text{-}1500\text{ cm}^{-1}$, there is the amide I band, representing the C-N and C=O bonds of the organic matrix. $1500 - 1350\text{ cm}^{-1}$ is the band for $\nu_3\text{CO}_3^{2-}$ while $\nu_2\text{CO}_3^{2-}$ is located between $900 - 850\text{ cm}^{-1}$. $\nu_1\text{PO}_4^{3-}$, $\nu_3\text{PO}_4^{3-}$ and $\nu_4\text{PO}_4^{3-}$ are observed in the regions respectively ~ 960 , $1200 - 900$, and $565 - 605\text{ cm}^{-1}$ (Thompson et al., 2011; Greenwood, 2014).

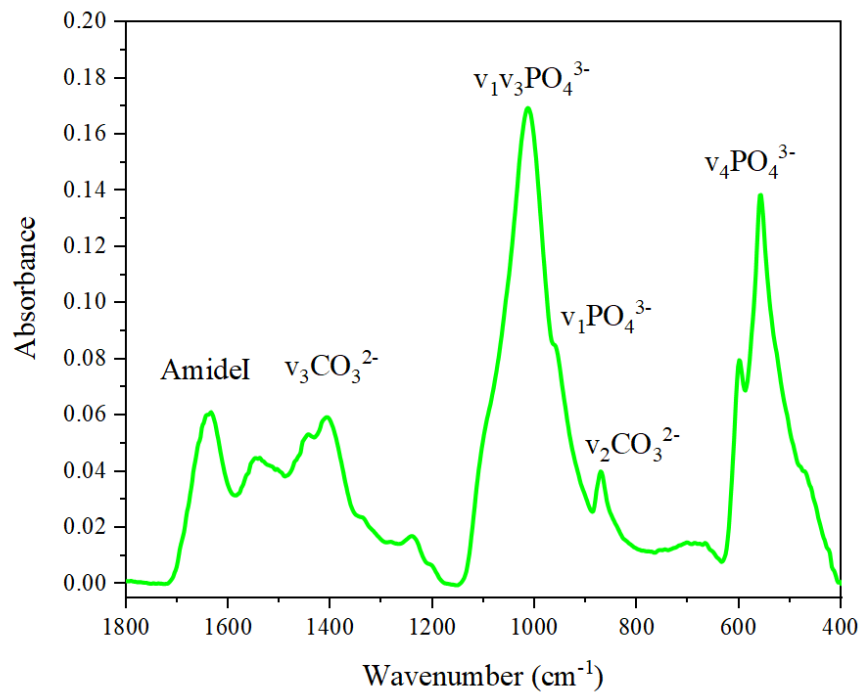


Figure 5.10: FTIR spectrum of human rib cortical bone.

Paschalis et al. (2001, 2003, 2011, 2014, 2017) largely employed this method in order to understand cross-links behaviour in relation to various factors such as type of bone (cortical, trabecular), ageing and pathological conditions (i.e. osteoporosis). Another common

field of application for spectroscopy is the analysis of mineral crystallinity in heat treated remains (Thompson et al., 2011, 2013; Greenwood et al., 2013) or due to age-driven ion exchange (Rey et al., 1989, 1991, 2007, 2009). To conclude, spectroscopy shows several advantages. The examination is quick, easy and inexpensive while providing a large amount of information regarding the molecular structure of the sample. Despite these advantages, this method can be complex and can provide ambiguous results when dealing with mixtures because it becomes more difficult to interpret what molecule the peak represents. Finally, a water peak between 3500 to 1600 cm^{-1} masks all the molecules solved in water (Smith, 2011). In forensic anthropology, FTIR was employed for determining *post mortem* interval (PMI). Wang et al. (2017) investigated taphonomic changes in 112 skull samples by means of FTIR. The specimens were artificially buried in different condition for a PMI between 76 and 552 days as well as left degrading on the surface of protection cage to avoid scavenging activities. Results for this experiment showed an increase in carbonate content and a decrease in organic for the buried bones. Furthermore, the authors were able to predict accurately the PMI of ~ 50 days for buried bones and ~ 70 days for unburied bones (Wang et al., 2017). These applications show the great potential versatility of this technique and is the reason why it was involved in the study.

In this study, spectra were collected by means of ALPHA T Platinum spectrometer (Bruker Optics[®]) in attenuated total reflectance mode (ATR). The range analysed is 4000-400 cm^{-1} with 4 cm^{-1} resolution for a total of 64 scans. Approximately 3 mg ($\sim 106 \mu\text{m}$ particle size) of bone powder were analysed. Due consideration is given to clean the holder and the crystal with deionised water before the first, and after each measurement. The measurements for the entire sample were carried out in the same conditions to maximise consistency. Spectral analysis was performed in Spectrum software 10.2 (Perkin Elmer). Due to the high variation in the spectral profiles due to levels of hydration of the powder, contact area between the crystal and the sample and amount of powder used during the examination spectra were not directly comparable. The aim of this examination is to offer semi-quantitative information of organic matrix, calcium and phosphate content of the bone matrix. The area under the curve was obtained by linear integration for the

Table 5.3: FTIR Variables (A = area of the peak, I = intensity of the peak). Baseline was set for all the different peaks separately.

Parameter	Abbreviation	Explanation
MM	$A_{1200-900cm^{-1}}/A_{1750-1600cm^{-1}}$	Integrated value of $\nu 3PO_4^{3-}$ over Amide I bands
CP	$A_{890-850cm^{-1}}/A_{1200-900cm^{-1}}$	Integrated value of $\nu 2CO_3^{2-}$ over $\nu 3PO_4^{3-}$ bands
CI	$I_{605cm^{-1}} + I_{565cm^{-1}}/I_{595cm^{-1}}$	Mineral crystallinity index calculated from the $\nu 4PO_4^{3-}$ peak
CC	$A_{1750-1600cm^{-1}}/A_{1200-900cm^{-1}}$	Integrated value of AmideI and $\nu 3PO_4^{3-}$ bands

peaks under investigation and the and the values were rationed. Mineral to matrix matrix ratio (MM) was calculated by the integrated area under the $\nu 3PO_4^{3-}$ bands ($1200-900\text{ cm}^{-1}$) and amide I ($1750-1600\text{ cm}^{-1}$) (Paschalis et al., 2017) and represents the amount of mineral normalised to the amount of matrix analysed. Similarly, carbon substitution (CP) was calculated by the band $\nu 2CO_3^{2-}$ ($890-850\text{ cm}^{-1}$) over $\nu 3PO_4^{3-}$ ($1200-900\text{ cm}^{-1}$) (Paschalis et al., 2017). Collagen content (CC) was calculated by Amide I band over $\nu 3PO_4^{3-}$ (Lebon et al., 2016). Finally, mineral crystallinity (CI) was calculated according to Thompson et al. (2011, 2013) investigating the distance between symmetric bands 565 cm^{-1} and 605 cm^{-1} of $\nu 4PO_4^{3-}$. Crystallinity is an overall indicator of crystal size and crystal lattice perfection of HAp. In contrast, mineral maturity is associated with the translation of unstable non-apatitic substance into more crystallised and stable ones, indicating the biological age of bone mineral. Variables are reported in Table 5.3.

5.7 Mechanical Analysis

Indentation remains one of the most effective tools in order to measure mechanical properties of the microstructure of several materials (Oliver and Pharr, 1992). This allows the calculation of hardness, defined as the measure of the resistance to yielding under pressure. In other words, it is the ability of a material to resist deformation due to a load applied. It is measured in units of pressure (load/contact area): Vickers hardness in normally mea-

sured in Kg/mm^2 while universal hardness values (H_{IT}) in GPa or MPa. Nanoindentation employs a pyramid shaped indenter (Berkovich diamond) in order to apply an impression on the material's surface. Different from microhardness, nanoindentation offers the possibility to know contact area at any point of the experiment allowing the calculation of the real hardness value and at the same time, estimate elastic modulus (Oliver and Pharr, 1992; Lewis and Nyman, 2008).

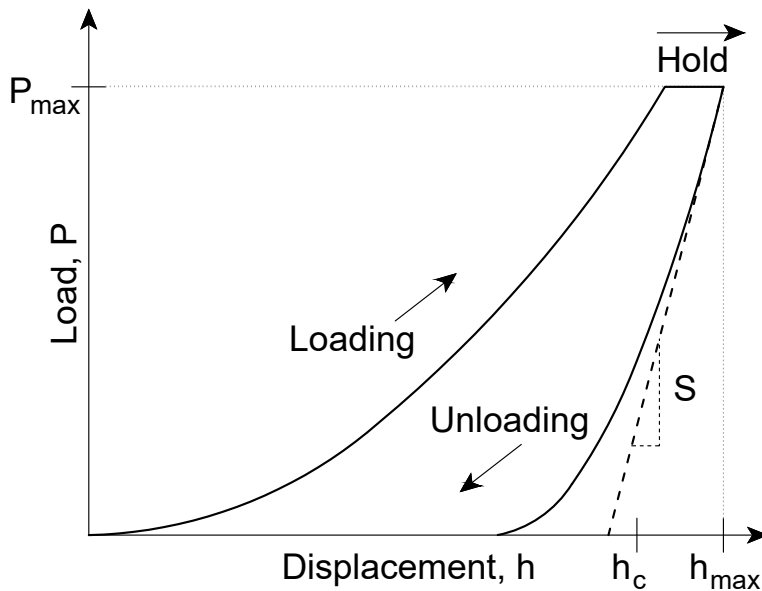


Figure 5.11: calculation of total work from the two portions of the indentation curve. The point G is where hardness is calculated and it is the point where load is maximum. After this point the unloading phase of the indentation curve starts and a tangent function is used to calculate elastic modulus.

Figure 5.11 shows the protocol normally applied to bone analysis with the load curve. Hardness is calculated at the end of the load at maximum depth (h_c and J) and maximum load (F_m and G) (Equation 5.12). In contrast, the elastic modulus can be obtained by the load/depth curve as the stiffness of the unloading portion of the indentation starting from the point G, given the Poisson's for the material ($\nu = 0.3$ for bone). From this experiment, hardness is calculated by Equation 5.12 (Oliver and Pharr, 1992):

$$H_{IT} = \frac{P_{Max}}{A} \quad (5.12)$$

Where P_{Max} is maximum load and A is the total area of the impression resulting from the indentation. The E_r , effective modulus is calculated using Equation 5.13, where S is the initial loading stiffness, A is the contact area and h_c contact depth. β for the triangular-based pyramid indenter is 1.034.

$$E_r = \frac{2\beta}{\sqrt{A(h_c)}} \quad (5.13)$$

Equation 5.13, when reduced for indenter-specimen combination, is also equal to:

$$E_{eff} = \left[\frac{1 - \nu_s^2}{E_s} + \frac{1 - \nu_i^2}{E_i} \right]^{-1} \quad (5.14)$$

Where ν_i and E_i refer to the Poisson's ratio and the elastic modulus of the indenter respectively and ν_s to the Poisson's ratio in the sample, assuming that the latter is homogeneous.

Additionally, the elastic work involved in the indentation was taken in consideration in order to better understand elastic properties of the material. This is achieved calculating the percentage value of the ratio between work under the elastic (W_{elast}) deformation portion of the load/depth curve and the sum of plastic and elastic deformation ($W_{total} = W_{plast} + W_{elast}$) according to 5.15 (Sawa, 2010). Figure 5.12 shows the areas under the curve considered for the calculation of the parameter.

$$\eta_{IT} = \frac{W_{elast}}{W_{total}} \times 100 \quad (5.15)$$

To conclude, the visco-elastic behaviour of bone will be analysed by means of indentation creep at the point when load is held stable over time. In practice, when the load is stable creep is given by the variation in indentation depth. This is a way to quantify the delayed response of the material to stress or strain. Although this parameter does not show the necessary consistency to assess age estimation, creep behaviour is found important in

order to understand qualitative changes associated with mechanical properties degeneration (Fischer-Cripps, 2004). Indentation creep is calculated by equation 5.16

$$C_{IT} = \frac{h_2 - h_1}{h_1} \times 100 \quad (5.16)$$

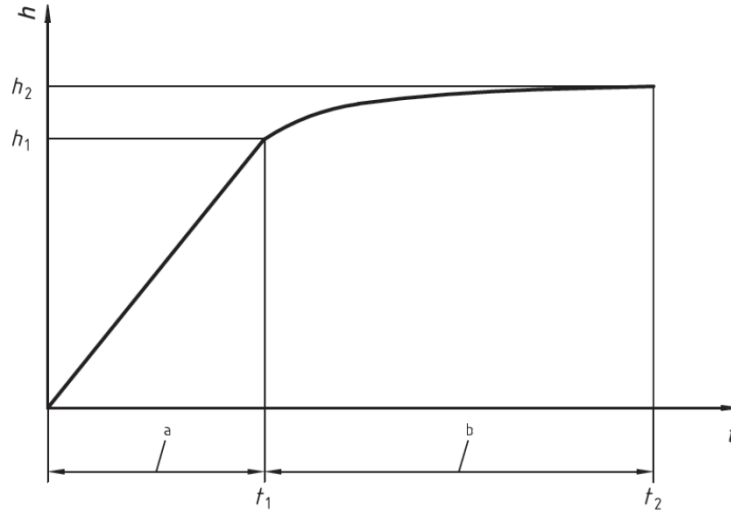


Figure 5.12: Indentation creep calculation from the time vs depth curve. h_1 is the indentation depth at time t_1 when maximum load is reached. h_2 is the indentation depth after t_2 when force is held constant.

In the present study, nanoindentation was performed using a CSM-NHT (system v.3.75, CSM, 2034 Peseux, Switzerland) instrument, at 10 mN maximum hold load (20 mN/min loading/unloading speed) with 30s long load/hold/unload stages. In order to perform this test, ~ 2 mm thick sections of bone are embedded in resin. The preparation procedure does not affect testing and supports the bone to allow enough stability for the very sensitive indenter to acquire the data (Rho et al., 2002). For each specimen, eight indentations were performed on each of four different secondary osteons and in the four surrounding interstitial bone areas nearby (Figure 5.13). Each osteon was chosen from different sectors of the bone (two from the pleural surface and two from the cutaneous surface, chosen according to the regularity of the surface). Universal hardness was calculated from load and contact area while elastic modulus was obtained (assuming Poisson's ratio value of ν

= 0.3) in the unloading phase as per the Oliver and Pharr method. Indentation creep was calculated by the proportional increase in depth occurring while the load is held at its maximum level (for 30s) and its measurement reflects the visco-elasticity of the tissue. The elastic portion of the indentation work was obtained by examining the percentage ratio of the elastically recovered energy over the total energy (elastic + plastic) input during an indentation sequence. Figure 5.12 shows a typical nanoindentation curve. During the test, attention was paid to avoiding factors that produce ‘experimental noise’, such as levelling the sample to allow the indenter to penetrate at right angles, minimising the external vibrations and discarding any asymmetric or problematic readings. Furthermore, the choice of load and depth of indentation would avoid any variations introduced by surface roughness. Ten lamellae per osteon were tested in order to obtain a meaningful mean value, avoid the effect of the rotated-plywood structure between consecutive lamellae and the variation in composition reported by (Ascenzi and Bonucci, 1968).

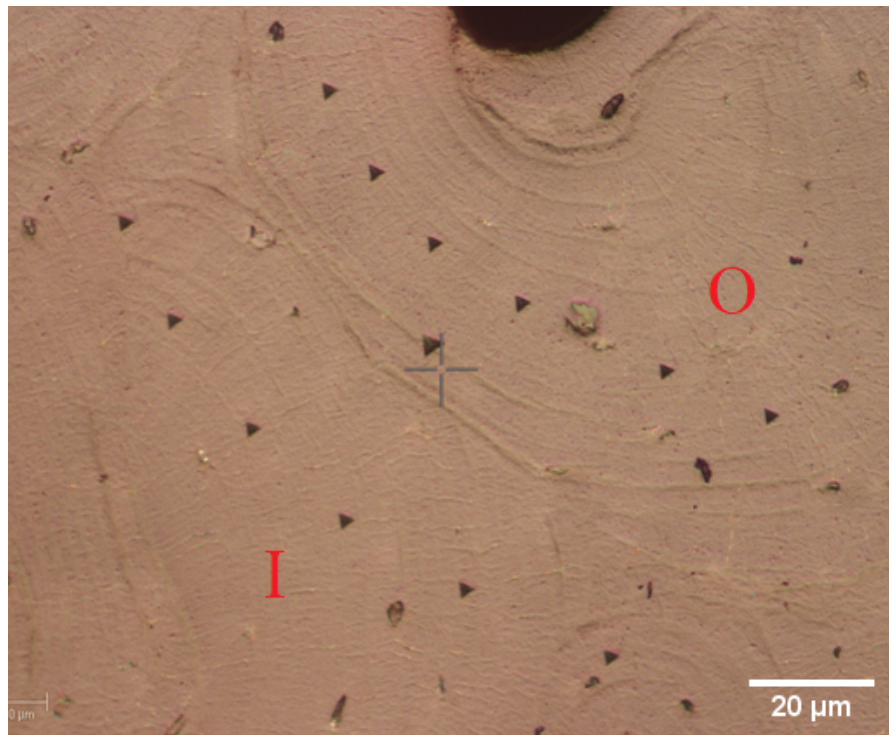


Figure 5.13: Nanoindentation impression on osteon (O) and interstitial bone (I). The small black triangle are the indentation impressions.

Vickers hardness (microhardness) testing procedure was developed by Smith and Sandly (1922). The diamond indenter of the square-based pyramid tip of the indenter leaves an impression on the surface of the sample that can be measured. Hardness is calculated from the ratio of force over area. This technique is still widely employed due to the fact that the procedure is easy and quick to do and results show very high consistency. Walden et al. (2017) have shown the potential of the application of this procedure in order to determine postmortem interval. They deposited femora, tibiae and fibulae of pigs in controlled burial conditions to understand how diagenesis affected bone matrix. Results showed that there is decrease in microhardness in both surface and burial depositions when tested along the transverse axis while it increases along the longitudinal axis. This variation is explained to be caused by changes in hydration and organic matrix (Walden et al., 2017). Similarly, due to consistency in results, microhardness tested was shown to be a good predictor of age (Bonicelli et al., 2017). In the multifactorial approach chosen for the study, the combination of micro-, nano-hardness and compositional analysis of the matrix showed promising results: age was predicted with 92% of accuracy and mean absolute error of 4.41 years (Bonicelli et al., 2017). An INDENTEC HWDM-7 instrument, equipped with a square-shaped pyramid diamond tip of $\theta = 136^\circ$, was employed to produce Vickers microhardness values for osteonal and interstitial bone areas for each specimen. The maximum load in these tests was set at 10 gf. The same areas selected for nanoindentation testing were examined applying one indentation on the osteon and one on the surrounding matrix for a total of eight indentations per section. Figure 5.14 shows how nanoindentation (triangle) allows to indent between lamellae.

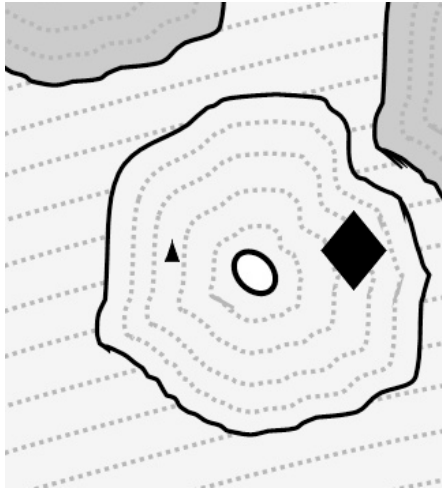


Figure 5.14: Schematic representation of a single osteon. The dashed grey lines represent the concentric lamellae while the solid black line the cement line. Nanoindentation (triangle) and microindentation (rhombus) location are shown.

5.8 Statistical Analysis

Statistical analysis was carried out in R 3.6.0 and the data for graphical representation of this section were randomly generated using the "simstudy" package ([CRAN.R-project.org/package = simstudy](http://CRAN.R-project.org/package=simstudy)) based on 30 data points. Descriptive statistics were first employed to inspect the entire set of variables and then divided by sex. Particular attention was paid to kurtosis and skewness as indicators for normal distribution. The value should fall in the ± 2 threshold to indicate normal distribution. Normality was further investigated using Shapiro-Wilk Test (S-W) with significance value set at $p = 0.05$. S-W is based on the correlation of data and corresponding normal scores (10) is the commonly used test for sample size < 40 . It assumes a null hypothesis that the sample is normally distributed and if the score shows significance, this hypothesis is rejected. It is the most widely performed test for its power of detecting small variation in normality. Although small variations are often shown, they should not account for major statistical violations (Shapiro and Wilk, 1965; Lucy, 2005; Ghasemi and Zahediasl, 2012).

5.8.1 Chloroform-methanol Defatting Procedure

Ten randomly chosen individuals were selected to explain what the effect of the previously described defatting procedures involving chloroform, methanol and ethanol consecutive baths (section 5.2). For these specimens a portion of the bone intended for powdering was spun in a plastic tube for twelve hours to remove superficial organic tissue and then milled following the procedure described in section 5.2. XRD, ATR-FTIR and thermal analysis were carried out according to the same protocol in order to evaluate changes in the matrix associated with the different preparation protocols. After assessing normal distribution of the two sets of measurements, differences for the two sets were investigated using analysis of variance (ANOVA).

5.8.2 Sex differences and General Variable Correlation

Sex differences were tested using the Mann–Whitney U test (M-W). M-W was applied as it is commonly used for two unrelated sets and because it does not include normality as one of its assumptions. Differences between males and females are normally easy to identify and this test represents the ideal choice for testing group differences. Variation between the two groups are considered with Z-score over 1.96 and p at 0.05 (Sheskin, 2003).

For all the normally distributed and homogeneous variables, T-test and analysis of variance (ANOVA) were also applied to evaluate mean differences considering significance at $p \leq 0.05$. These aim to test the hypothesis that the groups' means are equal (H_0). The same tests were applied after splitting the sample in individuals < 40 and > 40 years of age in order to understand the extent of differences before and after skeletal maturity. These age ranges were decided after visual assessing age variation by means of loess curve (Lucy, 2005).

In order to investigate physiological changes between different properties with age, Pearson's two-tailed correlations were applied to the entire pool of parameters. For those variables that do not show normal distribution, Spearman correlations were also used and

results for the two methodologies were compared (Lucy, 2005). The relationship between compositional and mean mechanical properties for the tissue as well as the relationship between compositional parameters of mineral and collagen was further investigated with backward stepwise regression analysis (Cook, 2005).

5.8.3 Age estimation

For age estimation, three tools were employed: linear regression models (LM), backward and forward stepwise regression and Bayesian information criterion (BIC) regression. In order to perform regression analysis, the dependent (response) variable was the known age-at-death for each individual. Independent variables (predictors) are the empirically calculated matrix properties. The relationship between predictors and response is shown in Equation 5.17 where Y is the response, X is the predictor, β_0 represent the intercept, β_1 is the coefficient of linear regression and ε is the mean-zero random error term (Lucy, 2005).

$$Y = \beta_0 + \beta_1 X + \varepsilon \quad (5.17)$$

This produced a model based on the best linear fit minimizing the least square criterion. Figure 5.15 shows a graphic representation of real values (x_1) and fitted values (y_1) where the full line shows the best fit and the errors are represented by the dashed lines.

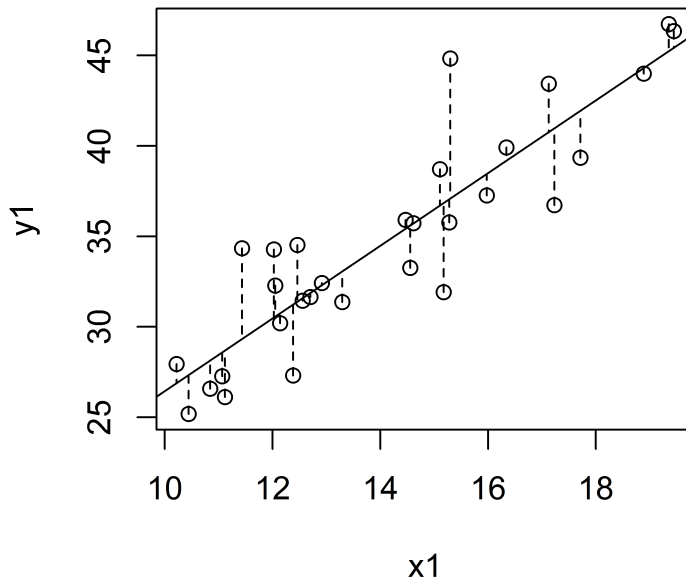


Figure 5.15: Example of best fit line and errors in dashed lines for each sample ($x1$ = real values, $y1$ = predicted values).

At first, the full set of variables was used to produce the unrestricted parameter selection. This aimed to simulate the ideal condition in which the entire set of tests could be performed without time restrictions in order to achieve the highest accuracy possible. To this model, stepwise selection was applied in order to automatically select the best combination of parameters that could give the highest degree of accuracy without compromising statistical integrity of the model. In each step, the variables are considered for subtraction based on the adjusted R^2 value reducing the loss of accuracy of the model (Lucy, 2005). Similarly, BIC variables selection aims to reduce the number of predictors in order to obtain the most reliable model based on the rule of the lower the values for AIC and BIC, the better the model performs. The main advantage of this technique is the increased accuracy for models involving large sample size. Overall, it is shown to perform better than R^2 based selection techniques (Gagné and Dayton, 2002).

In order to perform restricted selection criteria to meet different working conditions such as facility availability and time constraints, single linear models were produced for the parameters gathered with one or different combinations of predictors. The same automatic selection was applied to this model to achieve the best combination of significant parameters (Lucy, 2005).

Sex effect on age estimation was further investigated by analysis of covariance (ANCOVA) hierarchical linear regression. Sex was transformed into a dummy variables (male = 0, female = 1) to include it into the main linear regression models: PR1, PR2 and PR3. The predicted values of the original model and the one incorporating sex as a predictor were later tested using F statistic and chi-square test (Lucy, 2005). Three sex specific formulas were created. Despite the very high number of predictors and the fact that number of males and females is not equal, the choice of automatic parameter selection aims to maintain statistical robusticity of the models. Furthermore, in the following section a large number of regression diagnostic will be presented.

5.8.4 Regression Diagnostic

The accuracy of the models were evaluated by means of residual standard error (RSE), R^2 , R^2 -adj, Akaike information criterion (AIC) and Bayesian information criterion (BIC), multi-collinearity (tolerance level at <10) check and via visual assessment. Distribution of residuals was evaluate by means of S-W and autocorrelation of the model using Durbin-Watson test statistic (D-W) that ranges between 0 to <2 indicating positive autocorrelation and >2 to 4 is negative autocorrelation, with 2 showing no autocorrelation.

RSE is evaluated by mean standard deviation of ϵ according to Equation 5.18. This provides an absolute value of standard deviation in which the unit measure is the one of the independent variables (Lucy, 2005).

$$RSE = \sqrt{\frac{1}{n-2} \sum_{i=1}^n (y_i - \hat{y}_i)^2} \quad (5.18)$$

R represents the fraction of residual sum of squares (RSS) and the total (explained)

sum of squares (TSS) and therefore explains the amount of variance according to Figure 5.16 and Equation 5.19. It indicates the goodness of fit for the regression model and its value is between 0 and 1, with values close to 1 indicating a better fit (Lucy, 2005).

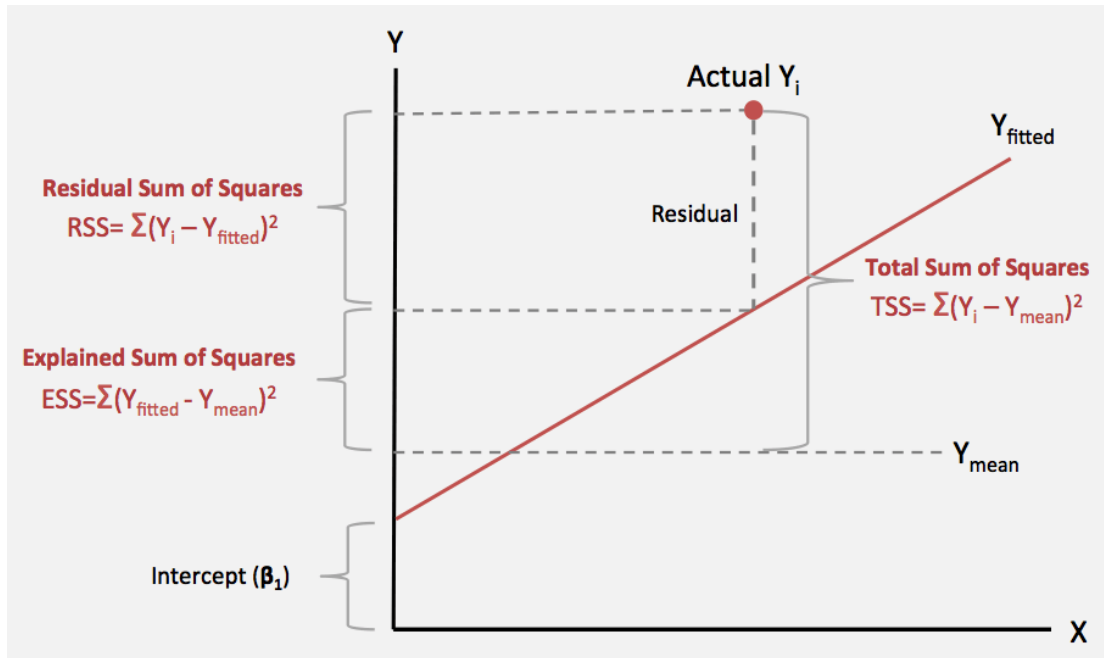


Figure 5.16: Graphic representation of R^2 calculation (www.machinelearningplus.com).

$$R^2 = 1 - \frac{RSS}{TSS} \quad (5.19)$$

In addition, R^2 -adj was used to compare different models. The main advantage relies on the fact that the increase in predictors does not necessarily determine an increase in R^2 -adj. It is calculated according to Equation 5.20, where MSE is the mean squared error and MST is the mean squared total.

$$R^2 - adj = 1 - \frac{MSE}{MST} \quad (5.20)$$

AIC and BIC are the other two parsimony indicators employed to understand the predictive power and robustness of the models. AIC is a measure of similarity between the observed model and the true model produced by the sample when potential of prediction

is considered. BIC, on the other hand, evaluates the probability that the model considered is the one appropriate for the sample (Burnham and Anderson, 2004; Kuha, 2004). Equations 5.21 - 5.22 show the calculation for AIC and BIC where θ is the maximum likelihood of the present model and p is the number of variables to be included in the model. AIC is an indicator of goodness of fit and the prediction error comparing model fit and complexity. BIC suggests the correct model against all given models.

$$AIC = 2[l(\hat{\theta}_2 - \hat{\theta}_1)] - 2(p_2 - p_1) \quad (5.21)$$

$$AIC = 2[l(\hat{\theta}_2 - \hat{\theta}_1)] - \log n(p_2 - p_1) \quad (5.22)$$

In Figure 5.17 it is possible to see the diagnostic plot for the regression models. First, the Residuals vs Fitted is useful to display non-linearity via the deviation between the red line and the best fit line. This plot also displays outliers, marking them with a number. Normal Q-Q plot was employed to assess distribution of the residuals against the ideal fit and the deviation from the line indicates a non-normal distribution of the residuals. The Scale-Location plot suggests variance of the distribution and should have equal distance from each point. Influential observations are evaluated using the Residuals vs Leverage plot (Lucy, 2005).

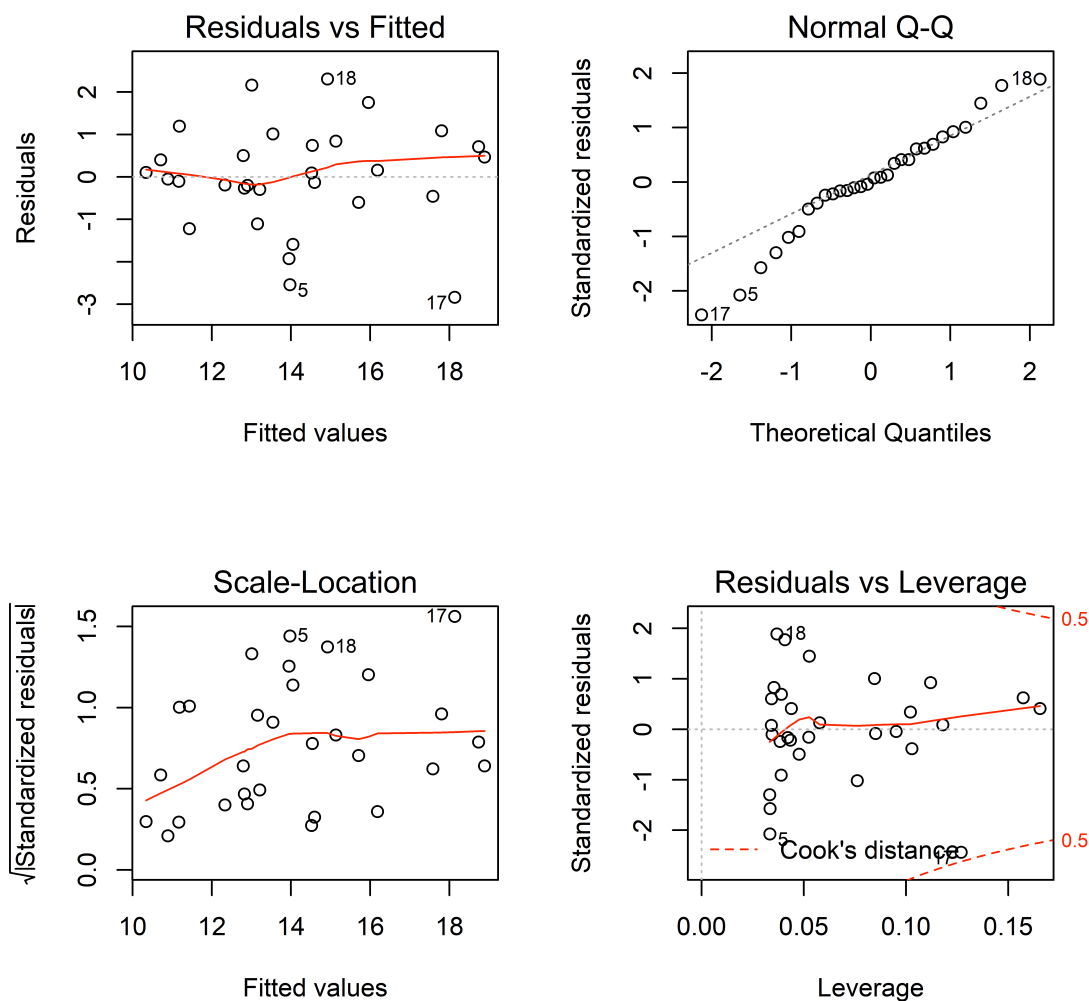


Figure 5.17: Diagnostic plots for regression analysis.

5.8.5 Cross-validation (CV)

As previously described in Section 5.8.3, cross validation of a prediction model involves splitting the sample into training and test sub-sample sets: 80% of the entire sample is used to develop the model while the remaining 20% is used to test the model accuracy. The sample was split avoiding modifying the mean value by 1-sigma. In this case, the assessment quality will be affected by the number of observations that are involved in

generating the model (Picard and Cook, 1984). This methodology was therefore excluded and other techniques were applied. K-fold cross validation was first applied to all the models developed. This resampling technique is based on the fact that k represents the number of groups the sample is divided into for testing the model. Each time, the entire dataset is randomly shuffled and one of these groups is used for testing the model while the rest is used as a training set. This represents a less biased cross-validation technique compared to the train/test splitting procedure (Bengio and Grandvalet, 2004; Fushiki, 2011). In this thesis, 10-fold and 10-fold repeated 3 times were performed. Finally, leave-one-out CV will be applied in order to test the accuracy of the models. In this case, k is equal to total number of data points and therefore the model is trained on the entire sample except for one point and the procedure is repeated a number of times equal to sample size (Arlot and Celisse, 2009). These techniques will be applied to all the models developed and mean absolute error (MAE).

5.9 Concluding Remarks

A broad variety of experimental procedures adopted were employed in this study in order to fully understand the composite and heterogeneous nature of bone at its age related modifications. This allowed investigation of both structural and compositional characteristics of organic and mineral phase as well as functional-mechanical properties of bone as a material.

Powder XRD is routinely used in crystallography and largely employed in the study of HAp crystallite structure. Different interpretation procedures were chosen in order to tackle the limitations given by the directional dependence of peak broadening in apatitic material. ATR-FTIR, is accessible and versatile, commonly used as a complement to XRD, for the possibility of simultaneously investigating both mineral and organic phase of HAp. The main limitation for this analytical technique is peak overlapping. To obtain a more broad understanding of organic matrix variation, DSC was employed to evaluate enthalpy changes during heat treatment and combined with TGA to record weight variation and obtain mineral content, an essential parameter to understand mechanical behaviour

of bone. Finally, mechanical analysis was carried out at tissue and microscopic level. This procedure has been proved to give extremely consistent results and allowed an understanding of the difference between structural levels. Figure 5.1 shows the procedures involved in this study and the different preparation methods of the samples. All the procedure were thoroughly explained in order to make the experiments repeatable and limit the impact of personnel experience in age-at-death estimation. The experimental design was conceptualised and realised in order to discuss the following aspects of the research:

- mechanical properties of cortical bone matrix;
- compositional properties of collagen and mineral phase;
- relationship between compositional and mechanical properties;
- structural relationship between mineral and organic matrix;
- effect of chemical preparation on chemical and physical analysis.
- Age related trends in physicochemical and mechanical changes of cortical bone rib matrix

CHAPTER 6

RESULTS

This study combines the mechanical and physicochemical analysis of rib cortical bone matrix using a multidisciplinary approach. The primary objective of which is to estimate the age-at-death while removing the influence of personnel experience. This was accomplished by means of DSC and TGA for thermal analysis, spectroscopy to characterise mineral and organic phase and XRD to obtain an indication of crystal size and crystallinity. Mechanical analysis was carried out by means of nano- and micro-indentation. The correlation between all these parameters would give a thorough understanding of the relation of structural and functional behaviour of bone with age.

This chapter will present the results of the various methods and analyses used in this research. In order to present the results systematically, the sections of this chapter are divided as follows:

- Section 6.1 will present the variation induced by the chloroform-methanol preparation method in the physicochemical properties
- Section 6.2 will present data distribution for all the variables.
- The sexual dimorphism's impact on specific variables is presented in Section 6.3.
- Subsequently, the trend analysis for different variables with respect to age is detailed in Section 6.4.
- The mineral-collagen interaction was investigated in this study and the results are presented in Section 6.5. The motivation for this arises from the lack of understanding of the mineral and collagen phase in ontogeny.
- Section 6.6 shares the results of the methods investigating the variation of the mechanical properties with age.

- Section 6.7 will provide results that will help to understand skeletal maturity in rib cortical bone.
- Unrestricted parameter selection was explored and the different models using all the variables available are tested (Section 6.8). The cross-validation methodology is also detailed.
- When restricted by the limitations of the testing machines, the variables were divided accordingly and the results of this process are detailed in Section 6.9. Sex specific formulas are presented in Section 6.10.

6.1 Chloroform-methanol Preparation

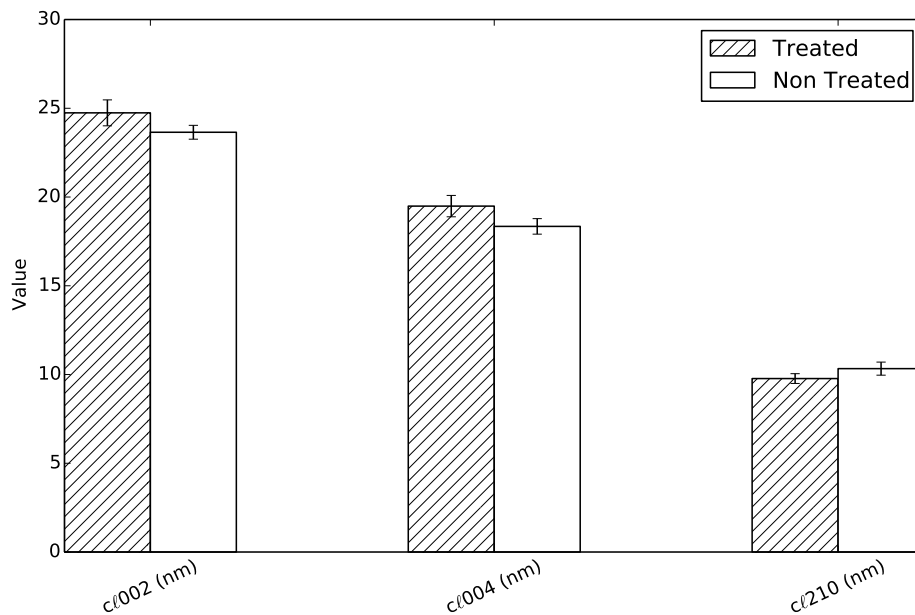


Figure 6.1: *Effect of treatment on coherence length at 002, 004 and 210 peaks.*

There is statistically significant difference between the two groups for CAH as determined by one-way ANOVA ($F(1,9) = 11.476$, $p = 0.01$) due to the reduced amount of grease in the treated sample. Additionally, the untreated group shows higher values for structural

water ($F(1,9) = 7.895$, $p = 0.023$). No other statistical difference were found for thermal analysis or infrared spectroscopy.

The main changes induced by this procedure are recorded for coherence length at several peaks (Figure 6.1). The treatment causes increased values for CL002 ($F(1,9) = 6.973$, $p = 0.03$) and CL004 ($F(1,9) = 9.4425$, $p = 0.02$) while values for CL210 are higher for native bone ($F(1,9) = 5.9113$, $p = 0.04$). This can be explained by an increase in size for the first two parameters and a decrease for CL210. In contrast, strain is lower for CL002 and CL004 and increased for CL210.

Water plays a central role in collagen quality. A very strong positive correlation was found between collagen thermal stability and $W\%$ ($p < 0.001$ and $R = 0.65$). This not only suggests that young collagen is in a better hydrated state but also that the defatting procedure allows removal of surface water, thereby preserving bone water. Furthermore, Unal et al. (2019) suggested negative correlation between water content and porosity is indicative of only bound water, while the opposite behaviour would suggest the presence of surface water. Considering the negative correlation between these two parameters ($R = 0.27$, $p = 0.003$), this parameter is intended to be bound/structural water.

Overall, the procedure proved to be effective in degreasing bone and removing surface water leaving structural water and collagen properties unaltered. Unfortunately, it induces ion substitution that causes alteration in crystallite size and variations in microstrain that need to be considered when designing an experiment. It is, therefore, appropriate for mechanical testing, thermal analysis and FTIR while could be problematic in the interpretation of XRD results.

6.2 Variables Distribution

Descriptive statistics for the entire set of variables are detailed in Tables 6.2 and 6.3. Age (mean = 45.23, SD = 16.66), which is treated as a dependant variable for estimation, shows normal distribution. A number of variables are not normally distributed, verified using the S-W test. $Po.Ar\%$ does not show any extreme values for skewness and kurtosis but S-W tests show different results (S-W = 0.98, $p = 0.03$). Considering mechanical properties,

only two variables are not normally distributed: ^{On}E (S-W = 0.98, $p = 0.04$) and ^{It}H (S-W = 0.96, $p = 0.001$). DSC parameters violate normal distribution. LΔH and CΔH do not violate the rules for skewness and kurtosis but S-W tests disagree with these results and show S-W = 0.97, $p = 0.01$ and S-W = 0.98, $p = 0.04$, respectively. Moreover, Ash_% show S-W = 0.96, $p = 0.004$. All the ATR-FTIR results violate the assumption for S-W test, while only collagen content tends to violate kurtosis assumptions. The final variable that violates kurtosis and distribution test is Size (S-W = 0.98, $p < 0.001$). Spearman Rank correlation method was employed to corroborate Pearson's results. This confirms the same relationship despite the violation of normalcy. Despite the fact that a number of variables violate normal distribution assumption this is not supposed to affect parametric methods and regression analysis. The non-normal distribution is here attributed to the large sample size ($N > 40$) (Ghasemi and Zahediasl, 2012). Table 6.1 shows results for Saphiro-Wilk test.

Table 6.1: Results for S-W test shows violation of normal distribution for certain variables due to the large sample size (*: $p \leq 0.05$).

Variable	Statistic	p-value	Variable	Statistic	p-value
Age	0.982	0.119	Or _%	0.987	0.338
PoAr _% *	0.974	0.0267	Ash _% *	0.963	0.004
^{On}H	0.981	0.116	MO*	0.923	6.188^{-06}
^{On}E *	0.976	0.0409	CP*	0.923	6.373^{-06}
$^{On}C_{IT}$	0.994	0.906	CI*	0.773	6.428^{-12}
$^{On}\eta_{IT}$	0.987	0.377	CC*	0.807	7.163^{-11}
^{It}H *	0.957	0.001	Strain	0.987	0.325
^{It}E	0.980	0.091	Size*	0.844	1.483^{-9}
$^{It}C_{IT}$	0.983	0.150	CL002	0.992	0.724
$^{It}\eta_{IT}$	0.991	0.695	CL004	0.980	0.091
^{On}HV	0.989	0.518	CL030	0.990	0.555
^{It}HV	0.979	0.066	CL210	0.994	0.902
LΔH*	0.970	0.012	'a' axis	0.984	0.210
CΔH*	0.976	0.042	'c' axis	0.984	0.193
W _%	0.986	0.272			

Table 6.2: Descriptive statistic for mechanical parameters (*SD* = standard deviation; *Min* = minimum; *Max* = maximum; *Se* = standard error; *Mad* = mode).

Variable	Mean	SD	Median	Trimmed	Mad	Min	Max	Range	Skewness	Kurtosis	SE
Age	45.23	16.66	45.00	44.87	19.27	12.00	84.00	72.00	0.14	-0.74	1.57
Po.Ar%	5.95	2.07	5.85	5.88	2.49	2.07	10.60	8.53	0.23	-0.77	0.20
<i>On</i> H	46.01	9.40	45.29	46.01	11.10	24.85	69.19	44.34	0.06	-0.79	0.88
<i>On</i> E	17.75	2.14	17.75	17.73	2.48	13.73	22.86	9.13	0.06	-0.88	0.20
<i>On</i> C _{IT}	4.93	0.80	4.93	4.95	0.77	2.68	6.84	4.16	-0.13	-0.13	0.08
<i>On</i> C _{IT}	21.69	2.06	21.56	21.63	1.70	16.94	27.33	10.39	0.29	0.06	0.19
<i>It</i> H	50.22	9.97	49.38	50.10	12.57	32.71	69.93	37.22	0.10	-1.18	0.94
<i>It</i> E	20.17	2.49	20.03	20.11	2.34	15.31	26.34	11.03	0.27	-0.52	0.23
<i>It</i> C _{IT}	5.33	0.66	5.37	5.35	0.64	3.43	6.80	3.38	-0.36	0.07	0.06
<i>It</i> C _{IT}	20.84	1.78	20.81	20.81	1.55	16.41	26.95	10.54	0.23	0.62	0.17
<i>On</i> HV	33.36	5.14	33.75	33.49	4.71	21.10	47.70	26.60	-0.08	-0.08	0.48
<i>It</i> HV	39.20	5.00	39.43	39.49	5.19	25.58	48.75	23.17	-0.44	-0.33	0.47

Table 6.3: Descriptive statistic for physicochemical parameters (*SD* = standard deviation; *Min* = minimum; *Max* = maximum; *Se* = standard error; *Mad* = mode).

Variable	Mean	SD	Median	Trimmed	Mad	Min	Max	Range	Skewness	Kurtosis	SE
LΔH	159.84	17.45	156.40	159.33	17.91	121.80	197.79	75.99	0.28	-0.56	1.64
CΔH	3307.84	280.13	3276.54	3292.93	290.25	2714.55	3974.58	1260.03	0.41	-0.46	26.35
W _%	8.60	0.65	8.59	8.60	0.62	7.23	9.96	2.74	0.05	-0.51	0.06
Or _%	28.09	1.02	28.02	28.04	0.97	25.70	30.82	5.12	0.35	-0.05	0.10
Ash _%	63.31	1.36	63.51	63.42	1.25	59.24	65.96	6.72	-0.69	0.14	0.13
MM	6.82	0.78	6.97	6.91	0.64	4.45	8.05	3.60	-1.06	0.94	0.07
CP	0.02	0.00	0.02	0.02	0.00	0.01	0.03	0.01	0.97	0.84	0.00
CI	0.99	0.06	1.01	1.00	0.02	0.80	1.09	0.29	-1.55	1.56	0.01
CC	0.15	0.02	0.14	0.14	0.01	0.12	0.22	0.10	1.89	3.84	0.00
Strain	0.01	0.00	0.01	0.01	0.00	0.00	0.01	0.01	0.34	-0.02	0.00
Size	32.31	3.37	31.95	31.95	2.37	25.53	49.67	24.14	2.04	7.25	0.32
CL002	23.73	0.86	23.73	23.72	0.95	21.79	25.79	4.00	0.03	-0.54	0.08
CL004	18.83	1.02	18.77	18.82	1.11	16.45	20.97	4.52	0.08	-0.63	0.10
CL030	8.23	0.38	8.26	8.23	0.32	7.20	9.43	2.22	0.04	0.67	0.04
CL210	9.74	0.93	9.70	9.73	0.89	7.61	12.17	4.56	0.08	-0.27	0.09
'a' axis	9.42	0.00	9.42	9.42	0.00	9.41	9.43	0.02	0.24	0.17	0.00
'c' axis	6.90	0.00	6.90	6.90	0.00	6.89	6.91	0.02	0.21	0.53	0.00

6.3 Sex Differences

The non-parametric M-W test proves that sexual dimorphism only affects three of the variables. $C\Delta H$ is significantly higher for the male group ($U = 1752$, $p = 0.024$) while the opposite trend is shown with respect to crystal size ($U = 901$, $p = 0.003$).

Further investigation by T-test and ANOVA proved that sexual dimorphism affects the same two variable and $Or_{\%}$. T-test shows significant differences for $C\Delta H$ ($t = 2.17$ and $p = 0.03$) with higher values of thermal stability in the combustion peak for samples of male in comparison to female. This result is supported by sex related differences in $Or_{\%}$ and the weight loss for the organic combustion, which follows a similar trend as before ($t = 1.98$ and $p = 0.04$). In contrast, values of crystallite size are higher for females compared to their male counterparts ($t = 2.08$ and $p = 0.04$). Similar results are obtained from the ANOVA analysis and reported in Tables 6.4 and 6.5. In terms of age estimation, the effect of sex will be presented according to results obtained by hierarchical linear regression for the main prediction models in the following sections. Figure 6.2 shows the three variables that proved to be different.

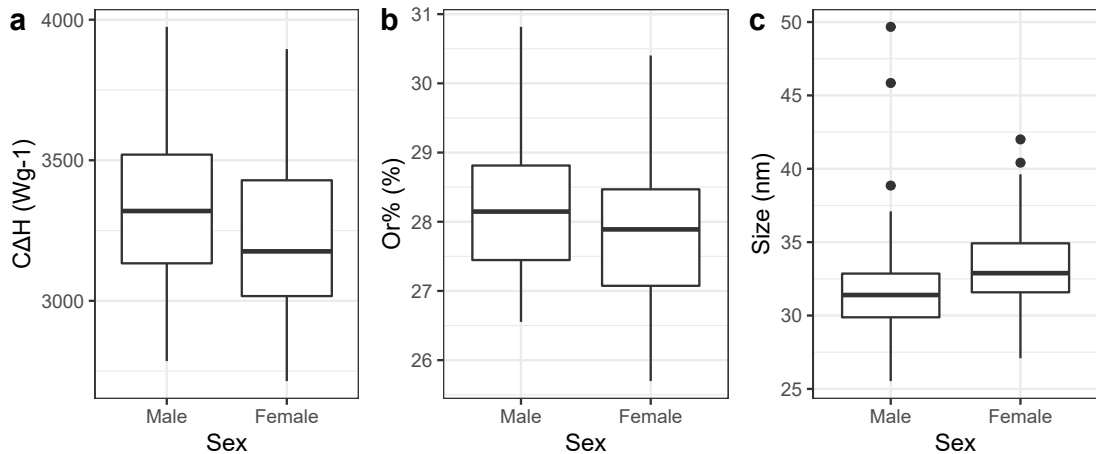


Figure 6.2: Box plots of the variables that show significant difference according to sex.

Table 6.4: Mean values and standard deviation for the sample split between male and female for mechanical parameters. Results for t-test and ANOVA (SD = standard deviation; *: $p \leq 0.05$).

Parameter	Male (N = 77)		Female (N = 36)		Anova		T-test	
	Mean	SD	Mean	SD	F-value	P-value	t-value	P-value
Po.Ar%	6.036	2.148	5.774	1.925	0.625	0.533	0.3901	0.533
^{On}H	45.432	9.802	47.252	8.456	0.959	0.340	0.920	0.340
^{On}E	17.616	2.120	18.043	2.171	0.990	0.325	0.979	0.325
$^{On}C_{IT}$	4.984	0.719	4.826	0.958	0.971	0.334	0.943	0.334
$^{On}\eta_{IT}$	21.466	1.930	22.167	2.269	1.700	.0919	2.891	0.092
^{It}H	49.703	10.375	51.313	9.081	0.799	0.426	0.638	0.426
^{It}E	19.971	2.377	20.581	2.692	1.219	0.226	1.485	0.227
$^{It}C_{IT}$	5.381	0.639	5.223	0.711	1.177	0.242	1.386	0.242
$^{It}\eta_{IT}$	20.713	1.638	21.099	2.043	1.08	0.283	1.1667	0.283
^{On}HV	33.019	5.079	34.102	5.274	1.043	0.299	1.089	0.299
^{It}HV	38.827	4.926	39.994	5.144	1.157	0.250	1.338	0.250

Table 6.5: Mean values and standard deviation for the sample split between male and female for physicochemical parameters. Results for t-test and ANOVA (SD = standard deviation; *: $p \leq 0.05$).

Parameter	Male (N = 77)		Female (N = 36)		Anova		T-test	
	Mean	SD	Mean	SD	F-value	P-value	t-value	P-value
LΔH	159.524	17.503	160.520	17.549	0.282	0.779	0.079	0.779
CΔH*	3346.229	263.782	3225.740	299.735	2.165	0.0325	4.688	0.0325
W _%	8.619	0.629	8.558	0.686	0.472	0.638	0.223	0.638
Or _% *	28.219	0.984	27.815	1.057	1.984	0.050	3.934	0.0498
Ash _%	63.161	1.363	63.627	1.304	1.717	0.089	2.948	0.0886
MM	6.781	0.735	6.893	0.869	0.714	0.477	0.510	0.477
CP	0.019	0.003	0.019	0.003	0.280	0.780	0.079	0.780
CI	0.992	0.057	0.981	0.063	0.898	0.371	0.808	0.371
CC	0.149	0.019	0.146	0.021	0.953	0.343	0.908	0.343
Strain	0.007	0.00	0.007	0.001	1.098	0.275	1.205	0.275
Size*	31.867	3.413	33.263	3.127	2.078	0.040	4.319	0.040
CL002	23.622	0.841	23.956	0.864	1.956	0.053	3.826	0.0530
CL004	18.843	1.036	18.811	0.998	0.155	0.877	0.024	0.877
CL030	8.208	0.378	8.263	0.378	0.721	0.472	0.520	0.472
CL210	9.672	0.948	9.876	0.882	1.091	0.278	1.190	0.278
'a' axis	9.416	0.003	9.417	0.003	.813	0.418	0.660	0.418
'c' axis	6.904	0.003	6.903	0.003	1.620	0.108	2.625	0.1081

6.4 Age Related Changes

In this section, the significant trends between the different variables and age will be described using Pearson's correlation coefficient and R value. Each subsection is dedicated to individual experimental procedures employed in this study.

6.4.1 Optical porosity

Porosity showed the most promising correlation with age among all the variables. The strong increase is described by $p < 0.001$ and $R = 0.83$. The deviation tends to increase regularly until 40-45 years of age while the variation from the regression relationship (regression line) increases for older ages. This is best explained by the probability of variations due to pathological conditions or normal individual in Figure 6.3.

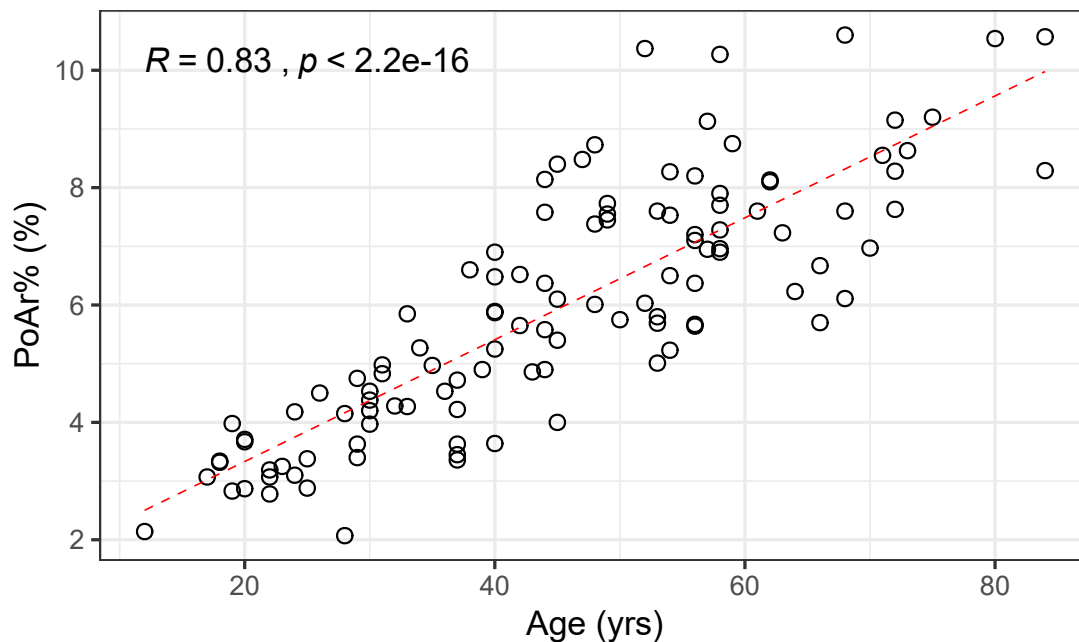


Figure 6.3: Scatter plot of the increase in $Po.Ar\%$ with ageing. It can be seen that there is a decrease in correlation with the increase of age.

Surprisingly, no significant difference between sexes is shown for this variable that is the most affected by the impaired turnover induced by hormonal changes (e.g. menopause). There is also a negative correlation between porosity measurement and the properties

related to the organic matrix. In specific with $L\Delta H$, $W\%$, $Or\%$ and CC (respectively $p < 0.001$, $p = 0.003$, 0.011 and 0.003). Moreover, $Ash\%$ ($p < 0.001$) and CP ($p < 0.001$) increase with increasing porosity.

6.4.2 Thermal Analysis

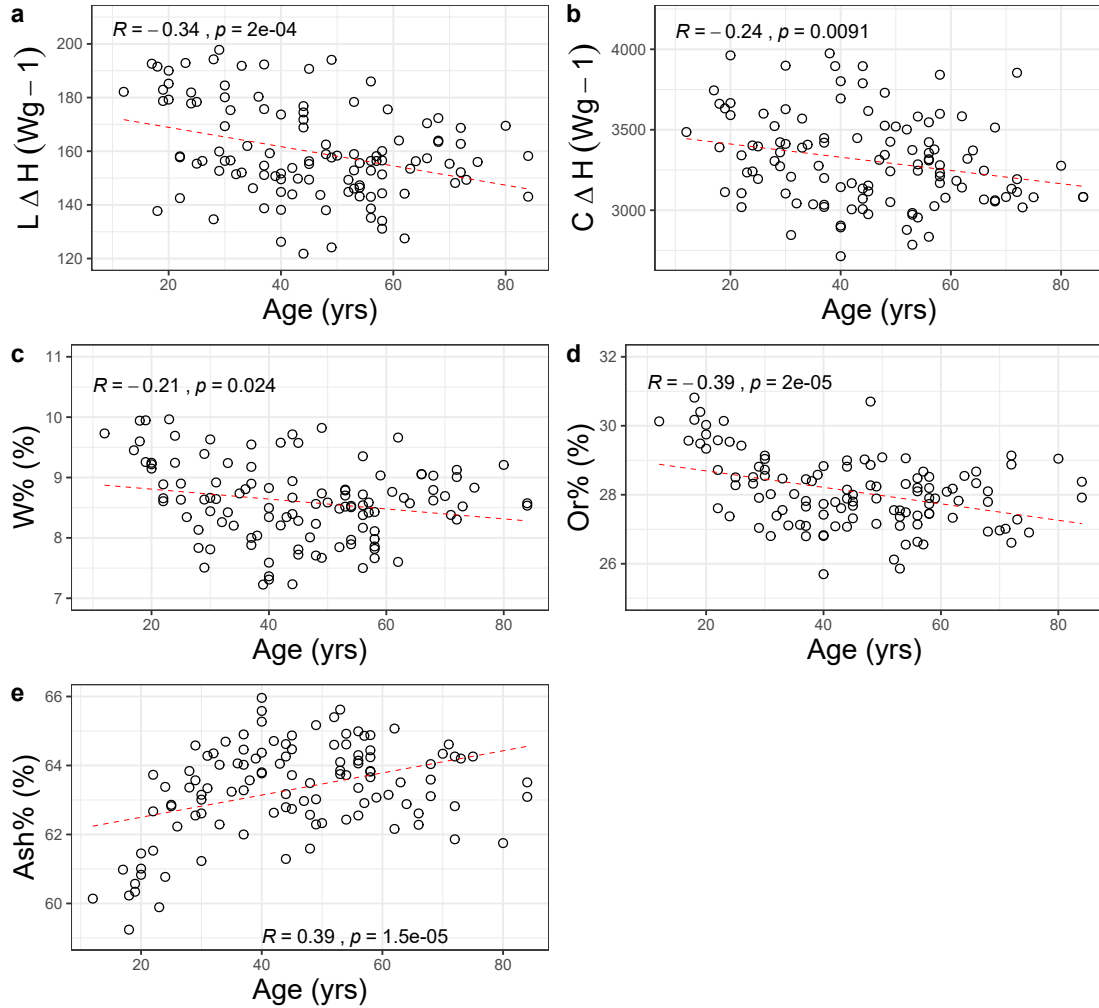


Figure 6.4: Variation of thermal analysis parameters at different ages. With age there is a general increment in mineral content (e) combined with the degeneration of collagen quality and content.

Dynamic heating of bone powder showed that both collagen shrinkage and organic matrix combustion decrease their enthalpy values with age. For instance, $L\Delta H$ and $C\Delta H$ negative

correlation with age is explained by $p < 0.001$ and $p = 0.009$, respectively. As can be seen from Figure 6.4, the peak responsible for the triple helix degradation (a) shows better correlation compared to the exothermic peak (b) possibly due to the fact that enthalpy responsible for the organic combustion involves other non-collagenous proteins present in bone.

There were no statistical differences between sexes for LΔH. Similarly, a decrease in water content ($p = 0.024$, $R = 0.21$) and organic weight loss ($p < 0.001$, $R = -0.39$) due to combustion was seen and quantified with thermogravimetric analysis. In contrast, the ash content tends to increase ($p < 0.001$, $R = 0.39$). The pattern shows a degree of non-linearity, with a rapid increase at peaks between 30 and 40 years. The trend then tends to stabilise, with a slight variation (increment or decrease) for older ages according to the parameter. Statistical difference is only shown for Or% when tested with anova and t-test as described in Section 6.3, while no clear differences are present for the others.

However, the behaviour of the gravimetric parameters is seen not to follow a clear linear trend and, therefore, the logarithmic scale was applied to better understand the behaviour of the properties. Figure 6.5 shows a clear improvement of the relationship with age suggesting that the variation in matrix composition is composed by two phases: a first increase and later in life a stabilisation. Ash% shows $p < 0.001$ and $R = 0.51$. Correlation coefficient value for Or% is improved from -0.39 to -0.47 and W% from -0.21 to -0.29. Although this behaviour was found during the preliminary investigation of the parameters, for the sake of age estimation they were treated with linear regression.

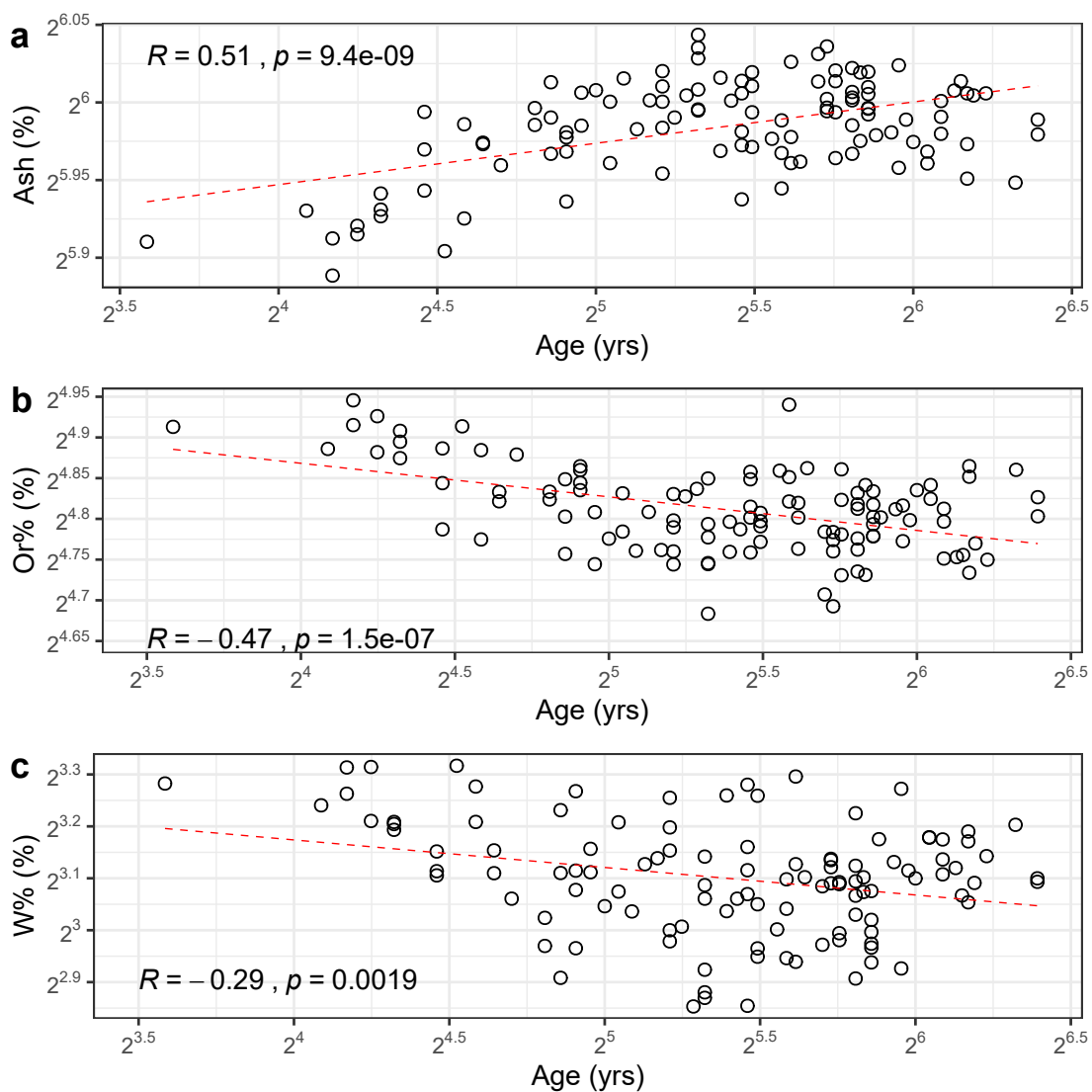


Figure 6.5: Logarithmic scale for the examination of matrix composition variation with age suggests a non linear behaviour of mineral (a), organic (b) and water phase (c).

6.4.3 Powder X-ray Diffraction and Fourier Transform Infrared Spectroscopy

Crystallite size shows a significant increase with age ($p = 0.018$, $R = 0.22$). This parameter was also reported to be sex specific with smaller crystallite size for males compared to females. An interesting inference from this method is the negative relationship with 'a'

axis ($p = 0.016$, $R = -0.20$). This is supported by the significant decrease of CL030 with $p = 0.016$, $R = -0.20$. No other significant trends have been found with age. Only one of the variables obtained from FTIR analysis was found to be significant with age. CP increases with age $p < 0.001$ and $R = 0.36$. The contradictory results between 'a' axis and size/CL030 indicates that crystal tends to achieve a more elongated shape along their major axis. This could be confirmed by 'c' axis relationship, but unfortunately shows no significance. Trends are shown in Figure 6.6.

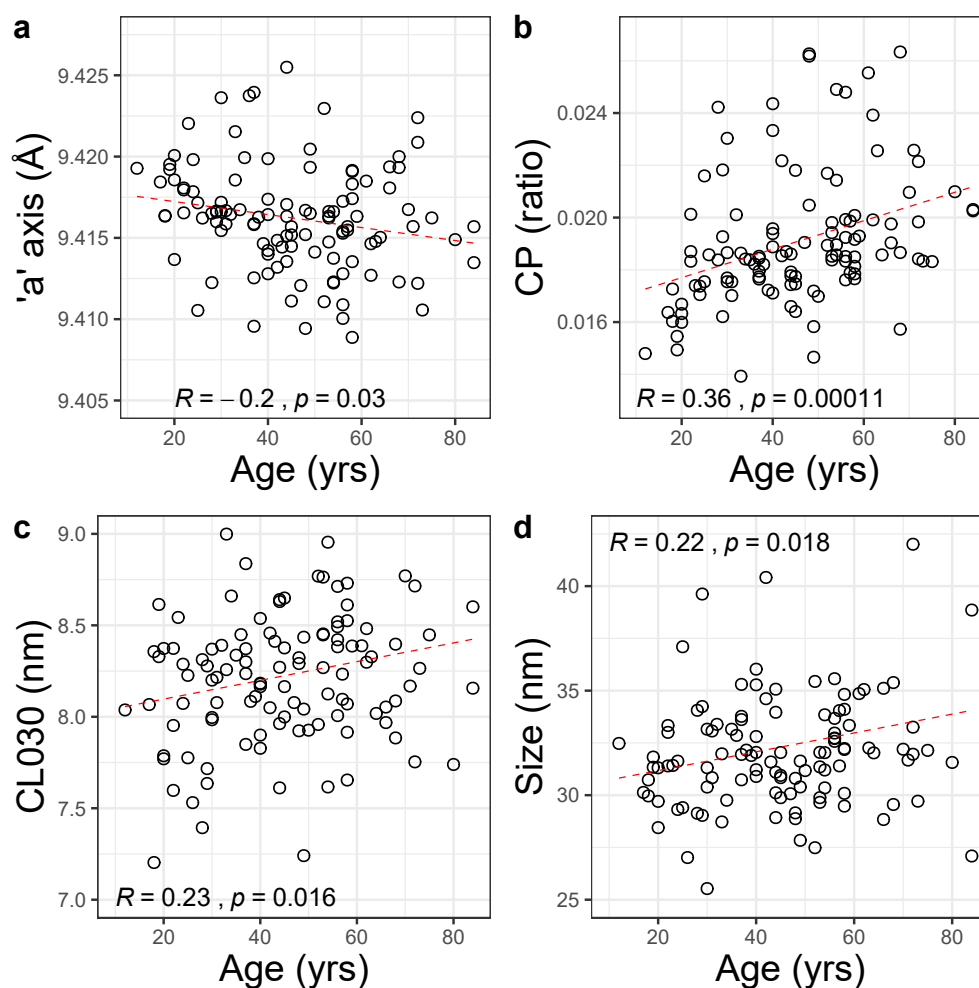


Figure 6.6: Variation of FTIR and XRD parameters with age. There is an overall increase in size of the crystals (c, d) and shrinkage of crystal lattice (a). This is associated with the increase in carbonation of the matrix (b).

6.4.4 Mechanical Analysis

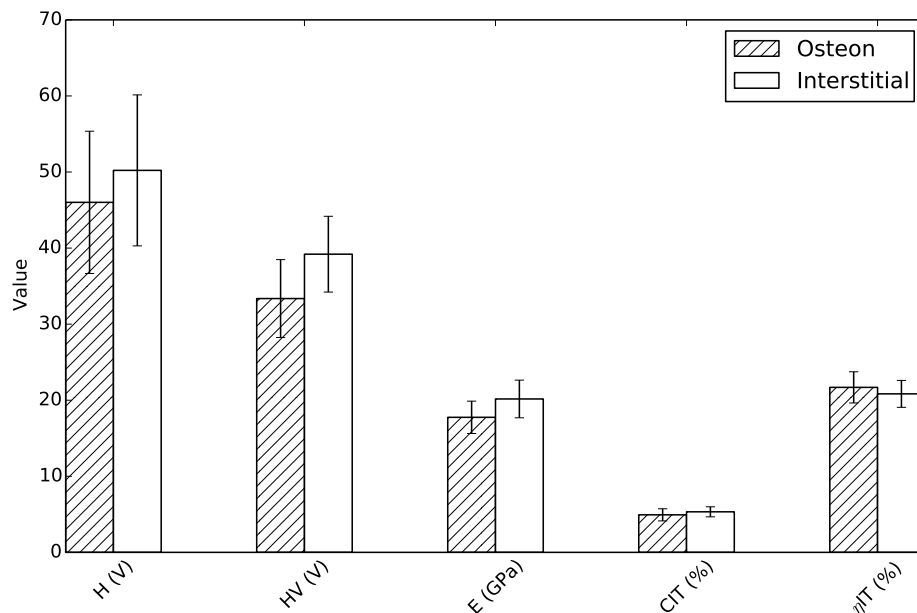


Figure 6.7: Variation of mechanical parameter between osteonal and interstitial bone. All mechanical properties are higher for osteons except for indentation creep.

For all the mechanical properties, variation between osteons and interstitial bone was tested using ANOVA and t-test. As can be seen in Figure 6.7, all of them differ significantly when taken from either of the locations and, therefore, the trends were analysed separately. Overall, interstitial bone shows consistently higher values for nanohardness ($F(1,224) = 10.644$, $p = 0.02$), elastic modulus ($F(1,224) = 61.265$, $p < 0.001$), microhardness ($F(1,224) = 74.708$, $p < 0.001$) and indentation creep ($F(1,224) = 16.422$, $p < 0.001$). η_{IT} is the only mechanical parameter that shows higher values for osteons compared to interstitial bone ($F(1,224) = 11.106$, $p < 0.001$). Elastic modulus (E) reflecting behaviour was strongly positively correlated with H ($R = 0.85$, $p < 0.001$) reflecting the plastic nature of hardness. Results for ANOVA and t-test are reported in Table 6.6.

Table 6.6: Mean values and standard deviation for the sample split between osteon and interstitial area for mechanical parameters. Results for t-test and ANOVA (SD = standard deviation; *: $p \leq 0.05$).

Parameter	Osteon (N = 226)		Interstitial (N = 226)		Anova		T-test	
	Mean	SD	Mean	SD	F-value	P-value	t-value	P-value
H*	46.012	9.395	50.216	9.969	10.644	0.001	-3.262	0.001
E*	17.752	2.136	20.165	2.486	61.265	< 0.001	-7.827	< 0.001
C_{IT} *	4.933	0.802	5.330	0.664	16.422	< 0.001	-4.052	< 0.001
η_{IT} *	21.689	2.060	20.836	1.778	11.106	0.001	3.333	0.001
HV*	33.364	5.143	39.199	5.004	74.708	< 0.001	-8.643	< 0.001

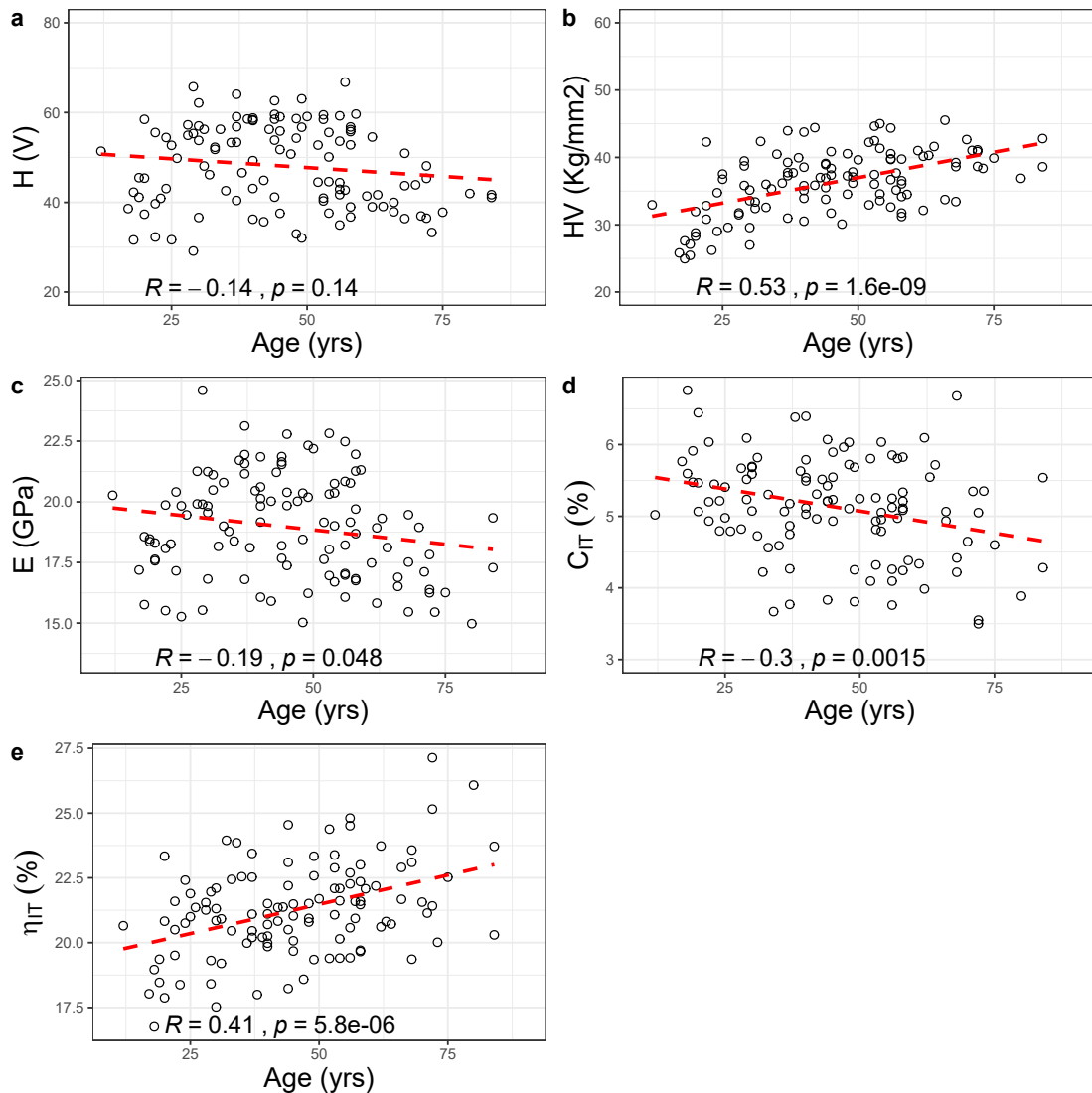


Figure 6.8: Behaviour of mechanical properties with age. Elastic modulus (c), and indentation creep (d) is seen to decrease with age. In contrast, microhardnes (b) and indentation work ratio (e) increase significantly with age. The only variable not significant with age is nanohardness (a).

At tissue level, considering the behaviour of mean values of mechanical properties (average between osteon and interstitial results) in relation to age (Figure 6.8), H shows a decrease with age, although the results are not significant. The elastic modulus of osteons is seen to decrease ($p = 0.048$, $R = -0.19$). Very similar results for indentation creep values that reveals a negative relationship with age ($p < 0.001$, $R = -0.30$). Elastic portion

of indentation show the best correlation with a considerable increment ($p < 0.001$, $R = 0.41$). Finally, microhardness increases linearly showing a high degree of correlation ($p < 0.001$, $R = 0.53$). Table 6.7 shows the entire set of correlations between age and mechanical properties.

Considering now the two locations separately, it is possible to identify a very similar trend. Both indentation modulus and creep for the osteonal area exhibit significant negative correlation with age (respectively $p = 0.048$, $R = -0.19$ and $p < 0.001$, $R = -0.41$). Conversely, microhardness decreases with age ($p < 0.001$, $R = -0.53$) as well as elastic/plastic behaviour ($p < 0.001$, $R = -0.41$). Nanohardness still does not show any significant results. Regarding interstitial bone values, both nanohardness and elastic modulus are not significant with age, while microhardness ($p < 0.001$, $R = 0.55$) and elastic/plastic work ($p < 0.001$, $R = 0.38$) increase significantly. Creep show negative correlation with age ($p < 0.001$, $R = 0.27$). Although Vicker hardness values are higher for interstitial compared to osteonal bone as previously described for nanohardness, in this case with the advancement of age, there is also a very clear increase in microhardness (Figures 6.8a/b). This is in contrast with tissue hardness. In fact, nanoindentation allows to experimental testing between each lamella, aiming to investigate tissue properties. Microindentation tests a number of lamellae that have the function to enhance the mechanical behaviour of bone. Hypermineralised lamellae and cement lines function to stop the occurrence and growth of microdamages increasing mechanical resistance of the the tissue (Figure 5.14).

Table 6.7 shows the cross correlation between mechanical properties of the two areas combined. There is a robust positive relationship between hardness and modulus suggesting that plastic deformation is related to elastic modulus. Furthermore, results shows that indentation creep is negatively correlated with the elastic/total work of the indentation. This suggest that when the elastic work is increase there is a reduction in the creep resistance.

Table 6.7: Pearson's correlation between age and mechanical properties for interstitial and osteonal bone (^a: $p \leq 0.5$; ^b: $p \leq 0.01$; ^c: $p \leq 0.001$).

	Age	Po.Ar%	<i>On</i> H	<i>On</i> E	<i>On</i> C _{IT}	<i>On</i> η _{IT}	<i>It</i> H	<i>It</i> E	<i>It</i> C _{IT}
Age	1								
Po.Ar%	0.834 ^c	1							
<i>On</i> H	-0.125	-0.005	1						
<i>On</i> E	-0.202 ^a	-0.128	0.864 ^c	1					
<i>On</i> C _{IT}	-0.290 ^b	-0.066	-0.014	0.159	1				
<i>On</i> η _{IT}	0.399 ^c	0.182	0.179	-0.102	-0.837 ^c	1			
<i>It</i> H	-0.144	0.022 ^a	0.820 ^c	0.743 ^c	0.042	0.025	1		
<i>It</i> E	-0.145	-0.065	0.570 ^c	0.689 ^c	0.056	-0.112	0.824 ^c	1	
<i>It</i> C _{IT}	-0.270 ^b	-0.112	-0.017	0.124	0.807 ^c	-0.702 ^c	-0.076	-0.033	1
<i>It</i> η _{IT}	0.384 ^c	0.202 ^a	0.159	-0.071	-0.720 ^c	0.810 ^c	0.154	-0.102	-0.762 ^c

6.5 Bone Matrix Compositions: Reciprocal changes in mineral and organic

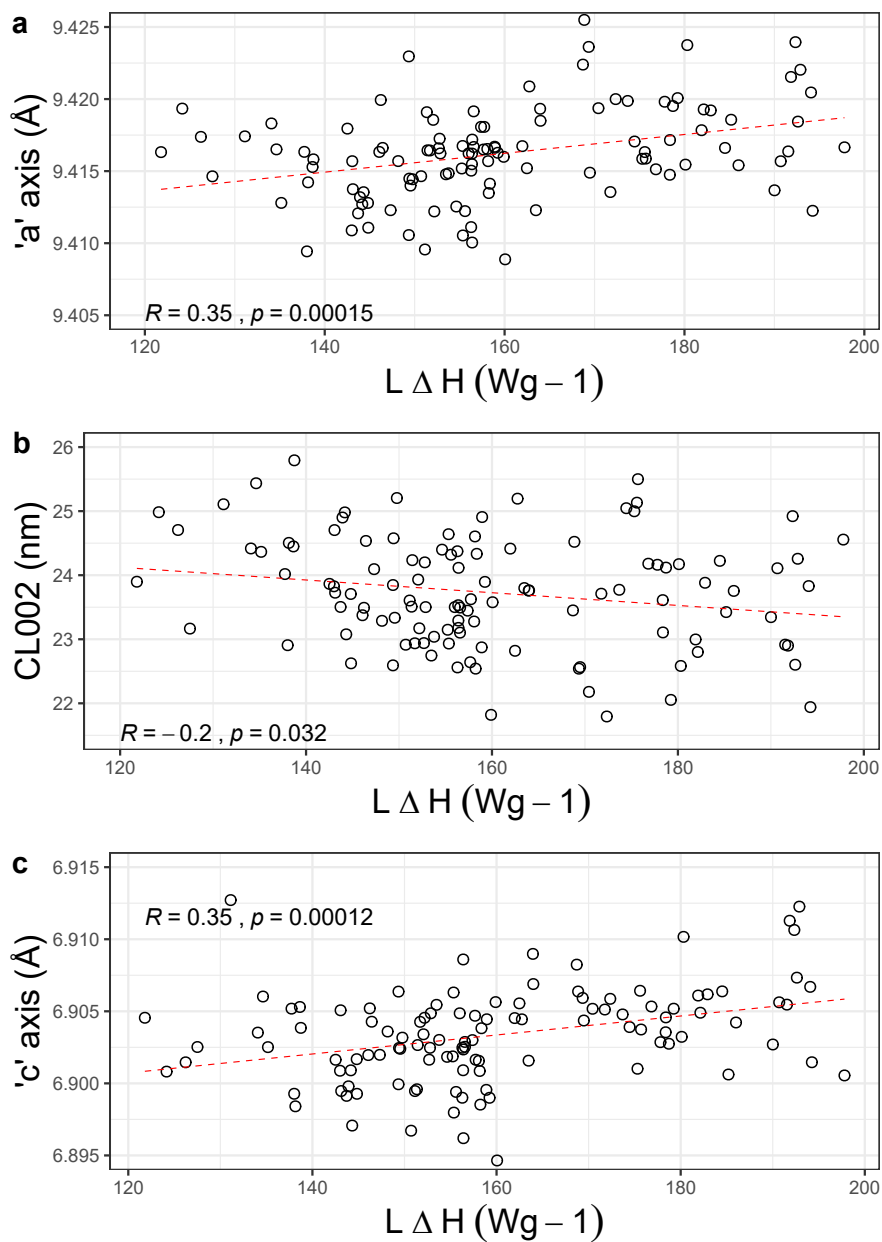


Figure 6.9: Correlation between crystal geometry and collagen degradation. Young collagen, characterised by high thermal stability, is associated with small crystals (b). In contrast, lattice parameters is positively correlated with collagen thermal stability (a and c).

As previously described the role of collagen as a template is generally accepted while its role in inducing mineralisation and the growth of mineral crystal is still a topic open for debate (Olszta et al., 2007). The current study found that collagen could play a role in determining changes in mineral geometry. If considered, the direct relationship of coherence length (CL002) and collagen thermal stability (L Δ H) (Figure 6.9), it is immediately clear that high thermal stability, characteristic of good quality collagen fibres, is correlated with low crystallite size (newly formed crystals) and high microstrain ($p = 0.032$ and $R = -0.20$).

There is a clear, positive correlation between L Δ H and both 'a' axis ($p < 0.001$ and $R = 0.35$) and 'c' axis ($p < 0.001$ and $R = 0.35$). This suggests that crystal growth is not limited to one lattice direction. A negative correlation was also found between C Δ H and CL002 ($p = 0.011$ and $R = -0.24$). These results are also supported by gravimetric analysis that show negative correlation between Or% and Size $p = 0.019$ and $R = -0.22$), CL002 ($p < 0.001$ and $R = -0.25$) and CL030 ($p = 0.02$ and $R = -0.22$). Considering collagen content (CC), negative correlation was detected with CL002 ($p = 0.033$ and $R = -0.20$) and 'a' axis ($p = 0.025$ and $R = -0.21$). These results confirm the hypothesis that young bone that has increased amount of collagen also shows small crystal size. It is possible that young collagen induces strain of the crystals that consequently increase in size. Finally, carbonate substitution (CP), that increases with age, induces a significant decrease in 'a' axis ($p = 0.002$, $R = -0.29$). Additionally, an increase in crystallite size tends to determine an increment in mineral content as suggested by the positive correlation between mineral/organic matrix (MO) and 'a' axis ($p = 0.015$ and $R = 0.23$), and CL002 ($p = 0.043$ and $R = 0.19$). This is corroborated by the significant increment of Ash% and crystallite size ($p = 0.016$ and $R = 0.23$) and CL002 ($p = 0.013$ and $R = 0.23$). One last aspect on mineral crystal is the variation of crystallinity index (CI) that indicates the size, strain and perfection of HAp. This is observed to drastically decrease with the increase of carbonate substitution ($p < 0.001$ and $R = -0.77$) and is negatively correlated with mineral strain ($p = 0.034$ and $R = -0.20$). It seems that the increase of crystallinity could be attributed to an increase in size as suggested by the positive correlation with: 'a' axis

($p = 0.005$ and $R = 0.26$), 'c' axis ($p < 0.001$ and $R = 0.32$), CL002 ($p = 0.035$ and $R = 0.20$) and CL004 ($p = 0.007$ and $R = 0.25$).

It is possible to confirm that, with age, there is an increase in ash content and a consequent decrease in water and organic matrix. This is supported by the robust negative correlation between Ash% and Or% ($p < 0.001$ and $R = -0.89$) and between Ash% and W% ($p < 0.001$ and $R = -0.69$). These results are also supported by the decrease in collagen content (CC) with the increase in Ash% ($p = 0.006$ and $R = 0.26$) and *vice versa*, the decrease in mineral/organic ratio (MO) with Or% ($p < 0.001$ and $R = -0.37$). To conclude, collagen thermal stability (L Δ H) shows a very robust, significant positive correlation with both structural water and the increase in organic content as seen in Figure 6.10. Similarly, there is a significant increase in 'c' axis ($p < 0.001$ and $R = 0.41$) and 'a' axis ($p = 0.024$ and $R = 0.21$) with the increment of structural water, indicating a growth along the major axis of the crystal.

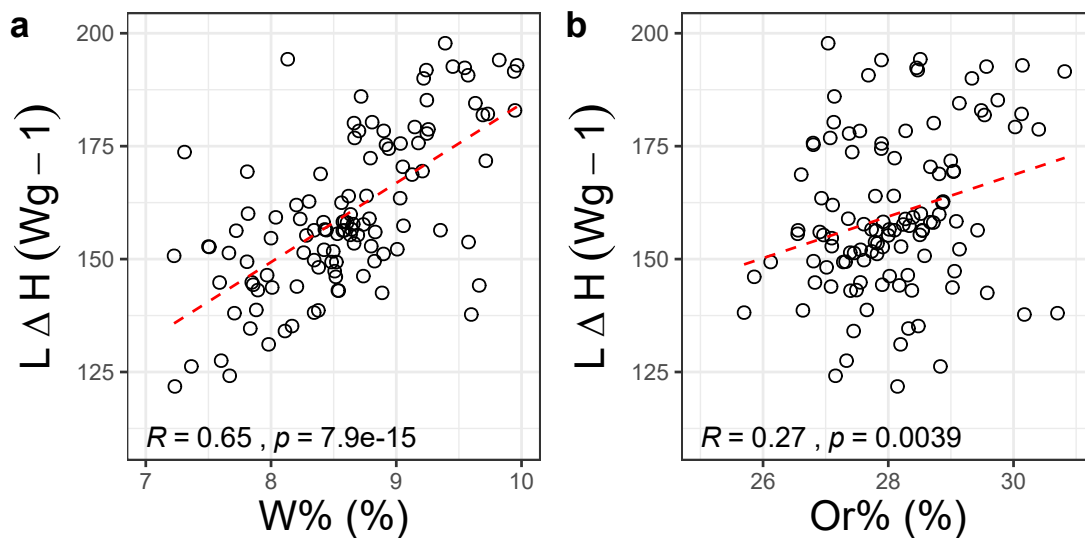


Figure 6.10: Collagen thermal stability is related to the amount of structural water (a) that allows the creation of hydrogen bonds that keeps the triple-helix configuration intact. The increase in collagen thermal stability is also associated with increased collagen content (b).

6.5.1 Stepwise Regression Relationship - Collagen vs. Mineral

Further investigation of the relationship between collagen and mineral required a stepwise regression approach. The two parameters that show promising results are CI and CP. The CI, that indicates the crystallinity of the mineral crystals, is predominantly affected by $W_{\%}$ and CC with a negative relationship between crystallinity index and the two parameters. This is indicative of decrease in CC. A loss in thermal stability induces an increase in crystallinity (Table 6.8). The model explains 36.5% of the variance.

Similarly, for CP, the predominant factor is CC, which shows a positive trend. The negative effect of $W_{\%}$ and $C\Delta H$ is also pronounced (Table 6.9). This model explains 34% of the changes in carbonate substitution.

Table 6.8: Stepwise regression analysis of CI vs Compositional parameters of the organic matrix, $R^2 = 0.36$ (SE: standard error; *: $p \leq 0.05$; **: $p \leq 0.01$; ***: $p \leq 0.001$).

Parameter	β	SE	t value	P value
Intercept	72.289483	1.252863	57.699	2e-16 ***
CC	-1.665402	0.224205	-7.428	2.51e-11 ***
$W_{\%}$	0.021831	0.006952	3.140	0.00217 **

Table 6.9: Stepwise regression analysis of CP vs Compositional parameters of the organic matrix with $R^2 = 0.34$ (SE: standard error; *: $p \leq 0.05$; **: $p \leq 0.01$; ***: $p \leq 0.001$).

Parameter	β	SE	t-value	P-value
Intercept	3.187e-02	4.048e-03	7.873	2.75e-12 ***
CC	5.996e-02	1.013e-02	5.918	3.83e-08 ***
$W_{\%}$	-1.422e-03	3.153e-04	-4.511	1.64e-05 ***
$C\Delta H$	-2.860e-06	7.398e-07	-3.866	0.000188 ***

The last parameter predicted is 'c' axis. Carbonate substitution did not show any relationship using Pearson's method with the lattice parameter. Stepwise regression, in contrast, shows a highly significant positive correlation with 'c' axis. Finally, the most interesting aspect of Table 6.10 is the predominant role of carbonate ratio and crystallinity in determining the increase in length along the 'c' axis. It is also interesting to note that

collagen quality and quantity, coupled with water fraction, induce an increment in lattice size along the 'c' axis.

Table 6.10: Stepwise regression analysis of 'c' axis vs Compositional parameters of the organic matrix with $R^2 = 0.33$ (SE: standard error; *: $p \leq 0.05$; **: $p \leq 0.01$; ***: $p \leq 0.001$).

Parameter	β	SE	t-value	P-value
Intercept	6.821e+00	1.517e-02	449.790	2e-16 ***
CI	3.633e-02	7.454e-03	4.874	3.81e-06 ***
CP	6.645e-01	1.762e-01	3.770	0.000267 ***
W _o %	1.104e-03	5.370e-04	2.056	0.042196 *
Or _o %	6.281e-04	2.878e-04	2.182	0.031283 *
LΔH	3.863e-05	1.983e-05	1.948	0.054022

Additional models were developed and assessed. However, the models with an $R \leq 0.20$ were not presented as they are unsuitable when attempting to infer relationships between the parameters.

6.6 Matrix Composition and Mechanical Properties

This research revealed that the variation of mechanical properties with age is highly dependent on both changes of the mineral and organic phase at matrix level.

For mean tissue values, HV is the only parameter that shows negative correlation with LΔH ($p < 0.001$, $R = -0.33$). Enthalpy values for the combustion peak (CΔH) also correlate negatively with C_{IT} ($p < 0.001$, $R = -0.38$) and positively with η_{IT} ($p = 0.015$, $R = 0.23$) and HV ($p < 0.001$, $R = 0.38$), suggesting the organic content plays a central role in viscoelastic behaviour of bone. The increase in structural water induces a significant decrease in nanohardness ($p < 0.001$, $R = -0.35$), elastic modulus ($p = 0.012$, $R = -0.24$) and microhardness ($p = 0.03$, $R = -0.27$). It is interesting to note that the predominant effect is on hardness rather than elastic modulus suggesting that organic content modifications linked to the loss of structural water are more linked to plastic behaviour. Surprisingly, no correlations are found between nanohardness and Or_o%, while there is good positive correlation with C_{IT} ($p = 0.001$, $R = 0.30$), and negative correlation with E ($p = 0.034$, $R =$

-0.20) and η_{IT} ($p = 0.002$, $R = -0.29$). The best correlation was the negative relationship with microhardness ($p < 0.001$, $R = -0.52$) that supports the aforementioned hypothesis. Finally, considering the degree of mineralisation that was found to increase with age, results are shown in Figure 6.11 and confirm the correlation between plastic behaviour and mineral content. These are also supported by the combined increment in MM and HV ($p < 0.001$, $R = 0.34$) and the decrease of C_{IT} ($p = 0.015$, $R = -0.23$) with the increase in mineral content (MM).

Regarding the modifications in mechanical properties linked to the osteonal and interstitial, $Ash_{\%}$ shows a number of significant correlations with mechanical behaviour a nano- and micro-level. Osteons show significant correlation between ^{On}H ($p = 0.029$, $R = 0.21$), ^{On}E ($p = 0.028$, $R = 0.21$) and $^{On}\eta_{IT}$ ($p < 0.001$, $R = 0.24$) and increase of mineral content. $Or_{\%}$ show a positive correlation with $^{On}\eta_{IT}$ ($p = 0.006$, $R = 0.26$) and negative $^{On}C_{IT}$ ($p = 0.004$, $R = -0.27$). In contrast, the decrease in $W_{\%}$ induces an increase in ^{On}H ($p < 0.001$, $R = 0.34$), ^{On}E ($p = 0.009$, $R = 0.24$). Additionally, mineral/organic matrix (MO) induces a decrease in $^{On}C_{IT}$ ($p = 0.021$, $R = -0.21$) while the opposite trend is found with collagen content (CC) ($p = 0.007$, $R = 0.25$). Very similar results are found for the interstitial area and are reported in Table 6.14 at the end of this subsection.

Turning now to the experimental evidence regarding modifications of crystal structure, the increase in coherence length that quantifies the lattice dislocation in a specific direction is seen to influence the mechanical properties of bone matrix. With the exception of η_{IT} and HV, all the nanoindentation parameters are significantly correlated with increase in coherence length at CL002 peak as shown in Figures 6.12. Table 6.11 shows the very similar pattern of CL004 while, changing the crystallographic direction, CL030 only correlates with C_{IT} and η_{IT} . The increase in CL210 only induces a weak increment in nanohardness ($p = 0.018$, $R = -0.22$). Furthermore, It can be seen that the predominant effect of mineral crystal changes is on the elastic deformation properties. The crystallinity index (CI) do not show correlations with any of the mean tissue properties while there is a negative relationship between carbonate substitution (CP) and and elastic modulus ($p = 0.011$, $R = -0.24$) and positive with HV ($p = 0.047$, $R = 0.19$).

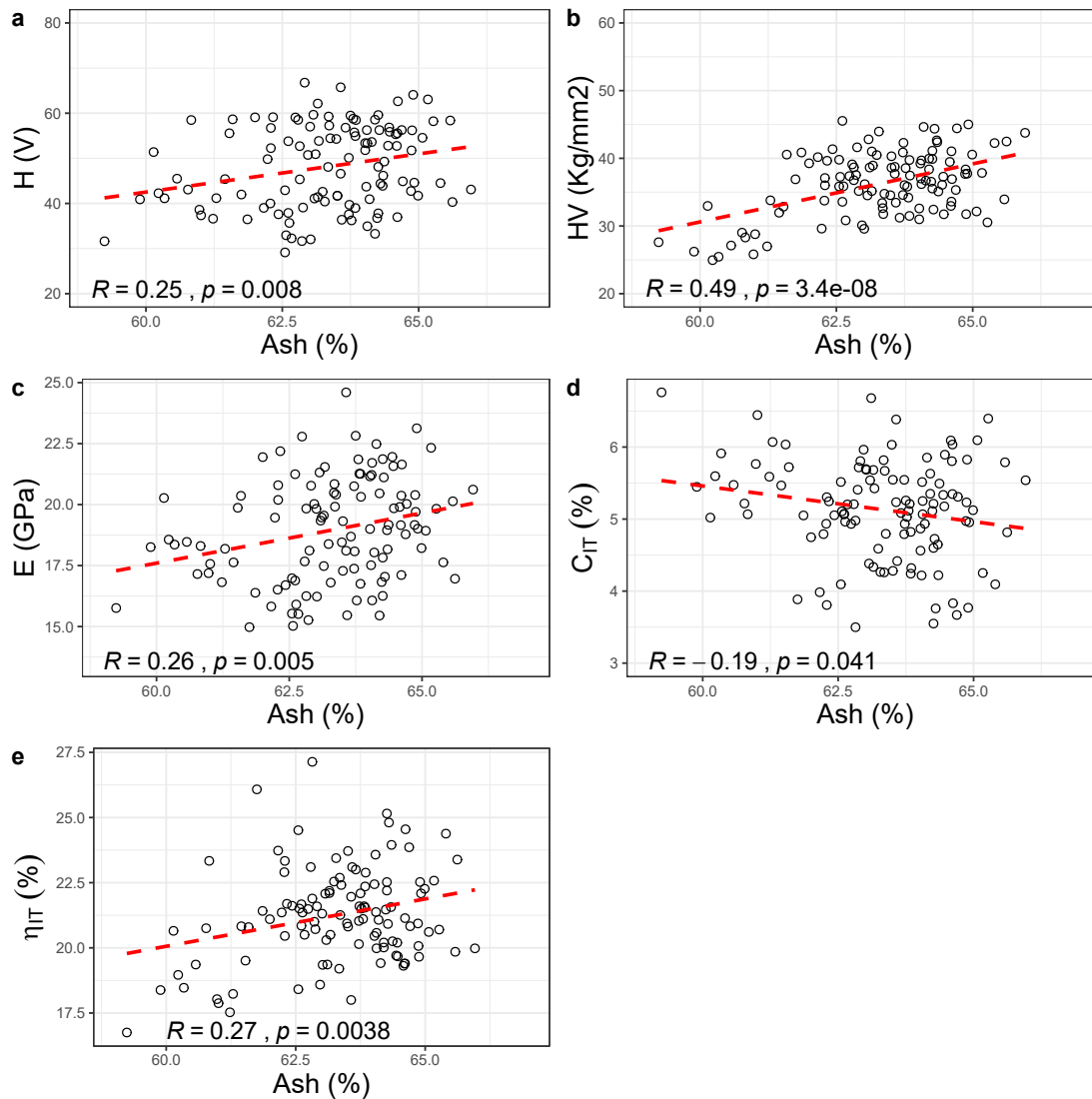


Figure 6.11: Influence of mineral content on mean tissue mechanical properties. The only property negatively affected by mineral content is indentation creep (d).

Turning now to the experimental evidence regarding modifications of crystal structure, the increase in coherence length that quantifies the lattice dislocation in a specific direction is seen to influence the mechanical properties of bone matrix. With the exception of η_{IT} and HV, all the nanoindentation parameters are significantly correlated with increase in coherence length at CL002 peak as shown in Figures 6.12. Table 6.11 shows the very similar pattern of CL004 while, changing the crystallographic direction, CL030 only correlates

with C_{IT} and η_{IT} . The increase in CL210 only induces a weak increment in nanohardness ($p = 0.018$, $R = 0.22$). Furthermore, It can be seen that the predominant effect of mineral crystal changes is on the elastic deformation properties. The crystallinity index (CI) does not show correlations with any of the mean tissue properties while there is a negative relationship between carbonate substitution (CP) and and elastic modulus ($p = 0.011$, $R = -0.24$) and positive with HV ($p = 0.047$, $R = 0.19$). These results suggest that the increase in crystal length is the main contributor in improving the mechanical behaviour of bone matrix, with the exception of η_{IT} . Increase in the mineral thickness/width account for the increase in elastic work of the indentation and reduction in C_{IT} . To conclude, crystallite strain seems to induce a number of mechanical changes of the bone matrix. It induces a decrease in H ($p = 0.002$, $R = -0.29$) and E ($p < 0.001$, $R = -0.36$). Additionally it is found the combined increase in strain and HV ($p = 0.002$, $R = 0.29$).

Table 6.11: *Correlation Matrix of mechanical properties for interstitial bone and coherence length for the 004 and 030 peak (^a: $p \leq 0.05$; ^b: $p \leq 0.01$; ^c: $p \leq 0.001$).*

	CL004	CL030	H	E	C_{IT}	η_{IT}
CL004	1					
CL030	0.084	1				
H	0.410 ^a	-0.058	1			
E	0.510 ^a	-0.065	0.852 ^c	1		
C_{IT}	-0.257 ^b	-0.342 ^c	-0.015	0.085	1	
η_{IT}	0.026	0.273 ^b	0.139	-0.112	-0.839 ^c	1

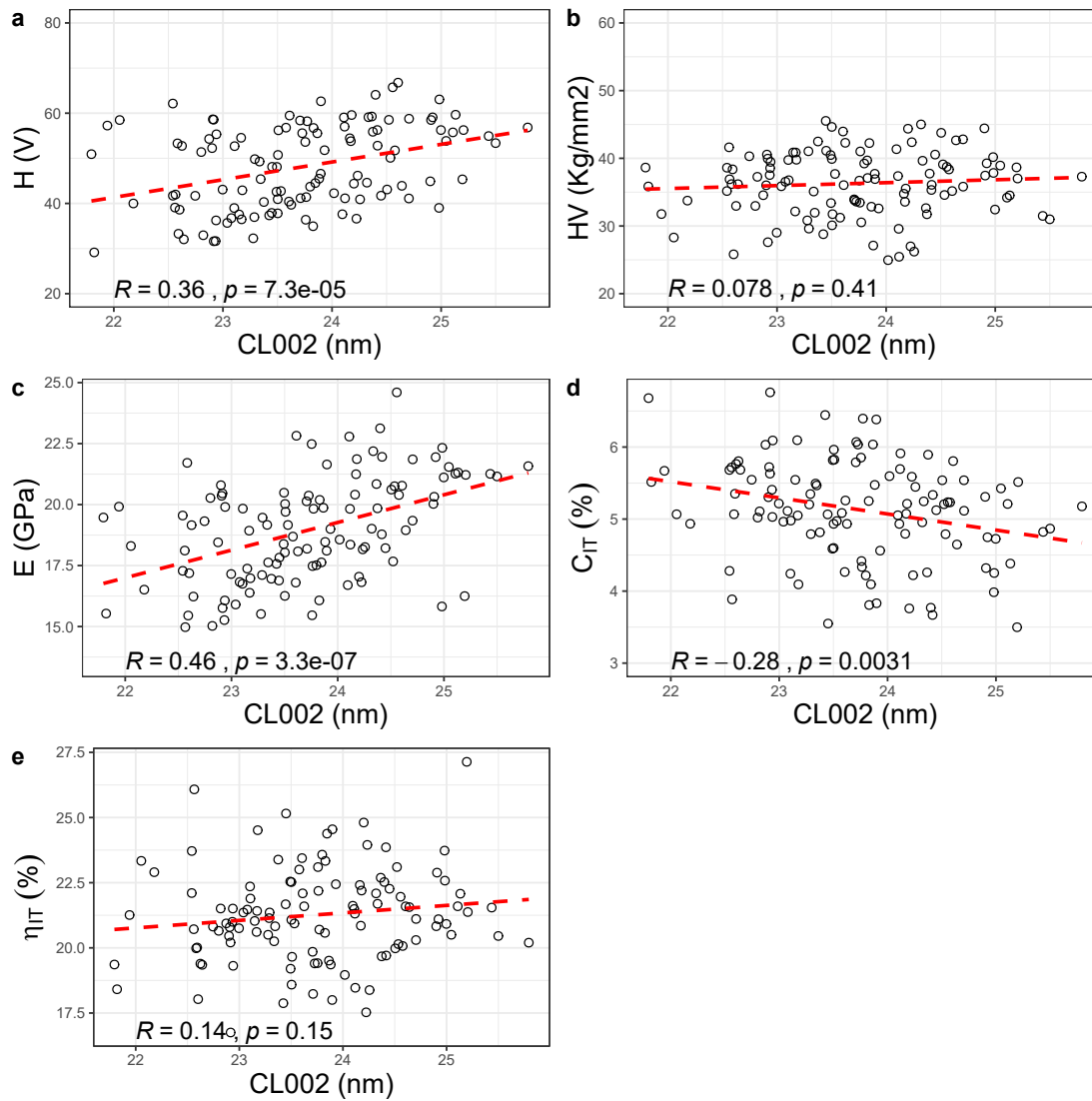


Figure 6.12: Influence of coherence length at 002 peak on mechanical properties of the entire tissue. It is possible to see the predominant role of crystals' modification in the elastic behaviour of bone.

Comparing results for osteons and interstitial bone, it can be seen that carbonate substitution does not affect osteonal bone while there is a negative correlation with ${}^I E$ ($p = 0.008$, $R = -0.25$) and a positive one with ${}^I HV$ ($p = 0.028$, $R = 0.21$). A similar behaviour is shown by the crystallinity index that only induces a mild increase in ${}^I E$ ($p = 0.017$, $R = 0.22$) and decrease ${}^I C_{IT}$ ($p = 0.003$, $R = -0.21$). In contrast CL002 shows positive correlation with ${}^{On} H$ ($p < 0.001$, $R = 0.36$), ${}^{On} E$ ($p < 0.001$, $R = 0.40$) and ${}^I C_{IT}$

($p = 0.002$, $R = 0.29$). The same trends are found with the interstitial area and respectively are $p < 0.001/R = 0.34$, $p < 0.001/R = 0.44$ and $p = 0.016/R = 0.23$. Tables 6.12 and 6.13 summarise the same trends discussed for mean tissue values in relation to the two areas of investigation. CL210 correlates positively with ^{On}H ($p = 0.039$, $R = 0.19$), ^{It}H ($p = 0.016$, $R = 0.23$) and ^{It}E ($p = 0.023$, $R = 0.21$). Surprisingly, the increase in size only determines an increase in microhardness for both osteons ($p = 0.013$, $R = 0.21$) and interstitial area ($p = 0.002$, $R = 0.29$). None of the lattice parameter value seem to induce any variation in mechanical properties.

Table 6.12: Correlation Matrix of mechanical properties for osteonal bone and coherence length at 004 and 003 (a : $p \leq 0.05$; b : $p \leq 0.01$; c : $p \leq 0.001$).

	CL004	CL030	^{On}H	^{On}E	$^{On}C_{IT}$	$^{On}\eta_{IT}$
CL004	1					
CL030	0.084	1				
^{On}H	0.339 ^c	-0.072	1			
^{On}E	0.376 ^c	-0.091	0.864 ^c	1		
$^{On}C_{IT}$	-0.224 ^b	-0.331 ^c	-0.014	0.159	1	
$^{On}\eta_{IT}$	0.047	0.219 ^a	0.179	-0.102	-0.837 ^c	1

Table 6.13: Correlation Matrix of mechanical properties for interstitial bone and coherence length at 004 and 003 (a : $p \leq 0.05$; b : $p \leq 0.01$; c : $p \leq 0.001$).

	CL004	CL030	^{It}H	^{It}E	$^{It}C_{IT}$	$^{It}\eta_{IT}$
CL004	1					
CL030	0.084	1				
^{It}H	0.441 ^c	-0.040	1			
^{It}E	0.548 ^c	-0.034	0.824 ^c	1		
$^{It}C_{IT}$	-0.269 ^b	-0.318 ^c	-0.076	-0.033	1	
$^{It}\eta_{IT}$	-0.002	0.307 ^c	0.154	-0.102	-0.762 ^c	1

Finally, there are significant correlation between interstitial mechanical properties and crystallinity index and carbonate substitution. Figure 6.13 shows the significant decrease in elastic modulus with the increase on CP. In contrast it seems that carbonation has a

positive effect on microhardness (Figure 6.13). In contrast, the increase in crystallinity (CI) have a positive effect on elastic modulus ($p = 0.017$, $R = 0.22$) and negative with the indentation creep ($p = 0.027$, $R = -0.21$). This is not surprising if considering the strong negative correlation between CP and CI ($p < 0.001$, $R = -0.77$). The behaviour for interstitial bone follows the same trends and is shown in Table 6.14.

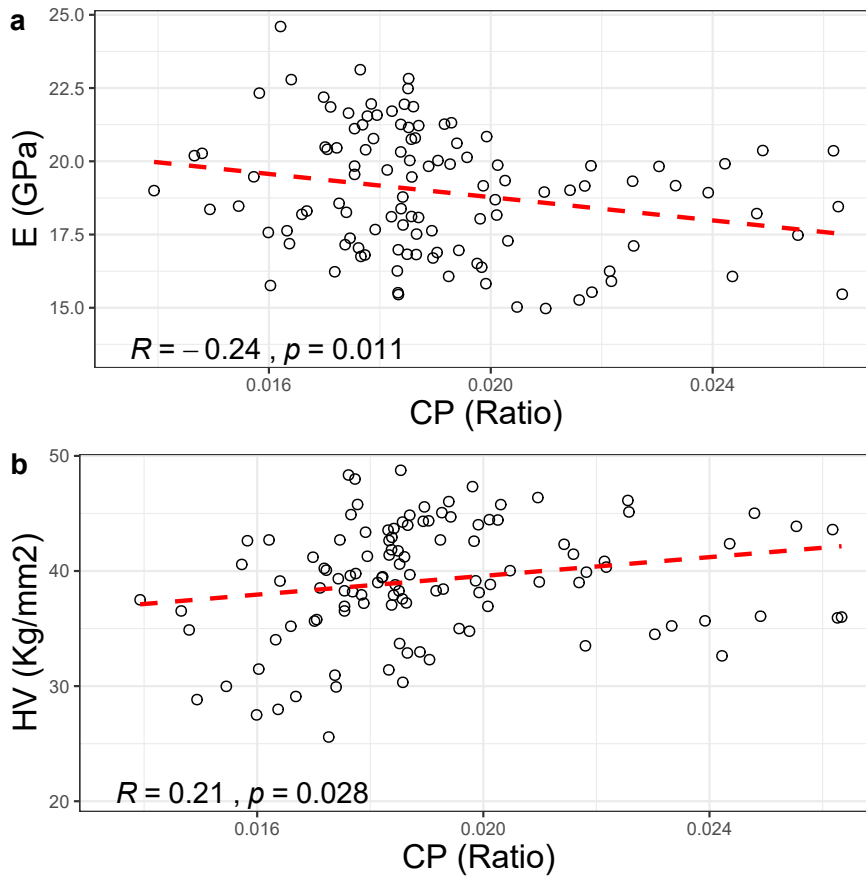


Figure 6.13: Relationship between carbonate substitution and mechanical properties. It almost equally affect plastic and elastic deformation of bone.

Table 6.14: Correlation Matrix of mechanical properties for interstitial bone and physicochemical changes (^a: $p \leq 0.05$; ^b: $p \leq 0.01$; ^c: $p \leq 0.001$).

	I^tH	I^tE	I^tC_{IT}	$I^t\eta_{IT}$	LΔH	CΔH	W _%	Or _%	Ash _%	MM	CP	CI
I^tH	1											
I^tE	0.824 ^c	1										
I^tC_{IT}	-0.076	-0.033	1									
$I^t\eta_{IT}$	0.154	-0.102	-0.762 ^c	1								
LΔH	0.044	0.005	0.061	-0.058	1							
CΔH	0.144	-0.090	0.361 ^c	-0.163	0.159	1						
W _%	-0.332 ^c	-0.193	-0.065	-0.106	0.649 ^c	-0.208 ^a	1					
Or _%	-0.144	-0.238 ^a	0.319 ^c	-0.296 ^c	0.270 ^b	0.489 ^c	0.289 ^c	1				
Ash _%	0.266 ^b	0.270 ^b	-0.209 ^a	0.273 ^a	-0.512 ^c	-0.269 ^a	-0.693 ^c	-0.890 ^c	1			
MM	0.083	0.180	-0.219 ^a	0.174	-0.063	-0.098	-0.127	-0.366 ^c	0.335 ^c	1		
CP	-0.173	-0.247 ^a	0.051	0.122	-0.307 ^c	-0.150	-0.277 ^b	-0.179	0.267 ^b	-0.457 ^c	1	
CI	0.087	0.225 ^a	-0.207 ^a	-0.001	0.167	-0.043	0.216 ^a	-0.104	-0.024	0.611 ^c	-0.769 ^c	1
CC	-0.056	-0.163	0.244 ^a	-0.164	-0.001	0.190	0.041	0.319 ^c	-0.260 ^b	-0.882 ^c	0.398 ^c	-0.555 ^c

6.6.1 Stepwise Regression Relationship - Mechanical Properties vs. Composition

The relationship between compositional parameters (independent) and mechanical properties (dependent) was further investigated by means of stepwise regression in order to understand the extent of their effect on the dependent variables. The values for osteonal and interstitial bone were averaged to obtain mean tissue properties. At first, the four mechanical properties were compared to the compositional parameters by backward stepwise regression in order to identify the effect of the independent variables and their dominance.

Table 6.15: *Effect of compositional parameters on nanohardness (SE: standard error; *: $p \leq 0.05$; **: $p \leq 0.01$; ***: $p \leq 0.001$).*

Parameter	β	SE	t-value	P-value
Intercept	6.009e+01	3.366e+01	1.785	0.0771
L Δ H	2.366e-01	5.264e-02	4.495	1.78e-05 ***
W _%	-9.132e+00	1.360e+00	-6.71	3.971e-10 ***
CP	-1.039e+03	4.227e+02	-2.457	0.0156 *
CI	-3.805e+01	1.788e+01	-2.128	0.0356 *
Strain	-1.270e+03	4.943e+02	-2.569	0.0116 *
CL002	3.998e+00	8.186e-01	4.884	3.70e-06 ***

Nanohardness can be predicted by a combination of parameters related to both organics and mineral matrix with R values equal to 0.46, as shown in Table 6.15. It is interesting to note that only the increase in collagen thermal stability and coherence length at 002 have a positive effect on hardness. Furthermore, ion substitution (CP) and crystallinity index (CI) have a negative effect on hardness. Dominant parameters are mostly related to organic matrix and its quality. Crystal geometry also plays a relevant role in defining nanohardness.

Table 6.16: *Effect of compositional parameters on elastic properties. It is possible to see how the parameters related to mineral modifications have increased in the attempt of explaining the behaviour of elastic properties (SE: standard error; *: $p \leq 0.05$; **: $p \leq 0.01$; ***: $p \leq 0.001$).*

Parameter	β	SE	t-value	P-value
Intercept	6.13176	5.55595	1.104	0.272250
L Δ H	0.04874	0.01162	4.195	5.68e-05 ***
W $_{\%}$	-1.42089	0.30623	-4.640	1.00e-05 ***
Strain	-689.36339	172.69763	-3.992	0.000121 ***
Size	0.18812	0.07159	2.628	0.009877 **
CL002	1.05115	0.20394	5.154	1.19e-06 ***
CL030	-1.09848	0.41768	-2.630	0.009810 **

Regression results show that the increase of organic matrix quality plays a positive role in determining elastic properties of bone. Considering the strong correlation between W $_{\%}$ and L Δ H, it is not surprising that these two variables account for most of the variance in the model. Interestingly, the increase in crystal size, which accounts for a decrease in Strain, has a positive correlation with E, proving that longer crystal are characteristic of more elastic tissue. Considering that coherence length increase accounts for an increment in size and a decrement in strain at crystal level, the results obtained for CL002 and CL030 confirm this inference. The overall performance of the model is R = 0.48 (Table 6.16). For the remaining mechanical testing, only lesser than 30% of the variance could be explained by the compositional parameters and, therefore, results do not allow a detailed and final interpretation.

Finally, microhardness (Table 6.17) was predicted with R = 0.442 and it is observed that mineral density plays a preponderant role in predicting this variable. However, C Δ H is still one of the variables selected for the model, suggesting that organic matrix plays a role in plastic deformation.

Table 6.17: Effect of compositional parameters on microhardness (SE: standard error; *: $p \leq 0.05$; **: $p \leq 0.01$; ***: $p \leq 0.001$).

Parameter	β	SE	t-value	P-value
Intercept	-8.620810	19.221284	-0.449	0.65469
CΔH	-0.005367	0.001279	-4.197	5.57e-05 ***
Ash%	1.302701	0.275714	4.725	6.97e-06 ***
MM	1.272703	0.465124	2.736	0.00727 **
CL004	-1.513028	0.340958	-4.438	2.20e-05 ***

Overall, plastic deformation (post yield) is primarily affected by changes in organic matrix while elastic deformation (pre-yield) is predominantly determined by variations in mineral content and crystallite architecture. Additionally, newly interstitial bone is more affected by age related changes in matrix compared to newly formed bone.

6.7 Skeletal Maturity

Considering that skeletal maturity is reached approximately at 35 years of age (Zioupos, 2001), all the variables were plotted against age using loess curves to evaluate the age at which the peak of physicochemical parameters and mechanical properties is reached before change in the trend. This trend is very clear for mechanical properties (Figure 6.14). Nanohardness and indentation modulus follow the same trend: positive until 35 years and negative afterwards. Microhardness, in contrast, increases steadily for the entire age range but this increase is of significance only until the age of 35 ($p = 0.005$, $R = 0.48$) as can be seen in Figure 6.14. Similarly, η_{IT} increase significantly for 0-35 years ($p < 0.001$, $R = 0.40$) and 35-85 ($p < 0.001$, $R = 0.40$) while indentation creep (C_{IT}) decreases significantly along the entire age range, respectively $p = 0.002$, $R = 0.29$ and $p = 0.002$, $R = 0.29$. These changes combined suggest that after 35 years of age the risk of accumulation of microdamage that would lead to overall fracture of the bone increase.

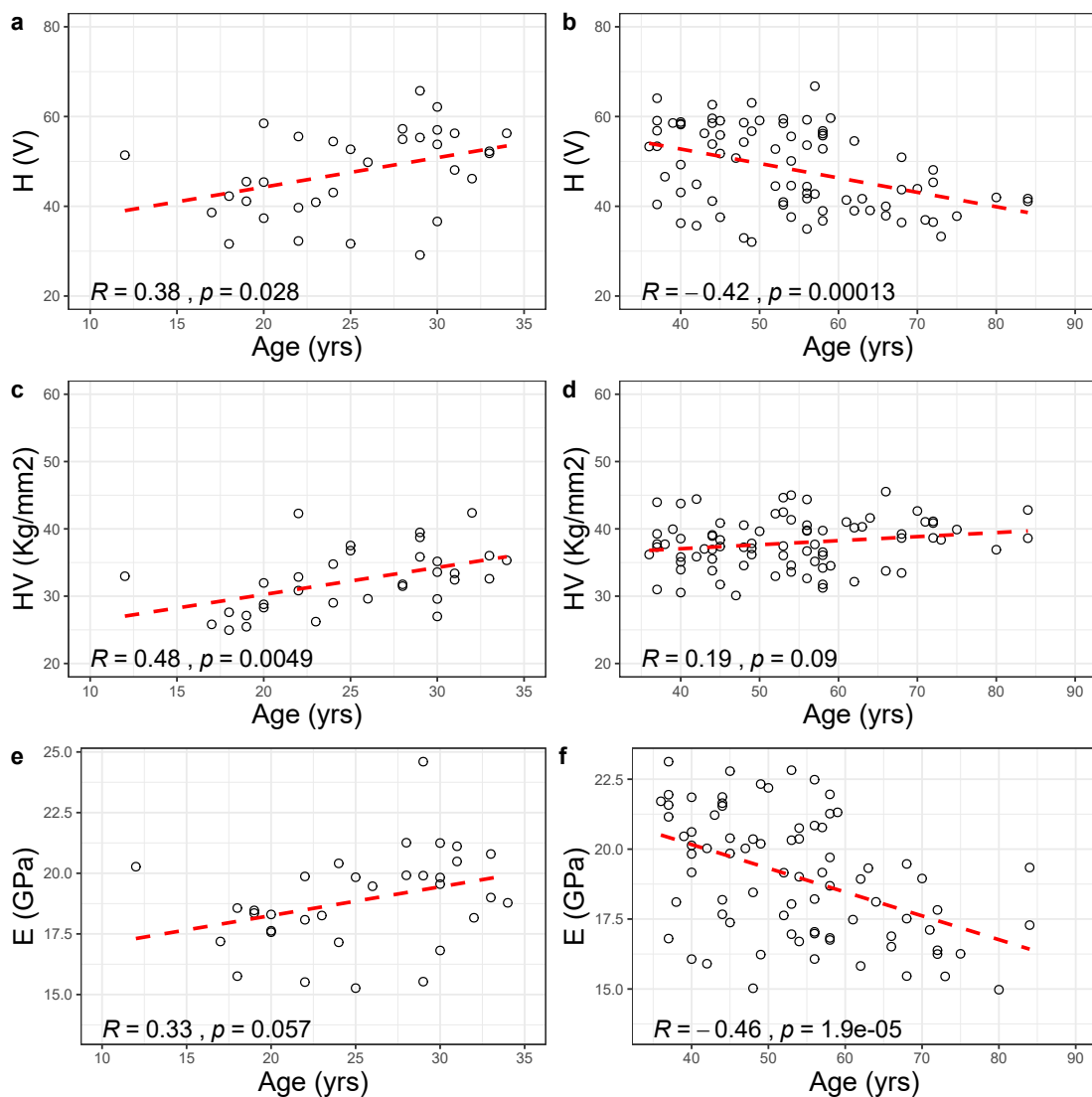


Figure 6.14: Behaviour mechanical properties with age explain by loess curve shows a peak in mechanical properties at ~40 years of age.

Considering physicochemical changes the situation is more complex and different components mature at different ages. Considering thermal analysis, no clear changes are to be reported for enthalpy values for the combustion peak (ΔH). However, maturation of this parameter is believed to be set at 40 years of age by comparison with the gravimetric analysis of the organic weight loss that shows a steep decrease ($p < 0.001$, $R = -0.72$) to then reduce its variation to a non-significant slight decrease, as can be seen in Figure 6.15

a/b and e/f. Similarly, structural water drops until the same point in life ($p < 0.001$, $R = 0.57$) to later increase moderately. As a consequence, the increase in mineral content is drastic and highly significant until 40 years ($p < 0.001$, $R = 0.77$) and after plateaus until 80 years.

Further, a number of architectural parameters of mineral crystals seems to mature at 40 years of age. For instance, CL002 increases and then decreases with approximately the same intensity for both age ranges as can be seen in Figure 6.16a/b. The same decrease is seen after 40 years of age for CL004 but no other significant changes were found. This suggest that the increase in length of the crystal is followed by shrinkage.

Considering the compositional changes analysed by FTIR, from Figure 6.17e/f, collagen content steeply decreases until the age of 30 years ($p = 0.034$, $R = -0.44$) while no clear changes are shown afterwards. In contrast, the degree of mineralisation of the matrix (MM) do not show any clear changes. Turning now to the mineral composition and architecture, mineral crystallinity does not show clear trends with age and therefore does not allow any inference (Figure 6.17g/h) the carbonate substitution clearly increases along the entire age range: the intensity is higher before 30 years ($p < 0.001$, $R = 0.65$) compared to afterwards ($p = 0.014$, $R = 0.26$).

There are, however, other parameters for which maturity is reached later in life. For instance, collagen thermal stability ($L\Delta H$), that explains the energy required to break the hydrogen bonds in the triple helix configuration, show a significant decrease until the age of 50 years ($p = 0.0013$, $R = 0.38$), without showing any specific trends afterwards. Further, lattice size along the 'a' axis constantly decreases until the age of 50 years (Figure 6.18). No other variables were identified to show this two phase behaviour.

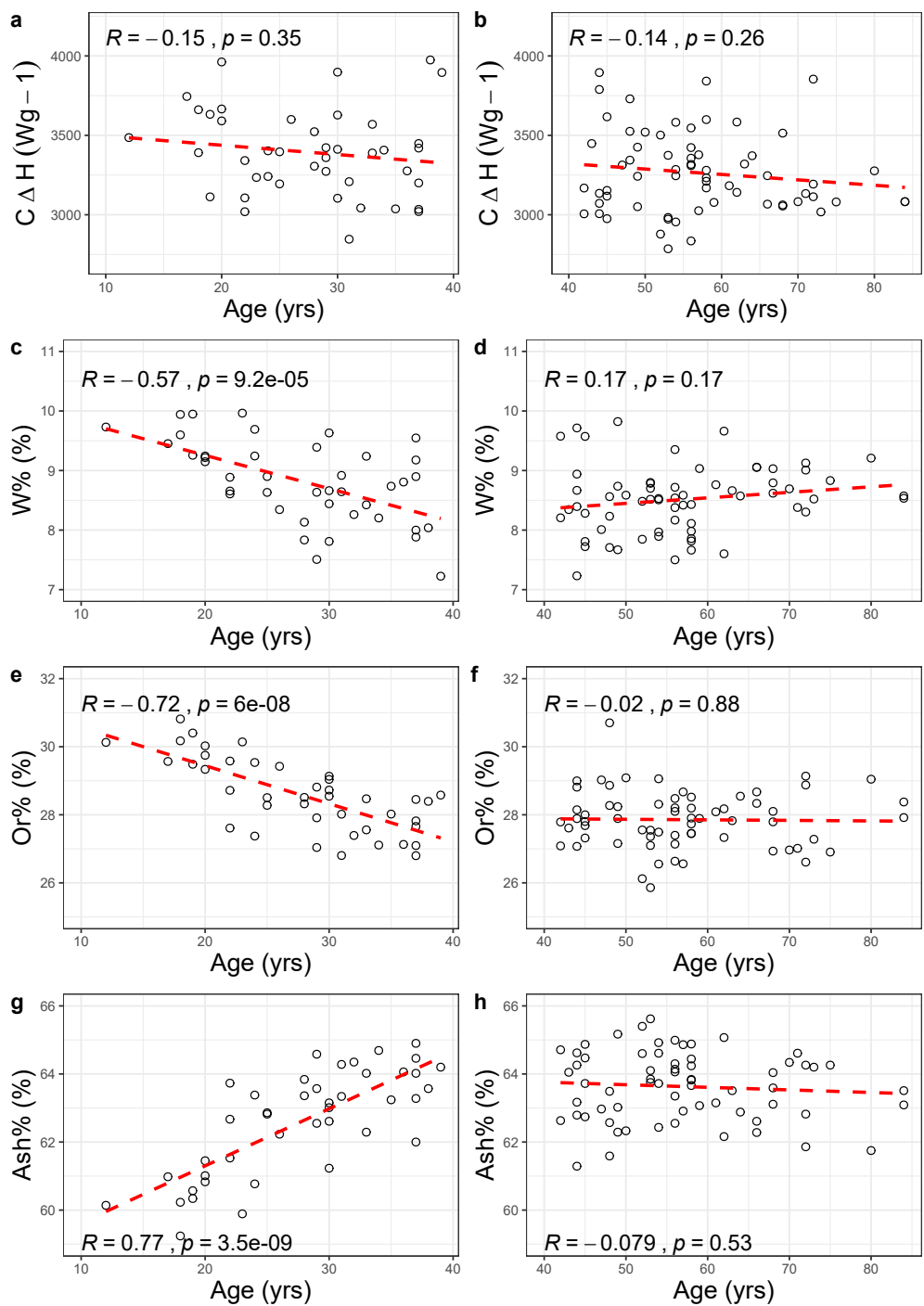


Figure 6.15: Behaviour of collagen and mineral related physicochemical parameters acquired by thermal analysis show an increase in mineral content and a decrease in organic and water phase.

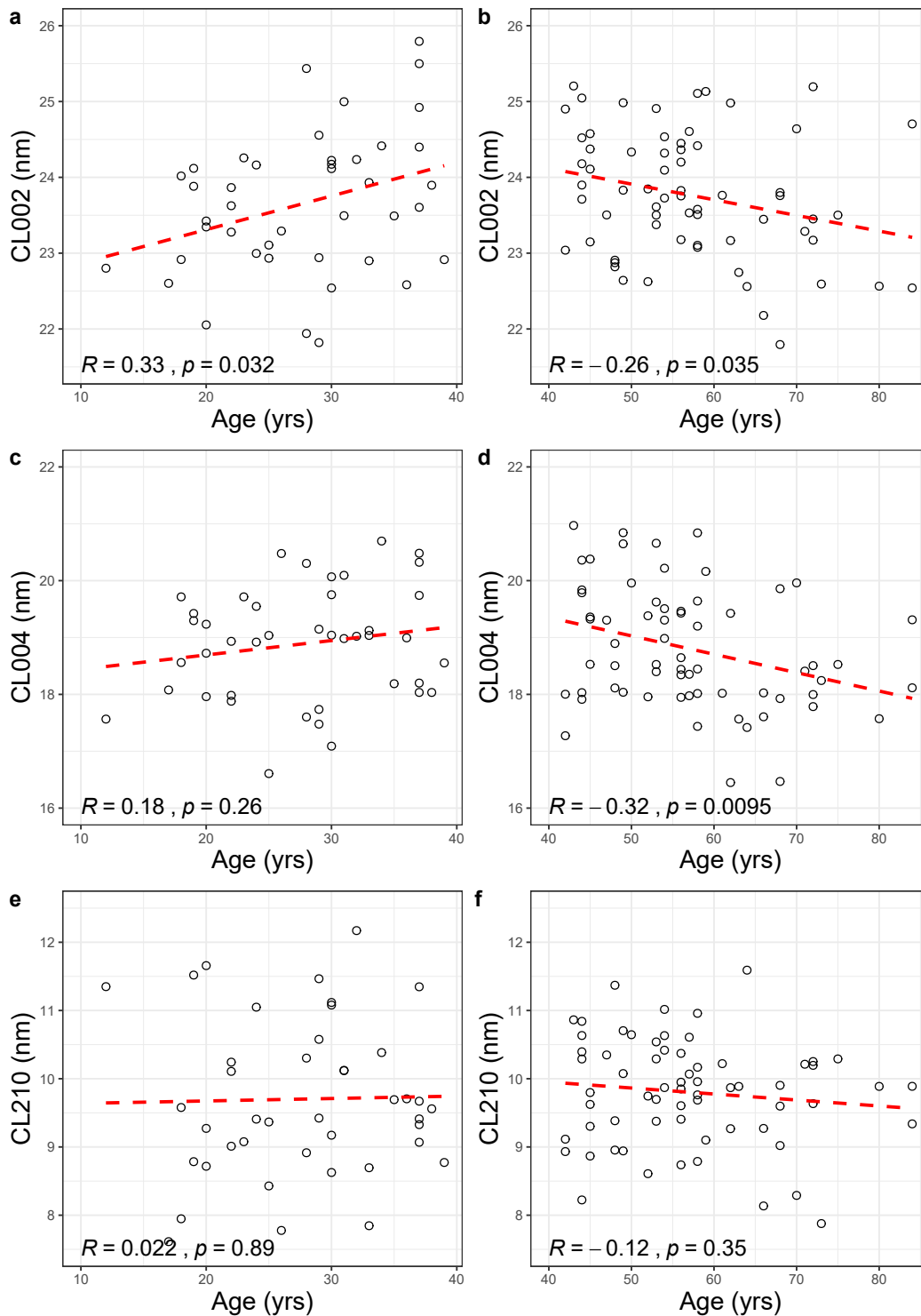


Figure 6.16: mineral crystal length reaches its maximum at 40 years. The first increase is associated with carbonate substitution (Figure 6.17c/d) and followed by crystal size reduction.

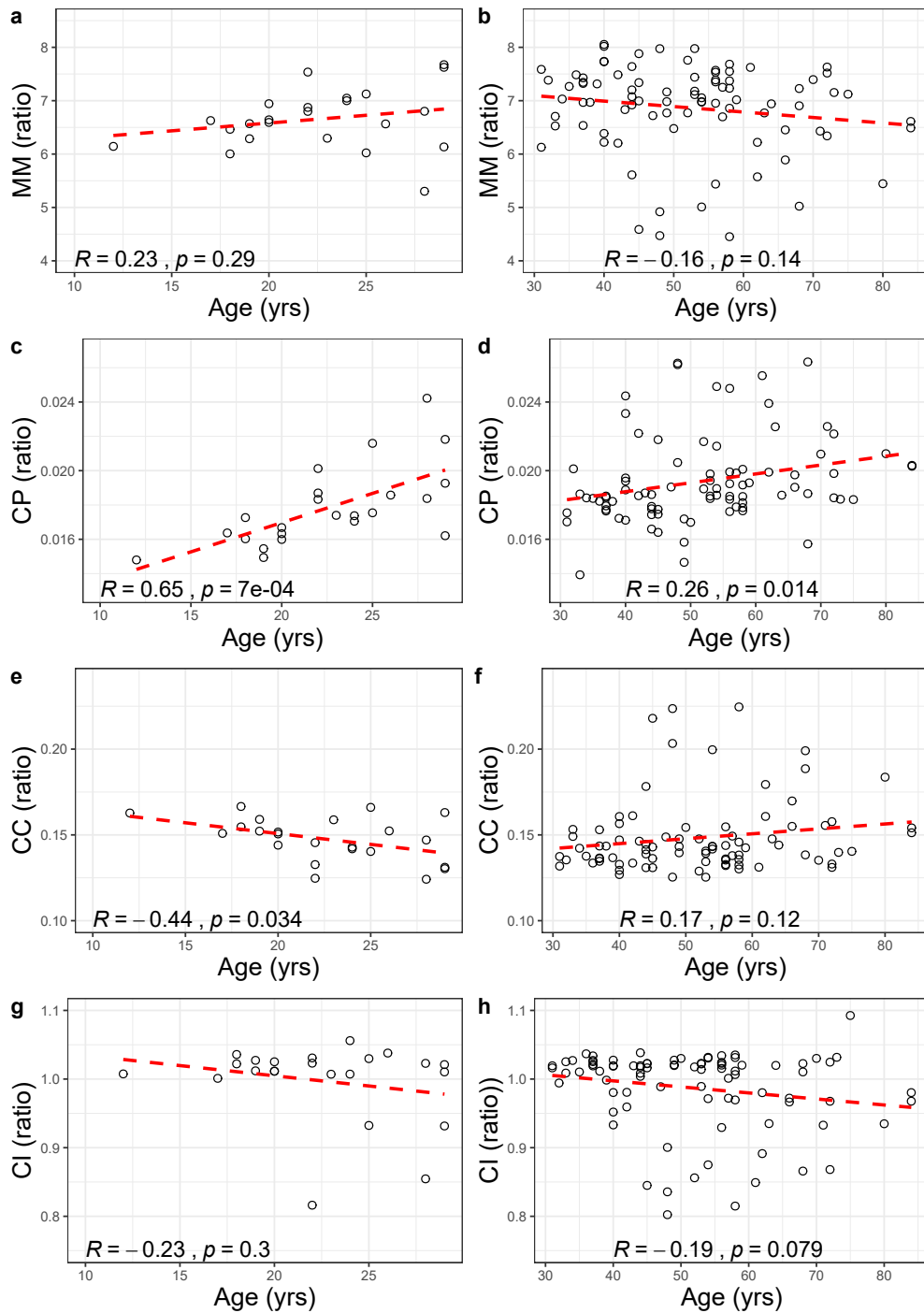


Figure 6.17: Infrared spectroscopy shows that the majority of this variation occurs until the age of 30 years. However, no clear trends are shown by mineral to matrix ratio and crystallinity index.

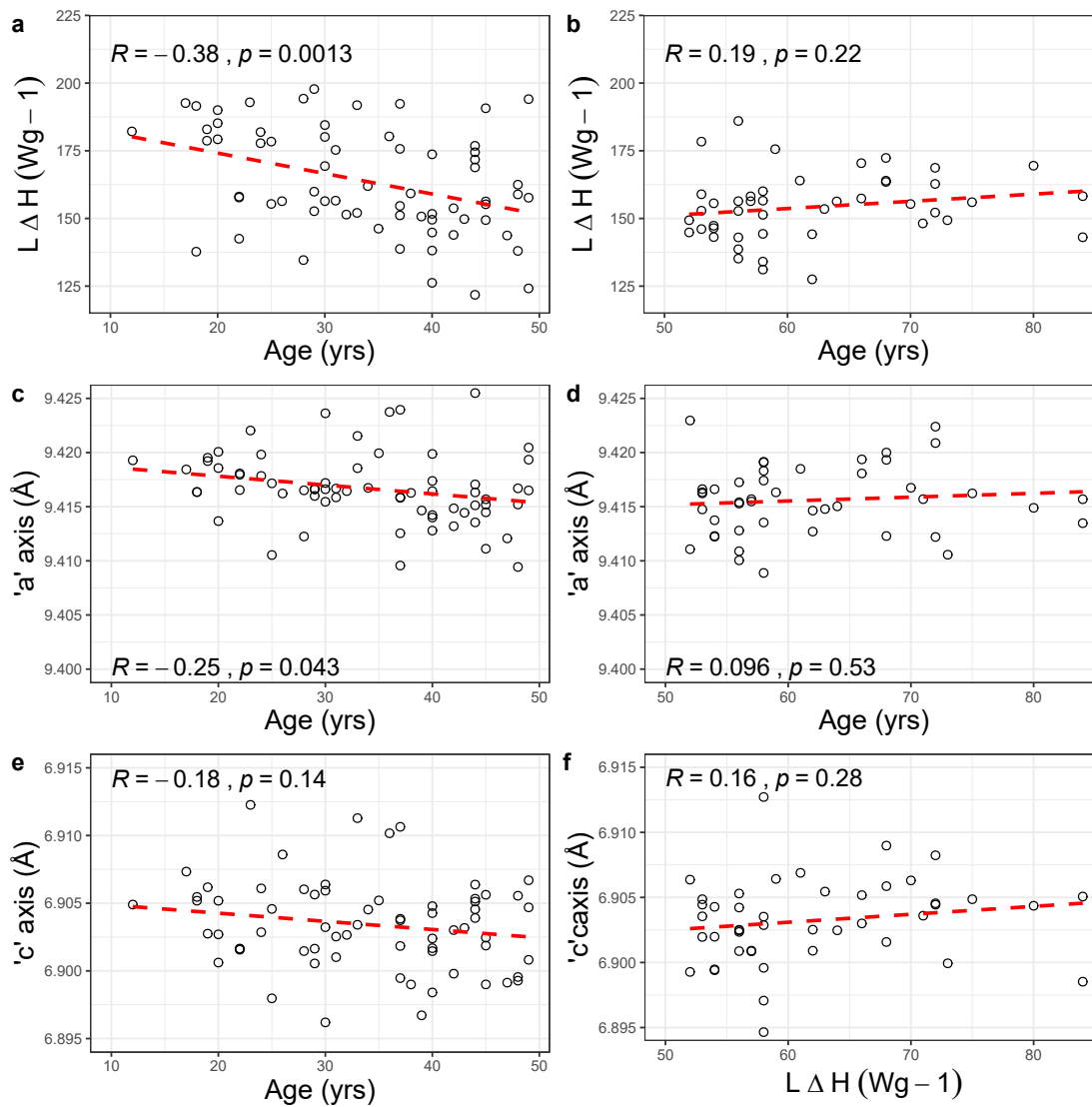


Figure 6.18: *thermal stability and 'a' axis decrease until 50 years of age compared to what shown for the other physicochemical parameters. It is interesting to note that the behaviour of the lattice parameter is opposite compared to the crystallite size ones but, the lack of clear correlations does not allow confident speculations.*

Overall, according to the present results different components of bone matrix reach maturity at different ages and this determines the complex mechanical behaviour of bone matrix. For the properties for which no clear trends are shown, the cause is attributed to the low sensibility of the methodology rather than the intrinsic behaviour of the matrix.

6.8 Age estimation - Unrestricted Parameter Selection

The first step in age estimation for this study was to produce different models involving the entire set of parameters based on backward (PR1) and forward stepwise selection (PR2), and BIC selection (PR3).

Table 6.18: Parameter selection based on the entire set of parameters (*: $p \leq 0.05$; **: $p \leq 0.01$; ***: $p \leq 0.001$).

Variable	PR1	PR2	PR3
Intercept	-141.122**	-6697.083	-70.449***
Po.Ar%	6.317***	6.327***	5.895***
$^{On}\eta_{IT}$	1.885***	1.764	1.261***
^{It}H	-0.393**	-0.541	-0.215**
^{It}E	1.089*	1.342	
$^{It}C_{IT}$	2.263	3.366	
^{On}HV	0.285	0.191	
^{It}HV	0.409	0.342	0.763***
LΔH	0.072	0.094	
MM	-3.884	-3.670	
CP	1063.700*	876.608	
CI	36.270	36.115	
CC	-159.743*	-139.770	
Size	0.286	0.367	
CL030	5.032**	5.166*	4.151*
^{On}H		-0.060	
^{On}E		0.449	
$^{On}C_{IT}$		1.091	
$^{It}\eta_{IT}$		1.333	
CΔH		-0.005	
W%		63.570	
Or%		65.904	
Ash%		65.379	
Strain		-297.445	
CL002		-0.089	
CL004		0.062	
CL210		-0.320	

This was aimed at achieving a higher accuracy without taking into consideration the

time and facilities constraints. Results are shown in Table 6.18. Table 6.19 shows the parameters use to test model accuracy for unrestricted parameters selection. Plots showing real age and predicted age and diagnostic plots for PR4 to PR7 are reported in Appendix C.

Table 6.19: (*RSE: residual standard error; *: $p \leq 0.05$; **: $p \leq 0.01$; ***: $p \leq 0.001$; (R^2 : coefficient of estimation; RSE: residual standard error; AIC: Aikake information criterion; BIC: Bayesian information criterion)*).

Variable	PR1	PR2	PR3
RSE	6.352	6.596	6.819
R^2	0.873	0.880	0.840
R^2 -adj	0.855	0.843	0.832
BIC	798.041	848.524	781.456
AIC	754.403	772.157	762.364
p	<0.001	<0.001	<0.001

For backward stepwise regression (PR1), a selection of 15 mechanical and physico-chemical parameters was used to calculate the age-at-death. This was done with a significant regression equation ($F(14,98) = 48.02, p < 0.001$) that explains 87% of the total variance. The mean error of the estimate was found to be 6.35 years.

The regression slope is significant with $p < 0.01$, with only few predictors significant with age ($Po.Ar\%$, ${}^t\eta_{IT}$, tH , tE , CP, CC and CL030). All the variables fall into an acceptable range for multi-collinearity. Residuals present normal distribution ($W = 0.98, p = 0.51$) and the acceptable results are shown for autocorrelation with $D-W = 2.21$ and $p = 0.37$. Table 6.20 shows that residuals do not show skewness or kurtosis, and have equal variance (heteroscedasticity). Link function proves a good relationship between the linear model and response variables.

Diagnostic plots (Figure 6.19) confirm linearity, normal distribution and homogeneity of variance for residuals. Even though outliers are present, they do not influence the estimation as ascertained from tests with Cook's distance. Figure 6.19 shows that three outliers are present in the estimation with a general tendency of overestimation.

Table 6.20: Linear model assumption with global test based on 4 degree of freedom for PR1.

	Value	p-value	Decision
Skewness	0.6302	0.4273	Assumptions acceptable
Kurtosis	1.3718	0.2415	Assumptions acceptable
Link Function	2.4634	0.1165	Assumptions acceptable
Heteroscedasticity	0.1378	0.7105	Assumptions acceptable

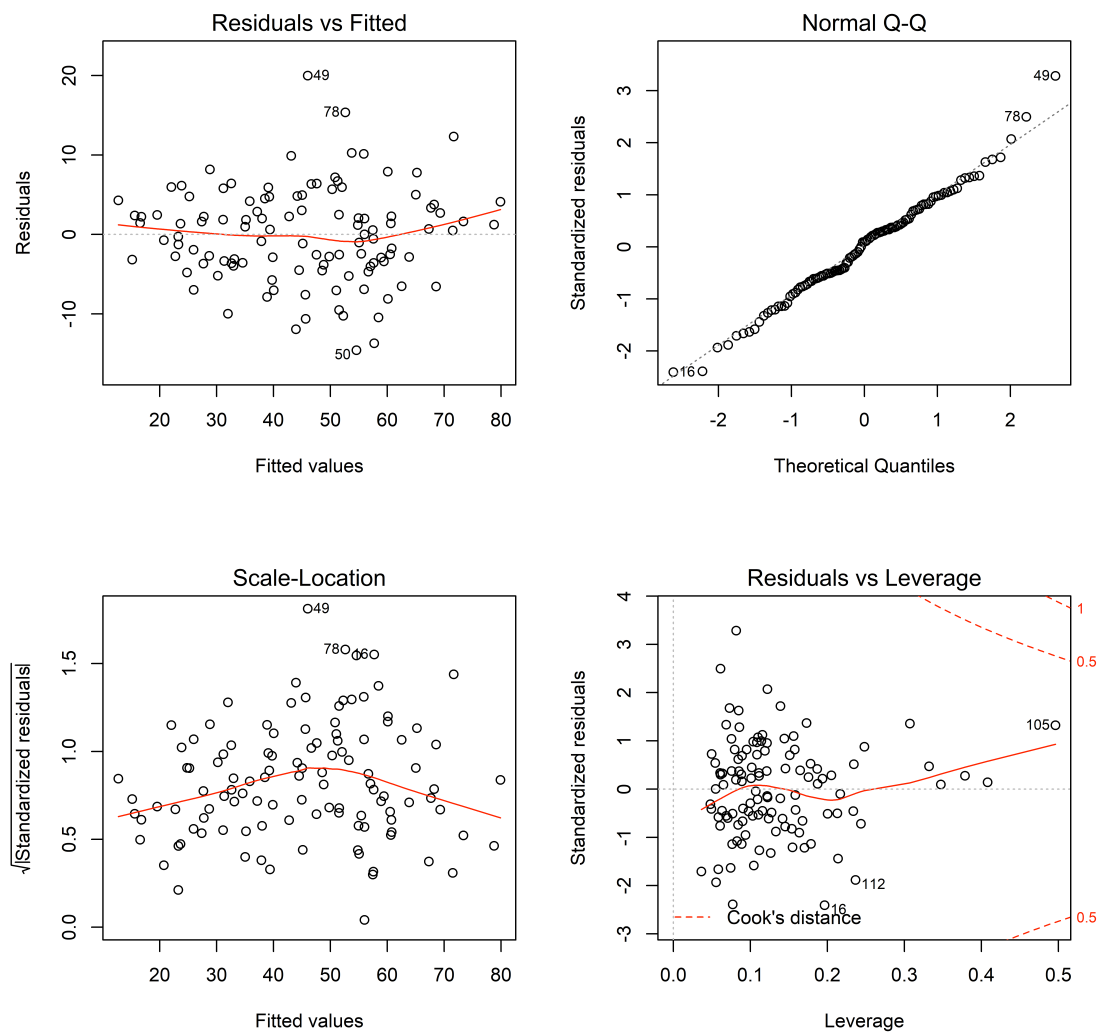


Figure 6.19: Visual diagnostic for backward selection of the full model (PR1).

PR2 involves forward stepwise parameter selection. The resulting equation (Table 6.18, $F(26,86) = 24.17$, $p < 0.001$) involves a larger number of predictors compared to the previous model with only Po.Ar% and CL030 being statistically significant. It shows $R^2 = 0.88$ and $R^2\text{-adj} = 0.84$. The standard error of the estimate is 6.59 years, showing a slightly poorer performance in comparison to the previous model. All the variables comply with the multicollinearity assumption.

Linear assumptions are all met as shown in Table 6.21. When tested, distribution of the residuals and autocorrelation does not show any significant correlation with S-W tests, showing $W = 0.99$, $p = 0.67$ and D-W test = 2.12 and $p = 0.61$. Considering the diagnostic plots in Figure 6.20, the roughly straight line in the Residuals vs Fitted plot confirms a good linear distribution of the residuals as well as the good fit of the Q-Q plot. Homoscedasticity is visible in the residual distribution of the Scale-Location plot, with a slight decrease towards older age ranges. The absence of outliers is confirmed by the Residuals-Leverage plot and all the individuals are below 1 for the Cook's distance.

Table 6.21: *Linear model assumption with global test based on 4 degree of freedom for PR2.*

	Value	p-value	Decision
Skewness	0.1492	0.69931	Assumptions acceptable
Kurtosis	1.322	0.25030	Assumptions acceptable
Link Function	3.714	0.05395	Assumptions acceptable
Heteroscedasticity	0.441	0.99470	Assumptions acceptable

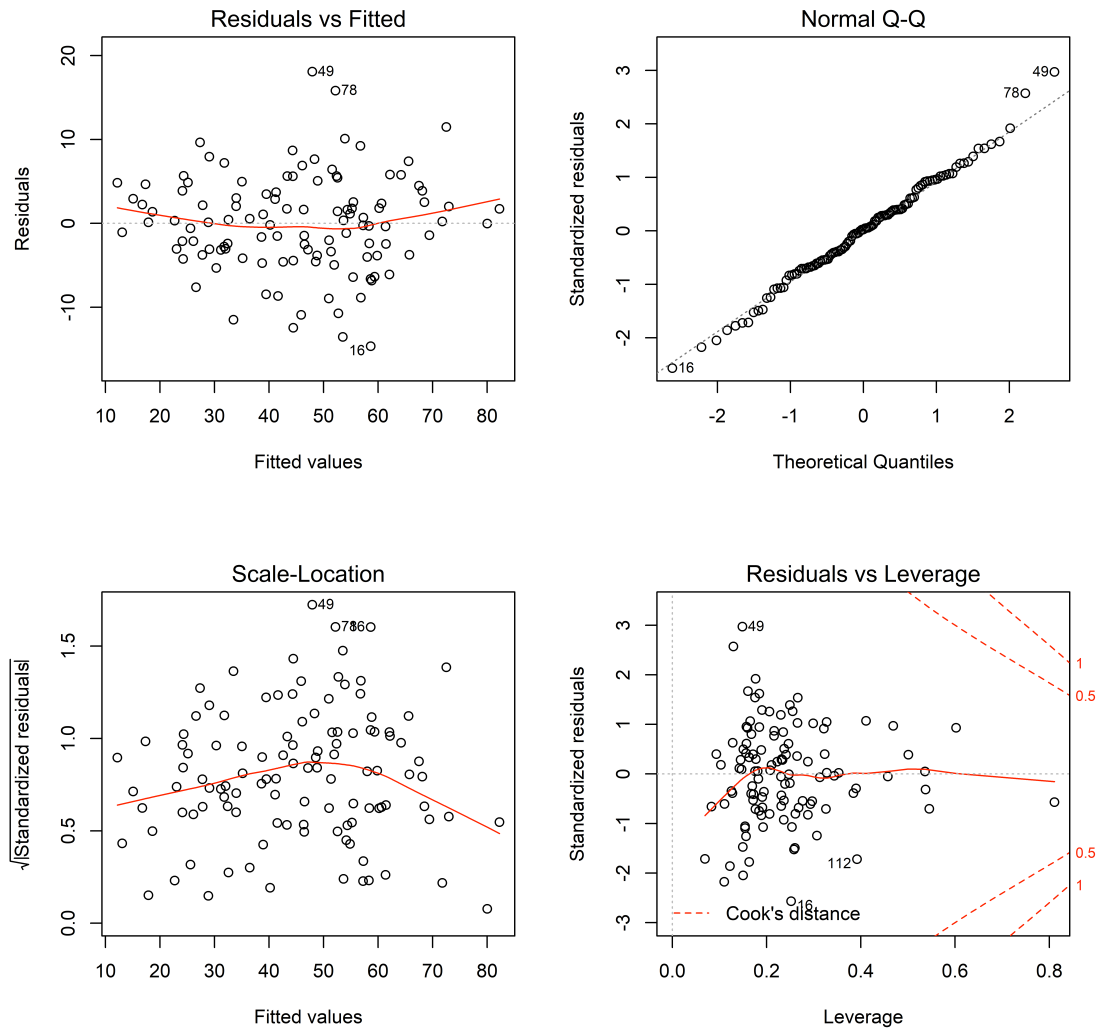


Figure 6.20: Visual diagnostic for forward selection of the full model (PR2).

The final model (PR3) in this study was developed using Bayesian selection. Age-at-death was predicted by $Po.Ar\%$ and CL030 as structural parameters and three mechanical parameters ($^{On}\eta_{IT}$, ^{It}H and ^{It}HV). All the predictors are found to be significant and none of them shows collinearity. The model is not affected by autocorrelation (D-W = 1.952388, $p = 0.756$). Distribution was also evaluated as shown in Table 6.22.

Table 6.22: Linear model assumption with global test based on 4 degree of freedom for PR3.

	Value	p-value	Decision
Skewness	2.040	0.15317	Assumptions acceptable
Kurtosis	3.015	0.08249	Assumptions acceptable
Link Function	1.351	0.24504	Assumptions acceptable
Heteroscedasticity	1.532	0.21584	Assumptions acceptable

In terms of accuracy, the model presents $R^2 = 0.84$ and $R^2\text{-adj} = 0.83$ with a mean error of 6.82 years. It is the equation with lower predictive power between the ones developed from the entire set of predictors. Residuals are found to be normally distributed (S-W: $W = 0.98$, $p = 0.054$). These results are confirmed by the diagnostic plots in Figure 6.21 and no outliers are present when considering Cook's distance.

The only statistical difference according to sex for the entire pool of variables was found for $Po.Ar\%$ and $C\Delta H$. When hierarchical multiple regression is applied to these three models with the inclusion of sex as a variable, PR1 showed a slight increase in accuracy with $R^2 = 0.872$ for the original model and $R^2 = 0.874$ for the model incorporating sex as a categorical variable. Predicted values are proved not to be statistically different. PR2 and PR3 show very similar results with no significant difference and an increase in R value of 0.001. Considering the inconclusive results, no further investigation was carried out for estimating the age.

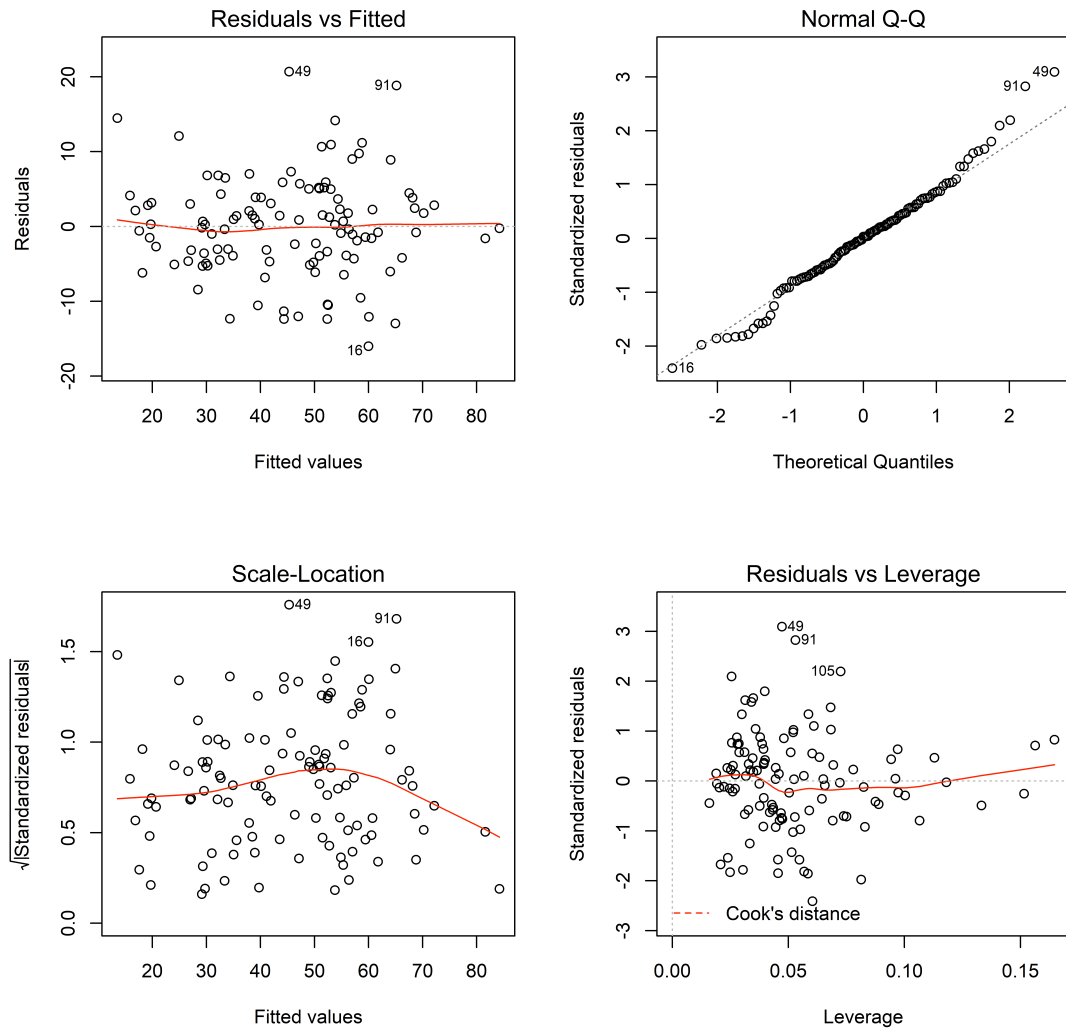


Figure 6.21: Visual diagnostic for forward selection of the full model (PR3).

6.9 Age estimation - Restricted Parameter Selection

Restricted parameters selection was based on limitation of testing machines available. In order to achieve this, parameters were divided by experimental procedure and BIC selection was applied. The same diagnostic tools were used to test these estimation models and the relevant graphics are reported in Appendix C.

The first model (PR4) was developed using the parameters obtained with the nanoin-

denter. Preparation involves section cutting and defatting procedure for a total of 36 hours. The clean sections are then dried out overnight, mounted in resin and polished. These steps take approximately 36 hours after which the mounted samples is ready for testing. The total experimental procedure takes a duration of three days. In addition to mechanical parameters, it allows calculation of Po.Ar% using BoneJ. Equation 6.1 shows the variables selected.

$$Age = -62.0633 + Po.Ar\% \times 6.0734 + {}^{It}H \times -0.6235 + {}^{It}E \times 1.6347 + {}^{It}\eta_{IT} \times 2.2082 + {}^{It}HV \times 0.5989 \quad (6.1)$$

The prediction model ($F(5,107) = 111.1, p < 0.001$) shows a good accuracy with $R^2 = 0.839$ and $R^2\text{-adj} = 0.831$ and a mean error of 6.85 years. All the variables are significant at $p < 0.01$ and the model shows no autocorrelation ($W = 1.91, p = 0.54$). No multi-collinearity was detected and all the assumptions for skewness, kurtosis and heteroscedastic are acceptable. M-W confirms normal distribution of the residuals ($W = 0.98, p = 0.2162$). Cook's distance verifies the absence of outliers. BIC is 782.44 and AIC 763.35.

In contrast, thermal analysis employs bone powder that has a preparation time of approximately 12 hours while the experimental procedure takes two hours. Results (PR5) do not show the same degree of accuracy with a model ($F(4,108) = 8.988, p < 0.001$) with an error of 14.69 years and $R^2 = 0.250$ and $R^2\text{-adj} = 0.222$ (Equation 6.2). Although almost all general linear assumptions are met with the exception of the link function (value = 7.60 and $p = 0.006$), null hypothesis for autocorrelation is rejected when tested with D-W (1.57, $p = 0.012$). M-W test also proves non-normal distribution of the residuals with $W = 0.971$ and $p = 0.017$. Some of the individuals also violate Cook's distance. All variables except LΔH violate the collinearity assumption. Distribution of the predicted age seems to have a linear behaviour until the age of 40 years and then exponentially increases. AIC and BIC are respectively 934.91 and 951.29.

$$Age = -1.017e^5 + L\Delta H \times -3.001e^{-1} + Wt_{\%} \times 1.022e^3 + Or_{\%} \times 1.014e^3 + Ash_{\%} \times 1.020e^3 \quad (6.2)$$

Similar results are given by the model (PR6) developed using ATR-FTIR (Equation 6.3). Although preparation time and experimental execution is the shortest of all the methods, the examination results do not show acceptable accuracy in a forensic setting. The model ($F(3,109) = 9.154$, $p < 0.001$) is tested and an inaccuracy of 15.09 years is obtained. There is the same loss of accuracy detected for individuals over the skeletal maturity age as explained before. This inference is drawn from an R^2 value of 0.201 and R^2 -adj 0.179, with $AIC = 939.99$ and $BIC = 953.63$. Skewness and kurtosis assumptions are respected, as well as heteroscedasticity, while link function is violated with value = 6.410 and $p = 0.232$. None of the parameters showed multicollinearity. However, the model shows a slight positive autocorrelation and residuals are not normally distributed ($D-W = 1.776$ and $p = 0.218$; $M-W = 0.965$ and $p = 0.005$).

$$Age = -149.957 + 12.532 \times MM + 2968.906 \times CP + 358.070 \times CC \quad (6.3)$$

The last model (PR7) was developed employing the same bone powder to run XRD. Results are not satisfying with $R^2 = 0.104$, R^2 -adj = 0.088 and $MSE = 15.91$ years ($F(2,111) = 6.41$), $p = 0.002$ (Equation 6.4). Nevertheless, all linear model assumptions are acceptable. No outliers are detected and residuals are normally distributed ($M-W = 0.986$ and $p = 0.283$). A slight negative autocorrelation was observed but not significant ($D-W = 1.606$, $p = 0.015$). Collinearity assumption is respected. AIC and BIC , which are the highest recorded, are 950.93 and 961.84, respectively.

$$Age = 1118.099 + d'axis \times -1185.671 + CL030 \times 11.145 \quad (6.4)$$

6.10 Age Dtermination - Sex Specific Regression Formulas

Analysis of covariance (ANCOVA) showed that only two of the entire sets of variables were significant. There is a significant effect of sex on age after controlling Po.Ar% in function of age , $F(1,110) = 4.359$, $p = 0.039$. Furthermore, there is also an effect of sex on CAH when involved in age estimation ($F(1,110) = 4.269$, $p = 0.041$).

Table 6.23 compares the models developed with backward stepwise regression (Table D.1 in Appendix D). Results for the male individual samples show an improvement in all the regression diagnostic. Residuals are normally distributed ($w = 0.98$, $p = 0.43$) and the model does not show autocorrelation ($D-W = 1.78$, $p = 0.28$). Finally, results for multi-collinearity are acceptable. For females, there is an increment in R^2 compared to the unknown sex model but it remains lower than the male one. However, RSE is the lowest for all the models as well as AIC and BIC, indicating a lower degree of overfitting for this model. This could be due to the reduced sample size. Normal distribution of residual ($w = 0.94$, $p = 0.051$), autocorrelation ($D-W = 1.79$, $p = 0.38$) and collinearity are all respected. Regression plots in Appendix D do not show any anomalies for both groups. No issues were found in diagnostic plots (Appendix D).

Table 6.23: *Comparison between models created with backward selection for the entire sample and split between male and female.*

Variable	PR1	PR1 - Male	PR1 - Female
Observations	113	77	36
R^2	0.873	0.903	0.898
R^2 -adj	0.855	0.879	0.873
RSE	6.352	5.860	5.829
F	48.021 (df = 14; 98)	37.955 (df = 15; 61)	35.234 (df = 7; 28)
AIC	798.041	506.868	238.037
BIC	754.403	546.713	252.288

Similarly, results for PR2 show an increase in R^2 for the sex specific formulae and an improvement in AIC and BIC. No substantial variation is seen in the estimation error, however the model for the female group presents the worst performance. Residuals are

normally distributed for both male ($w = 0.98$, $p = 0.43$) and female ($w = 0.91$, $p = 0.051$). In the same way, autocorrelation is respected (male: $D-W = 1.78$, $p = 0.31$; female: $D-W = 1.78$, $p = 0.37$). Collinearity is violated for several variables for the female model. Additionally, diagnostic plots (Appendix D) for PR2 - samples from female individuals show that there are a number of outliers that violate Cook's distance. Overall, the female specific model is unsuitable for age estimation due to statistical reasons.

Table 6.24: Comparison between models created with forward selection for the entire sample and split between male and female.

Variable	PR2	PR2 - Male	PR2 - Female
Observations	113	77	36
R^2	0.880	0.907	0.932
R^2 -adj	0.843	0.858	0.737
RSE	6.596	6.349	8.375
F	24.169 (df = 26; 86)	18.725 (df = 26; 50)	4.771 (df = 26; 9)
AIC	848.524	525.914	261.272
BIC	772.157	591.541	305.610

Finally, Table D.3 presents results for specific groups regression. What is immediately evident is the fact that all the variables are in this case significant for age estimation. Best results are shown for the male group with the highest R^2 and the lowest residual of the estimation. Durbin-Watson does not show autocorrelation ($D-W = 1.78$, $p = 0.28$), residuals are normally distributed ($w = 0.98$, $p = 0.36$) and no collinearity is shown for any of the variable. From the diagnostic plots no issue raised (Appendix D). The model for females normal distribution is respected ($w = 0.99$, $p = 0.98$) but there is positive autocorrelation ($D-W = 1.44$, $p = 0.044$). No collinearity was detected. AIC and BIC are the lowest between the three groups (Table 6.25) and accuracy is higher compared to the entire sample results.

Table 6.25: Comparison between models created with backward selection for the entire sample and split between male and female.

Variable	PR3	PR3 - Male	PR3 - Female
Observations	113	77	36
R ²	0.840	0.886	0.856
R ² -adj	0.832	0.867	0.843
RSE	6.819	6.153	6.476
F	112.280 (df = 5; 107)	46.069 (df = 11; 65)	63.484 (df = 3; 32)
AIC	848.524	511.268	242.431
BIC	772.157	541.737	250.348

6.11 Cross-validation

To simulate the application to unknown skeletal remains and to fully understand the potential of the three models in forensic settings, leave-one-out (LOO) cross-validation was first applied. For the unrestricted parameter selection, PR1 and PR2 show a considerable loss in R² while only an increase in mean absolute error (MAE) of ~1 year. PR3 retains the accuracy compared to the previous models with the increase in mean absolute error (MAE) of less than 1 year. Similar results are shown by PR4, that is the second best performing models in terms of accuracy after cross-validation. This also involves a limited number of machinery reducing the expertise necessary for the experimental procedure. The remaining models show a generalised loss in accuracy and results are not suitable for age estimation in forensic setting.

After k-fold cross-validation (in Table 6.26), the best model is PR5, including mechanical and histological analysis. The only difference recorded is an increase in MAE by 0.14 years. Very similar chance for the unrestricted selection models, while the rest of the results confirms how the rest of the models are not suitable for the AAD. Repeating k-fold procedure three times (in Table 6.26) shows that the smallest MAE is given by PR3 (MAE = 5.23 years) while the best performing method in terms of accuracy remains PR4 with R² = 0.838 compared with R² = 0.835 of PR3.

Table 6.26: Comparison between original results and cross-validated for the unrestricted parameter selection (MAE = mean absolute error; CV: cross-validated).

Model	Leave-one-out				10-fold				10-fold x 3			
	R ²	MAE	CV R ²	CV MAE	R ²	MAE	CV R ²	CV MAE	R ²	MAE	CV R ²	CV MAE
PR1	0.873	4.72	0.808	5.68	0.873	4.72	0.814	5.72	0.873	4.72	0.826	5.55
PR2	0.880	4.47	0.809	5.60	0.880	4.47	0.847	5.66	0.880	4.47	0.827	5.75
PR3	0.840	4.96	0.822	5.23	0.835	5.28	0.818	5.73	0.840	4.96	0.846	5.18
PR4	0.839	5.10	0.821	5.38	0.839	5.10	0.839	5.24	0.839	5.10	0.848	5.40
PR5	0.251	12.05	0.186	12.59	0.251	12.05	0.22	12.7	0.251	12.05	0.232	12.51
PR6	0.201	12.61	0.152	12.96	0.201	12.61	0.189	13.04	0.201	12.61	0.234	12.95
PR7	0.104	12.09	0.062	13.35	0.104	12.09	0.148	13.23	0.104	12.09	0.171	13.25

CHAPTER 7

DISCUSSION

The results presented in the previous chapter gave an insight into the age-related variation of mineral and organic matrix. Furthermore, the structural relationship between collagen and mineral have been presented as well as the effect of various components on the mechanical behaviour. Finally, results regarding skeletal maturity and age estimation were presented. These results and their inferences are further discussed in this chapter. A total of 113 specimens were analysed using XRD from different crystallographic directions to understand the modification of crystal size and strain with age. These results were combined with spectroscopic and thermal analysis of the organic matrix to investigate not only the deterioration with age but also the effect of collagen degeneration on the mineral strain and consequently on crystal size. This research is aimed to combine different physico-chemical and mechanical parameters to understand their potential for age estimation of unidentified remains in forensic contexts.

This chapter will consider the results of this research and compare them with what is previously presented in the literature. It will discuss the effect of chemical preparation procedures on the quantification of physicochemical parameters (Section 7.1). Further, the variation of mechanical properties with sex and age, with particular attention on skeletal maturity (Sections 7.2, 7.3 and 7.5) are also discussed. Understanding the mechanical behaviour of bone is of utmost importance as it represents one of the main challenges for medical and forensic applications. The chapter will discuss the interaction between organic and mineral phase, and possible interpretations regarding the combined changes in organic and mineral matrix (Section 7.4). The chapter will conclude with comparing the method developed in this thesis with the most commonly used laboratory-based protocols for age-at-death estimation considering advantages, disadvantages, applicability and accuracy (Section 7.6).

7.1 Chloroform-methanol Preparation

After considering the methods currently used for sample degreasing, the choice of chloroform-methanol preparation was made due to its consistency and effectiveness reported in literature for removing organic material and non-structural water. This preparation method was tested before adoption for assessing all the samples in the study. The advantage is that it does not affect the physiological properties but impacts the crystal size. The preparation method is key as a choice of a different method can affect the age estimation and diverges from the protocol detailed in this thesis. The author suggests that if a user would like to employ the age estimation method it is necessary to apply the degreasing protocol in order to obtain consistent results despite what regression model is chosen.

First, the effects of particle size and homogeneity of powder on spectroscopic and diffraction analysis is well known (Kontopoulos et al., 2018; Londoño-Restrepo et al., 2019). Data reported an increment in crystallinity and a decrease in $\nu 2\text{CO}_3^{2-}$ to $\nu 3\text{PO}_4^{3-}$ ratio with decreasing particle size (Kontopoulos et al., 2018). It is also pointed out that there was an increase in absorbance when the particle size decreases and a shift towards higher wavenumber values of most of the components (Kontopoulos et al., 2018). In the regard of XRD analysis the effect of increased particle size leads to a broadening of the peaks (Londoño-Restrepo et al., 2019). For this reason the powder was processed in order to obtain homogeneous 106 μm powder that allows consistent data acquisition. To date, not a large amount of work has been done on investigating the physicochemical changes induced by the chloroform-methanol defatting protocol. Therefore, it is appropriate to begin the discussion with understanding how the bone matrix is affected by this procedure. Not surprisingly, the most striking outcome of the experiment was the reduced enthalpy values for the exothermic peak responsible for organic components combustion for treated and untreated bone. As previously explained, the bone organic matrix is composed primarily by type I collagen but also by other types of collagen in a smaller percentage and several non-collagenous proteins (Currey, 2002). As noted by different studies, collagen thermal denaturation varies according to the choice of pre-treatments (Lozano et al., 2003;

Miculescu et al., 2011). In the present study, no statistical differences were shown in collagen denaturation and shrinkage suggesting that the treatment does not affect molecular stability and successfully removes the excess of fat and bone marrow increasing the consistency of the results. This is shown by the significant reduction in enthalpy value for the organic combustion peak that is lower due to the removal of superficial grease and marrow removal (Section 6.1). Additionally, one significant difference was found in the water fraction. These results were also expected as the second purpose of this procedure was to eliminate non-bound (surface) water left in the pores in cortical bone. The final ethanol bath aims to remove the viscous chloroform and methanol residues from the bone surface (Unal and Akkus, 2015; Unal et al., 2019) and simultaneously reduce the non-structural water in the sample allowing the measurement of bound water. This is achieved as the water measurements did not show any statistical difference between the two groups. However, this specific treatment and the potential for surface water removal needs to be further tested with NMR.

With regards to the mineral matrix, the objective was to evaluate any compositional modification induced by the consecutive bath sequences. No statistical difference was shown by infrared results suggesting little or no variation in ion substitution or crystallinity index as explained in Section 6.1. The similarity of mineral to matrix between the two groups suggests that the examination is extremely effective in the quantification of HAp and no biasing effect is introduced by the defatting procedure. As seen in Figure 6.1, there is a variation of approximately 1 nm for coherence lengths at almost all peaks. For 002 and 004, results show an increase while there is a decrease for 210. In contrast, no statistical difference was found for CL030. This is consistent with the results of Su et al. (2018) that could not find variation between treated and untreated bone. The difference, however, was expected and it is believed to be due to the increase in ion substitution induced by the solution. This is supported by Bas and Cardona (2018) who found a significant increase in both $\delta^{15}\text{N}$ and $\delta^{13}\text{C}$ isotope ratios after the use of chloroform-methanol delipidation treatment of fish bone.

The use of consecutive baths in methanol–chloroform solution and ethanol have been

employed in different fields to eliminate fat and bone marrow from specimens. It is used in mechanical characterisation (Zioupos, 2001; Rho et al., 2002; Cook and Zioupos, 2009), X-ray diffraction (Rogers and Daniels, 2002; Dicken et al., 2016) and spectroscopic analysis (Karampas et al., 2013; Paschalis et al., 2014; Gamsjaeger et al., 2017). It has also been used in pre-operative sterilisation procedures (Kaku et al., 2002; Bettin et al., 2003). However, several different procedures have been developed for both deproteinisation and decalcification of bone to isolate and better investigate the two components separately. These have been seen to induce both structural and compositional changes to bone. This could represent an important limitation when trying to obtain real data regarding the bone as well as introducing bias when these techniques are applied to forensic anthropology. However, the amount of grease, marrow and surface water that is retained by the structure is proportional to porosity and, therefore, age. The removal of these components increases consistency of the results by ensuring that the actual properties are analysed.

In terms of efficiency, Jimson et al. (2014) compared several decalcification agents normally used in bone histology considering parameters essential for experimental design such as time constraint, degree of mineralisation and staining techniques to be applied. They showed that the use of strong acid (e.g. 5 % nitric acid) is the most efficient in terms of time but it induces a loss in nuclear staining and damages soft tissues. Similarly, the use of neutral tetra-sodium ethylenediamine tetra-acetic acid (EDTA), largely applied in biomechanics, induces some degree of distortion of collagen fibres but shows good potential for maintaining intercellular structures, although it remains the most time-consuming amongst the agents reviewed. Solutions of 10% formic acid, in contrast, prevent cellular and collagen shrinkage (Jimson et al., 2014). Overall, EDTA is concluded to be the most efficient and less invasive procedure and therefore it is very often employed for the analysis of collagen via infrared spectroscopy (Paschalis et al., 2001, 2003, 2011).

The opposite procedure of demineralisation is deproteinisation, that allows isolation of the mineral matrix. Approaches are various and the most direct is the heat treatment. The main disadvantage of this procedure is the increase of crystal size after exposure to heat for long periods (e.g. 600°C for 24 hours). Chemical methods are also often employed in de-

fattening and deproteinization of bone, mainly chloroform and methanol, hydrogen peroxide, and acetone (Liu et al., 2013). The main drawback of these chemical approaches is that no sources are available to explain the destruction induced by these treatments to the mineral. Su et al. (2018) tested the effect of different deproteinisation procedures on porcine cortical bone to understand the modifications induced by these to XRD, SEM, TGA spectroscopic techniques. The team treated the bone sample with sodium hypochlorite (NaOCl), hydrogen peroxide (H₂O₂), sodium hydroxide (NaOH) and potassium hydroxide (KOH) over a period of 15 days, applying at the end the delipidation procedure involving a 2:1 solution of chloroform and methanol. Results showed no significant changes in XRD analysis. However, spectroscopy revealed that after four days in NaOCl the collagen bands disappeared while Amide III remains unaltered as well as bands relative to both carbonate and phosphate. In general, mineral is less affected by H₂O₂ and NaOCl rather than NaOH and KOH. It is possible to conclude that NaOCl is the treatment that better allows preservation of both mineral and organic matrix integrity.

The defatting procedure minimally affects bone matrix physicochemical properties and, simultaneously, removes excess of surface water, grease and bone marrow. This allows better estimation of the age-related loss in organic phase and structural water. This is essential to understand the relationship between bone composition and mechanical behaviour. Although the use of deionised water is widely accepted, the procedure induces a small degree of ion substitution that results in statistical difference between the two groups. It is important to stress that due to the increment induced by the procedure of crystal size, failing to apply this preparation step when using the protocol for age estimation would result in incorrect age-at-death. The main aim of the present study is not to infer of that mechanism that cause this changes but simply to quantify variations connected with the defatting procedure. Overall, the application of consecutive chloroform-methanol baths represent a methodological choice that aims to reduce the number of biasing factors that could affect parameters acquisition and needs to be followed for correct replication of the protocol.

7.2 Age- and Sex-related Variation of the Bone Matrix

Bone strength is the ability of the tissue to dissipate stress through the increase of strain and structural modification. The hierarchical organisation of bone (macro-, micro-, nano- and molecular structure) accounts at different levels for this ability. This ability is representative of the bone morphology, composition and physicochemical properties of these components. Although it is largely accepted that changes in bone architecture (e.g. variations porosity, trabecular organisation) account for approximately 70% of bone strength, modifications at matrix level of mineral, organic and water phase should not to be overlooked and are essential in order for the treatment to be effective for certain pathological conditions (e.g. bisphosphonate for osteoporosis) (Fonseca et al., 2014; Ma et al., 2017; Burr, 2019). It is also well known that, despite the fact that compositional changes mostly affect nano- and micro-mechanical properties, they have an effect on bone mechanical behaviour at the macroscopic scale. Generally, bound water has a positive effect on toughness and post-yield toughness. In contrast, crystallinity has a beneficial effect on elastic modulus. Finally, mineralisation has a positive effect on both elastic and plastic deformation (Yerramshetty and Akkus, 2008; Boskey and Imbert, 2017; Unal et al., 2019). This is supported by the results produced by nanoindentation of the bone samples in this study. As shown in Section 6.6, the physicochemical parameter related to the organic matrix shows more robust correlation with the elastic modulus while those related to mineral parameters better explain the hardness behaviour. A comprehensive understanding of the physicochemical modification of the bone matrix is essential in order to evaluate mechanical resistance of bone.

7.2.1 Mineral Content

In the present study, mineral content is seen to increase with age. This variation is associated with increase in mineral size and carbonate substitution as well as the decrease in organic and water fraction. Furthermore, this phenomenon has a positive effect on mechanical properties of the mineralised collagen fibres.

These results corroborate early findings by Currey et al. (1996) that identify a robust positive relationship between ash content and age: the authors also confirmed that this variation induces a decrease in impact energy and work of fracture. Further, Zioupos et al. (2000b) combined microhardness and elastic modulus with ash content for the rostrum of a male *Mesoplodon Densirostris* and compared with the bone tissue from other species in order to explain the effect on hypermineralisation in mechanical properties. Results showed at microscopic level mineral content has a beneficial effect on hardness and elastic modulus but, somehow, an extreme concentration of mineralised tissue leads to extreme brittleness as explained by the low stress tolerance in fatigue testing by Zioupos et al. (2000b). In human bone, the effect of the variation in mineral content has been seen to increase until the age of 35 years and then slowly decrease (Zioupos, 2001). Results for the present study are in agreement with what was found previously in research and there is an important increment until 40 years with a stabilisation afterwards. This is confirmed by the fact that, considering the age range 10-80 years, there is not a clear linear relationship ($p < 0.001$ $R = 0.39$) while when transforming the relationship into logarithmic scale, the correlation is clearly improved ($p < 0.001$ $R = 0.51$) as shown in Figure 6.5. This complex behaviour is due to a number of other physicochemical variations that account for the increase in mineral content. For instance, in the present work crystal size increase with age is associated with the increase in mineral content as well and carbonation of the matrix. Overall, this variation is coupled with a decrease in organic and water fraction and is highly correlated with all mechanical properties with the exception of indentation creep (Section 6.6).

This modification has a considerable influence on bone tissue mechanics while there are other factors that have a more pronounced effect on strength at macroscopic level such as decrease in density and increase in porosity (Unal et al., 2018). However, hypermineralisation has a negative effect on mechanical resistance to fracture. The importance of combining results at different levels could help in predicting accurately fracture risks, a task that at this stage is mainly achieved by dual X-ray absorptiometry or quantitative computer tomography at the clinical level (Greenwood et al., 2015; Kranioti et al., 2019). The

limitation of these approaches are linked to the fact that they do not account for structural and compositional changes of the bone matrix. The combination of these methods with trans-cutaneous noninvasive Raman tomographic imaging could improve the potential in fracture prediction (Schulmerich et al., 2006, 2007, 2008).

7.2.2 Organic Matrix

In order to investigate different aspects of the organic matrix (collagen content and collagen quality assessed by thermal stability and percentage of structural water), thermal analysis and spectroscopy techniques were employed. The results show that there is a decrease in collagen content and quality with decreasing thermal stability and reduced amount of structural water. This suggests the presence of lesser hydrogen bonds between collagen fibres in the bone sample that affects the strength of the triple helix, Figure 7.1.

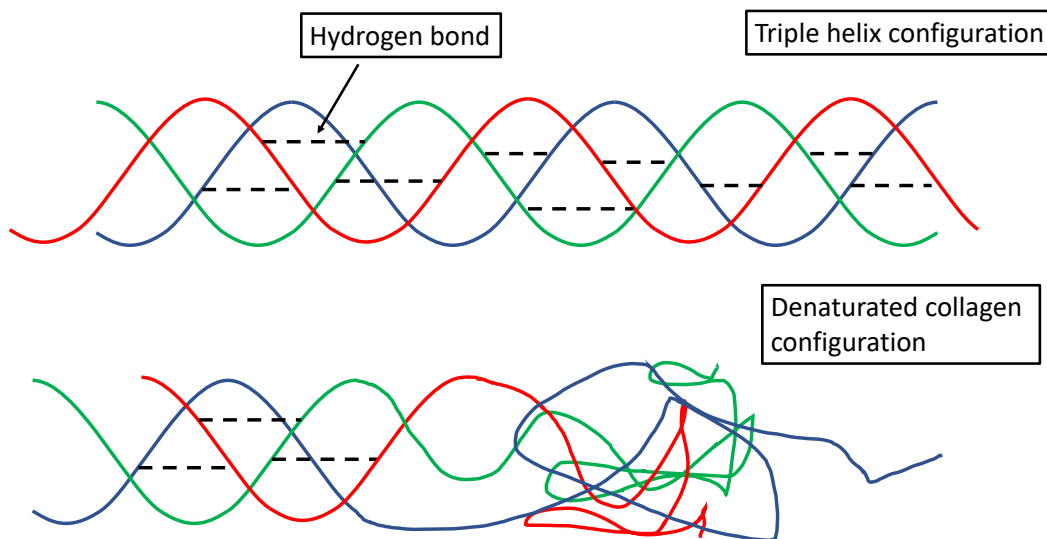


Figure 7.1: Schematic representation of two collagen molecules. The hydrogen bonds (black dashed line) maintain the triple helix configuration of the collagen fibres.

Concerning organic matrix variation with age, a series of enzymatic and non-enzymatic processes induce changes in collagen molecular configuration that will eventually affect the strength of bone (Zioupou and Currey, 1998; Zioupou, 2001; Burr, 2019). An early

study from Danielsen (1994) showed the same behaviour as that detected in the present study for 41 specimens from crista iliaca with a decrease of collagen shrinkage temperature with age. This phenomenon was further investigated by Zioupos (2001) in human femur cortical bone at different age and showed the decrease of temperature at which the triple helix of collagen degenerates with the increase of ageing. The present study shows the same decrease in thermal collagen stability with age (Figure 6.4) which can be attributed to two main factors: (1) molecular degeneration of collagen fibrillar structure (Danielsen, 1994) and (2) decreased level of hydration of the organic matrix (Burr, 2019). Regarding level of hydration, TGA results provided an insight into the behaviour of mineralised collagen in cortical bone. A significant decrease in structural water (Figure 6.4) was highlighted which is in agreement with published studies (Miles et al., 2005; Bridelli et al., 2017; Kerch, 2018). The relationship between these thermal stability and structural water parameters is robust ($R = 0.65$) resulting in the the coupled increase of fibrillar stability and water content. This confirms the role of hydration in favouring the increment in hydrogen bonds that are believed to increase collagen network strength. These have a direct effect on mechanical behaviour at all levels of magnification (Wang et al., 2002a; Unal and Akkus, 2015). Figure 7.1 shows how collagen, in its spiral organisation, is supported by hydrogen bonds and the denatured arrangement due to degeneration. According to the present study, the amount of structural water is proportional to the thermal stability. This suggests that the decrease in hydrogen bonds with age is responsible for the compromised stability of collagen and consequently, for decreasing mechanical properties of bone.

Further, the enthalpy value for the exothermic peak indicates the combustion of the organic matrix, including the various types of collagen and non-collagenous proteins. The decrease shows a steep decrease until the age of 40 and afterwards a stabilisation with a very slight negative variation. This is also supported by the same behaviour of $Or_{\%}$ results as can be seen in the plots in Figure 6.15. In contrast, mineral content measured with TGA and mineral to matrix ratio shows a clear increase, suggesting that the reduction in the organic matrix is coupled with an increase in mineral content. The fact that after skeletal maturity is reached, there is a clear reduction in the variation of both organic

and mineral matrix can be explained by the main role of remodelling increasing the mean tissue mineralisation. This hypothesis is supported by Akkus et al. (2003) in a study that compared primary and secondary bone, reporting the increase of highly mineralised areas on cortical bone. This is due to the increase of mineral content for Haversian systems as well as the increase in mineral size, crystallinity and ion substitution that characterises non-remodelled primary lamellae. As a consequence, there is an increase in brittleness that results in the accumulation of micro-cracks that leads to an increased risk of fracture.

Currey et al. (1996), on the other hand, showed the same increase in mineral content but linearly correlated. The unclear relationship noted in the different studies could be due to the heterogeneous behaviour of bone remodelling in different individuals. ΔH and $Or_{\%}$ have also shown statistical differences according to sex suggesting a higher concentration of organic matrix in male individuals. To discuss this finding, one needs to consider that the mean age of the total sample is approximately 46 years of age. This suggests that skeletal maturity is reached for the majority of the sample and degeneration of the matrix has already started. Contextualising this with the fact that there is an incidence of 17% per 10,000 women per year affected by osteoporosis-related hip fractures and 30.2 cases per 10,000 women with radius/ulna fracture, the lifetime risk is approximately 50% of women in Wales and England suffered from fractures after the age of 50 (van Staa et al., 2001). It is easy to understand that several hormonal changes induce different degeneration paths for the two sexes that result in heterogeneous physicochemical properties of bone matrix. What is surprising is the absence of a statistically significant difference between males and females for mineral content values as it would have been expected as shown in Table 6.5. This could be linked again to the heterogeneous nature of remodelling and a large number of factors that affect this phenomenon but a better understanding of this phenomenon could be gained by introducing in the study sample a cohort of post-menopausal women and osteoporotic men that normally are affected by impaired remodelling and abnormal mineralisation. Furthermore, a more systematic investigation of post-translational modification of collagen and the evaluation of the different cross-links that accumulate with age would be beneficial in order to understand the effect of ageing on the mechanical

behaviour of the bone matrix.

7.2.3 Carbonate Substitution and Crystallinity

When evaluating the changes in carbonate substitution and crystallinity of mineral platelets, an increase along the entire age range was observed for the first and no clear trends for the latter. This is due to the high micro-strain of the mineral domain that induces ion substitution. A clear difference of carbonate substitution is observed below and above 30 years of age, an inference drawn from the experimental analysis in this study. Conversely, crystallinity showed no change with age. This could be related to the remodelling rate of the bone rather than the chronological age.

The poor crystalline nature of HAp is characterised by the different type of lattice substitutions such as magnesium, potassium, sodium, acidic phosphate and carbonate that affect not only crystal geometry but also the solubility (Paschalis et al., 2017). Changes in size and shape account for crystallinity while the purity of the stoichiometric compound is defined as maturity. The ageing of HAp crystals is explained by Rey et al. (2007), considering the numerous non-apatitic environments in bone crystals at their embryonic stage. Before water is lost, these environments are in a hydrated state inducing ion exchange. Between the ions, carbonate plays a central role in crystal maturation and growth inhibition. Carbonate ions are also seen to be permanently incorporated in the lattice, reducing the vacancies in the crystals. In the present study, the carbonate to phosphate ratio is used to understand ion substitution. This shows a clear increase with age before 30 years ($R = 0.65$), which tends to decrease after maturation (Akkus et al., 2003; Yerramshetty et al., 2006). Results for this thesis (Figure 6.17) showed a very similar pattern with a very steep increase before 30 years of age ($p < 0.001$, $R = 0.65$) and a much less marked variation after this point ($p = 0.014$, $R = 0.26$). The increase of carbonation is largely supported and can be also related to the behaviour of the splitting factor (crystallinity index) that shows a decrease with age, although not significant. When comparing carbonate content and crystallinity, there is significant negative correlation between the two parameters ($R = -0.77$) that suggests carbonate reduces crystallinity decreasing size/strain balance and mineral

perfection. This has been experimentally confirmed by Yerramshetty et al. (2006) who, by means of Raman spectroscopy, suggested that crystallinity is an indicator in growing mineral crystal size along the major axis. Therefore, results disagree what found in previous studies who detected a positive correlation between carbonate content and crystallinity. This can be explained by the fact that the turnover rate, that is very high until skeletal maturity and later slows down, is probably the main contributor to crystal composition, size and crystallinity.

Another important aspect to highlight is the experimental evidence of the relationship between crystallinity and the effect of carbonate is the variation of lattice size. The increase in crystallinity is correlated to crystal growth at both 'a' and 'c' axis while carbonate substitution does not show any significant variations with crystal size. In agreement with Greenwood et al. (2016), there is a reduction in 'a' axis with the increase of carbonate content, while the absence of correlations with 'c' axis is somehow unexpected, explained in Section 6.5. Overall, the negative correlation between crystallinity and carbonate substitution suggests that the increase in carbonation with age induces a decrease in the lattice perfection. However, the absence of a clear correlations found between crystallinity and age suggests the the effect of carbonate concentration is probably responsible for alterations at lattice level rather than crystallite size. It is however complex to interpret the behaviour of crystallinity calculated by means of splitting factor from $\nu_4\text{PO}_4^{3-}$ of ATR-FTIR as results are not as consistent as other parameters related to mineral geometry.

These results are in agreement with previously published studies Boskey (2003) and are applicable to bones other than the rib. At this stage, it is important to note that crystallinity is a valuable yet unexplored parameter that should be further studied using histomorphometry rather than the various methods used for superficial physical analysis. When bone turnover rate is high small crystal are found in the matrix with high carbonate content and extended surface area that facilitate substitution (Greenwood et al., 2016). It is not surprising that in the present study we found increased crystal size around 40 years of age later. One last aspect that is needed to better understand the behaviour of mineral matrix at the nanoscale is the employment of spectroscopy combined with imaging (e.g. FTIRI or

μ FTIR) to analyse precise distribution and heterogeneity of crystallinity and carbonation across old interstitial bone and newly remodelled osteons.

7.2.4 Crystal Geometry

With increasing age, the bone crystals encountered are larger in comparison to younger age samples, i.e. along the 'c' axis which is along the major axis of the collagen. However, upon closer examination, a steep increase can be seen until the age of 40 which is followed by a shrinkage of the physical crystal in the bone sample. This can be seen in Figure 7.2.

Powder XRD has been applied to understand compositional and structural changes of bone mineral phase according to age, type of bone and pathological conditions. With age, the lattice parameter increases by approximately 0.00015 Å/year along the 'a' axis while the same variation is reported to be less drastic along the 'c' axis with only 0.00005 Å/year (Handschin and Stern, 1992). This translates to the modification of the crystals into a more squared structure, maintaining their elongated shape with the major axis along the 'c' axis, aligned longitudinally with collagen fibres. These results are in agreement with the present study that shows significant reduction along the 'a' axis but not along the 'c' axis (Figure 6.18). Another key aspect is the variation of crystallinity according to different age ranges. It was pointed out by Handschin and Stern (1992) that in bone samples from individuals younger than 30 years of age, there is a noticeable increase of crystallinity while no appreciable variations are shown by older individuals. Similarly, Handschin and Stern (1995) showed that the reflection for 002 seems to vary with the same pattern along the 'c' axis. From Figure 7.2, it is possible to observe the coherence length at 002 peak, where there is an increase until the age of 40 years ($R = 0.33$, $p = 0.032$) followed by a significant decrease until the age of 85 ($R = -0.26$, $p = 0.035$). When considering the entire age range, it was not possible to appreciate any variations, due to the lack of significance between coherence length and age. This could be explained by the lack of sensitiveness of the test to such a small variation in the parameter for bone sample. CL004 follows the same pattern with a considerable decrease after 40 years ($p < 0.001$). In contrast, CL030 only shows a significant increase with age when considering the entire age range as shown

in Figure 6.6 ($p = 0.016$). The increase in crystallite size confirms the previously reported results (Handschin and Stern, 1992, 1995). No clear relationship is found between age and strain. To conclude, the increase in size determines an increase in ash content, indicating that longer crystals are connected with the increase of mineral density in the bone.

The negative relationship between ash content and the length of the lattice parameter along the two axes is unexpected. The overall increase with age is interesting as there is a steep increment before skeletal maturity is reached. Afterwards, the individual variability seems to increase making it difficult to identify clear trends. Boskey (2003) explains how diet, cell viability and disease are important factors that affect crystal size. For instance, in osteoporotic bone, increased crystal size was found compared to healthy individuals at the same age. Unfortunately, for the sample employed in this study, no information regarding diet and pathological conditions is available and this does not allow the studies to draw any specific inferences.

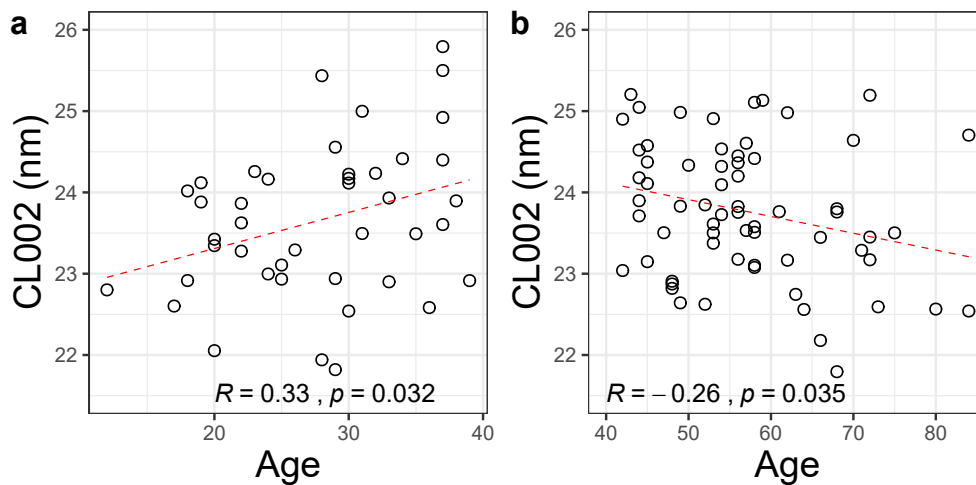


Figure 7.2: Coherence length shows a very specific pattern that can be explained by a steep increase before maturity to then decrease at a much lower pace.

7.3 Mechanical, Physicochemical Properties and Heterogeneity of Human Cortical Bone

The heterogeneous and hierarchical structure of bone has been largely discussed in the initial part of the thesis as well as the degeneration that bone is subject to, relative to age. The remodelling process has the main function of maintaining the structural and mechanical integrity of bone. However, differences in mineralisation and, more in general, in composition are seen between old primary bone and newly remodelled one (Rho et al., 1995). Indentation has been commonly applied to investigate the variation of these two areas with age and pathological conditions. Nanoindentation has been largely employed to investigate mechanical properties of the microstructure of bone. The resolution of this instrument can be up to 1 μm offering the possibility to test the intrinsic mechanical properties of mineralised collagen fibrils avoiding the effect of microstructural features of bone (Rho et al., 1998, 1999; Lewis and Nyman, 2008). To fully understand the mechanical behaviour of a material, the relationship between compositional properties of the mineral and organic matrix will be discussed in the following sections (Farlay et al., 2010; Paschalis et al., 2011).

7.3.1 Osteon vs. Interstitial Bone

Comparison between osteon and interstitial bone proved the presence of well-defined differences in this study. Osteonal bone shows a decrease of approximately 15% in elastic modulus and 8% in hardness compared with interstitial bone and analysis of variance shows significance for both variables as shown in Figure 6.7. These results corroborate Rho et al. (2002), who proved the same behaviour for the indentation test of the femur. In this case, the ribs show lower values compared to those provided for the femur. The same increment is seen for indentation creep while the elastic behaviour at hold is higher for osteons compared to the interstitial area. Microhardness shows higher values for interstitial bone by approximately 15%.

No correlation between age and nanohardness is shown in the present study while elas-

tic modulus decreases significantly with age ($p = 0.048$ and $R = -0.19$). This is supported by Hoffler et al. (2000) who suggested that the changes could be related to alterations in the tissue composition and organisation, independent of age and sex. In contrast, a very weak negative relationship was shown between elastic modulus of osteons ($p = 0.032$ and $R = -0.20$), mean tissue value ($p = 0.048$ and $R = -0.19$) and age as previously reported in literature (Rho et al., 2002). Good negative correlations, however, are found between C_{IT} and age for mean tissue value and all the locations (Table 6.7). The other unexpected outcome related to microhardness is the increase with age that is opposite to nanoindentation calculated hardness (Figure 6.8). This could be explained by the different equipment resolutions of the investigations. Nanoindentation has a resolution in the order of a few microns that allows testing of bone as a tissue. Microindentation resolution at a scale of $100 \mu\text{m}$, allowing to investigate a single osteon, accounting for several lamellae that have the function of increasing bone resistance. One can, therefore, suggest that secondary osteons show higher values of hardness due to their architecture rather than the chemical composition of their matrix. The presence of osteons and, specifically in the hypermineralised cement lines that enclose several concentric lamellae is seen to prevent linear microdamage propagation. However, this structure contributes to the increase in stiffness that does not prevent the formation of such damage but only the propagation behaving as a barrier with different properties that dissipate energy (Burr et al., 1988; Diab and Vashishth, 2007; Milovanovic et al., 2018). This is an example that shows how mechanical properties are the result of composition and structure rather than one of the two aspects taken separately.

This difference is correlated with the remodelling rate. For instance, old unremodelled bone has time to fulfil secondary mineralisation and therefore increase mineral size and content enhancing most of the mechanical properties. In contrast, the decreased values for indentation creep are believed, in the present study, to be attributed to the time-related degeneration of collagenous matrix.

7.3.2 Tissue Mechanical Properties: Effect of Crystal Modifications

The increase in crystal size along all the axes is seen to have a positive effect on nanohardness, elastic modulus, plasticity and nanohardness of the bone sample. In contrast, indentation creep is inversely affected by the increase of crystal size. Furthermore, carbonate substitution has a negative impact on the mechanical properties of the bone.

To compare physicochemical and mechanical properties of rib cortical bone, HAP powder was tested by means of XRD and FTIR. This did not allow the evaluation of the compositional difference between osteons and surrounding non-remodelled matrix. For this reason, mechanical properties from osteons and interstitial areas were averaged in order to obtain mean tissue values. It is normally accepted that collagen maturity and integrity play a central role in determining plastic deformation resistance in bone. This was tested by Bala et al. (2011) who applied nanoindentation and FTIR microscopy on femoral cortical bone and found robust correlation between collagen maturity and plastic deformation rather than elastic one. They also did not find any link between mineral crystallinity and tissue mechanical properties. In contrast, a similar study employing Raman microscopy and macromechanical analysis by Yerramshetty and Akkus (2008) reported the association of crystallinity with both monotonic and fatigue properties. In the present study, no correlation was shown between crystallinity (intended as Splitting Factor calculated from the symmetric bands intensity of the $\nu_4\text{PO}_4^{3-}$ peak) and any of the indentation mechanical properties (Section 6.6). Findings for the present study reinforce results of Bala et al. (2011), who suggested that it could be due to the sample employed in their study. Postmenopausal osteoporotic female individuals are characterised by the imbalance between bone formation and resorption that reduces the consistent increase in crystallinity in cortical bone. However, the absence of correlation in the results for this thesis suggest that there is hardly any observable correlation between age and crystallinity. This is indicative of the high inter-individual variation of this parameter. Similarly, no relationship between lattice parameters and mechanical properties are found (Section 6.6). However, when considering crystallite strain and size, many correlations may account for the re-

relationship between crystal modifications and mechanical behaviour of the matrix. The increase of strain has a negative effect on nano- and micro-hardness and elastic modulus. Considering that strain induces an increase in crystal size, a similar behaviour can be expected. Surprisingly, the only positive relationship that was found is with microhardness (Section 6.6). It remains difficult to understand whether either organic or mineral matrix plays a more prominent role in determining the mechanical properties of bone. It is the combination of the two that gives bone its unique behaviour (Rho et al., 1998).

Coherence length affects almost all the mechanical properties, equally for osteon and interstitial bone. Coherence length derived from 002 and 004 peaks primarily influences positively nanohardness and elastic modulus while there is a decrease in indentation creep suggesting a decrease in the viscoelastic behaviour of the matrix (Section 6.6). Increased CL at 030 peaks seems to have a positive relationship with C_{IT} and negative with η_{IT} . It may be the case therefore that the increases in crystal size have a primary impact of reducing viscoelasticity of the bone at the matrix level. Finally, CL at the 210 peak shows a positive correlation with both nanohardness and elastic modulus, especially for the interstitial area. Overall, these results provide further support for the hypothesis that the increase in crystal size and the consequent decrease in crystal strain have a beneficial effect on both nanohardness and elastic modulus, and no significant variation is present between osteons and interstitial areas. These results in this thesis corroborate the findings of a great deal of the previous work in Yerramshetty et al. (2006) and Yerramshetty and Akkus (2008). They suggested that longer and more mature crystal can affect bone deformation. This is related to the fact that longer crystals leave less areas of unreinforced bone that reduce the elongation capability of the entire tissue. In contrast, smaller crystals would induce greater post-yield deformation (Yerramshetty and Akkus, 2008). Additionally, heterogeneity of crystal sizes and its distribution have been recently suggested to be responsible for enhanced mechanical behaviour (Boskey, 2003; Tai et al., 2007; Renders et al., 2011; Donnelly et al., 2012). This functional mechanism of tissue mechanics remain open to debate and need to be further investigated.

Previous studies evaluating the effect of carbonate on mechanical properties presented

inconsistent results on the effect of carbonate amount on bone elastic properties. This was the case due to the inconsistency in the spatial distribution of carbonate on the cortical surface (Akkus et al., 2004). In the present study, carbonate to phosphate ratio exhibits a clear decrease in elastic modulus ($p = 0.011$ and $R = -0.24$), which seems to be more marked after the age of thirty. Similarly, hardness decreases with the increase of carbonate in HAp crystals ($p = 0.030$ and $R = -0.23$), as well as microhardness. One more aspect to be noted is that the interstitial area is the most affected site for these modifications. The longer the bone matrix remains unremodelled the larger the crystal size and the higher the carbonate content is. This is due to the fulfilling of secondary mineralisation that accounts for matrix maturation and influences bone mechanical behaviour. On one side, the increase in carbonation have a negative effect on mechanical properties. In contrast, the increase in crystal size improves tissue mechanical properties. The closer HAp is to its stoichiometric ideal composition, the better mechanical performance the bone shows at the matrix level. The behaviour changes for microhardness are seen as the toughening effect of concentric lamellae, which induces an increase in hardness and elastic properties, despite the increase in carbonation. The combined evaluation of carbonation level and crystallinity index could have explained how crystal composition could affect matrix functional behaviour. Unfortunately, crystallinity did not correlate with any of the mechanical properties as depicted in Figure 5.14.

Although the results clearly indicate that bigger crystals improve mechanical properties of the matrix with the exception of indentation creep, further attention should be focused on the distribution of the crystal size on the matrix to decipher the macro-scale mechanical properties of the bone. Additionally, a better understanding of bone turnover is essential to gain a comprehensive understanding of the time-related compositional and mechanical modification of the bone matrix.

7.3.3 Tissue Mechanical Properties: Mineral and Organic Matrix

The amount of mineral context in the bone sample has a positive impact on all the mechanical properties with the exception of indentation creep. However, hypermineralisation

increases the brittleness of the bone, making the bone more prone to fracture. Simultaneously, an opposite behaviour is noted when considering the collagen and its impact on the mechanical properties.

Currey et al. (1996) reported the tendency of older bone to developed hypermineralised areas that represent the ideal location for the accumulation of microdamage. This phenomenon has been related to the decrease of toughness of cortical bone (Zioupos, 2001). However, in the present study, there is both an increase in elastic modulus, and nano- and micro-hardness with the increment of ash content, as previously reported by Boivin et al. (2008). This is linked to the turnover rate that eliminates older osteons before the completion of secondary mineralisation. This could also explain the higher values for interstitial bone, that have completed secondary mineralisation, compared to osteons. It is also worth mentioning the good correlation present between ash content and mechanical properties of interstitial bone that are the non-remodelled highly mineralised areas as suggested by Currey (2003a). This study confirms that individual components of bone are not sufficient to explain variations in mechanical behaviour. The variations of mineral content in the bone with ageing are concomitant with the ones affecting the organic matrix. However, the increase in mineral content induces an increase in all the mechanical parameters with the exception of indentation creep that decreases significantly, as can be seen in Figure 6.11. Currey (2003a) showed how a simple increase in the mineral content increases the toughness of bone but also makes it brittle and more prone to the accumulation of microdamage.

When discussing the collagen and the effect of the organic matrix on the mechanical properties of bone, Currey (2003a) used ^{60}Co gamma-ray to degrade collagen. Results showed that this has an antagonist effect on toughness but does not affect stiffness. Further investigation involving nanoindentation and spectroscopic analysis also provided evidence that collagen has an impact on the viscoelastic behaviour of bone matrix (Bala et al., 2011). In the present study, thermal stability did not show any correlation with parameters acquired using nanoindentation but there is a negative correlation with microhardness, for both osteon/interstitial and mean tissue value (Section 6.6). Nevertheless, when consid-

ering the amount of organic matrix rather than its quality, it is clear that it affects several mechanical properties except elastic modulus. It causes an increase in microhardness for both interstitial bone and osteons but only nanohardness for osteons. The best positive correlation is seen with the indentation creep that suggests an increase in viscoelasticity for young bone rich in collagen. In contrast, there is a clear decrease of η_{IT} . Bala et al. (2011) confirmed that collagen maturity is linked to plastic deformation. In this study, results for collagen quantification via ATR-FTIR show a negative relationship with microhardness while the increase of viscoelastic behaviour and collagen content is coupled. In contrast to these earlier findings, however, there is evidence that the organic component might also influence the estimation of the elastic properties and is not only related to plastic deformation as suggested by Bala et al. (2011). Decrease of $Or_{\%}$ has a negative effect on the elastic properties of the tissue and it is seen also to affect the elastic modulus for interstitial bone. $Or_{\%}$ also induces a decrease in the viscoelastic properties and an increase in indentation creep. To conclude, increased $W_{\%}$ has a negative effect on both elastic modulus and hardness. This interpretation is to be limited to indentation tests as other types of mechanical modes could have different behaviours according to hydration level. According with what just mentioned, if it is possible to confirm that organic matrix have a major influence in plastic behaviour and mineral content on elastic deformation, it is otherwise true that is the combination of the components of bone matrix that determines the complex behaviour of bone.

In conclusion, when considering the plastic and elastic deformations, collagen has a greater effect on the former while the degree of mineralisation effects the latter.

7.3.4 Stepwise Regression – Mechanics vs. Physicochemical Properties

The relationship of the single structural/compositional and functional (mechanical) parameter could represent a constraint in the interpretation of the ageing process. The composite nature of bone does not allow the complete isolation of individual components to under-

stand their role in determining nano-mechanical properties of bone. Therefore, stepwise regression was applied to identify the independent variable that could explain the mechanical behaviour of bone as a material.

The model showed that elastic modulus and hardness share several predictors when stepwise selection is applied. $L\Delta H$ is the predominant parameter for both, indicating that collagen is not the only component responsible for plastic behaviour. Water ($W\%$) fraction also influences plasticity (Table 6.16). Previous studies showed the importance of structural water not only to collagen stability but also in enhancing ion substitution (Rey et al., 2009; Burr, 2019). Finally, the negative relationship between crystallite strain indicates that young crystals that show high strain values are normally correlated with poor mechanical behaviour (both nanohardness and elastic modulus). This is supported by the presence of CL002 in both models.

Considering nanohardness separately, it is possible to see that carbonate ratio has a positive correlation with this mechanical property (Table 6.15). This is not surprising as the increase in carbonate content is known to increase stiffness of bone the both micro- and macro-level (Martin et al., 2015). Additionally, the increase of crystallinity with age induces a decrease in hardness as previously reported in literature (Bi et al., 2011; Morris and Mandair, 2011). Finally, slightly different results are found between microhardness and mechanical properties and nano-structural level (Table 6.17). In this case, the degree of mineralisation plays a predominant role in predicting microhardness; both mineral content parameters ($Ash\%$ and MO) are included in the model. CL004 is also in the model suggesting that increase in size of crystal reduces hardness values. The selection of $C\Delta H$, finally, consolidates the belief regarding the complex behaviour of bone. Mineral and organic matrix play a combined role to maintain mechanical integrity.

7.4 Mineral and Organic Matrix Interaction

In the study, correlation was found between the degree of mineralisation, including variations in crystallite geometry, and collagen integrity. Results for the present study showed that bone matrix with larger crystals is also characterised by reduced collagen stability.

This could also mean that the organic portion quality decreases with age as mineral crystals grow. This could be due to a combination of two reasons. On one side, collagen physically limits the crystal growth and, therefore, when collagen is strong crystals are small in size. On the other hand, when bone turnover slows down and there is more time for secondary mineralisation crystals grow and collagen quality and quantity is reduced. The confirmation of this could be an avenue for future research involving *In vitro* mineralisation techniques.

In vitro studies have used calcium-ion-binding polymer to induce intra-fibrillar and extra-fibrillar mineralisation obtaining calcium, phosphate and carbonate ions from the extracellular matrix. Wang et al. (2012) showed that collagen can initiate mineralisation and influence not only size but also the 3D distribution of crystals. An implication of this is the possibility that, after mineralisation, crystal growth could still be partially driven by collagen. These results are supported by Nudelman et al. (2010) who showed the possibility of mineralisation in the presence of nucleation inhibitors which suggests the contribution of collagen to the mineralisation process.

In contrast, it has been suggested, that collagen, during bone formation may limit mineral growth (Boskey, 2003; Nudelman et al., 2010). Although this hypothesis is based primarily on observational data, it still remains feasible if one considers the inverse relationship of mineral and organic content (Zioupos, 2005; Greenwood et al., 2013). This mechanical restriction applied to mineral growth tends to be acceptable if considering the inverse relationship between organic and mineral phase. Taking into account TGA results, it is noted that the increase in Ash% is coupled with a proportional decrease in organic material as suggested by Zioupos et al. (2000a).

The current study found that collagen amount and stability could influence crystal changes with ageing as shown in Section 6.5.1. One interesting finding is the relationship between collagen thermal stability and crystal size obtained by Williamson-Hall plot, shows that high thermal stability levels, that indicate young and resilient collagen, are typical of bone tissue characterised by small crystals. This is characteristic of newly formed mineralised collagen. Conversely, with age, when collagen has already degenerated, crys-

tals show an increased size. The increase in crystal size occurs both along the 'a'- and 'c'-axes. Considering the reciprocal interaction between strain and size, this result may be explained by the fact that stable collagen is also associated with high values of strain (domain vacancies that will be filled by ion substitution) and polarisation that is reduced with age and leads to an increase in crystal size with ageing. This confirms that collagen plays a role in modifying mineral geometry. This role is interpreted as a physical impediment of crystal growth.

What is also interesting is the increase of carbonate content with the decrease in thermal stability found in the present study that could, most likely, be interpreted in the light of ion chemical process of ion substitution rather than induced by collagen. This phenomenon is supported by the findings of this study. These results also broadly support the work of other studies in this area (Nudelman et al., 2010, 2013). Overall, this suggests that there is not only a combined variation in organic and mineral content but also collagen quality could be involved in limiting crystal growth.

In addition to the collagenous matrix, the water phase plays a key role in mineralisation. The main function of water is known to be stabilisation of collagen fibrils via hydrogen bonds. Structuring and orientation of crystals have been already proved to be water-mediated (Wang, 2013). It was also confirmed by NMR studies on powder from bovine femora that there is a 2.3–2.55 Å ordered hydrated layer from carbonate apatite (Wilson et al., 2005). In contrast, synthetic apatite showed the presence of hydroxide bonds with phosphate and carbonate of the mineral phase (Wilson et al., 2006). Further studies have shown the presence of this structure also in the mineral lattice (Yoder et al., 2012; Pasteris et al., 2014). It is possible considering the results of the present study that this hydrated layer is responsible for ion exchange and therefore modification in crystal size and geometry (Cazalbou et al., 2005; Rey et al., 2009). According to the results from this thesis, correlations were found between $W_{\%}$ and several structural and compositional parameters (Table 6.14). First of all, one can confirm the role of water in collagen stability with a robust positive correlation ($p < 0.001$ and $R = 0.65$). Additionally, when considering the lattice parameter, the major effect of water is the steep increase along the

'c' axis and the more moderate increase along the 'a' axis suggesting that water fraction stimulates lattice growth. This could be related to the reduction of water content inducing the increase in crystallinity. The interpretation of crystallinity and carbonate substitution is more complex. It is expected that high levels of hydration would lead to an increase in size and therefore crystallinity, while low level of hydration corresponds to low substitution. However, there is a conflicting trend in the values for water content that could be due to different levels of dehydration after the chloroform-methanol defatting procedure. This procedure that involves mechanical spinning of bone specimens could be heavily affected by the increase in porosity associated with age: young, dense bone has an increased surface area exposed to the solution and therefore, might retain grease and non-structural water. These findings raise intriguing questions regarding the nature of the relationship between water fraction and mineral phase, but it is of utmost importance to apply and test a procedure that could maintain hydration and collagen integrity to further investigate this aspect.

The present study does not take into consideration is the reduced turnover rate that is associated with the advancement of age. This phenomenon slows down bone resorption and allows bone to initiate and fulfil secondary mineralisation process, responsible for crystal maturation and increase in size (Boskey, 2003). Taking into account that that remodelling is also responsible for laying down newly formed collagen, it is easy to imagine that collagen of old and non remodelled bone is subject to post-translational modification that affect its normal structure and quality (Cazalbou et al., 2005). Further study should account the effect of turnover rate in order to better understand the combined changes of mineral crystal and collagen fibres.

7.4.1 Stepwise Regression – Mineral vs. Organic

In order to gain a better insight into the processes involved in crystal modifications and mineral composition, stepwise regression was applied to compare variables related to mineral phase obtained using XRD and ATR-FTIR and, as independent variables, the ones related to the organic matrix and water content.

In the current study, crystallinity and carbonate substitution are the two predominant parameters to explain the behaviour related to collagen content and level of hydration. For crystallinity, the negative relationship with collagen content suggests that young individuals have low indices of crystallinity. This increases with ageing. The main cause of this increase is opposing decrease in crystallite strain and simultaneous increase in size. This is also coupled with the increased carbonate substitution. This is supported by the fact that the relationship between carbonate: phosphate and collagen content in the second model is inverse (Table 6.8). The same trend is seen for $W_{\%}$ which shows a positive correlation with splitting factor and inverse correlation with collagen content. Furthermore, in the second model (Table 6.9), carbonate substitution is also predicted by $C\Delta H$ showing that high enthalpy values, typical of young individuals and is characteristic of low substitution level. Finally, modifications of crystal lattice along the 'c' axis show more complex behaviour (Table 6.10). The results confirm what is previously stated regarding the role of collagen in determining an increase in crystal size. It is possible that collagen controls both mechanical and molecular crystal growth. Due to the observational approach of the present study, further research should take into consideration the molecular interaction between collagen and mineral. The 'c' axis seems to show an increment with both $C\Delta H$, $Or_{\%}$ and $W_{\%}$. However, between the selected factors in predicting 'c' axis, carbonate substitution and, consequently, mineral crystallinity show moderate correlation.

7.5 Cortical Bone Maturity: the Rib Example

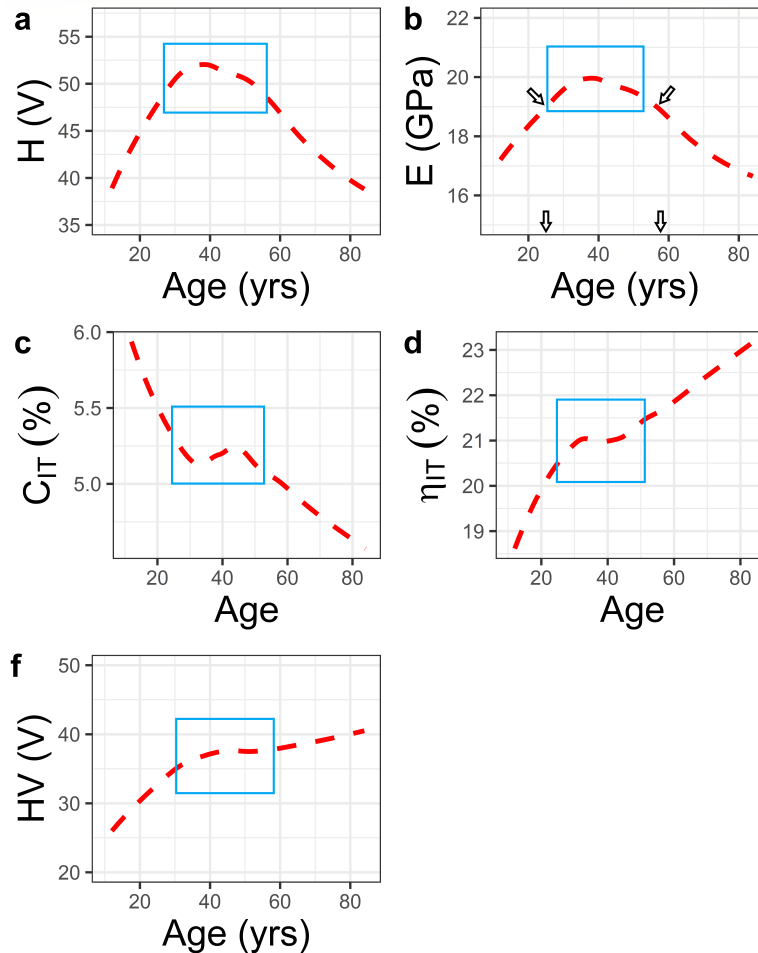


Figure 7.3: Loess curves show how mechanical properties change with age and the different behaviour between them. The blue squares approximately between 30 and 50 years show how the combination of all the physicochemical changes reaching maturity at different ages affect the transition between increase and degeneration of mechanical properties.

When considering the behaviour of matrix composition and mechanics, the present study reveals that certain variables have different behaviours when the sample is divided into two age ranges as can be seen in Figure 7.3. Zioupos (2001) explains that it is common knowledge that human bone achieves skeletal maturity between 30 and 35 years of age. Before this point, there is an increase in mineral content that is related to the increase of stiffness of the tissue. In contrast, after skeletal maturity, bone starts to deteriorate. In

the present study, the decision was made to analyse all the variables visually by means of locally estimated scatter plot smoothing (loess) to evaluate if compositional and structural variables have the same maturity age. Results showed that different variables of the matrix reach their maximum development at different ages, i.e. between 30 years up to 50 years (approximately). This can explain why, considering mechanical properties, there is, between 30 and 40 years, a small variation that was not expected. This change in the behaviour is not smooth (Figure 7.3, blue square). This could also represent an issue when employing certain variables for age estimation. In Figure 7.3 b, the arrows clearly show that for a value of 19 GPa of elastic modulus can be attributed to both an individual slightly older than 20 years and to one slightly younger than 60 years. This would lead to an erroneous estimation of age at death. For this reason, ideal parameters from AAD estimation should have a linear relationship with age. However, the multifactorial approach proposed in this thesis could be further improved by selecting and combining different parameters that can adjust the estimation in precise age ranges. An example is given by microhardness (Figure 7.3 f) that shows a distinct increase until 40 years of age and then remain more or less stable. This variable can be useful to estimate age for individuals <40 years but then should be combined with other parameters for the estimation of older ages like for example indentation work ratio (in Figure 7.3 e) that shows a clear variation after this age.

Results for the present study agree with what presented by Zioupos (2001) regarding maturity of mechanical properties. It can be clearly seen in Figure 7.3 a and b that both nanohardness and elastic modulus reach their peak at approximately 35 years of age to then quickly degenerate. A similar behaviour is shown for microhardness (7.3 f) that shows the same increment to then plateau. As shown before in Figure 5.14, microhardness does not have the necessary resolution to investigate material properties of the tissue but it is influenced by the structure of the osteon (e.g. number and mineralisation of the lamellae). Therefore, for discussing this feature, further research should account for microstructure of osteons and interstitial bone. The last two parameters (indentation creep and work ratio), in contrast, show a monotonic behaviour with age as can be seen in Figure 7.3 c and d. The same maturity limit was found also for carbonate substitution (CP) and collagen content

(CC) (Figure 6.17). CP increases significantly for the entire age range, losing intensity after 30 years. In contrast, CC decreases significantly only before 30 years.

In contrast, the set of variables that seems to mature at 40 years include mineral, organic and water weight loss as well as coherence length at the 002 and 004 peaks (Figure 6.16). Changes in coherence length indicate a first increase in size and subsequently, a decrease. This could be interpreted as a consequence of the increase in lattice strain up to 40 years followed by a decrement in the intensity but due to the lack of significance this is to be further investigated. This increase can be explained if associated with the rapid increase in carbonate in the crystal domain. LeGeros et al. (1969) explain that the increase in carbonate is responsible for the increase in crystal length and these findings are supported by the present study. The maturation point set at 40 years of age for crystal seems to bring slightly different results compared with previous studies that demonstrated that most of the variation in size for crystal lattice occurs between 0 and 30 years (Handschin and Stern, 1992, 1995). However, one needs to bear in mind that the previous studies employed Crista Iliaca (Section 7.2.4) which has a weight-bearing function and undergoes different amounts of stress throughout life. These factors could account for the difference in both mineral and organic matrix. The increased stress applied to a weight bearing bone increases the rate of remodelling that increase crystal size and the deposition of new collagen. Overall, crystal size is found to consistently decrease with the increase in carbonate substitution. Mineral content increases rapidly until 40 years but does not show a clear behaviour afterwards. This agrees in part with Zioupos et al. (1996) who did not found a regular trend after 25 years. The difference in the maturity point could be attributed to the fact that in the sample employed in the present study, a larger number of specimen and a better age distribution is present.

The last group of variables was found to reach maturity at 50 years of age and are collagen thermal stability and crystal cell size along the 'a' axis. Correlation for the decrease is moderate but suggests a decrease in collagen thermal stability and, therefore, quality. No clear trends could be seen after maturity. In contrast, lattice parameter does not show clear and robust correlations a part from the the weak decrease of crystal cell along the 'a'

axis. The acquisition of these parameters should be repeated with a better instrument as the experiment set for this thesis did not show enough sensibility to appreciate age changes in the lattice parameter.

It was previously suggested that the behaviour of compositional and structural changes of bone matrix could also explain the variation of mechanical properties with age. Both hardness and elastic modulus increase until the age of 30/35 years and this phase is followed by a stable segment with very limited variation. From approximately 45 years of age, there is a more marked decrease that could be due to the sudden change in crystal structural properties and collagen integrity. Despite this, the results corroborate the findings commonly shared in previous work (Akkus et al., 2003). It would be advisable, however, to cautiously consider the fact that different components of bone matrix behave differently. It is possible to state that mechanical proprieties reach their peak at approximately 40 years of age. In contrast, the behaviour of mineral and organic matrix might show some slight variation that needs further investigation. These results differ from those suggested by Zioupos (2001) who set skeletal maturity for the femur at 35 years of age. There are multiple factors that influence the dynamics of age-related changes and this could be the case for these diverging results. Furthermore, the femur is a weight-bearing bone and this induces higher levels of stress which results in the acceleration of bone turnover that is responsible for compositional and structural changes. Despite this, the present study demonstrates in general, that different features of bone matrix mature between different age ranges and the development of mechanical properties of mineralised collagen fibres is the result of all these physicochemical modifications.

The final aim of understanding changes in matrix composition is to have a better understanding of mechanical degradation of bone and to predict the increase of fracture risk. This would allow the identification of the best treatments. An example is given by osteoporosis, a metabolic disorder that occurs with advanced age and hormonal changes (i.e. menopause). Ma et al. (2017) give a comprehensive overview of numbers and costs related to osteoporosis. It is said that, of the ~ 200 million people affected by this metabolic disorder, 8.9 million annually are affected by fragility fracture. European treatments alone

cost 37 billion euros and with the raise of life expectancy this number could increase. Bisphosphonates are very common antiresorptive treatments that aim to reduce bone loss and increase bone mass in order to reduce fracture risks. Zimmermann et al. (2016) proved that, although an increase in mineral density is successfully obtained during a six-year treatment with alendronate mechanical properties of the bone matrix are reduced and the overall risk of fracture remains high. This example shows how understanding the behaviour of bone matrix is essential in order to understand the main components of bone strength and how to prevent fracture.

Overall, this study highlighted differences in the maturation point of compositional, structural and mechanical properties and showed the importance of the extensive evaluation of physicochemical and mechanical properties. This is also an essential step in identifying efficient markers in order to predict age accurately in forensic anthropology. Finally, further studies should consider different skeletal elements and a more extensive sampling in order to further understand the physiology of bone ageing.

7.6 Age-at-death Estimation

The final aim of this research is the development of age estimation based on physicochemical and mechanical parameters of bone matrix. To achieve this goal, different types of regression models were developed with a total of 28 parameters (Table 6.18). A total of seven models showed different degrees of accuracy and applicability in forensic settings. The rationale behind the selection was to explore the potential of the combination of the full matrix analysis and each aspect separately. Also, different combinations of parameters reduce the number of experimental procedures and the time for data acquisition. Based on R^2 , AIC, BIC and standard error of the estimation, three models were selected for their better performance in terms of accuracy. These three models were developed using the different stepwise selection strategies (detailed in Section 5.8.3).

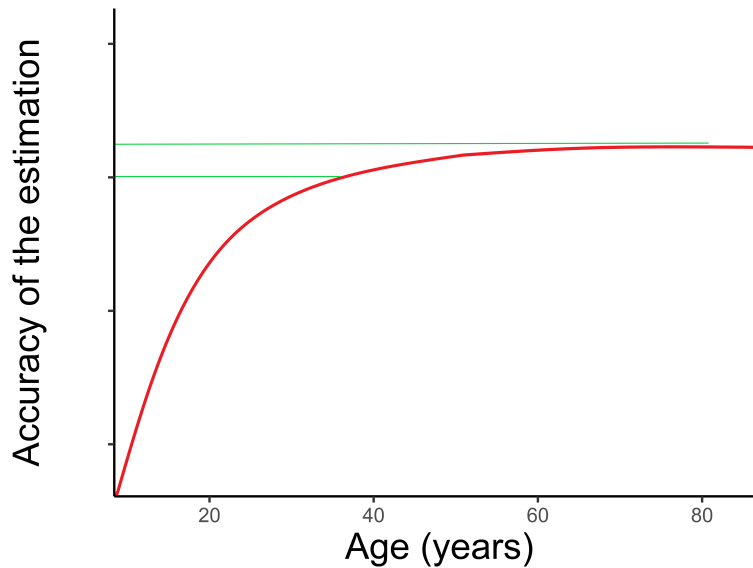


Figure 7.4: *The sketch represents the issue with age estimation. The increase in age drastically reduces the accuracy of the majority of the methods as shown by the area between the green lines.*

The accuracy of the age estimation methodology faces a key problem. With samples from older individuals, the estimation algorithm’s accuracy plateaus beyond a certain point. For instance, in Figure 7.4, the accuracy of the age estimation algorithms is low for bone samples from younger individuals. In order to solve this problem of sensitivity of models for age-at-death estimation, the current study focused on developing multifactorial models that can be robust and accurate in their estimations. The multifactorial approach involves the selection of different variables which have characteristic variations in certain age ranges. The combination of all these variables allows a more accurate estimation of age-at-death.

7.6.1 Unrestricted Parameter Selection

The first model (PR1), which employs backwards stepwise regression, shows the best performance in terms of standard error, with a deviation from the real age of only ± 6.35 years. R^2 -adj is still the highest achieved in all the models. The lower AIC indicates that there is no over or underfitting. The rest of the regression diagnostic have been thoroughly

presented in the results section. However, PR1 involves all the experimental procedures that increase the experimental time significantly. Moreover, several variables (e.g. $^{IT}C_{IT}$, $L\Delta H$ and MO) do not show significance. For age estimation, the selection of these variables is the ideal combination which allows age assessment with best accuracy and lowest residual. Nonetheless, considering that no collinearity was detected for this model, it is possible to overcome the statistical weakness with the good results provided by the model.

The second model (PR2) uses forward stepwise regression for parameter selection. Results are very similar to model PR1 with a decrease in all the indicators used for diagnostic. A key observation is the selection of 26 out of the 28 parameters. Although this model is shown to respect collinearity and autocorrelation for all variables, the list of independent variables most certainly contains "noise variables." Only $Po.Ar\%$ and $CL030$ are significant at $p < 0.05$ in this model. Although this model scores among the better performing models, the large number of experimental procedures involved and the fact that most of them did not show statistical significance does not make it the first choice for age estimation.

The final of the three best performing models (PR3) employed BIC based selection. This selection technique is the most appropriate from a statistical and forensic point of view. It employs only 5 variables from two different experimental procedures: nanoindentation ($Po.Ar\%$, $^{On}\eta_{IT}$, ^{IT}H , ^{IT}HV) and XRD ($CL030$). All the variables are significant at $p < 0.05$. Additionally, the time for the experimental procedure is R^2 hrs and the loss in accuracy is minimal (-0.33). Similarly, the deviation between predicted and real age shows satisfactory results (± 6.82 years). BIC is the lowest of all three suggesting that is the best combination of variables to predict the age of death based on the entire pool of variables.

Considering the most common parameters selected, porosity is highly significant and present in all the models. In accordance with the results presented in this study, previous studies have demonstrated this relationship (Feik et al., 1997; Zioupos, 2001; Zioupos et al., 2008). Three mechanical parameters are also included in each of the models. Considering that two are related to interstitial area suggests that these areas are less subject to

heterogeneity compared to osteons (Rho et al., 2002). Moreover, both variables are related to hardness properties (nanohardness and microhardness).

7.6.2 Restricted Parameter Selection

For restricted parameters selection, facilities and time availability was the rationale behind factor selection and each experimental procedure was considered independently to produce four additional models. For restricted selection, criterion selection was based on the results obtained in unrestricted parameter selection. As a result, PR4 involves the use of nanoindenter to acquire mechanical properties of interstitial and osteonal bone, and optical porosity. The model shows good accuracy with R^2 -adj of 0.831 and 6.85 years of deviation from the real age. All the regression diagnostics are shown to be acceptable. The main advantage is that the entire procedure can be done in 36 hours. One interesting aspect is that all the mechanical variables are taken from interstitial bone that implies that the ageing processes of this location are more consistent compared with osteonal bone.

The remaining models employ the analysis of bone powder in order to obtain different information on bone matrix composition. None of the models shows appropriate accuracy for forensic settings and the standard deviation is very high as can be seen in Table 7.1. For example, PR5 involves four of the five parameters acquired using TGA/DSC3+. For the first time, this model also shows autocorrelation and residuals are not normally distributed. There is an increase in accuracy for the age range over 30 years but the overall accuracy ($R = 0.25$) is too low to be acceptable. Therefore, both from a statistical point of view and considering possible applications this model is not suitable for age estimation. The only advantage is that the method can be potentially applied in 24 hours. Very similar results are found for PR6 that employs ATR-FTIR. The last model (PR7) performs the poorest of all the considered models. With $R = 0.10$ and $MSE = 15.91$ years, this method cannot be used for age estimation.

Table 7.1: Table summarising results for all the models developed showing the effectiveness of the multifactorial approach: reducing the number of factors obtained with different experimental procedures there is a decrease in the inaccuracy of the prediction. PR1, developed with backward stepwise regression, is the best performing model in terms of accuracy and statistical robusticity (R^2 : coefficient of determination; RSE: residual standard error; AIC: Aikake information criterion; BIC: Bayesian information criterion).

Model	RSE	R^2	R^2 -adj	BIC	AIC
PR1	6.352	0.873	0.855	754.403	754.403
PR2	6.596	0.880	0.843	848.524	772.157
PR3	6.819	0.840	0.832	781.456	762.364
PR4	6.849	0.839	0.831	782.443	763.351
PR5	14.69	0.250	0.222	951.279	934.914
PR6	15.09	0.201	0.179	953.633	939.996
PR7	15.91	0.104	0.088	961.839	950.930

7.6.3 Sex Specific Formulas

According to the results of this study, male individuals showed higher organic content compared to females that instead have longer crystals. The decrease in organic content is normally accompanied by dehydration of collagen molecules and the increase in mineral content. Similarly, the increase in mineral size with age is also characteristic of increased mineralisation of bone matrix. Although, with age, both sexes experience a decline in the BMU activity and bone formation, this is accentuated in females by the age of 40 years and affects primarily bone architecture (Ma et al., 2016, 2017). However, the increase in crystal size is also characteristic in osteoporosis and it could explain the observations presented in the previous paragraph (Guerado et al., 2016).

Due to this variation, sex specific formulas were produced. Overall, the backward and criterion stepwise selection generated models that primarily involve variables describing the mechanical behaviour of cortical bone for the female sample while the formulas developed for males involve both of them. This is due to the fact that at a certain age female individuals are affected by a number of hormonal changes that heavily affect composition of bone matrix. Therefore, physicochemical parameters are not reliable predictors. Preferentially, models to predict age-at-death for female individuals will be based on me-

chanical properties. In terms of results, no great difference was shown between the model developed on different groups. However, when applying the method, it is recommended to choose a sex specific formula when sex is known. Further research should focus on collecting a sample comprising of clinical history in order to evaluate potential bias in the age estimation

7.7 Comparison with Other Age Estimation Methods

At the outset, it is of importance to mention that the previously mentioned need to estimate age-at-death from a multifactorial approach using multiple parameters has been successfully achieved. The focus of this chapter shifts to placing the results of this thesis within the context of existing methods. This will help understand the significance of the results and the contribution of this thesis. Further, it will also discuss the advantages, disadvantages, applicability and degree of accuracy of physicochemical and mechanical analysis of human cortical bone. Zioupos et al. (2014) employed analysis of femoral matrix, which was the starting point for the present research. This procedure considers bone from macro- to nano-level showing the potential applicability of this principle with a ± 1 year of accuracy. The author proposed several different combinations of variables to reduce experimental time to 24 hours. However, the anatomical target of this technique is the femur, a weight-bearing bone not easily accessible during normal autopsy procedure (Bonicelli et al., 2017). Moreover, the method may be robust but the sample size ($N = 12$) is too small to establish this with certainty.

Another study showed the potential of this approach on ribs (Bonicelli et al., 2017). This site is accessible during autopsies and employs a very small segment of bone (~ 5 cm). Ribs offer the advantage of being less affected by mechanical stress compared to the femur and therefore, less prone to hormonal and metabolic changes (Zioupos, 2001). Results were very promising (mean residual error of 2.13 years ± 0.4) although with a total of 28 variables and only 24 specimens, it is difficult to clearly understand the applicability of this methodology. This study also considered two different Mediterranean populations (Greek and Albanian), showing no difference between the two (Bonicelli et al., 2017). The present

study is the continuation and implementation of these previous pilot studies and focuses on mainly compositional and structural parameters of the matrix with only indentation (micro and nano) as mechanical testing. The total number of parameters are 33 and, considering the larger sample size, it allows researchers to fully understand the potential for age estimation. The results do not prove to be as accurate as those of the previous methodologies (Zioupos et al., 2014; Bonicelli et al., 2017) with maximum accuracy with R^2 of 87.3 and mean residual error of 6.69 years. This could be due to several factors. First, the increased sample size increases inter-population variation depicted in the values. In other words the more the sample the greater the variability and the lower the predicted accuracy. However, information criteria were employed in variable selection for multiple linear regression that are shown to be better than stepwise selection (Gagné and Dayton, 2002). Second, for the sample employed in this study maximum age is 84 years with a large number of individuals over 60 years of age. It is known that due to the heterogeneous behaviour of age-related changes, accuracy noticeably decreases with the increment of age (Márquez-Grant, 2015). It is possible to state that, although the present methodology loses some degree of accuracy in determining age for an older individual, results remain acceptable for forensic age-at-death estimation.

Comparing R^2 , which is the proportion of the variance in the age that is explained by the regression model in each case and the mean residual error, with other methodologies, it is possible to evaluate performance and discuss the applicability of the proposed technique. As previously stated, AAR is one of the most efficient procedures for age estimation and several tests have been carried out (Ohtani, 1995b; Arany et al., 2004; Sakuma et al., 2012). However, these methodologies require a considerable amount of time, specialised equipment and personnel. Moreover, they have been proved to be inaccurate and inappropriate for certain categories according to age and sex (i.e. older females) and for post mortem interval larger than 20 years (Franklin, 2010). Finally, considering the incidence of caries on teeth, the most accurate target for AAR application, this could represent a biasing factor for age estimation (Griffin et al., 2008). One should consider that pathological conditions such as osteoporosis or osteogenesis imperfecta could have an impact on age

estimation using physicochemical and mechanical properties of cortical bone (Bonicelli et al., 2017). Another interesting approach for age estimation developed by Schmitt et al. (2010) on root translucency and periodontosis proved once more the inappropriateness for individuals > 60 years of age and sex-related variations that were not shown in our test.

Histological analysis has been largely proved to be an efficient methodology for age estimation. Since Kerley (1965) different procedures have been developed for mineralised bone (Stout and Gehlert, 1980; Maat et al., 2006; Goliath et al., 2016), demineralised bone (Martrille et al., 2009; Cannet et al., 2011) and on tooth cementum (Jankauskas et al., 2001; Kagerer and Grupe, 2001). Results are reported in the table below and show good accuracy. It is not affected by taphonomic changes but sex, diet and pathological condition can heavily affect the age assessment (Gómez García-Donas, 2018). To the author personal experience, the issue with these procedures relies on the fact that the preparation is time-consuming and the data acquisition is complex and requires knowledge of micro-anatomy to obtain an accurate count of the features. It is, however, correct to infer that the estimation method developed in this thesis requires some degrees of knowledge in bone micro-anatomy although the sampling technique speeds the data acquisition and simplifies the reading of cortical bone features.

Several molecular methods have been introduced at the beginning of this report. Martin-De Las Heras et al. (1999) have presented work on age-related changes in collagen. They provided two innovative approaches that unfortunately did not give appropriate results for age estimation. However, the authors suggest that this could represent a useful and complementary method in combination with other morphological and biochemical procedures on teeth, such as histology or AAR (Martin-De Las Heras et al., 1999, 2003). Zubakov et al. (2010, 2016) showed the potential of molecular ageing methods. DNA methylation was applied by Huang et al. (2015) with very similar results to the present study (SD approximately ± 6 years). They highlighted that methylation could be highly population specific in contrast to the physicochemical and mechanical properties for age estimation employed in this thesis. Telomere length observed by Takasaki et al. (2003) shows a reduction in R^2 compared to the previously presented studies (Zubakov et al., 2010, 2016)

but the standard error remains very low as can be seen in Table 7.2. The main limitation is that this phenomenon does not occur in dry conditions. This intense influence of environmental conditions on the estimation based on telomere shortening. In contrast, for individuals who died by drowning the amount of shortening is increased, affecting accuracy of the estimation. Contamination and taphonomic deterioration of the remain make this methodology unsuitable for forensic application. Finally, evaluation of telomere repeat has been shown to be of minimal or no applicability for forensic estimation due to 22 years of deviation between real and predicted age (Karlsson et al., 2008).

It can be seen in Table 7.2 that the present study involves a large number of studies compared to the other cited methodologies. The study involving blood samples are comparable to the present one in terms of sample size. However, the possibility of sampling easily blood from a large number of individuals is indeed an advantage in planning the experimental process. The only invasive study involving a larger sample size is Kerley (1965). Furthermore, in terms of R^2 remains one of the best-performing methods, if considering both sample size and overall performance. Noticeable less accuracy can be seen when the present protocol is compared with Zioupos et al. (2014) and Bonicelli et al. (2017) but this is due to the great difference in sample size. The present study employs the same multi-factorial approach that necessitates of a large number of specimens to have statistical robusticity. Overall, it is possible to state the the present study achieves the main goal of producing an accurate and versatile tool for age estimation of unknown skeletal remains.

Table 7.2: Main laboratory methods applied in forensic anthropology for age-at-death estimation (R^2 : coefficient of determination; RSE: residual standard error; SDE: standard deviation of residual standard error).

Reference	Method	Target	R^2	RSE	SDE
PR1	Mechanical and physicochemical	Rib (N=113)	0.87	6.35	5.94
PR2	Mechanical and physicochemical	Rib (N=113)	0.88	6.60	5.77
PR3	Mechanical and physicochemical	Rib (N=113)	0.84	6.82	6.66
Bonicelli et al. (2017)	Mechanical and physicochemical	Rib (N=24)	0.949	2.14	0.4
Zioupos et al. (2014)	Mechanical and physicochemical	Femur (N=12)	0.997	0.6	0.31
Ohtani (1995b)	AAR	Teeth (N=24)	-	3	-
Griffin et al. (2008)	AAR	Teeth (N=31)	-	4.35	-
Sakuma et al. (2012)	AAR	Teeth (N=12)	0.87–0.96	7.4–3.9	-
Schmitt et al. (2010)	Translucency and periodontosis	Teeth (N=12)	0.33	13.7	-
Kerley (1965)	Histomorphometry	Fibula (N=126)	0.973	5	-
Thompson and Galvin (1983)	Histomorphometry	Tibia (N=53)	-	9.13	-
Stout and Paine (1992)	Histomorphometry	Rib and clavicle (N=40)	77.6	2.6	2.2
Stout et al. (1996)	Histomorphometry	Rib (N=83)	-	5.5	-
Jankauskas et al. (2001)	Histomorphometry	Teeth (N=49)	0.772	8.63	6.46
Martin-De Las Heras et al. (1999)	Collagen cross-link	Teeth (N=22)	0.47	14.3	-
Martin-De Las Heras et al. (2003)	AGEs - spectroradiometry	Teeth (N=287)	0.7 0	13.7	-
Zubakov et al. (2010)	T-cell DNA	Blood (N= 195)	0.835	8.9	0.36
Zubakov et al. (2016)	Telomere length	Blood (N=390)	0.86	7.62	-
Takasaki et al. (2003)	Telomere length	Teeth (N=100)	0.562	7.52	-
Huang et al. (2015)	DNA methylation	Blood (N=89)	0.819	7.87	-
Karlsson et al. (2008)	Telomere repeats	Blood (N=100)	0.3	22	-

7.8 Research Limitations

The design of this study took into consideration any potential biasing factors to create ideal experimental conditions to produce the final methodology. However, some limitations are to be examined for both the forensic application and more qualitative evaluation of bone matrix determination.

To better understand the relationship between compositional, structural and functional properties of and the reciprocal effect on mineral and organic phase and the impact that they have on bone mechanical properties, the two phases should be isolated before analysis. There are a large number of procedures for deproteinization and demineralisation that have been applied in biomedical research (Liu et al., 2013; Jimson et al., 2014). This could be appropriate also for age estimation as some of the changes (e.g. collagen cross-link and AGEs products) could show very consistent behaviour with age. One specific aspect that needs further investigation is the dehydration protocol. In this study and in literature (Unal and Akkus, 2015; Unal et al., 2019), it is assumed that the degreasing procedure could remove non-binding water and retain structural water. This aspect could be further tested using solid-state NMR as water represents an essential component in the bone. Limited research has been carried out from the FTIR spectra and there is still potential for further investigation of carbonate substitution. This phenomenon is essential to understand the crystal architecture and the degeneration of mechanical properties.

The fundamental aim of this study was to investigate the potential of physicochemical and mechanical examination for age estimation based on a bench top instrument protocol. The main limitation for such an analysis is the sample size. Having ascertained that the total number is satisfactory for a dependable result, the amount of variables is very high and increasing the number of samples could make the method more robust. Furthermore, although basic demographic information and health status (known pathology and cause of death) were present for this sample, it would have been beneficial to acquire more information such as body weight and height and to test the methodology in different groups according to ethnicity and pathological conditions (e.g. diagnosed osteoporotic). If one

considers that bisphosphonate is a common treatment for osteoporosis, this treatment increases significantly mineral content and would drastically affect the estimation of age. This could allow a more accurate age estimation and also a better understanding of the physiological changes in bone matrix with age. Regarding the sample choice, one aspect that is essential to consider is the potential bias that affect the prediction when the method is applied to a different population other than the reference. From a twin study, Bjørnerem et al. (2015) showed that genetic factors account for 47% to 68% of the variance in trabecular volumetric bone mineral density account at the distal radius and 67% and 61% for total cortical porosity at the distal tibial for example. Overall, genetic factors are accountable for 55% to 62% in remodelling markers. This proves, that not only genetic distance that affect histomorphometry and physicochemical properties of bone that would reflect on the mechanical behaviour, but also environmental factors could play a role in inducing inaccuracy in the age-at-death estimation.

One further limitation of the study is also the invasiveness of the procedure. However, the small amount of bone to be sampled and the location of the sampling (rib) would induce minimal damages to the completeness of the remains. Finally, the most accurate models involve several bench top analytical techniques that may not always be available. To face this issue different models were developed based on the employment of only one of these techniques. The reduction in the number of predictors in the model inevitably induces a decrease in the model performance. However, this is an intrinsic issue of the multifactorial approach that can only be solved by finding parameters that better describe and consistently correlate with age.

It was not possible to assess diagenesis and, therefore, it is unknown how *post mortem* interval and conditions can affect age estimation. A pilot study was carried out to evaluate this issue at a preliminary stage but a more systematic experiment should be designed. For example, the effect of heat treatment on crystal morphology have been largely studied using different techniques: XRD results suggested that an increase in temperature induces loss of lattice incorporated water, variation in ion exchange (particularly the loss of carbonate) and thermal expansion (Greenwood et al., 2013). Similarly, Thompson et al. (2011),

by means of FTIR, showed an increase in crystallinity directly proportional not only with the increase of burning intensity but also with the time of exposure to the heat source and the temperature. It is therefore essential to include this aspect in order to understand the full potential of the age-at-death method developed in this thesis in different conditions. The same necessity is to be expanded to the decay of the organic matrix and the modification of mechanical properties as it could introduce bias in the estimation (Collins et al., 2002; Turner-Walker, 2011; Lau et al., 2013).

CHAPTER 8

CONCLUSIONS

The main objective of the study in this thesis was to develop a new age-at-death method that could address the necessary requirements of accuracy, replicability and applicability that have been seen to be essential in forensic anthropology (Garvin and Passalacqua, 2012). Focusing on these requirements prepares the resulting method to be applicable in legal scenarios. The approaches chosen based on physicochemical and mechanical properties of bone have shown to meet all these requisites. Simultaneously, it was possible to investigate variation of physicochemical and mechanical properties of ribs gaining essential information for biomedical research and mechanical engineering. It was proved that the combination of experimental procedures gives a comprehensive understanding of mineral and organic matrix and their involvement in determining bone mechanical resistance. The following conclusions can be drawn from the results and the study as a whole.

8.1 Chloroform-methanol Procedure

Chloroform-methanol preparation is an efficient procedure to eliminate the excess of fat and bone marrow from a fresh bone. It does not affect the organic matrix compositional properties. It also induces the removal of the excess of water from the sample due to the last step in ethanol, allowing to evaluate variations of water phase with age. Due to ion substitution induced by the treatment, an increase in CL002 and CL004 was found as well as a reduction in CL210. According to these results, caution is warranted when formulating the experimental design as these procedures can affect the outcome. Considering age estimation, the increased organic content is typical of young individuals and causes underestimation. Similarly, older individuals with increased porosity would retain more grease compared to dense younger individuals that would represent a confounding factor that would be scored in a lower age range. Furthermore, coherence length has been

shown to increase with age. The fact that in at the 002 and 004 peaks values higher for the treated group and for the 210 peak lower, would represent a further biasing factor. As a consequence, the method developed and presented in this thesis must be carried out on rib cortical bone after the treatment to avoid incorrect results.

8.2 Structural Relationship between Collagen and Mineral

This study confirms a close relationship between collagen ageing and mineral growth. Although no molecular mechanism of mineral and collagen interaction were taken into consideration and inferences were only drawn on the basis of observational data, it appears that highly organised and young collagen could induce an increase of strain resulting in mineral crystal growth width. Additionally, it is not to exclude that the shrinkage of collagen molecules could reduce the mechanical stress applied on the crystals inducing an increase in size. It is important to consider that there are other processes (e.g. ion substitution) that affect mineral growth and further investigation is necessary to entirely understand this relationship. In addition, simultaneous occurrence of these events could have a complex impact which needs to be understood. It was shown that carbonate substitution induces the increase in size, especially along the 'a' axis, indicating that older bone is characterised by broader crystals. The only conclusion made with certainty is that there is a general increase in crystal size coupled with collagen shrinkage. Concerning the overall bone composition, the linear decrease in water and organic content is coupled with the increase in mineral. These trends are mostly in agreement with previous literature. However, it was found that for the rib, the magnitude of these phenomena is reduced due to the lower metabolic activity of the rib cage and the reduced stress the area is subject to.

8.3 Age Related Changes and Comparison of Mechanical and Physicochemical Parameters

Considering sex-related differences, there was minimal variation between male and female for bone matrix analysis. The three variables affected are $C\Delta H$, $Or\%$ and crystal size. The first two variables are related to the amount of organic matrix present in the bone and

could represent the best age-at-death predictors. Crystal size, on the other hand, could be affected by to pathological conditions and diet. It is to be noted that according to demographic data, none of the individuals presented metabolic diseases (e.g. osteoporosis, osteogenesis imperfecta) that are highly sex-specific but full clinical history would be beneficial in understanding variations. For this small degree of variation between sexes, rib bones are a suitable target for age estimation.

According to the correlation between compositional and mechanical parameters, the study revealed that the combination of the physicochemical changes of mineral and organic matrix affects mechanical behaviour of bone. Overall, variations in mineral content and crystal structure better describe the mechanical behaviour. The increase in crystallite size and related increase in ash content have a positive effect on both elastic and plastic deformation. However, stepwise regression proved that elastic properties are better described by parameters related to the mineral phase while hardness is equally dependent from variations of mineral and organic phase.

8.4 Skeletal Maturity

It was possible to state that skeletal maturity for rib cortical bone is reached approximately at 40 years of age. This is unequivocally true for mechanical properties with both elastic modulus and harness increasing until this point in life and then decreasing drastically. However, if this is unequivocally true for mechanical properties and mineral content, it was shown using DSC and XRD that mineral architecture and collagen stability follow a more complex development and degeneration that can be correlated with the behaviour of mechanical properties.

8.5 Age-at-death Estimation

It was possible to develop an efficient and accurate age-at-death estimation method that is potentially free from inter-observer error. The method that ranks best for better scoring in terms of predictive power and the sample size is sufficient to be representative for the population (R^2 and standard deviation 6.35 years). It is highly replicable and does not require

specific knowledge in bone anatomy and physiology, allowing laboratory technicians to carry out an unbiased evaluation of age-at-death. This multifactorial approach could benefit from the incorporation of other variables that could be gathered with the experimental procedures chosen in this thesis such as histomorphometry that would however require the presence of highly specialised personnel to be carried out. In order to increase applicability, different predictive relationships were produced to manage time and facilities constraints as well as sex specific models. Overall, this new method could represent an efficient tool for forensic anthropology. Although, it is a fully developed method based on a sample size adequate to be representative and hold its statistical merit, caution is recommended as the effect of diagenesis remains unknown and would require further systematic approach for evaluation.

8.6 Future Work

Future research beyond this thesis directly stems from the observations of this study and the limitations mentioned previously. Age estimation is an essential step for the identification of unknown skeletal remains. A considerable number of methodologies have been developed to allow anthropologists the ability to ascertain the age of bone samples in different conditions. The methodological choice is always case driven and depends mainly on the type of remains, preservation, completeness and availability of equipment. Microscopic and biochemical procedures proved to be extremely accurate and free from observer bias (Franklin, 2010; Garvin and Passalacqua, 2012). However, they necessitate specific equipment that could represent an impediment to application universally in any and all conditions. Multifactorial approach involving the examination of different developmental or degeneration indicators offers increased accuracy compared to other methods (Franklin, 2010; Basset et al., 2011).

This project is the first comprehensive investigation of physicochemical and mechanical properties in service of age estimation. Therefore, literature does not offer specific reviews on its efficiency and applicability. A natural progression of this work is to combine histomorphometry and the variables acquired in the present study to evaluate the

potential for age estimation. This implementation would have the double advantage of giving a better understanding of the ageing process and increasing the accuracy for anthropological purposes. Furthermore, it would be easy to apply as the bone embedded in the epoxy resin can be analysed under reflected light for this purpose. This would give better understanding of the degeneration of the bone matrix concerning turnover. Furthermore, histomorphometric variables have been largely employed in age estimation could improve the estimation. However, the methodology requires improvement to be adapted to the different microscopy techniques applied in this study. Genetic variation and environmental factors should be always be considered when including such variables for age assessment. The study should be repeated using bone from different animal species. The potential of histomorphometry characterisation for segregating human vs. non-human and different species have been largely proved. Yet, the combination of all these parameters using regression analysis could show improved results. Finally, the bone targeted in this study was the rib. Nonetheless, other skeletal sites could be more suitable for age estimation. More locations should be evaluated and compared, and combined where possible, to improve the accuracy of the estimation. Additionally, this method employs bone segments towards the sternal end of 4th of forth ribs from autopsy material. When sampling the necessary specimens, it would be advisable to detach and macerate the very final part of the rib to apply the method developed by Işcan et al. (1984) and combine it with results from the matrix analysis. This could give an initial orientation on the age of unknown skeletal remains and facilitates development of models specific for different age ranges to optimise accuracy and applicability. Furthermore, there are a series of variables to consider before understanding the full potential of this approach for age estimation.

The application of this method to other skeletal elements and variation across the thoracic cage, along the rib and between the two sides should be further investigated. Several studies have investigated diagenetic processes that affect bone collagen, mineral and mechanical process (Thompson et al., 2011; Tătar et al., 2014). Taphonomic changes, therefore, must have a negative effect on the accuracy of the estimation. A short study based on two ribs retrieved from a seashore showed that the methodology retained good accuracy

and precision after a one-month post-mortem interval (Bonicelli et al., 2017). However, a more systematic investigation should be conducted to elucidate this aspect for this specific combination of variables. The variation in compositional properties evaluated by means of FTIR was tested by Wang et al. (2017) that showed the difference between unburied (e.g. increase in organic and carbonate content) and buried bone (e.g. decrease in organic and carbonate content). This chemical modification induced by post-depositional processes is seen to affect various ageing techniques: contributes to denaturation of collagen triple helix increasing racemization of peptide-bound aspartic acid (Torres et al., 2014) and affects extraction of sample for methods based on molecular biology increasing the risk of contamination (Zapico and Ubelaker, 2013). Similarly, heat treatment has been shown to heavily affect mineral phase (Thompson et al., 2011; Greenwood et al., 2013). These compositional changes induce modification in mechanical behaviour, with a general decrease in performances with the increment in PMI (Walden et al., 2017). The new systematic experiment should consider different time intervals, temperature, environment acidity and humidity in order to acquire a deep understanding of the bias introduced by taphonomic factors to the method developed in this thesis.

Finally, pathological conditions could play a central role in affecting age-at-death estimation. For instance, changes induced by osteoporosis on bone architecture and composition have been largely studied in the biomedical domain (Parfitt, 1979; Mkukuma, 2005; Bernhard et al., 2013). When considering the incidence of this condition that affects 50% of women over 50 years of age in the UK (van Staa et al., 2001), it is clear that this parameter is of utmost importance to reach an exhaustive accuracy level.

To conclude, in this study linear regression was employed to produce predictive formulas. The issues related to sample size and the number of predictors are well known. Different statistical approaches should be evaluated to avoid overestimation associated with linear regression, such as the Bayesian approach. The methodology in this thesis works with rib bone samples. Once expanded to include other bones from different locations of the body and including a greater sample size in the study, the number of parameters increase drastically. However, modern technologies such as neural networks and machine

learning offer solutions that can handle such a high data volume and inter-data variability. It would be a challenging yet rewarding venture to assess the applicability of such technologies to provide a holistic assessment for estimation of age-at-death.

Overall, the degree of accuracy and versatility showed the potential of a multidisciplinary approach to forensic age estimation. This response to the standard requirements explained in the introduction part and reviewed by several critical reviews (Ritz-Timme et al., 2000; Cattaneo, 2007; Franklin, 2010) and could help medico-legal investigation and assessment of the biological profile of unknown individuals. This study showed the potential of the application of material sciences to forensic anthropology in order to obtain accurate age estimation.

8.7 Summary

To conclude, in this study a new age-at-death estimation protocol was developed based on the combination of a number of physicochemical and mechanical properties. Results outstripped most of the methods normally applied for age-at-death estimation in the forensic setting. Furthermore, it meets the standards recently established for the forensic application. More validation work is however needed in order to fully explore the applicability. Regard the five research question set prior the investigation, outcome are summarised below:

1. Overall, the degreasing protocol chosen for the study proved to efficiently remove the superficial organic matter (e.g. grease and marrow) and well as superficial water. On the other hand, it was found that this induces an increase in crystal length. It was possible to provide a satisfactory explanation of the effect of the protocol and suggestions have been given regarding its application.
2. The study found a general degeneration of the mechanical behaviour in relation to age. Considering composition, a drastic increment in mineral content and the decrease in organic was found. This was also accompanied by increase in carbonate

content and crystallite size. Overall, this is in agreement with literature with the exception that the present sample size is one of the largest analysed.

3. Conclusive results for the structural interaction between collagen and mineral were found. They show that the degeneration of collagen matrix is coupled with the increase in mineral content, crystallite size and carbonate substitution. Further research should evaluate the molecular mechanism of this age related process.
4. The present study provides clear results that indicate that it is not possible to isolate one component of bone matrix to explain its mechanical behaviour. However, it can be seen that the mineral phase has a predominant role in nanomechanical properties determination. The comparison between mechanical testing typical of other structural levels could be beneficial to better understand functional behaviour of bone.
5. Regarding skeletal maturity, results confirmed that mechanical properties reach their maximum performance at approximately 35 years of age. However, structural and compositional characteristic of bone matrix were found to give different intervals rather than providing a uniform age limit. Further research is necessary to better evaluate this aspect and more comprehensive study should be designed to answer this complicated question.

Bibliography

- Adserias-Garriga, J. and Wilson-Taylor, R. (2019). Chapter 5 - skeletal age estimation in adults. In Adserias-Garriga, J., editor, *Age Estimation*, pages 55 – 73. Academic Press.
- Akkus, O., Adar, F., and Schaffler, M. B. (2004). Age-related changes in physicochemical properties of mineral crystals are related to impaired mechanical function of cortical bone. *Bone*, 34(3):443–453.
- Akkus, O., Polyakova-Akkus, A., Adar, F., and Schaffler, M. B. (2003). Aging of Microstructural Compartments in Human Compact Bone. *Journal of Bone and Mineral Research*, 18(6):1012–1019.
- Akkus, O. and Rimnac, C. M. (2001). Cortical bone tissue resists fatigue fracture by deceleration and arrest of microcrack growth. *Journal of Biomechanics*, 34(6):757–764.
- Allen, M. R. and Burr, D. B. (2013). Bone Modeling and Remodeling. *Basic and Applied Bone Biology*, pages 75–90.
- Andrade, M. G. S., Sá, C. N., Marchionni, A. M. T., Bório dos Santos Calmonde Bittencourt, T. C., and Sadigursky, M. (2008). Effects of freezing on bone histological morphology. *Cell and Tissue Banking*, 9(4):279–287.
- Arany, S., Ohtani, S., Yoshioka, N., and Gonmori, K. (2004). Age estimation from aspartic acid racemization of root dentin by internal standard method. *Forensic Science International*, 141(2-3):127–130.
- Arlot, S. and Celisse, A. (2009). A survey of cross-validation procedures for model selection. *Statistic Surveys*, 4:40–79.
- Ascenzi, A., Baschieri, P., and Benvenuti, A. (1990). The bending properties of single osteons. *Journal of Biomechanics*, 23(8):763–771.

- Ascenzi, A., Baschieri, P., and Benvenuti, A. (1994). The torsional properties of single selected osteons. *Journal of Biomechanics*, 27(7):875–84.
- Ascenzi, A. and Bonucci, E. (1967). The tensile properties of single osteons. *The Anatomical Record*, 158(4):375–386.
- Ascenzi, A. and Bonucci, E. (1968). The compressive properties of single osteons. *The Anatomical Record*, 161(3):377–391.
- Ascenzi, A., Bonucci, E., and Simkin, A. (1973). An approach to the mechanical properties of single osteonic lamellae. *Journal of Biomechanics*, 6(3):227–230.
- Aubert, G. and Lansdorp, P. M. (2008). Telomeres and Aging in Mammals. *Physiology Review*, 88:557–579.
- Augat, P. and Schorlemmer, S. (2006). The role of cortical bone and its microstructure in bone strength. *Age and Ageing*, 35(SUPPL.2):27–31.
- Baccino, E., Ubelaker, D. H., Hayek, L.-A. C., and Zerilli, A. (1999). Evaluation of seven methods of estimating age at death from mature human skeletal remains. *Journal of Forensic Sciences*, 44(5):931–936.
- Bala, Y., Depalle, B., Douillard, T., Meille, S., Clément, P., Follet, H., Chevalier, J., and Boivin, G. (2011). Respective roles of organic and mineral components of human cortical bone matrix in micromechanical behavior: An instrumented indentation study. *Journal of the Mechanical Behavior of Biomedical Materials*, 4(7):1473–1482.
- Barthelat, F., Yin, Z., and Buehler, M. J. (2016). Structure and mechanics of interfaces in biological materials. *Nature Reviews Materials*, 1(4):16007.
- Bas, M. and Cardona, L. (2018). Effects of skeletal element identity , delipidation and demineralization on the analysis of stable isotope ratios of C and N in fish bone. *Journal of Fish Biology*, 92:420–437.

- Bassed, R. B., Briggs, C., and Drummer, O. H. (2011). Age estimation using CT imaging of the third molar tooth, the medial clavicular epiphysis, and the spheno-occipital synchondrosis: A multifactorial approach. *Forensic Science International*, 212(1-3):273.e1–273.e5.
- Bechbache, R. R. and Duffin, J. (1977). The Entrainment of Breathing Frequency by Exercise Rythm. *Journal of Physiology*, 272:553–561.
- Beckett, S. (2009). *Inter-species variation in bone mineral*. Phd, Cranfield University.
- Bellido, T. and Hill Gallant, K. M. (2013). *Hormonal Effects on Bone Cells*. Elsevier Inc.
- Bellido, T., Plotkin, L. I., and Bruzzaniti, A. (2014). Bone Cells. *Basic and Applied Bone Biology*, 14:27–45.
- Bengio, Y. and Grandvalet, Y. (2004). No Unbiased Estimator of the Variance of K-Fold Cross-Validation. *Journal of Machine Learning Research*, 5:1089–1105.
- Bernhard, A., Milovanovic, P., Zimmermann, E. A., Hahn, M., Djonic, D., Krause, M., Breer, S., Püschel, K., Djuric, M., Amling, M., and Busse, B. (2013). Micro-morphological properties of osteons reveal changes in cortical bone stability during aging, osteoporosis, and bisphosphonate treatment in women. *Osteoporosis International*, 24(10):2671–2680.
- Bettin, D., Polster, J., Rullkötter, V., Von Versen, R., and Fuchs, S. (2003). Good preservation of initial mechanical properties in lipid-extracted, disinfected, freeze-dried sheep patellar tendon grafts. *Acta Orthopaedica Scandinavica*, 74(4):470–475.
- Betts, F., Blumenthaland, N. C., and Posner, A. S. (1981). Bone Mineralization. *Journal of Crystal Growth*, 53:63–73.
- Bi, X., Patil, C. A., Lynch, C. C., Pharr, G. M., Mahadevan-Jansen, A., and Nyman, J. S. (2011). Raman and mechanical properties correlate at whole bone- and tissue-levels in a genetic mouse model. *Journal of Biomechanics*, 44(2):297–303.

- Bjørnerem, Å., Bui, M., Wang, X., Ghasem-Zadeh, A., Hopper, J. L., Zebaze, R., and Seeman, E. (2015). Genetic and environmental variances of bone microarchitecture and bone remodeling markers: A twin study. *Journal of Bone and Mineral Research*, 30(3):516–524.
- Blair, H. C. (1998). How the osteoclast degrades bone. *BioEssays*, 20(10):837–846.
- Bocklandt, S., Lin, W., Sehl, M. E., Sánchez, F. J., Sinsheimer, J. S., Hovrath, S., and Vilan, E. (2011). Epigenetic Predictor of Age. *PLoS ONE*, 6(6):e14821.
- Boivin, G. (2007). The hydroxyapatite crystal: A closer look. *Medicographia*, 29(2):126–132.
- Boivin, G., Bala, Y., Doublier, A., Farlay, D., Ste-Marie, L. G., Meunier, P. J., and Delmas, P. D. (2008). The role of mineralization and organic matrix in the microhardness of bone tissue from controls and osteoporotic patients. *Bone*, 43(3):532–538.
- Bonicelli, A., Xhemali, B., Kranioti, E., and Zioupos, P. (2017). Rib biomechanical properties exhibit diagnostic potential for accurate ageing in forensic investigations. *PLoS ONE*, 12(5):1–20.
- Boskey, A. (2003). Bone mineral crystal size. *Osteoporosis International*, 14(0):16–21.
- Boskey, A. L. (1998). Biomineralization: conflicts, challenges, and opportunities. *Journal of cellular biochemistry. Supplement*, 30-31:83–91.
- Boskey, A. L. and Coleman, R. (2010). Aging and Bone. *Journal of Dental Research*, 89(12):1333–1348.
- Boskey, A. L. and Imbert, L. (2017). Bone quality changes associated with aging and disease: a review. *Annals of the New York Academy of Sciences*, 1410(1):93–106.
- Boskey, A. L., Spevak, L., Paschalis, E., Doty, S. B., and McKee, M. D. (2002). Osteopontin deficiency increases mineral content and mineral crystallinity in mouse bone. *Calcified Tissue International*, 71(2):145–154.

- Bridelli, M. G., Stani, C., and Bedotti, R. (2017). Fourier transform infrared conformational investigation of type I collagen aged by in vitro induced dehydration and non-enzymatic glycation treatments. *Journal of Biological Research - Bollettino della Società Italiana di Biologia Sperimentale*, 90(1):45–50.
- Brooks, S. T. (1955). Skeletal Age At Death : the Reliability of Crania and Pubic Age Indicators. *American Journal of Physical Anthropology*, 3(13):567–597.
- Buckberry, J. and Chamberlain, A. (2009). Age Estimation from the Auricular Surface of the Ilium: A Revised Method. *American Journal of Physical Anthropology*, 239:231–239.
- Buikstra, J. and Ubelaker, D. (1994). *Standards for Data Collection from Human Skeletal Remains*. Fayetteville, AR.
- Burnham, K. P. and Anderson, D. R. (2004). Multimodel inference: Understanding AIC and BIC in model selection. *Sociological Methods and Research*, 33(2):261–304.
- Burr, D. (2003). Microdamage and bone strength. *Osteoporosis international*, 14 Suppl 5:S67–S72.
- Burr, D. B. (2002). The contribution of the organic matrix to bone's material properties. *Bone*, 31(1):8–11.
- Burr, D. B. (2019). Changes in bone matrix properties with aging. *Bone*, 120(October 2018):85–93.
- Burr, D. B. and Akkus, O. (2013). *Bone Morphology and Organization*. Elsevier Inc.
- Burr, D. B. and Martin, R. B. (1989). Errors in bone remodeling: Toward a unified theory of metabolic bone disease. *American Journal of Anatomy*, 186(2):186–216.
- Burr, D. B., Schaffler, M. B., and Frederickson, R. G. (1988). Composition of the cement line and its possible mechanical role as a local interface in human compact bone. *Journal of Biomechanics*, 21(11).

- Cannet, C., Baraybar, J. P., Kolopp, M., Meyer, P., and Ludes, B. (2011). Histomorphometric estimation of age in paraffin-embedded ribs: A feasibility study. *International Journal of Legal Medicine*, 125(4):493–502.
- Cattaneo, C. (2007). Forensic anthropology: developments of a classical discipline in the new millennium. *Forensic Science International*, 165(2-3):185–193.
- Cazalbou, S., Eichert, D., Ranz, X., Drouet, C., Combes, C., Harmand, M. F., and Rey, C. (2005). Ion exchanges in apatites for biomedical application. *Journal of Materials Science: Materials in Medicine*, 16(5):405–409.
- Charmas, B. (2013). TG and DSC studies of bone tissue: Effects of osteoporosis. *Thermochimica Acta*, 573:73–81.
- Chen, L., Jacquet, R., Lowder, E., and Landis, W. J. (2015). Refinement of collagen-mineral interaction: A possible role for osteocalcin in apatite crystal nucleation, growth and development. *Bone*, 71:7–16.
- Cho, H., Stout, S. D., Madsen, R. W., and Streeter, M. A. (2002). Population-Specific Histological Age-Estimating Method: A Model for Known African-American and European-American Skeletal Remains. *Journal of Forensic Sciences*, 47(1):12–18.
- Clarke, B. (2008). Normal bone anatomy and physiology. *Clinical Journal of the American Society of Nephrology*, 3(Suppl 3):131–139.
- Coats, A. and Redfern, J. (1963). Thermogravimetric analysis. *Analyst*, 88:906–924.
- Collins, M. J., Hiller, J., Smith, C. I., Roberts, J. P., Prigodich, R. V., Wess, T. J., and Millard, A. R. (2002). The Survival of Organic Matter in Bone: a Review. *Archaeometry*, 3(44):383–394.
- Cook, R. B. (2005). *Non-invasively assessed skeletal bone status and its relationship to the biomechanical properties and condition of cancellous bone*. Phd, Cranfield University.

- Cook, R. B. and Zioupos, P. (2009). The fracture toughness of cancellous bone. *Journal of Biomechanics*, 42(13):2054–2060.
- Cooper, D. M., Thomas, C. D. L., Clement, J. G., Turinsky, A. L., Sensen, C. W., and Hallgrímsson, B. (2007). Age-dependent change in the 3D structure of cortical porosity at the human femoral midshaft. *Bone*, 40(4):957–965.
- Cunha, E., Baccino, E., Martrille, L., Ramsthaler, F., Prieto, J., Schuliar, Y., Lynnerup, N., and Cattaneo, C. (2009). The problem of aging human remains and living individuals: A review. *Forensic Science International*, 193(1-3):1–13.
- Currey, J. D. (2002). *Bone: Structure and Mechanics*. Princeton University Press, Woodstock, ii edition edition.
- Currey, J. D. (2003a). Role of collagen and other organics in the mechanical properties of bone. *Osteoporosis International*, 14(0):29–36.
- Currey, J. D. (2003b). The many adaptations of bone. *Journal of Biomechanics*, 36(10):1487–1495.
- Currey, J. D., Brear, K., and Zioupos, P. (1996). The effects of ageing and changes in mineral content in degrading the toughness of human femora. *Journal of Biomechanics*, 29(2):257–260.
- Currey, J. D., Foreman, J., Laketic, I., Mitchell, J., Pegg, D. E., and Reilly, G. C. (1997). Effects of ionizing radiation on the mechanical properties of human bone. *Journal of Orthopaedic Research*, 15(1):111–117.
- Danielsen, C. C. (1994). Thermal Stability of Cortical Bone Collagen in Relation to Age in Normal Individuals and in Individuals with Osteopetrosis. *Bone*, 15(1):91–96.
- Diab, T. and Vashishth, D. (2007). Morphology, localization and accumulation of in vivo microdamage in human cortical bone. *Bone*, 40(3):612–618.

- Dicken, A. J., Evans, J. P., Rogers, K. D., Stone, N., Greenwood, C., Godber, S. X., Clement, J. G., Lyburn, I. D., Martin, R. M., and Zioupos, P. (2016). Classification of fracture and non-fracture groups by analysis of coherent X-ray scatter. *Scientific Reports*, 6(July):1–7.
- Dobberstein, R. C., Huppertz, J., von Wurmb-Schwark, N., and Ritz-Timme, S. (2008). Degradation of biomolecules in artificially and naturally aged teeth: Implications for age estimation based on aspartic acid racemization and DNA analysis. *Forensic Science International*, 179(2-3):181–191.
- Dobberstein, R. C., Tung, S. M., and Ritz-Timme, S. (2010). Aspartic acid racemisation in purified elastin from arteries as basis for age estimation. *International Journal of Legal Medicine*, 124(4):269–275.
- Donnelly, E., Meredith, D. S., Nguyen, J. T., Gladnick, B. P., Rebolledo, B. J., Shaffer, A. D., Lorch, D. G., Lane, J. M., and Boskey, A. L. (2012). Reduced cortical bone compositional heterogeneity with bisphosphonate treatment in postmenopausal women with intertrochanteric and subtrochanteric fractures. *Journal of Bone and Mineral Research*, 27(3):672–678.
- Ekizoglu, O., Hocaoglu, E., Inci, E., Can, I. O., Aksoy, S., and Sayin, I. (2015). Estimation of forensic age using substages of ossification of the medial clavicle in living individuals. *International Journal of Legal Medicine*, 129(6):1259–1264.
- Elliott, J. C., Wilson, R. M., and Dowker, S. E. P. (2002). Apatite structures. *Advances in X-ray Analysis*, 45(c):172–181.
- Falys, C. G. and Prangle, D. (2015). Estimating age of mature adults from the degeneration of the sternal end of the clavicle. *American Journal of Physical Anthropology*, 156(2):203–214.
- Farlay, D., Panczer, G., Rey, C., Delmas, P. D., and Boivin, G. (2010). Mineral maturity

- and crystallinity index are distinct characteristics of bone mineral. *Journal of Bone and Mineral Metabolism*, 28(4):433–445.
- Feik, S. A., Thomas, C. D. L., and Clement, J. G. (1997). Age-related changes in cortical porosity of the midshaft of the human femur. *Journal of Anatomy*, 191(3):407–416.
- Fischer-Cripps, A. C. (2004). A simple phenomenological approach to nanoindentation creep. *Materials Science and Engineering A*, 385(1-2):74–82.
- Florencio-silva, R.; Sasso, G.; Sasso-cerri, E.; Simões, M. J. & Cerri, P. S. (2015). Biology of Bone Tissue: Structure, Function, and Factors That Influence Bone Cells. *BioMed Research International*, pages 1–17.
- Fonseca, H., Moreira-Gonçalves, D., Coriolano, H. J. A., and Duarte, J. A. (2014). Bone quality: The determinants of bone strength and fragility. *Sports Medicine*, 44(1):37–53.
- Fraga, M. F., Ballestar, E., Paz, M. F., Ropero, S., Setien, F., Ballestar, M. L., Heine-Suner, D., Cigudosa, J. C., Urioste, M., Benitez, J., Boix-Chornet, M., Sanchez-Aguilera, A., Ling, C., Carlsson, E., Poulsen, P., Vaag, A., Stephan, Z., Spector, T. D., Wu, Y.-Z., Plass, C., and Esteller, M. (2005). From The Cover: Epigenetic differences arise during the lifetime of monozygotic twins. *Proceedings of the National Academy of Sciences*, 102(30):10604–10609.
- Franklin, D. (2010). Forensic age estimation in human skeletal remains: Current concepts and future directions. *Legal Medicine*, 12(1):1–7.
- Fratzl P, Gupta HS, Paschalis EP, and Roschger P (2004). Structure and mechanical quality of the collagen Mineral nano-composite in bone. *Journal of Materials Chemistry*, 14(14):2115–2123.
- Freire-Aradas, A., Phillips, C., Mosquera-Miguel, A., Girón-Santamaría, L., Gómez-Tato, A., Casares De Cal, M., Álvarez-Dios, J., Ansedé-Bermejo, J., Torres-Español, M., Schneider, P. M., Pośpiech, E., Branicki, W., Carracedo, and Lareu, M. V. (2016). Development of a methylation marker set for forensic age estimation using analysis of

- public methylation data and the Agena Bioscience EpiTYPER system. *Forensic Science International: Genetics*, 24:65–74.
- Frost, H. M. (1987a). Bone “ Mass ” and the “ Mechanostat ”: A Proposal. *The Anatomical Record*, 9:1–9.
- Frost, H. M. (1987b). Secondary osteon population densities: An algorithm for estimating the missing osteons. *American Journal of Physical Anthropology*, 30(8 S):239–254.
- Frost, H. M. (1997a). On our age-related bone loss: insights from a new paradigm. *Journal of Bone and Mineral Research*, 12(10):1539–1546.
- Frost, H. M. (1997b). Why do marathon runners have less bone than weight lifters? A vital-biomechanical view and explanation. *Bone*, 20(3):183–189.
- Frost, H. M. (2000). The Utah paradigm of skeletal physiology: an overview of its insights for bone, cartilage and collagenous tissue organs. *Journal of bone and mineral metabolism*, 18(6):305–316.
- Frost, H. M. (2001). From Wolff’s law to the Utah paradigm: Insights about bone physiology and its clinical applications. *Anatomical Record*, 262(4):398–419.
- Frost, H. M. (2004). A 2003 update of bone physiology and Wolff s law for clinicians. *Angle Orthodontist*, 74(1):3–15.
- Fushiki, T. (2011). Estimation of prediction error by using K-fold cross-validation. *Statistics and Computing*, 21(2):137–146.
- Gagné, P. and Dayton, C. M. (2002). Best regression model using information criteria. *Journal of Modern Applied Statistical Methods*, 1(2):479–488.
- Gamsjaeger, S., Robins, S. P., Tatakis, D. N., Klaushofer, K., and Paschalis, E. P. (2017). Identification of Pyridinoline Trivalent Collagen Cross-Links by Raman Microspectroscopy. *Calcified Tissue International*, 100(6):565–574.

- Garnero, P., Borel, O., Gineyts, E., Duboeuf, F., Solberg, H., Bouxsein, M. L., Christiansen, C., and Delmas, P. D. (2006). Extracellular post-translational modifications of collagen are major determinants of biomechanical properties of fetal bovine cortical bone. *Bone*, 38(3):300–309.
- Garvin, H. M. and Passalacqua, N. V. (2012). Current Practices by Forensic Anthropologists in Adult Skeletal Age Estimation. *Journal of Forensic Sciences*, 57(2):427–433.
- Gelse, K., Pöschl, E., and Aigner, T. (2003). Collagens - Structure, function, and biosynthesis. *Advanced Drug Delivery Reviews*, 55(12):1531–1546.
- Ghasemi, A. and Zahediasl, S. (2012). Normality Tests for Statistical Analysis: A Guide for Non-Statisticians. *International Journal of Endocrinology and Metabolism*, 10(2):486–489.
- Goliath, J. R., Stewart, M. C., and Stout, S. D. (2016). Variation in osteon histomorphometrics and their impact on age-at-death estimation in older individuals. *Forensic Science International*, 262:282.e1–282.e6.
- Gómez García-Donas, J. (2018). *Age estimation on two Mediterranean samples using rib histomorphometry*. Phd, University of Edinburgh.
- Greenwood, C. (2014). *Physicochemical Modification to Bone Mineral*. PhD thesis.
- Greenwood, C., Clement, J., Dicken, A., Evans, J. P., Lyburn, I., Martin, R. M., Rogers, K., Stone, N., and Zioupos, P. (2016). Towards new material biomarkers for fracture risk. *Bone*, 93:55–63.
- Greenwood, C., Clement, J. G., Dicken, A. J., Evans, J. P., Lyburn, I. D., Martin, R. M., Rogers, K. D., Stone, N., Adams, G., and Zioupos, P. (2015). The micro-architecture of human cancellous bone from fracture neck of femur patients in relation to the structural integrity and fracture toughness of the tissue. *Bone Reports*, 3:67–75.

- Greenwood, C., Rogers, K., Beckett, S., and Clement, J. (2012). Bone mineral crystallisation kinetics. *Journal of Materials Science: Materials in Medicine*, 23(9):2055–2060.
- Greenwood, C., Rogers, K., Beckett, S., and Clement, J. (2013). Initial observations of dynamically heated bone. *Crystal Research and Technology*, 48(12):1073–1082.
- Griffin, R. C., Moody, H., Penkman, K. E., and Collins, M. J. (2008). The application of amino acid racemization in the acid soluble fraction of enamel to the estimation of the age of human teeth. *Forensic Science International*, 175(1):11–16.
- Gross, K. A. and Berndt, C. C. (2002). Biomedical Application of Apatites. *Reviews in Mineralogy and Geochemistry*, 48(1):631–672.
- Grynepas, M. (1993). Age and disease-related changes in the mineral of bone. *Calcified Tissue International*, 53(Supp. 1):S57–S64.
- Grynepas, M. D. and Omelon, S. (2007). Transient precursor strategy or very small biological apatite crystals? *Bone*, 41(2):162–164.
- Guerado, E., Cruz, E., Cano, J. R., Crespo, P. V., Alaminos, M., Del Carmen Sánchez-Quevedo, M., and Campos, A. (2016). Bone mineral density aspects in the femoral neck of hip fracture patients. *International Journal of Care Injured*, 47:S21–S24.
- Hadjidakis, D. J. and Androulakis, I. I. (2006). Bone remodeling. *Annals of the New York Academy of Sciences*, 1092:385–396.
- Hamano, Y., Manabe, S., Morimoto, C., Fujimoto, S., Ozeki, M., and Tamaki, K. (2016). Forensic age prediction for dead or living samples by use of methylation-sensitive high resolution melting. *Legal Medicine*, 21:5–10.
- Handschin, R. G. and Stern, W. B. (1992). Crystallographic lattice refinement of human bone. *Calcified Tissue International*, 51(2):111–120.
- Handschin, R. G. and Stern, W. B. (1995). X-ray diffraction studies on the lattice perfection of human bone apatite (Crista Iliaca). *Bone*, 16(4 SUPPL.).

- Hernandez, C. J., Beaupré, G. S., Keller, T. S., and Carter, D. R. (2001). The influence of bone volume fraction and ash fraction on bone strength and modulus. *Bone*, 29(1):74–78.
- Hewakapuge, S., van Oorschot, R. A. H., Lewandowski, P., and Baidur-Hudson, S. (2008). Investigation of telomere lengths measurement by quantitative real-time PCR to predict age. *Legal Medicine*, 10(5):236–242.
- Hillson, S. and Bond, S. (1997). Relationship of enamel hypoplasia to the pattern of tooth crown growth: A discussion. *American Journal of Physical Anthropology*, 104(1):89–103.
- Hoffler, C. E., Moore, K. E., Kozloff, K., Zysset, P. K., Brown, M. B., and Goldstein, S. A. (2000). Heterogeneity of bone lamellar-level elastic moduli. *Bone*, 26(6):603–609.
- Huang, Y., Yan, J., Hou, J., Fu, X., Li, L., and Hou, Y. (2015). Developing a DNA methylation assay for human age prediction in blood and bloodstain. *Forensic Science International: Genetics*, 17:129–136.
- Hunt, H. B. and Donnelly, E. (2016). Bone Quality Assessment Techniques: Geometric, Compositional, and Mechanical Characterization from Macroscale to Nanoscale. *Clinical Reviews in Bone and Mineral Metabolism*, 14(3):133–149.
- Hurme, V. O. (1948). Standards of Variation in the Eruption of the First Six Permanent Teeth Author. *Child Development*, 19(4):213–231.
- Ilvesaro, J. M., Lakkakorpi, P. Y., and Väänänen, K. (1998). Inhibition of Bone Resorption in Vitro by a Peptide Containing the Cadherin Cell Adhesion Recognition Sequence HAV Is Due to Prevention of Sealing Zone Formation. *Experimental Cell Research*, 242(1):75–83.
- Itzstein, C., Coxon, F. P., and Rogers, M. J. (2011). The regulation of osteoclast function and bone resorption by small GTPases. *Small GTPases*, 2(3):1–14.

- Işcan, M. Y., Loth, S. R., and Wright, R. K. (1984). Metamorphosis at the sternal rib end: A new method to estimate age at death in white males. *American Journal of Physical Anthropology*, 65(2):147–156.
- Jankauskas, R., Barakauskas, S., and Bojarun, R. (2001). Incremental lines of dental cementum in biological age estimation. *HOMO- Journal of Comparative Human Biology*, 52(1):59–71.
- Jee, W. S., Hua Zhu, K., and Xiao Jian, L. (1991). Long-term anabolic effects of prostaglandin-E2 on tibial diaphyseal bone in male rats. *Bone and Mineral*, 15(1):33–55.
- Jenkins, R. and Snider, R. (1997). *Introduction to X-ray powder diffractometry*, volume 138. John Wiley & Sons Ltd., New Your, DC.
- Jimson, S., Balachander, N., Masthan, K. M. K., and Elumalai, R. (2014). A Comparative Study in Bone Decalcification Using Different Decalcifying Agents. *International Journal of Science and Research*, 3(8):2012–2015.
- Kader, F. and Ghai, M. (2015). DNA methylation and application in forensic sciences. *Forensic Science International*, 249:255–265.
- Kagerer, P. and Grupe, G. (2001). Age-at-death diagnosis and determination of life-history parameters by incremental lines in human dental cementum as an identification aid. *Forensic Science International*, 118(1):75–82.
- Kaku, N., Tsumura, H., Kataoka, M., Taira, H., and Torisu, T. (2002). Influence of aeration, storage, and rinsing conditions on residual ethylene oxide in freeze-dried bone allograft. *Journal of Orthopaedic Science*, 7(2):238–242.
- Karampas, I. A., Orkoula, M. G., and Kontoyannis, C. G. (2013). A quantitative bioapatite/collagen calibration method using Raman spectroscopy of bone. *Journal of Biophotonics*, 6(8):573–586.

- Karkhanis, S., Mack, P., and Franklin, D. (2015). Dental age estimation standards for a Western Australian population. *Forensic Science International*, 257:509.e1–509.e9.
- Karlsson, A. O., Svensson, A., Marklund, A., and Holmlund, G. (2008). Estimating human age in forensic samples by analysis of telomere repeats. *Forensic Science International: Genetics Supplement Series*, 1(1):569–571.
- Kerch, G. (2018). Distribution of tightly and loosely bound water in biological macromolecules and age-related diseases. *International Journal of Biological Macromolecules*, 118:1310–1318.
- Kerley, E. R. (1965). The microscopic determination of age in human bone. *American journal of physical anthropology*, 23(2):149–163.
- Kerley, E. R. and Ubelaker, D. H. (1978). Revisions in the microscopic method of estimating age at death in human cortical bone. *American journal of physical anthropology*, 49(4):545–546.
- Kontopoulos, I., Presslee, S., Penkman, K., and Collins, M. J. (2018). Preparation of bone powder for FTIR-ATR analysis: The particle size effect. *Vibrational Spectroscopy*, 99:167–177.
- Kopp, J., Bonnet, M., and Renou, J. P. (1989). Effect of Collagen Crosslinking on Collagen-Water Interactions (A DSC Investigation). *Matrix*, 9(6):443–450.
- Kranioti, E. F., Bastir, M., Sánchez-Meseguer, A., and Rosas, A. (2009). A geometric-morphometric study of the cretan humerus for sex identification. *Forensic Science International*, 189(1-3):2–9.
- Kranioti, E. F., Bonicelli, A., and García-donas, J. G. (2019). Bone-mineral density: clinical significance, methods of quantification and forensic applications. *Research and Reports in Forensic Medical Science*, 9:9–21.

- Kuha, J. (2004). AIC and BIC: Comparisons of assumptions and performance. *Sociological Methods and Research*, 33(2):188–229.
- Kular, J., Tickner, J., Chim, S. M., and Xu, J. (2012). An overview of the regulation of bone remodelling at the cellular level. *Clinical Biochemistry*, 45(12):863–873.
- Kvaal, S. I., Kolltveit, K. M., Thomsen, I. O., and Solheim, T. (1995). Age estimation of adults from dental radiographs. *Forensic Science International*, 74(3):175–185.
- Lamendin, H., Baccino, E., Humbert, J. F., Tavernier, J. C., Nossintchouk, R. M., and Zerilli, A. (1992). A Simple Technique for Age Estimation in Adult Corpses: The Two Criteria Dental Method. *Journal of Forensic Sciences*, 37(5):13327J.
- Landis, W. J. (1995). The strength of a calcified tissue depends in part on the molecular structure and organization of its constituent mineral crystals in their organic matrix. *Bone*, 16(5):533–544.
- Landis, W. J., Hodgens, K. J., Song, M. J., Arena, J., Kiyonaga, S., Marko, M., Owen, C., and McEwen, B. F. (1996). Mineralization of collagen may occur on fibril surfaces: Evidence from conventional and high-voltage electron microscopy and three-dimensional imaging. *Journal of Structural Biology*, 117(1):24–35.
- Lau, M. L., Lau, K. T., Ku, H., Cardona, F., and Lee, J. H. (2013). Analysis of heat-treated bovine cortical bone by thermal gravimetric and nanoindentation. *Composites Part B: Engineering*, 55:447–452.
- Lebon, M., Reiche, I., Gallet, X., Bellot-Gurlet, L., and Zazzo, A. (2016). Rapid quantification of bone collagen content by ATR-FTIR spectroscopy. *Radiocarbon*, 58(1):131–145.
- Lefèvre, T., Chariot, P., and Chauvin, P. (2016). Multivariate methods for the analysis of complex and big data in forensic sciences. Application to age estimation in living persons. *Forensic Science International*, 266:581.e1–581.e9.

- LeGeros, R. Z. (1981). Apatites in biological systems. *Progress In Crystal Growth And Characterization*, 4:1–45.
- LeGeros, R. Z., LeGeros, J. P., and Trautz, O. R. (1970). Conversion of Monetite, CaHPO₄, to Apatites: Effect of Carbonate on the Crystallinity and the Morphology of the Apatite Crystallites. *Advances in X-Ray Analysis*, 14:57–66.
- LeGeros, R. Z., Trautz, O. R., Klein, E., and LeGeros, J. P. (1969). Two types of carbonate substitution in the apatite structure. *Experientia*, 25(1):5–7.
- Levangie, P. K. and Norkin, C. C. (2005). *Joint structure and function: A comprehensive analysis*. F.A. Davis Co., Philadelphia, PA, 6th edition.
- Lewis, G. and Nyman, J. S. (2008). The use of nanoindentation for characterizing the properties of mineralized hard tissues: State-of-the art review. *Journal of Biomedical Materials Research - Part B Applied Biomaterials*, 87(1):286–301.
- Lewis, M. (2007). *The Bioarchaeology of Children*. Cambridge University Press., Cambridge, UK, 2nd edition.
- Liu, Q., Huang, S., Matinlinna, J. P., Chen, Z., and Pan, H. (2013). Insight into biological apatite: Physiochemical properties and preparation approaches. *BioMed Research International*, 2013.
- Londoño-Restrepo, S. M., Jeronimo-Cruz, R., Millán-Malo, B. M., Rivera-Muñoz, E. M., and Rodriguez-García, M. E. (2019). Effect of the Nano Crystal Size on the X-ray Diffraction Patterns of Biogenic Hydroxyapatite from Human, Bovine, and Porcine Bones. *Scientific Reports*, 9(1):1–12.
- Lovejoy, C. O. (1985). Dental wear in the Libbean population: Its functional pattern and role in the determination of adult skeletal age and death. *American Journal of Physical Anthropology*, 68:47–56.

- Lovejoy, C. O., Meindul, R. S., Pryzback, T. R., and Mensforth, P. (1985). Chronological metamorphosis of the auricular surface of the ilium. A new method for the determination of adult skeletal age at death. *American Journal of Physical Anthropology*, 68:15–28.
- Lozano, L., Pena-Rico, M., Heredia, a., Ocotlan-Flores, J., Gomez-Cortes, a., Velazquez, R., Belio, I., and Bucio, L. (2003). Thermal analysis study of human bone. *Journal of Materials Science*, 38:4777–4782.
- Lucy, D. (2005). *Introduction to Statistics Forensic Scientist*. John Wiley & Sons Ltd, Edinburgh, 2nd edition.
- Ma, S., Boughton, O., Karunaratne, A., Jin, A., Cobb, J., Hansen, U., and Abel, R. (2016). Synchrotron Imaging Assessment of Bone Quality. *Clinical Reviews in Bone and Mineral Metabolism*, 14(3):150–160.
- Ma, S., Goh, E. L., Jin, A., Bhattacharya, R., Boughton, O. R., Patel, B., Karunaratne, A., Vo, N. T., Atwood, R., Cobb, J. P., Hansen, U., and Abel, R. L. (2017). Long-term effects of bisphosphonate therapy: Perforations, microcracks and mechanical properties. *Scientific Reports*, 7(January):1–10.
- Maat, G. J., Maes, A., Aarents, M. J., and Nagelkerke, N. J. (2006). Histological age prediction from the femur in a contemporary Dutch sample: The decrease of nonremodeled bone in the anterior cortex. *Journal of Forensic Sciences*, 51(2):230–237.
- Madupalli, H., Pavan, B., and Tecklenburg, M. M. (2017). Carbonate substitution in the mineral component of bone: Discriminating the structural changes, simultaneously imposed by carbonate in A and B sites of apatite. *Journal of Solid State Chemistry*, 255(July):27–35.
- Márquez-Grant, N. (2015). An overview of age estimation in forensic anthropology: Perspectives and practical considerations. *Annals of Human Biology*, 42(4):306–320.

- Martin, B. R. and Burr, D. B. (1989). *Structure, Function, and Adaptation of Compact Bone*. Raven Press, New York.
- Martin, R. B. (2000). Toward a unifying theory of bone remodeling. *Bone*, 26(1):1–6.
- Martin, R. B. (2002). Is all cortical bone remodeling initiated by microdamage? *Bone*, 30(1):8–13.
- Martin, R. B., Burr, D. B., Sharkey, N. A., Fyhrie, D. P., Weaver, D. S., Martin, R. B., Burr, D. B., Sharkey, N. A., and Fyhrie, D. P. (2015). *Skeletal Tissue Mechanics*, volume 112. Springer, New York, 2nd edition.
- Martin-De Las Heras, S., Valenzuela, A., Bellini, R., Salas, C., Rubiño, M., and Garcia, J. A. (2003). Objective measurement of dental color for age estimation by spectroradiometry. *Forensic Science International*, 132(1):57–62.
- Martin-De Las Heras, S., Valenzuela, A., and Villanueva, E. (1999). Deoxyypyridinoline crosslinks in human dentin and estimation of age. *International Journal of Legal Medicine*, 112(4):222–226.
- Martrille, L., Irinopoulou, T., Bruneval, P., Baccino, E., and Fornes, P. (2009). Age at death estimation in adults by computer-assisted histomorphometry of decalcified femur cortex. *Journal of Forensic Sciences*, 54(6):1231–1237.
- Matzenauer, C., Reckert, A., and Ritz-Timme, S. (2013). Estimation of age at death based on aspartic acid racemization in elastic cartilage of the epiglottis. *International Journal of Legal Medicine*, 128(6):995–1000.
- McCalden, R. W., McGeough, J. a., and Court-Brown, C. M. (1997). Age-related changes in the compressive strength of cancellous bone. The relative importance of changes in density and trabecular architecture. *The Journal of Bone and Joint Surgery*, 79(3):421–427.

- McCudden, C. R. and Kraus, V. B. (2006). Biochemistry of amino acid racemization and clinical application to musculoskeletal disease. *Clinical Biochemistry*, 39(12):1112–1130.
- Mcfarlin, S. C., Terranova, C. J., Zihlman, A. L., Enlow, D. H., and Bromage, T. G. (2008). Regional variability in secondary remodeling within long bone cortices of catarrhine primates: The influence of bone growth history. *Journal of Anatomy*, 213(3):308–324.
- Meindl, R. and Lovejoy, C. (1985). Ectocranial suture closure: a revised method for the determination of skeletal age at death based on the lateralanterior sutures. *American Journal of Physical Anthropology*, 68(1):57–66.
- Meindl, R. S., Lovejoy, C. O., Mensforth, R. P., and Walker, R. A. (1985). A revised method of age determination using the os pubis, with a review and tests of accuracy of other current methods of pubic symphyseal aging. *American Journal of Physical Anthropology*, 68(1):29–45.
- Meinl, R. S. and Lovejoy, C. O. (1989). Age changes in the pelvis: implications for paleodemography. In Iscan, M. Y., editor, *Age markers in the human skeleton*. Charles C. Thomas, Springfield.
- Meissner, C. and Ritz-Timme, S. (2010). Molecular pathology and age estimation. *Forensic Science International*, 203(1-3):34–43.
- Miculescu, F., Antoniac, I., Ciocan, L. T., Brânzei, M., Ernuteanu, A., Batalu, D., and Berbecaru, A. (2011). Complex Analysis on Heat Treated Human Compact Bones. *U.P.B. Scientific Bulletin*, 73(4):203–212.
- Milenkovic, P., Djuric, M., Milovanovic, P., Djukic, K., Zivkovic, V., and Nikolic, S. (2014). The role of CT analyses of the sternal end of the clavicle and the first costal cartilage in age estimation. *International Journal of Legal Medicine*, 128(5):825–839.

- Miles, C. A., Avery, N. C., Rodin, V. V., and Bailey, A. J. (2005). The increase in denaturation temperature following cross-linking of collagen is caused by dehydration of the fibres. *Journal of Molecular Biology*, 346(2):551–556.
- Miles, C. A. and Bailey, A. J. (1999). Thermal denaturation of collagen revisited. *Proceedings of the Indian Academy of Sciences.*, 111(1):71–80.
- Milovanovic, P., vom Scheidt, A., Mletzko, K., Sarau, G., Püschel, K., Djuric, M., Amling, M., Christiansen, S., and Busse, B. (2018). Bone tissue aging affects mineralization of cement lines. *Bone*, 110:187–193.
- Mkukuma, L. D. (2005). Thermal stability and structure of cancellous bone mineral from the femoral head of patients with osteoarthritis or osteoporosis. *Annals of the Rheumatic Diseases*, 64(2):222–225.
- Mkukuma, L. D., Skakle, J. M., Gibson, I. R., Imrie, C. T., Aspden, R. M., and Hukins, D. W. (2004). Effect of the proportion of organic material in bone on thermal decomposition of bone mineral: An investigation of a variety of bones from different species using thermogravimetric analysis coupled to mass spectrometry, high-temperature X-ray diffraction,. *Calcified Tissue International*, 75(4):321–328.
- Moraitis, K., Zorba, E., Eliopoulos, C., and Fox, S. C. (2014). A Test of the Revised Auricular Surface Aging Method on a Modern European Population. *Journal of Forensic Sciences*, 59(1):188–194.
- Moreno, J. and Forriol, F. (2002). Effects of preservation on the mechanical strength and chemical composition of cortical bone: An experimental study in sheep femora. *Biomaterials*, 23(12):2615–2619.
- Mori, S. and Burr, D. B. (1993). Increased Intracortical remodeling Following Fatigue Damage. *Bone*, (14):103–109.
- Morris, M. D. and Mandair, G. S. (2011). Raman assessment of bone quality. *Clinical Orthopaedics and Related Research*, 469(8):2160–2169.

- Mote, V., Purushotham, Y., and Dole, B. (2012). Williamson-Hall analysis in estimation of lattice strain in nanometer-sized ZnO particles. *Journal of Theoretical and Applied Physics*, 6(1):2–9.
- Moze, K. and Roberts, G. (2012). Dental age assessment (DAA) of Afro-Trinidadian children and adolescents. Development of a Reference Dataset (RDS) and comparison with Caucasians resident in London, UK. *Journal of Forensic and Legal Medicine*, 19(5):272–279.
- Mulhern, D. M. and Jones, E. B. (2005). Test of revised method of age estimation from the auricular surface of the ilium. *American Journal of Physical Anthropology*, 126(1):61–65.
- Nassif, N., Gobeaux, F., Seto, J., Belamie, E., Davidson, P., Panine, P., Mosser, G., Fratzl, P., and Giraud Guille, M. M. (2010). Self-assembled collagen-apatite matrix with bone-like hierarchy. *Chemistry of Materials*, 22(11):3307–3309.
- Nazarian, A., Hermannsson, B. J., Muller, J., Zurakowski, D., and Snyder, B. D. (2009). Effects of tissue preservation on murine bone mechanical properties. *Journal of Biomechanics*, 42(1):82–86.
- Nevin, C. and Carroll, M. (2015). Sperm DNA Methylation, Infertility and Transgenerational Epigenetics. *Human Genetics & Clinical Embryology*, 1(4):1–9.
- Nielsen-Marsh, C. M., Hedges, R. E., Mann, T., and Collins, M. J. (2000). A preliminary investigation of the application of differential scanning calorimetry to the study of collagen degradation in archaeological bone. *Thermochimica Acta*, 365(1-2):129–139.
- Nikita, E. (2013). Quantitative assessment of the sternal rib end morphology and implications for its application in aging human remains. *Journal of Forensic Sciences*, 58(2):324–329.
- Nudelman, F., Lausch, A. J., Sommerdijk, N. A. J. M., and Sone, E. D. (2013). In vitro models of collagen biomineralization. *Journal of Structural Biology*, 183(2):258–269.

- Nudelman, F., Pieterse, K., George, A., Bomans, P. H., Friedrich, H., Brylka, L. J., Hilbers, P. A., De With, G., and Sommerdijk, N. A. (2010). The role of collagen in bone apatite formation in the presence of hydroxyapatite nucleation inhibitors. *Nature Materials*, 9(12):1004–1009.
- Ohtani, S. (1995a). Estimation of age from dentin by utilizing the racemization of aspartic acid: influence of pH. *Forensic Science International*, 75:181–187.
- Ohtani, S. (1995b). Estimation of Age from the Teeth of Unidentified Corpses Using the Amino Acid Racemisation Method with Reference to Actual Cases. *The American Journal of Forensic Medicine and Pathology*, 16(3):238–242.
- Ohtani, S. (1995c). Studies on Age Estimation Using Racemization of Aspartic Acid in Cementum. *Journal of Forensic Sciences*, 40(5):15388J.
- Ohtani, S., Ito, R., and Yamamoto, T. (2003). Differences in the D/L aspartic acid ratios in dentin among different types of teeth from the same individual and estimated age. *International Journal of Legal Medicine*, 117(3):149–152.
- Oliver, W. C. and Pharr, G. M. (1992). An improved technique for determining hardness and elastic modulus using load and displacement sensing indentation experiments. *Journal of Materials Research*, 7(1):1564–1583.
- Olszta, M. J., Cheng, X., Jee, S. S., Kumar, R., Kim, Y. Y., Kaufman, M. J., Douglas, E. P., and Gower, L. B. (2007). Bone structure and formation: A new perspective. *Materials Science and Engineering R: Reports*, 58(3-5):77–116.
- Orías, A. A. E., Deuerling, J. M., Landrigan, M. D., Renaud, J. E., and Roeder, R. K. (2009). Anatomic variation in the elastic anisotropy of cortical bone tissue in the human femur. *Journal of Mechanical Behaviour of Biomedical Material*, 2(3):255–263.
- Ottani, V., Martini, D., Franchi, M., Ruggeri, A., and Raspanti, M. (2002). Hierarchical structures in fibrillar collagens. *Micron*, 33(7-8):587–596.

- Panchbhai, A. S. (2011). Dental radiographic indicators, a key to age estimation. *Dentomaxillofacial Radiology*, 40(4):199–212.
- Parfitt, A. M. (1979). Quantum Concept of Bone Remodeling and Turnover : Implications for the Pathogenesis of Osteoporosis. *Calcif Tissue Int*, 28(1):1–5.
- Paschalis, E. P., Gamsjaeger, S., and Klaushofer, K. (2017). Vibrational spectroscopic techniques to assess bone quality. *Osteoporosis International*, 28(8):2275–2291.
- Paschalis, E. P., Gamsjaeger, S., Tatakis, D. N., Hassler, N., Robins, S. P., and Klaushofer, K. (2014). Fourier transform infrared spectroscopic characterization of mineralizing type i collagen enzymatic trivalent cross-links. *Calcified Tissue International*, 96(1):18–29.
- Paschalis, E. P., Mendelsohn, R., and Boskey, A. L. (2011). Infrared assessment of bone quality: A review. *Clinical Orthopaedics and Related Research*, 469(8):2170–2178.
- Paschalis, E. P., Recker, R., Dicarlo, E., Doty, S. B., Atti, E., and Boskey, A. (2003). Distribution of Collagen Cross-Links in Normal Human Trabecular Bone. *Journal of Bone and Mineral Research*, 18(11):1942–1946.
- Paschalis, E. P., Verdellis, K., Doty, S. B., Boskey, A. L., Mendelsohn, R., and Yamauchi, M. (2001). Spectroscopic characterization of collagen cross-links in bone. *Journal of Bone and Mineral Research*, 16(10):1821–1828.
- Pasteris, J. D., Yoder, C. H., and Wopenka, B. (2014). Minerals in the human body: Molecular water in nominally unhydrated carbonated hydroxylapatite: The key to a better understanding of bone mineral. *American Mineralogist*, 99(1):16–27.
- Pazzaglia, U. E., Congiu, T., Marchese, M., Spagnuolo, F., and Quacci, D. (2012). Morphometry and Patterns of Lamellar Bone in Human Haversian Systems. *Anatomical Record*, 295(9):1421–1429.

- Pazzaglia, U. E., Congiu, T., Pienazza, A., Zakaria, M., Gnechi, M., and Dell'Orbo, C. (2013). Morphometric analysis of osteonal architecture in bones from healthy young human male subjects using scanning electron microscopy. *Journal of Anatomy*, 223(3):242–254.
- Pelker, R. R., Friedlaender, G. E., Markham, T. C., Panjabi, M. M., and Moen, C. J. (1984). Effects of freezing and freeze-drying on the biomechanical properties of rat bone. *Journal of Orthopaedic Research*, 1(4):405–11.
- Penel, G., Leroy, G., Rey, C., and Bres, E. (1998). MicroRaman spectral study of the PO₄ and CO₃ vibrational modes in synthetic and biological apatites. *Calcified Tissue International*, 63(6):475–481.
- Pfau, R. O. and Sciulli, P. W. (1994). A Method for Establishing the Age of Subadults. *Journal of Forensic Sciences*, 39(1):13582J.
- Pfeiffer, H., Mörnstad, H., and Teivens, A. (1995a). Estimation of chronologic age using the aspartic acid racemization method. I. On human rib cartilage. *International Journal of Legal Medicine*, 108(1):24–26.
- Pfeiffer, H., Mörnstad, H., and Teivens, A. (1995b). Estimation of chronologic age using the aspartic acid racemization method. II. On human cortical bone. *International Journal of Fracture*, 108(1):24–26.
- Picard, R. R. and Cook, R. D. (1984). Cross-Validation of Regression Models. *Journal of the American Statistical Association*, 79(387):575– 583.
- Pidaparti, R. M. and Burr, D. B. (1992). Collagen fiber orientation and geometry effects on the mechanical properties of secondary osteons. *Journal of Biomechanics*, 25(8):869–880.
- Piga, G., Gonçalves, D., Thompson, T. J. U., Brunetti, A., Malgosa, A., and Enzo, S. (2016). Understanding the Crystallinity Indices Behavior of Burned Bones and Teeth

- by ATR-IR and XRD in the Presence of Bioapatite Mixed with Other Phosphate and Carbonate Phases. *International Journal of Spectroscopy*, 2016:1–9.
- Pilin, A., Pudil, F., and Bencko, V. (2007). Changes in colour of different human tissues as a marker of age. *International Journal of Legal Medicine*, 121(2):158–162.
- Poole, K. E. S., van Bezooijen, R. L., Loveridge, N., Hamersma, H., Papapoulos, A. E., Lowik, C. W., and Reeve, J. (2005). Sclerostin is a delayed secreted product of osteocytes that inhibits bone formation. *The FASEB Journal*, 18.
- Posner, A. S., Harper, R. A., Muller, S. A., and Menczel, J. (1965). Age Changes in the Crystal Chemistry of Bone Apatite. *Annals of the New York Academy of Sciences*, 131(2):737–742.
- Poulsen, K. and Simonsen, J. (2007). Computed tomography as routine in connection with medico-legal autopsies. *Forensic Science International*, 171(2-3):190–197.
- Prideaux, M., Findlay, D. M., and Atkins, G. J. (2016). Osteocytes: The master cells in bone remodelling. *Current Opinion in Pharmacology*, 28:24–30.
- Prince, D. A. and Ubelaker, D. H. (2002). Application of Lamendin’s Adult Dental Aging Technique to a Diverse Skeletal Sample. *Journal of Forensic Sciences*, 47(1):15209J.
- Qin, Y. X., Lin, W., Mitra, E., Xia, Y., Cheng, J., Judex, S., Rubin, C., and Müller, R. (2013). Prediction of trabecular bone qualitative properties using scanning quantitative ultrasound. *Acta Astronautica*, 92(1):79–88.
- Reilly, G. C. and Currey, J. D. (1999). The development of microcracking and failure in bone depends on the loading mode to which it is adapted. *The Journal of experimental biology*, 202(5):543–552.
- Renders, G. A., Mulder, L., van Ruijven, L. J., Langenbach, G. E., and van Eijden, T. M. (2011). Mineral heterogeneity affects predictions of intratrabecular stress and strain. *Journal of Biomechanics*, 44(3):402–407.

- Rey, C., Collins, B., Goehl, T., Dickson, I. R., and Glimcher, M. J. (1989). The carbonate environment in bone mineral: A resolution-enhanced fourier transform infrared spectroscopy study. *Calcified Tissue International*, 45(3):157–164.
- Rey, C., Combes, C., Drouet, C., and Glimcher, M. J. (2009). Bone mineral: Update on chemical composition and structure. *Osteoporosis International*, 20(6):1013–1021.
- Rey, C., Combes, C., Drouet, C., Sfihi, H., and Barroug, A. (2007). Physico-chemical properties of nanocrystalline apatites: Implications for biominerals and biomaterials. *Materials Science and Engineering C*, 27(2):198–205.
- Rey, C., Renugopalakrishnan, V., Collins, B., and Glimcher, M. J. (1991). Fourier Transform Infrared Spectroscopic Study of the Carbonate Ions in Bone Mineral During Aging. *Calcified Tissue International*, 49:251–258.
- Rho, J. Y., Hobatho, M. C., and Ashman, R. B. (1995). Relations of mechanical properties to density and CT numbers in human bone. *Medical Engineering and Physics*, 17(5):347–355.
- Rho, J. Y., Kuhn-Spearing, L., and Zioupos, P. (1998). Mechanical properties and the hierarchical structure of bone. *Medical Engineering and Physics*, 20(2):92–102.
- Rho, J. Y., Zioupos, P., Currey, J. D., and Pharr, G. M. (1999). Variations in the individual thick lamellar properties within osteons by nanoindentation. *Bone*, 25(3):295–300.
- Rho, J. Y., Zioupos, P., Currey, J. D., and Pharr, G. M. (2002). Microstructural elasticity and regional heterogeneity in human femoral bone of various ages examined by nanoindentation. *Journal of Biomechanics*, 35(2):189–198.
- Richardson, B. (2003). Impact of aging on DNA methylation. *Ageing Research Reviews*, 2(3):245–261.
- Ries, W. and Pöthig, D. (1984). Chronological and biological age. *Experimental Gerontology*, 19(3):211–216.

- Ritz, S., Schütz, H.-W., and Peper, C. (1993). Aspartic Acid Racemization in Intervertebral Discs As an Aid to Postmortem Estimation of Age at Death. *Journal of Forensic Sciences*, 105(5):289–293.
- Ritz, S., Turzynski, A., and Schütz, H. W. (1994). Estimation of age at death based on aspartic acid racemization in noncollagenous bone proteins. *Forensic Science International*, 69(2):149–159.
- Ritz, S., Turzynski, A., Schütz, H. W., Hollmann, A., and Rochholz, G. (1996). Identification of osteocalcin as a permanent aging constituent of the bone matrix: Basis for an accurate age at death determination. *Forensic Science International*, 77(1-2):13–26.
- Ritz-Timme, S., Cattaneo, C., Collins, M., Waite, E., Schütz, H., Kaatsch, H., and Borman, H. (2000). Age estimation : The state of the art in relation to the specific demands of forensic practise. *International Journal of Legal Medicine*, 113:129–136.
- Robling, A. G., Fuchs, R. K., and Burr, D. B. (2013). Mechanical Adaptation. *Basic and Applied Bone Biology*, pages 175–204.
- Rogers, K., Beckett, S., Kuhn, S., Chamberlain, A., and Clement, J. (2010). Contrasting the crystallinity indicators of heated and diagenetically altered bone mineral. *Palaeogeography, Palaeoclimatology, Palaeoecology*, 296(1-2):125–129.
- Rogers, K. D. and Daniels, P. (2002). An X-ray diffraction study of the effects of heat treatment on bone mineral microstructure. *Biomaterials*, 23(12):2577–2585.
- Rösing, F. W., Graw, M., Marré, B., Ritz-Timme, S., Rothschild, M. A., Röttscher, K., Schmeling, A., Schröder, I., and Geserick, G. (2007). Recommendations for the forensic diagnosis of sex and age from skeletons. *HOMO- Journal of Comparative Human Biology*, 58(1):75–89.
- Saito, M. and Marumo, K. (2010). Collagen cross-links as a determinant of bone quality: A possible explanation for bone fragility in aging, osteoporosis, and diabetes mellitus. *Osteoporosis International*, 21(2):195–214.

- Sakuma, A., Ohtani, S., Saitoh, H., and Iwase, H. (2012). Comparative analysis of aspartic acid racemization methods using whole-tooth and dentin samples. *Forensic Science International*, 223(1-3):198–201.
- Salo, J., Lehenkari, P., Mulari, M., Metsikkö, K., and Väänänen, H. K. (1997). Removal of osteoclast bone resorption products by transcytosis. *Science*, 276(5310):270–273.
- Salo, J. J., Reddy, S. V., Roodman, G. D., Hentunen, T. A., Lehenkari, P. P., Kaija, H., Vihko, P., and Va, H. K. (1999). Intracellular Fragmentation of Bone Resorption Products by Generated by Osteoclastic Phosphatase. *The Journal of Biological Chemistry*, 274(33):22907–22911.
- Sawa, T. (2010). Correlation between Nanoindentation Test Result and Vickers Hardness. In *IMEKO TC5 and TC22: Metrology in Modern Context November*, pages 171–174.
- Schaffler, M. B. and Burr, D. B. (1988). Stiffness of compact bone: effects of porosity and density. *Journal of Biomechanics*, 21(1):13–16.
- Schaffler, M. B., Choi, K., and Milgrom, C. (1995). Aging and matrix microdamage accumulation in human compact bone. *Bone*, 17(6):521–525.
- Scheuer, L. (2000). *Developmental Juvenile Osteology*. Academic Press, London.
- Scheuer, L. (2002). Application of osteology to forensic medicine. *Clinical Anatomy*, 15(4):297–312.
- Schmeling, A., Geserick, G., Reisinger, W., and Olze, A. (2007). Age estimation. *Forensic Science International*, 165(2-3):178–181.
- Schmeling, A., Olze, A., Reisinger, W., and Geserick, G. (2004). Forensic age diagnostics of living people undergoing criminal proceedings. *Forensic Science International*, 144(2-3):243–245.

- Schmitt, A., Saliba-Serre, B., Tremblay, M., and Martrille, L. (2010). An evaluation of statistical methods for the determination of age of death using dental root translucency and periodontosis. *Journal of Forensic Sciences*, 55(3):590–596.
- Schour, I. and Massler, M. (1941). The development of human dentition. *Journal of the American Dental Association*, 28:1153–1160.
- Schulmerich, M. V., Cole, J. H., Dooley, K. A., Morris, M. D., Kreider, J. M., Goldstein, S. A., Srinivasan, S., and Pogue, B. W. (2008). Noninvasive Raman tomographic imaging of canine bone tissue. *Journal of Biomedical Optics*, 13(2):020506.
- Schulmerich, M. V., Dooley, K. A., Vanasse, T. M., Goldstein, S. A., and Morris, M. D. (2007). Subsurface and transcutaneous Raman spectroscopy and mapping using concentric illumination rings and collection with a circular fiber-optic array. *Applied Spectroscopy*, 61(7):671–678.
- Schulmerich, M. V., Finney, W. F., Fredricks, R. A., and Morris, M. D. (2006). Subsurface Raman spectroscopy and mapping using a globally illuminated non-confocal fiber-optic array probe in the presence of Raman photon migration. *Applied Spectroscopy*, 60(2):109–114.
- Scott, E. C. (1979). Dental wear scoring technique. *American Journal of Physical Anthropology*, 51(2):213–217.
- Shapiro, A. S. S. and Wilk, M. B. (1965). An Analysis of Variance Test for Normality. *Biometrika*, 52(3):591–611.
- Shapses, S. A., Cifuentes, M., Spevak, L., Chowdhury, H., Brittingham, J., Boskey, A. L., and Denhardt, D. T. (2003). Osteopontin facilitates bone resorption, decreasing bone mineral crystallinity and content during calcium deficiency. *Calcified Tissue International*, 73(1):86–92.
- Sheskin, D. (2003). *Handbook of Parametric and Nonparametric Statistical Procedures*. CRC Press Company LLC, 3rd editio edition.

- Silver, F. H. and Landis, W. J. (2011). Deposition of apatite in mineralizing vertebrate extracellular matrices: A model of possible nucleation sites on type I collagen. *Connective Tissue Research*, 52(3):242–254.
- Simmons, D. J. (1985). Options for bone aging with the microscope. *American Journal of Physical Anthropology*, 28(6 S):249–263.
- Simmons, E. D., Pritzker, K. P., and Grynblas, M. D. (1991). Age-related changes in the human femoral cortex. *Journal of Orthopaedic Research*, 9(2):155–67.
- Sirin, N., Matzenauer, C., Reckert, A., and Ritz-Timme, S. (2018a). Age estimation based on aspartic acid racemization in dentine: What about caries-affected teeth? *International Journal of Legal Medicine*, 132(2):623–628.
- Sirin, N., Reckert, A., and Ritz-Timme, S. (2018b). Reply to the letter by Kumar and Kanchan “Age estimation based on aspartic acid racemization in cariesaffected teeth: need for further explorations”. *International Journal of Legal Medicine*, 132(5):1467–1468.
- Smith, B. C. (2002). Fundamentals of Molecular Absorption Spectroscopy. In *Quantitative Spectroscopy: Theory and Practice*, pages 1–41.
- Smith, B. C. (2011). *Fundamentals of fourier transform infrared spectroscopy*. CRC Press.
- Smith, B. H. (1984). Patterns of Molar Wear in Hunter– Gatherers and Agriculturalists. *American Journal of Physical Anthropology*, 63(1):39–56.
- Smith, R. L. and Sandly, G. E. (1922). An Accurate Method of Determining the Hardness of Metals, with Particular Reference to Those of a High Degree of Hardness. *Proceedings of the Institution of Mechanical Engineers*, 102(1):623–641.
- Srinivasan, B., Kopperdahl, D. L., Amin, S., Atkinson, E. J., Camp, J., Robb, R. A., Riggs, B. L., Orwoll, E. S., Melton, L. J., Keaveny, T. M., and Khosla, S. (2012). Relationship

- of femoral neck areal bone mineral density to volumetric bone mineral density, bone size, and femoral strength in men and women. *Osteoporosis International*, 23(1):155–162.
- Standring, S. (2008). *Gray's Anatomy. The Anatomical Basis of Clinical Practice*. Churchill Livingstone Elsevier, 40th edition.
- Stock, S. R. (2015). The Mineral–Collagen Interface in Bone. *Calcified Tissue International*, 97(3):262–280.
- Stout, S. D. and Gehlert, S. J. (1980). The relative accuracy and reliability of histological aging methods. *Forensic Science International*, 15(3):181–190.
- Stout, S. D. and Paine, R. R. (1992). Brief Communication: Histological Age Estimation Using Rib and Clavicle. *American Journal of Physical Anthropology*, 115:111–115.
- Stout, S. D., Porro, M. A., and Perotti, B. (1996). Brief Communication: A test and correction of the clavicle method for histological age determination of skeletal remains. *American Journal of Physical Anthropology*, 100:139–142.
- Su, F. Y., Pang, S., Ling, Y. T. T., Shyu, P., Novitskaya, E., Seo, K., Lambert, S., Zarate, K., Graeve, O. A., Jasiuk, I., and McKittrick, J. (2018). Deproteinization of Cortical Bone: Effects of Different Treatments. *Calcified Tissue International*, 103(5):554–566.
- Svenson, U. and Roos, G. (2009). Telomere length as a biological marker in malignancy. *Biochimica et Biophysica Acta - Molecular Basis of Disease*, 1792(4):317–323.
- Tai, K., Dao, M., Suresh, S., Palazoglu, A., and Ortiz, C. (2007). Nanoscale heterogeneity promotes energy dissipation in bone. *Nature Materials*, 6(6):454–462.
- Takasaki, T., Tsuji, A., Ikeda, N., and Ohishi, M. (2003). Age estimation in dental pulp DNA based on human telomere shortening. *International Journal of Legal Medicine*, 117(4):232–234.

- Ten Cate, A., Thompson, G., Dickinson, J., and Hunter, H. (1977). The estimation of age of skeletal remains from the colour of roots of teeth. *Dental Journal*, 43:83–86.
- Thompson, D. D. (1979). The Core Technique in the Determination of Age at Death in Skeletons. *Journal of forensic sciencess*, 24(4):902–915.
- Thompson, D. D. and Galvin, C. A. (1983). Estimation of age at death by tibial osteon remodeling in an autopsy series. *Forensic Science International*, 22(2-3):203–211.
- Thompson, T. J., Islam, M., and Bonniere, M. (2013). A new statistical approach for determining the crystallinity of heat-altered bone mineral from FTIR spectra. *Journal of Archaeological Science*, 40(1):416–422.
- Thompson, T. J. U., Islam, M., Piduru, K., and Marcel, A. (2011). An investigation into the internal and external variables acting on crystallinity index using Fourier Transform Infrared Spectroscopy on unaltered and burned bone. *Palaeogeography, Palaeoclimatology, Palaeoecology*, 299(1-2):168–174.
- Todd, T. W. (1920). Age changes in the pubic bone. I. The male white pubis. *American Journal of Physical Anthropology*, 3(3):285–334.
- Todd, T. W. (1921). Age changes in the pubic bone II. White females. *American Journal of Physical Anthropology*, 4(1):1 – 70.
- Torres, T., Ortiz, J. E., Fernández, E., Arroyo-Pardo, E., Grün, R., and Pérez-González, A. (2014). Aspartic acid racemization as a dating tool for dentine: A reality. *Quaternary Geochronology*, 22:43–56.
- Tsuji, A., Ishiko, A., Takasaki, T., and Ikeda, N. (2002). Estimating age of humans based on telomere shortening. *Forensic Science International*, 126(3):197–199.
- Turner, C. (1993). Age, Bone Material Properties, and Bone Strength. *Calcified Tissue International*, 53(Suppl. 1):S32–S33.

- Turner, C. H. (1999). Toward a mathematical description of bone biology: The principle of cellular accommodation. *Calcified Tissue International*, 65(6):466–471.
- Turner, C. H. (2002). Biomechanics of bone: Determinants of skeletal fragility and bone quality. *Osteoporosis International*, 13(2):97–104.
- Turner, C. H. and Burr, D. B. (1993). Basic biomechanical measurements of bone: A tutorial. *Bone*, 14(4):595–608.
- Turner-Walker, G. (2011). The mechanical properties of artificially aged bone: Probing the nature of the collagen-mineral bond. *Palaeogeography, Palaeoclimatology, Palaeoecology*, 310(1-2):17–22.
- Tătar, A.-s., Ponta, O., and Kelemen, B. (2014). Bone Diagenesis and Ftir Indices: a Correlation. *Studia Universitatis Babeş-Bolyai Biologia*, LIX(1):101–113.
- Ubelaker, D. (1989). *Human Skeletal Remains: Excavation, Analysis, Interpretation*. Taraxacum, Washington, DC, 3rd edition.
- Ubelaker, D. H. (1987). Estimating Age at Death from Immature Human Skeletons: An Overview. *Journal of Forensic Sciences*, 32(5):1117-6J.
- Unal, M. and Akkus, O. (2015). Raman spectral classification of mineral- and collagen-bound water's associations to elastic and post-yield mechanical properties of cortical bone. *Bone*, 81:315–326.
- Unal, M., Creecy, A., and Nyman, J. S. (2018). The Role of Matrix Composition in the Mechanical Behavior of Bone. *Current Osteoporosis Reports*, 16(3):205–215.
- Unal, M., Uppuganti, S., Timur, S., Mahadevan-Jansen, A., Akkus, O., and Nyman, J. S. (2019). Assessing matrix quality by Raman spectroscopy helps predict fracture toughness of human cortical bone. *Scientific Reports*, 9(1):7159.
- Väänänen, H. K., Zhao, H., Mulari, M., and Halleen, J. M. (2000). The cell biology of osteoclast function. *Journal of Cell Science*, 113:377–381.

- van Staa, T. P., Dennison, E. M., Leufkens, H. G. M., and Cooper, C. (2001). Epidemiology of Fractures in England and Wales. *ZBone*, 29(6):517–522.
- Viguet-Carrin, S., Gineyts, E., Bertholon, C., and Delmas, P. D. (2009). Simple and sensitive method for quantification of fluorescent enzymatic mature and senescent crosslinks of collagen in bone hydrolysate using single-column high performance liquid chromatography. *Journal of Chromatography B: Analytical Technologies in the Biomedical and Life Sciences*, 877(1-2):1–7.
- Villa, C., Buckberry, J., Cattaneo, C., and Lynnerup, N. (2013). Technical note: Reliability of suchey-brooks and buckberry-chamberlain methods on 3D visualizations from CT and laser scans. *American Journal of Physical Anthropology*, 151(1):158–163.
- Waite, E. R., Collins, M. J., Ritz-Timme, S., Schutz, H.-W., Cattaneo, D. C., and Borrman, H. I. M. (1999). A review of the methodological aspects of aspartic acid racemization analysis for use in forensic science. *Forensic Science International*, 103(103):113–124.
- Walden, S. J., Evans, S. L., and Mulville, J. (2017). Changes in Vickers hardness during the decomposition of bone: Possibilities for forensic anthropology. *Journal of the Mechanical Behavior of Biomedical Materials*, 65(May 2016):672–678.
- Wallace, J. M. (2013). *Skeletal Hard Tissue Biomechanics*. Elsevier Inc.
- Wang, Q., Zhang, Y., Lin, H., Zha, S., Fang, R., Wei, X., Fan, S., and Wang, Z. (2017). Estimation of the late postmortem interval using FTIR spectroscopy and chemometrics in human skeletal remains. *Forensic Science International*, 281:113–120.
- Wang, X. (2013). Cortical Bone Mechanics and Composition: Effects of Age and Gender. In *Skeletal Aging and Osteoporosis*, volume 5, pages 105–131.
- Wang, X., Bank, R. A., Tekkopele, J. M., and Mauli Agrawal, C. (2001). The role of collagen in determining bone mechanical properties. *Journal of Orthopaedic Research*, 19(6):1021–1026.

- Wang, X., Hua, R., Ahsan, A., Ni, Q., Huang, Y., Gu, S., and Jiang, J. X. (2018). Age-Related Deterioration of Bone Toughness Is Related to Diminishing Amount of Matrix Glycosaminoglycans (GAGs). *JBMR Plus*, 2(3):164–173.
- Wang, X., Li, X., Bank, R. A., and Agrawal, C. M. (2002a). Effects of Collagen Unwinding and Cleavage on the Mechanical Integrity of the Collagen Network in Bone. *Calcified Tissue International*, 71:186–192.
- Wang, X. and Ni, Q. (2003). Determination of cortical bone porosity and pore size distribution using a low field pulsed NMR approach. *Journal of Orthopaedic Research*, 21(2):312–319.
- Wang, X. and Puram, S. (2004). The toughness of cortical bone and its relationship with age. *Annals of Biomedical Engineering*, 32(1):123–135.
- Wang, X., Shen, X., Li, X., and Mauli Agrawal, C. (2002b). Age-related changes in the collagen network and toughness of bone. *Bone*, 31(1):1–7.
- Wang, Y., Azaïs, T., Robin, M., Vallée, A., Catania, C., Legriel, P., Pehau-Arnaudet, G., Babonneau, F., Giraud-Guille, M. M., and Nassif, N. (2012). The predominant role of collagen in the nucleation, growth, structure and orientation of bone apatite. *Nature Materials*, 11(8):724–733.
- Weaver, C. M. and Gallant, K. M. H. (2014). *Nutrition*. Elsevier Inc.
- Wei, M., Bostrom, T., and Grøndahl, L. (2003). Synthesis and characterization of hydroxyapatite, fluoride-substituted hydroxyapatite and fluorapatite. *Journal of Materials Science: Materials in Medicine*, 14(4):311–320.
- Weiner, S. (2006). Transient precursor strategy in mineral formation of bone. *Bone*, 39(3):431–433.
- Weiner, S. and Traub, W. (1992). Bone structure: from angstroms to microns. *The FASEB Journal*, 6(3):879–885.

- Weiner, S., Traub, W., Wagner, H. D., and Wagner, D. H. (1999). Lamellar Bone: Structure – Function Relations Lamellar. *Journal of Structural Biology*, 126:241–255.
- Willett, T. L., Dapaah, D. Y., Uppuganti, S., Granke, M., and Nyman, J. S. (2019). Bone collagen network integrity and transverse fracture toughness of human cortical bone. *Bone*, 120(July 2018):187–193.
- Williamson, G. K. and Hall, W. H. (1953). X-Ray broadening from filed aluminium and tungsten. *Acta Metallurgica*, 1:22–31.
- Wilson, E. E., Awonusi, A., Morris, M. D., Kohn, D. H., Tecklenburg, M. M., and Beck, L. W. (2006). Three structural roles for water in bone observed by solid-state NMR. *Biophysical Journal*, 90(10):3722–3731.
- Wilson, E. E., Awonusi, A., Morris, M. D., Kohn, D. H., Tecklenburg, M. M. J., and Beck, L. W. (2005). Highly ordered interstitial water observed in bone by nuclear magnetic resonance. *Journal of Bone and Mineral Research*, 20(4):625–634.
- Yang, Y., Cui, Q., and Sahai, N. (2010). How does bone sialoprotein promote the nucleation of hydroxyapatite? A molecular dynamics study using model peptides of different conformations. *Langmuir*, 26(12):9848–9859.
- Yeni, Y. N. and Norman, T. L. (2000). Fracture toughness of human femoral neck: Effect of microstructure, composition, and age. *Bone*, 26(5):499–504.
- Yerramshetty, J. S. and Akkus, O. (2008). The associations between mineral crystallinity and the mechanical properties of human cortical bone. *Bone*, 42(3):476–482.
- Yerramshetty, J. S., Lind, C., and Akkus, O. (2006). The compositional and physico-chemical homogeneity of male femoral cortex increases after the sixth decade. *Bone*, 39(6):1236–1243.
- Yoder, C. H., Pasteris, J. D., Worcester, K. N., and Schermerhorn, D. V. (2012). Structural

- water in carbonated hydroxylapatite and fluorapatite: Confirmation by solid state ^2H NMR. *Calcified Tissue International*, 90(1):60–67.
- Zampieri, M., Ciccarone, F., Calabrese, R., Franceschi, C., Bürkle, A., and Caiafa, P. (2015). Reconfiguration of DNA methylation in aging. *Mechanisms of Ageing and Development*, 151:60–70.
- Zapico, S. and Ubelaker, D. H. (2013). Applications of physiological bases of ageing to forensic sciences. Estimation of age-at-death. *Ageing Research Reviews*, 12(2):605–617.
- Zimmermann, E. A., Schaible, E., Gludovatz, B., Schmidt, F. N., Riedel, C., Krause, M., Vettorazzi, E., Acevedo, C., Hahn, M., Püschel, K., Tang, S., Amling, M., Ritchie, R. O., and Busse, B. (2016). Intrinsic mechanical behavior of femoral cortical bone in young, osteoporotic and bisphosphonate-treated individuals in low- and high energy fracture conditions. *Scientific Reports*, 6(21072):1–12.
- Ziopoulos, P. (2001). Ageing human bone: factors affecting its biomechanical properties and the role of collagen. *Journal of Biomaterials Applications*, 15:187–229.
- Ziopoulos, P. (2005). In vivo fatigue microcracks in human bone: Material properties of the surrounding bone matrix. *European Journal of Morphology*, 42(1-2):31–41.
- Ziopoulos, P. and Currey, J. (1998). Changes in the Stiffness, Strength, and Toughness of Human Cortical Bone With Age. *Bone*, 22(1):57–66.
- Ziopoulos, P., Currey, J. D., and Casinos, A. (2000a). Exploring the Effect of Hypermineralization in Bone Tissue by Using an Extreme Biological Example. *Connective Tissue Research*, 41(3):220–258.
- Ziopoulos, P., Currey, J. D., and Casinos, A. (2000b). Exploring the effects of hypermineralisation in bone tissue by using an extreme biological example. *Connective Tissue Research*, 41(3):229–248.

- Ziopoulos, P., Gresle, M., and Winwood, K. (2008). Fatigue strength of human cortical bone: Age, physical, and material heterogeneity effects. *Journal of Biomedical Materials Research - Part A*, 86(3):627–636.
- Ziopoulos, P., Wang, X. T., and Currey, J. D. (1996). The accumulation of fatigue micro-damage in human cortical bone of two different ages in vitro. *Clinical Biomechanics*, 11(7):365–375.
- Ziopoulos, P., Williams, A., Christodoulou, G., and Giles, R. (2014). Determining 'age at death' for forensic purposes using human bone by a laboratory-based biomechanical analytical method. *Journal of the Mechanical Behavior of Biomedical Materials*, 33(1):109–123.
- Zubakov, D., Liu, F., Kokmeijer, I., Choi, Y., van Meurs, J. B., van IJcken, W. F., Uitterlinden, A. G., Hofman, A., Broer, L., van Duijn, C. M., Lewin, J., and Kayser, M. (2016). Human age estimation from blood using mRNA, DNA methylation, DNA rearrangement, and telomere length. *Forensic Science International: Genetics*, 24:33–43.
- Zubakov, D., Liu, F., Van Zelm, M. C., Vermeulen, J., Oostra, B. A., Van Duijn, C. M., Driessen, G. J., Van Dongen, J. J., Kayser, M., and Langerak, A. W. (2010). Estimating human age from T-cell DNA rearrangements. *Current Biology*, 20(22):R970–R971.

Appendices

APPENDIX A

ETHICAL APPROVAL

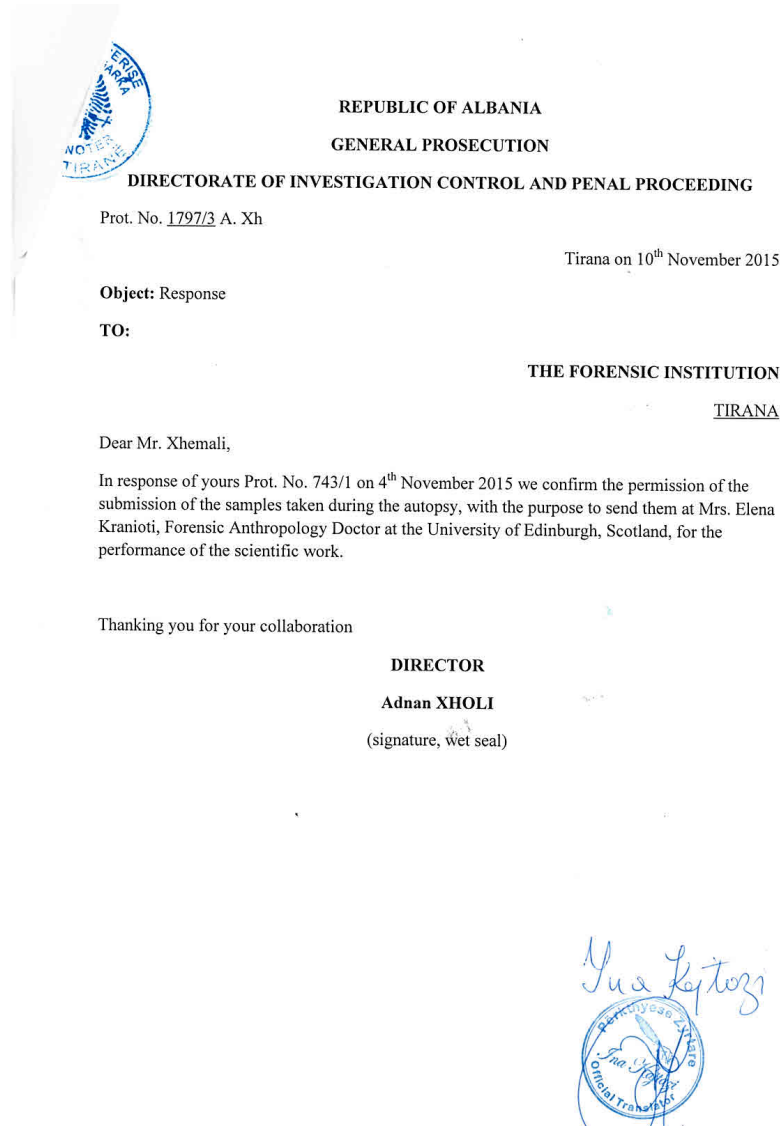


Figure A.1: *Ethical approval from the Directorate of Investigation Control and Penal Proceeding.*

Document Name	QF-TGU-A-TCIMAUD	VERSION 1.0	Review date	12-Feb-2019
---------------	------------------	-------------	-------------	-------------

NHS Lothian Tissue Governance

GENERAL AUDIT OF IMPORTED TISSUE COLLECTION

Principal Investigator:	Elena Kranioti MD, PhD Edinburgh Unit for Forensic Anthropology Director of MSc in Forensic Anthropology Archaeology, SHCA, University of Edinburgh Old Medical School, Teviot Place EH89AG, Edinburgh, UK Dr Peter Zioupos Cranfield Forensic Institute.
Nature of Tissue Resource / Collection:	Bone samples of routine and forensic autopsy cases (imported with permission from Greece and Albania)
Title of project:	Age Estimation based on Histological Examination of Ribs and Clavicles and the Investigation of the Effects of Alcohol on Bone Microstructure.
Tissue Governance reference number if relevant:	NA
Audit completed by:	Frances Rae
Date and venue:	09-Feb-2017 12.00am Dept of Archaeology, Teviot Place, Edinburgh University.

Non-conformances are categorised as:

Critical

Non conformances which constitute non compliance with NHS Lothian Tissue Governance policies, regulatory requirements, or accreditation standards. These must be corrected as high priority.

Major:

Non conformances which could potentially lead to a breach of any of the above. These must be corrected as priority.

Minor:

Non conformances which require some corrective action but cannot be classed as critical or major. These should be corrected but without the need for a high priority.

Author	: Frances Rae	Date	: 12-Feb-2015
Authority for Issue	: Craig Marshall	Date	: 12-Feb-2015
Quality Checked	: Craig Marshall	Date	: 12-Feb-2015

Figure A.2: *NHS Lothian Tissue Governance audit.*

Document Name	QF-TGU-A-TCIMAUD	VERSION 1.0	Review date	12-Feb-2019
---------------	------------------	-------------	-------------	-------------

CHECKLIST

		Findings
1) Type and approximate number of samples stored:	Small specimens of rib and clavicle from approximately 100 individuals with up to four samples from each donor. The specimens are frozen and stored at minus 20 degrees.	
2) Location of storage:	Currently in temporary storage at the University of Edinburgh, Archaeology Dept.	
3) Security of storage:	The samples are currently stored in laboratories which are locked when not in use. The freezers are also lockable for additional security. Once approval for use is confirmed, they will be moved to other suitable secure facilities within the University of Edinburgh and Cranfield Forensic Institute.	
4) Are samples de-identified in storage:	Yes, no donor identifiers are on the tubes. All tubes are marked with an anonymised code.	
5) System for anonymisation in place?	Yes. This is carried out by Dr Elena Kranioti at the time of receipt in her laboratory. The samples arrive with donor identifiers on them as the Institute of origin does not have the resources to de-identify them. All samples are used in a de-identified manner for the purposes of the research which is mainly student based.	
6) Secure database with sample inventory in place?	Yes. The database is held on Dr Kranioti's personal computer which is password protected and held in a lockable office.	

Author	: Frances Rae	Date	: 12-Feb-2015
Authority for Issue	: Craig Marshall	Date	: 12-Feb-2015
Quality Checked	: Craig Marshall	Date	: 12-Feb-2015

Document Name	QF-TGU-A-TCIMAUD	VERSION 1.0	Review date	12-Feb-2019
----------------------	------------------	-------------	--------------------	-------------

	There is a full sample inventory for each sample received with an audit trail from receipt, through to use and ultimate disposal. No samples have been disposed of yet, but when that time comes, they will be disposed of according to the local policies of the University of Edinburgh and/or Cranfield Forensic Institute.	
7) De-identified information only stored on database?	No. The donor names are held on the database. This is because it is the only means to track any further information required from forensic reports at the Institute of origin. This information is often not available at the time of receipt of the samples.	
8) Location of Database/Computer?	Dr Kranioti's office at the Dept of Archaeology.	
9) Country of origin of samples:	1 Crete, Greece 2 Albania	
10) Is consent in place?	1 Consent is in place for the Greek samples, either from the donor's next of kin, or in the case of tissue from forensic autopsies, from the Fiscal. The documents to substantiate this are held by the host Institution in Greece but are available if requested. 2 No consent is in place for the samples imported from Albania as there is no formal means to consent for the use of surplus tissue for research in this country. Letters of approval from the Public Prosecutor of the Ministry of Justice and the Head of the Forensic Institute are in place approving the use of the tissue samples by Dr Kranioti for her research in the University of Edinburgh and Cranfield Forensic Institute. These were seen in hard copy during the audit.	
11) Is there evidence of authority for use in this country?	Yes, letters of authorisation for the use of the samples by Dr Kranioti from both Albania (Protocol Number 1797/3 A. Xh.)	

Author	: Frances Rae	Date	: 12-Feb-2015
Authority for Issue	: Craig Marshall	Date	: 12-Feb-2015
Quality Checked	: Craig Marshall	Date	: 12-Feb-2015

Document Name	QF-TGU-A-TCIMAUD	VERSION 1.0	Review date	12-Feb-2019
---------------	------------------	-------------	-------------	-------------

	<p>and Crete were seen during the audit. The Ethics Committee at the University of Heraklion in Crete (Protocol Number 530) has also endorsed the use of the tissue samples for Dr Kranioti's research. A Permission Pass was also seen at the time of the audit. This was the equivalent of a Material Transfer Agreement which would be used in the UK.</p> <p>Courier documentation was also seen during the audit, permitting the samples to be transferred by TNT courier from Albania to Scotland.</p>	
12) Is ethical approval in place for the research studies to be carried out in Scotland?	<p>Yes, information on all studies proposing to use these samples, is sent to the School of History, Classics and Archaeology, University of Edinburgh ethics committee (Ethic assessment level 2), and no research is carried out until authorisation is given by this committee.</p>	
Auditor comments:	<p>Dr Kranioti has written to the Procurator Fiscal in Scotland and the Human Tissue Authority in the UK asking for their approval to use the imported samples in her research. Both have responded that this is not within their remit.</p> <p>Dr Kranioti has confirmed that the samples are all used in accordance with the guidelines given by Lothian Tissue Governance and this was checked at the time of audit.</p> <p>The function of the Tissue Governance team is mainly to oversee the governance of tissue samples from patients of NHS Lothian, but as we also have a responsibility to ensure the appropriate governance of the use of human tissue samples within the University of Edinburgh, it was agreed that this audit be carried out by the Tissue Governance Manager to ensure best practice is being followed, and that there is no breach of legislation.</p> <p>Having carried out this audit, we confirm that we are content that the tissue samples in question have been imported with appropriate authorisation from the countries of origin, and that they are now being used in accordance with our</p>	

Author	: Frances Rae	Date	: 12-Feb-2015
Authority for Issue	: Craig Marshall	Date	: 12-Feb-2015
Quality Checked	: Craig Marshall	Date	: 12-Feb-2015

Document Name	QF-TGU-A-TCIMAUD VERSION 1.0	Review date	12-Feb-2019
----------------------	-----------------------------------	--------------------	-------------

	<p>relevant local policies including having local ethical cover from a University Ethics Committee and maintaining good record keeping on how the samples are tracked, anonymised, stored, used and disposed of.</p> <p>No non-conformities were identified during the audit.</p>	
--	---	--

Signature of auditor:

Frances Rae

Tissue Governance Manager, NHS Lothian.

Signature of Designated Individual:

David Harrison

Professor David Harrison
 Director of Development, Laboratory Medicine, NHS Lothian

Tissue Governance audit reference number	ICA01/17
---	----------

Author	: Frances Rae	Date	: 12-Feb-2015
Authority for Issue	: Craig Marshall	Date	: 12-Feb-2015
Quality Checked	: Craig Marshall	Date	: 12-Feb-2015

APPENDIX B

PARAMETERS

Parameter	Instrument	Unit	Description
Po.Ar%	Image analysis	%	Optical porosity
O^nH	Nanoindentation	Vickers	Indentation nanohardness
O^nE	Nanoindentation	GPa	Indentation modulus
O^nC_{IT}	Nanoindentation	%	Indentation creep at hold
$O^n\eta_{IT}$	Nanoindentation	%	Elastic work over the total
I^tH	Nanoindentation	Vickers	Indentation nanohardness
I^tE	Nanoindentation	GPa	Indentation modulus
I^tC_{IT}	Nanoindentation	%	Indentation creep at hold
$I^t\eta_{IT}$	Nanoindentation	%	Elastic work over total work
O^nHV	Microindentation	g/mm^2	Indentation microhardness
I^tHV	Microindentation	g/mm^2	Indentation nmicrohardness
L Δ H	TGA/DSC3+	Wg^{-1}	Enthalpy measurement of the endothermic episode
C Δ H	TGA/DSC3+	Wg^{-1}	Enthalpy measurement of the endothermic episode
W%	TGA/DSC3+	%	Weight loss of dehydration step
Or%	TGA/DSC3+	%	Weight loss of combustion step
Ash%	TGA/DSC3+	%	Mineral content
MM	ATR-FTIR	Ratio	mineral to matrix matrix ratio
CP	ATR-FTIR	Ratio	Carbon substitution
CI	ATR-FTIR	Ratio	Crystallinity index
CC	ATR-FTIR	Ratio	Collagen content
Strain	XRD	Ratio	Lattice strain
Size	XRD	nm	Mineral size
CL002	XRD	nm	Coherence length at 002
CL004	XRD	nm	Coherence length at 004
CL030	XRD	nm	Coherence length at 030
CL210	XRD	nm	Coherence length at 210
'a' axis	XRD	Ångstrom	Length of crystal cell along a axis
'c' axis	XRD	Ångstrom	Length of crystal cell along c axis

Table B.1: Description of the parameters involved in the investigation.

APPENDIX C

REGRESSION DIAGNOSTIC

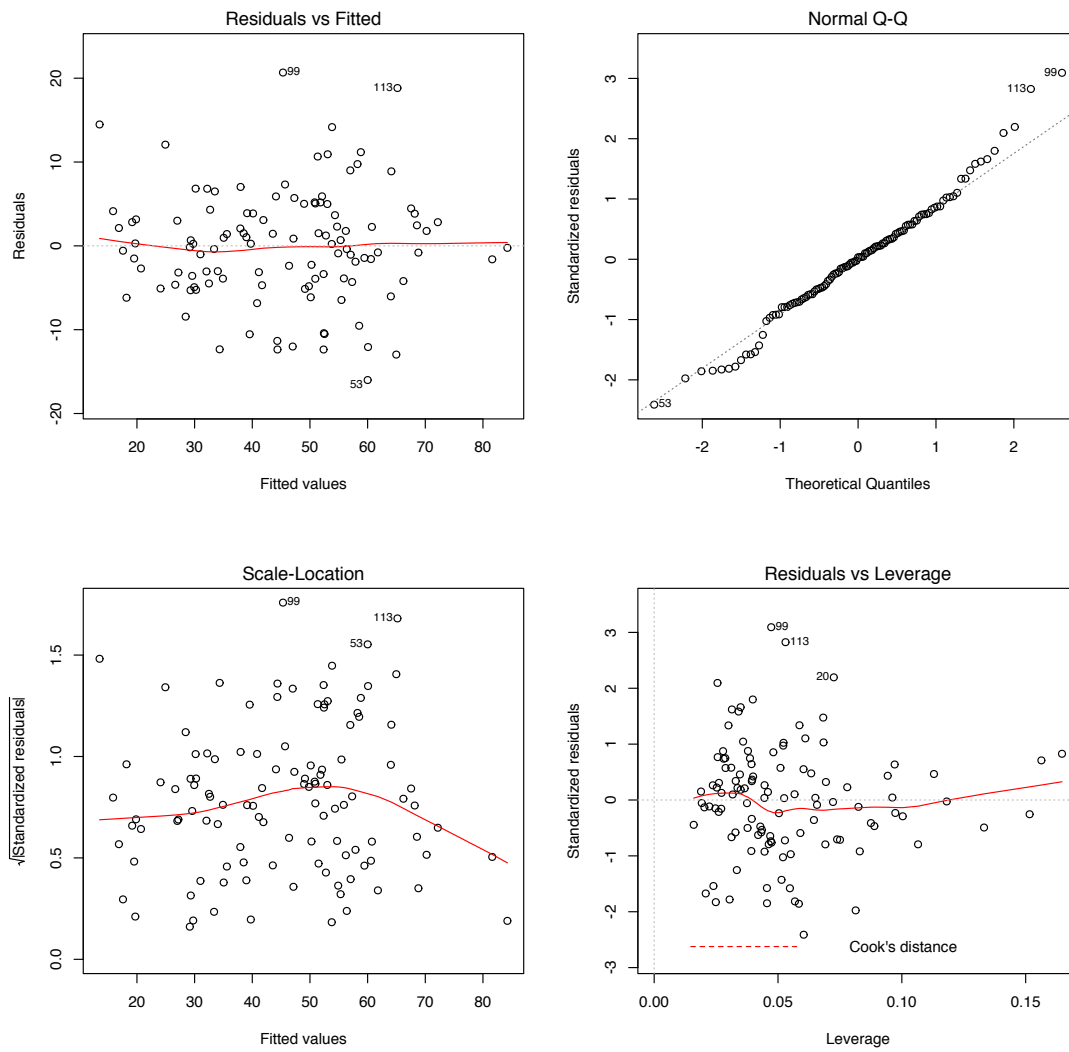


Figure C.1: Diagnostic plot for PR4.

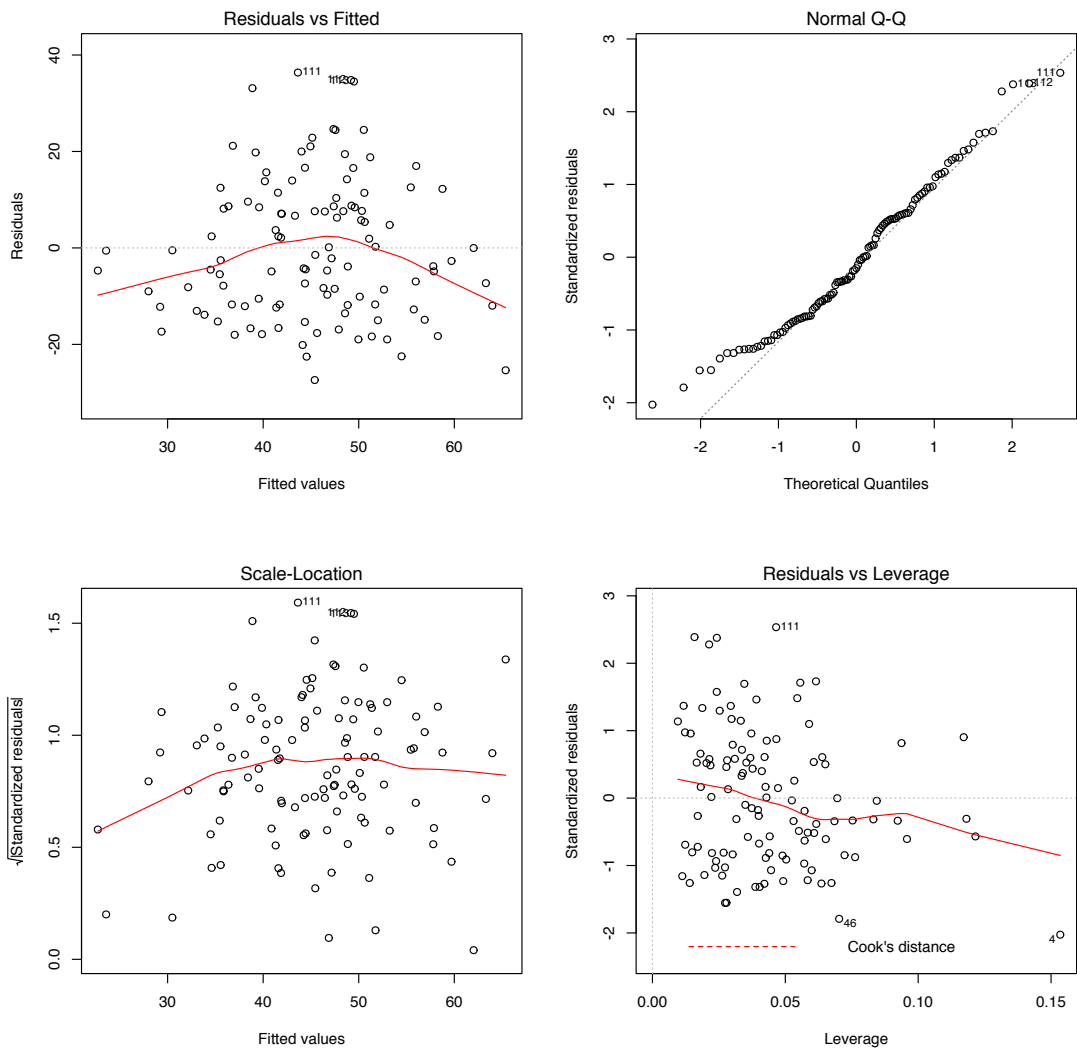


Figure C.2: Diagnostic plot for PR5.

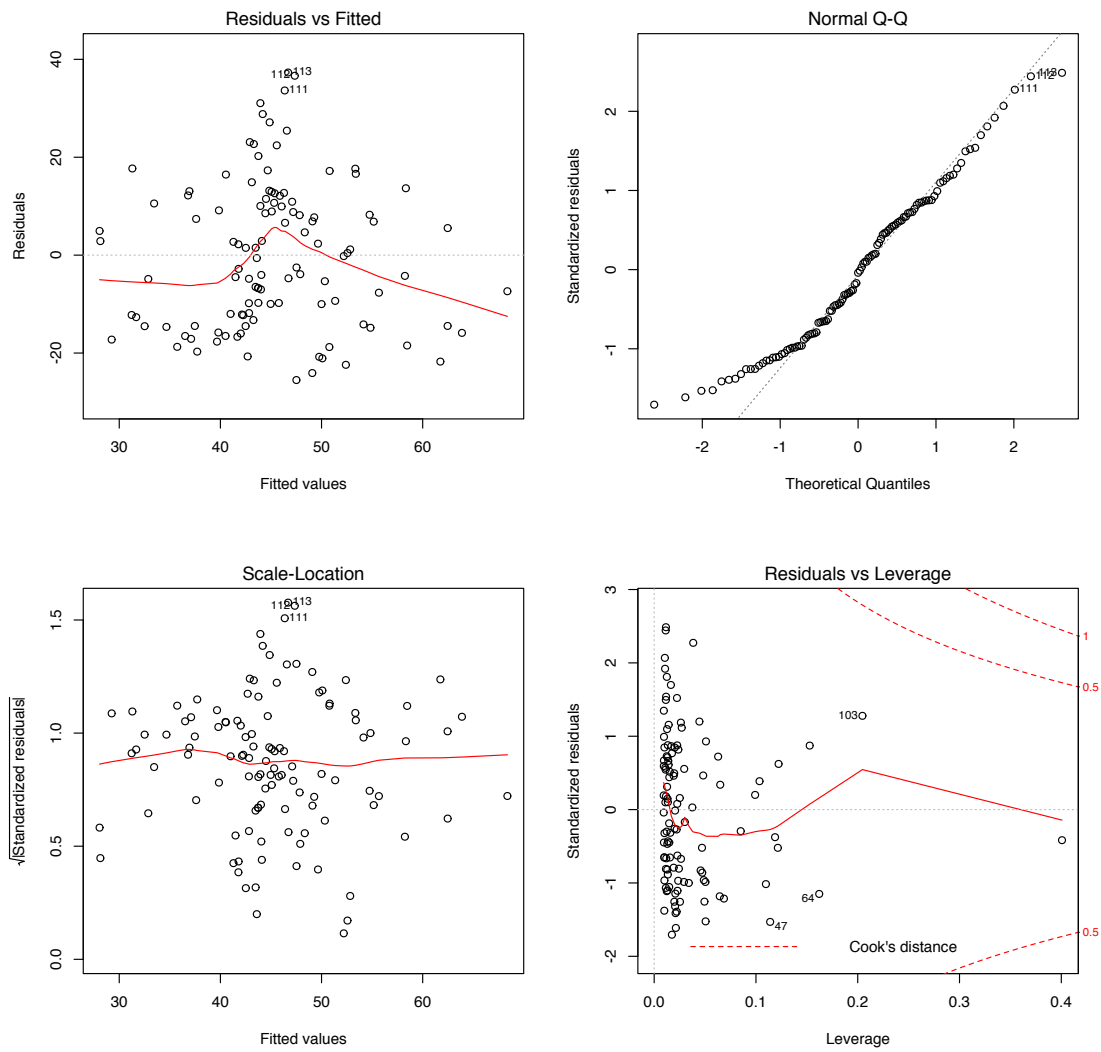


Figure C.3: Diagnostic plot for PR6.

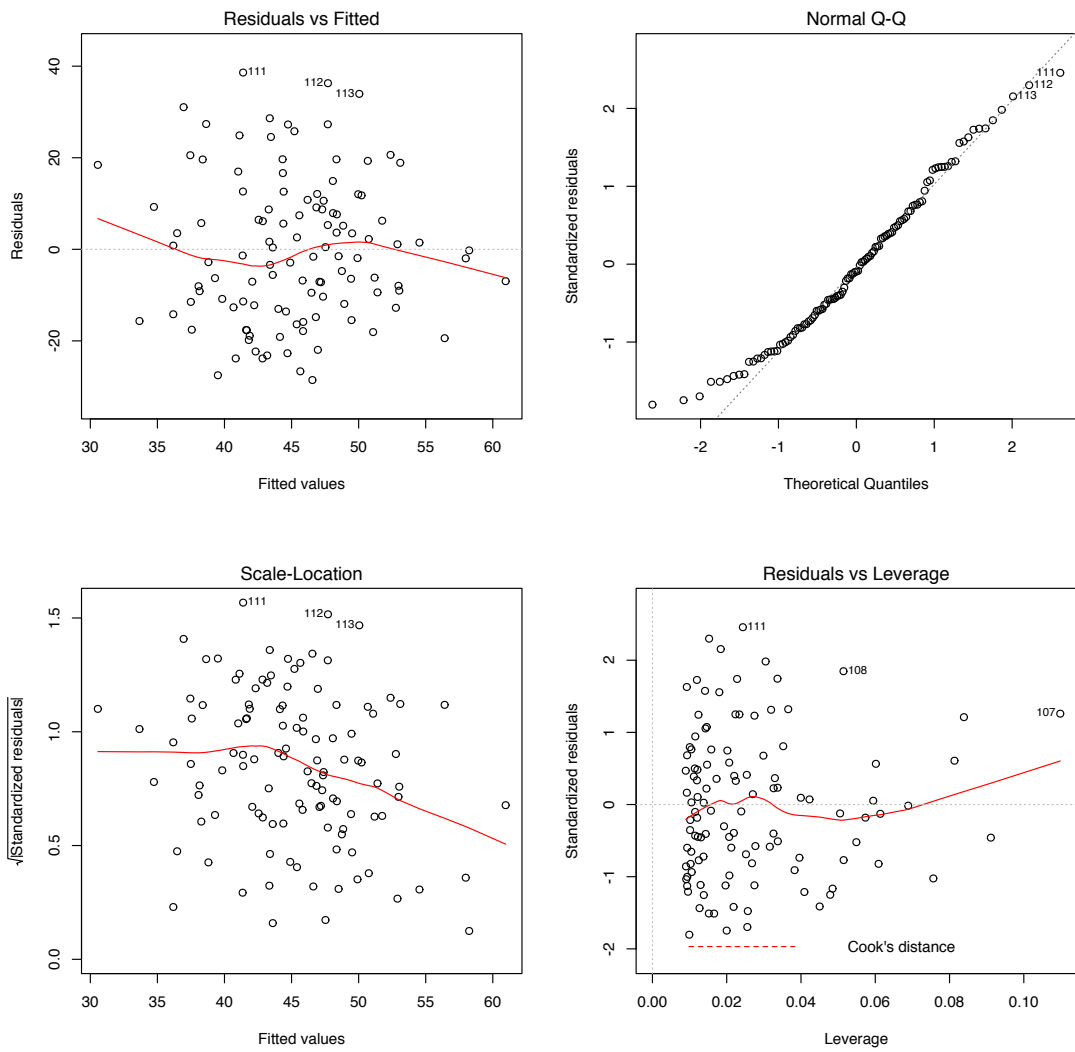


Figure C.4: Diagnostic plot for PR7.

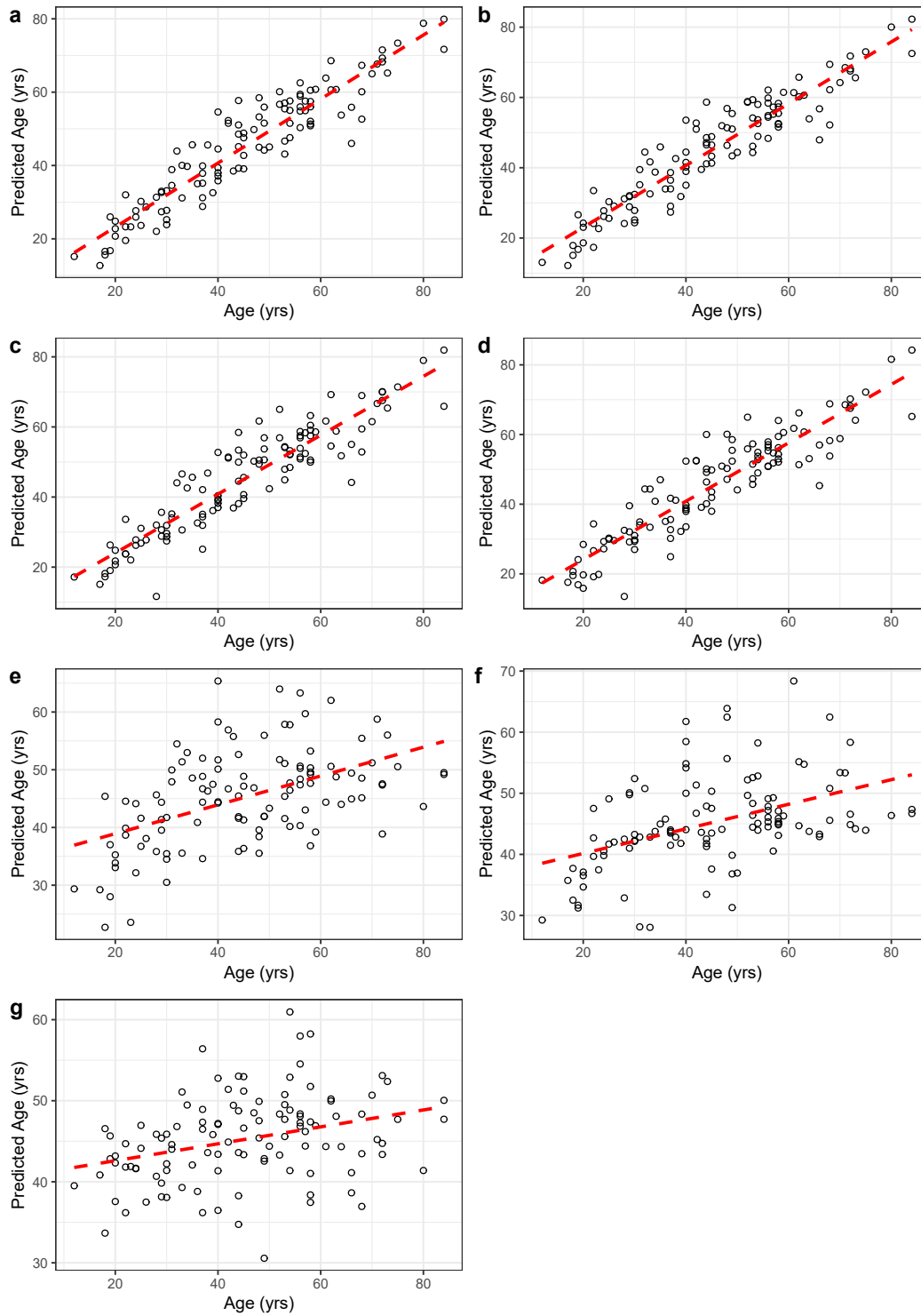


Figure C.5: Real age vs Predicted age for (a) PR1, (b) PR2, (c) PR3, (d) PR4, (e) PR5, (f) PR6 and (g) PR7. It is possible to note the decrease in accuracy from the first to the last model as variables are taken out from the models.

APPENDIX D

SEX SPECIFIC REGRESSION FORMULAS

Variable	PR1	PR1 - Male	PR1 - Female
Constant	-141.122***	-194.737***	-63.283*
Po.Ar%	6.317***	6.393***	4.145***
$On\eta_{IT}$	1.885***	1.132*	
ItH	-0.393***	-0.532**	
ItE	1.089**	1.811**	
OnH			-0.281**
OnC_{IT}			-3.411
ItC_{IT}	2.263	6.231***	7.292**
$OnHV$	0.285		0.577**
$It\eta_{IT}$		1.685	4.296***
$ItHV$	0.409*	0.488**	
LΔH	0.072*	0.071	
CΔH		-0.006	
MM	-3.884*	-5.082**	
CP	1,063.700**	1,563.821***	
CI	36.270*	64.768**	
CC	-159.743**	-216.187***	
Size	0.286	0.399*	-0.983**
CL030	5.032***	5.757***	

Table D.1: Comparison between models created with backward selection for the entire sample and split between male and female (*: $p < 0.05$; **: $p < 0.01$; ***: $p < 0.001$).

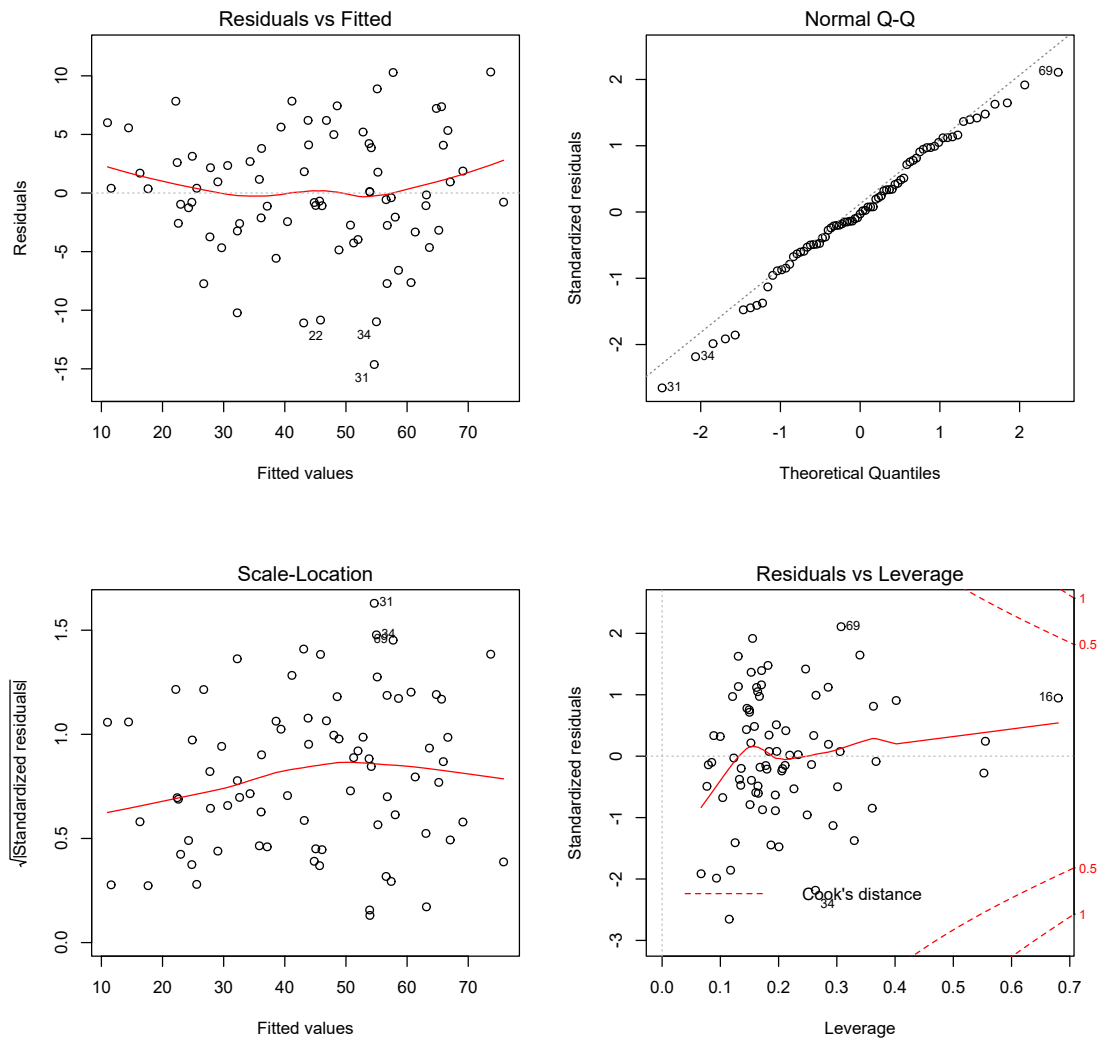


Figure D.1: Diagnostic plot for PR1 - Male.

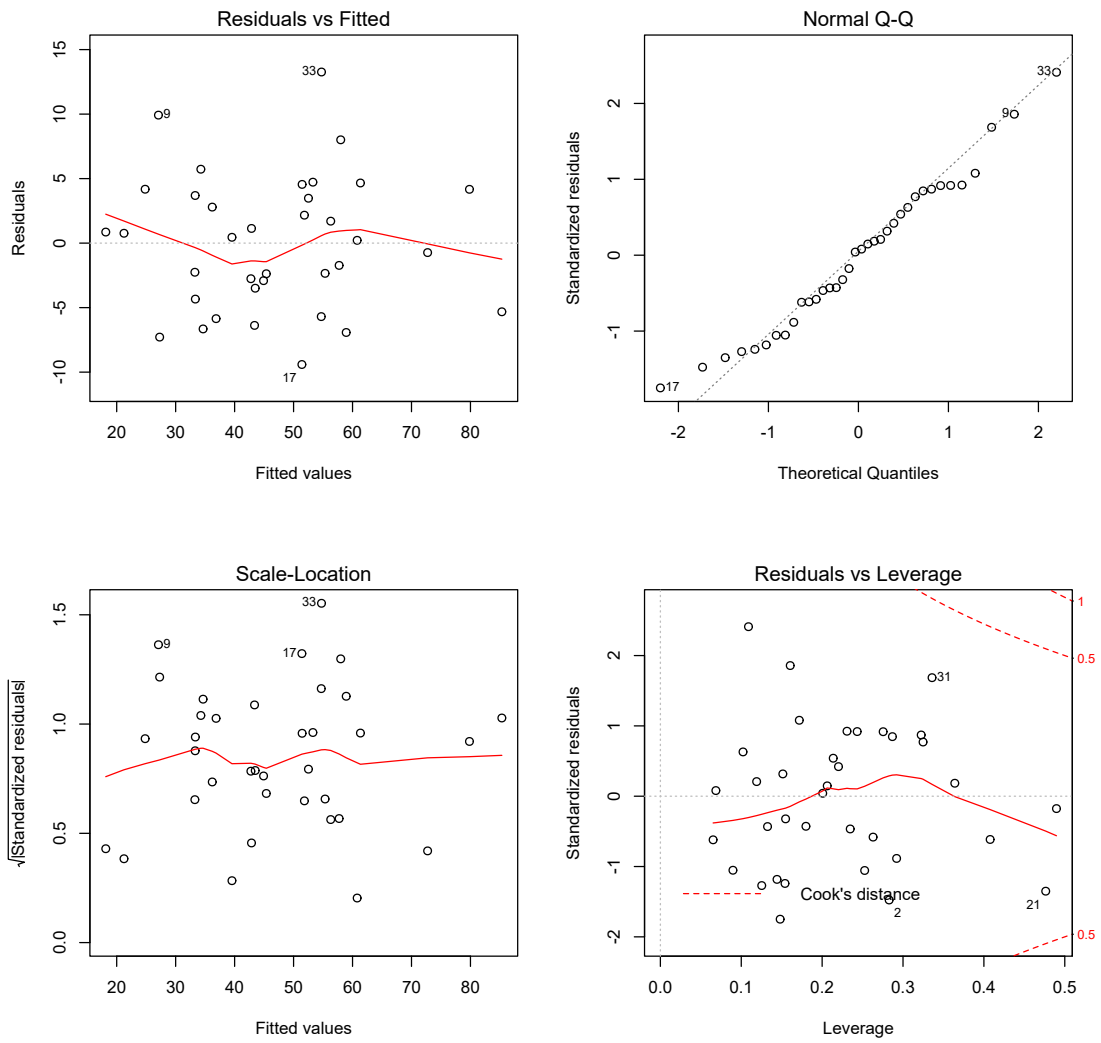


Figure D.2: Diagnostic plot for PR1 - Female.

Variable	PR2	PR2 - Male	PR2 - Female
Constant	-6,697.083	-259.725	23,358.290
Po.Ar%	6.327***	6.392***	2.136
<i>On</i> H	-0.060	-0.224	-0.606
<i>It</i> E	0.449	0.685	-0.304
<i>On</i> C _{IT}	1.091	1.824	-7.330
<i>On</i> η _{IT}	1.764*	1.849	-2.868
<i>It</i> H	-0.541*	-0.437	-0.341
<i>It</i> E	1.342	1.650	1.641
<i>On</i> C _{IT}	3.366	5.212*	8.488
<i>It</i> η _{IT}	1.333	1.459	8.160*
<i>On</i> HV	0.191	0.115	0.714
<i>It</i> HV	0.342	0.358	-0.340
LΔH	0.094	0.081	0.192
CΔH	-0.005	-0.005	-0.006
W%	63.570	0.384	-238.474
Or%	65.904	0.681	-232.581
Ash%	65.379	0.595	-230.041
MM	-3.670	-4.522	-3.952
CP	876.608*	1,561.542**	-1,518.926
CI	36.115*	59.398*	-95.787
CC	-139.770	-207.921**	-135.322
Strain	-297.445	-1,995.375	-202.461
Size	0.367	0.379	-1.119
CL002	-0.089	3.321	-4.080
CL004	0.062	-3.911	1.122
CL030	5.166**	5.394**	-2.844
CL210	-0.320	-0.366	0.891

Table D.2: Comparison between models created with forward selection for the entire sample and split between male and female (*: $p < 0.05$; **: $p < 0.01$; ***: $p < 0.001$).

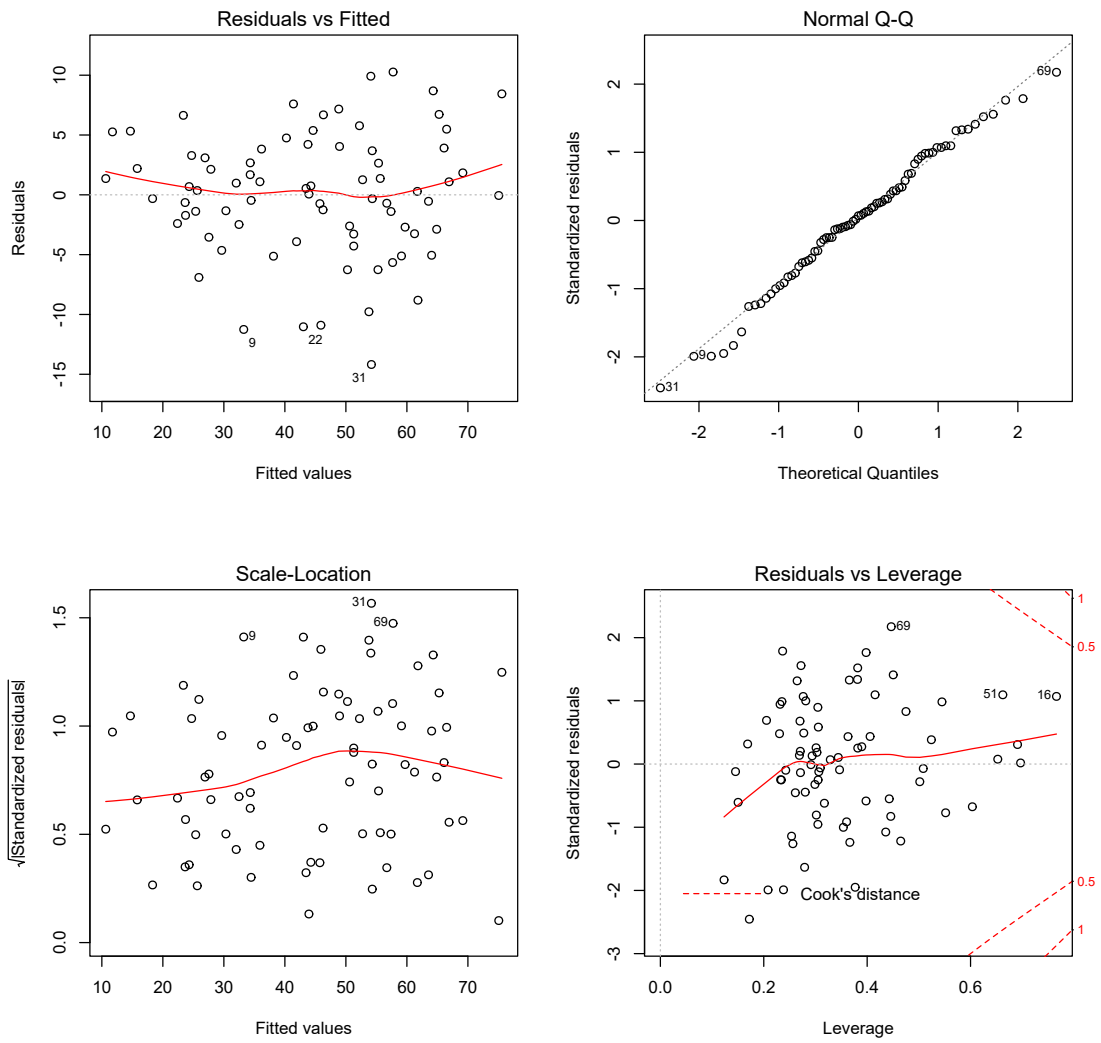


Figure D.3: *Diagnostic plot for PR2 - Male.*

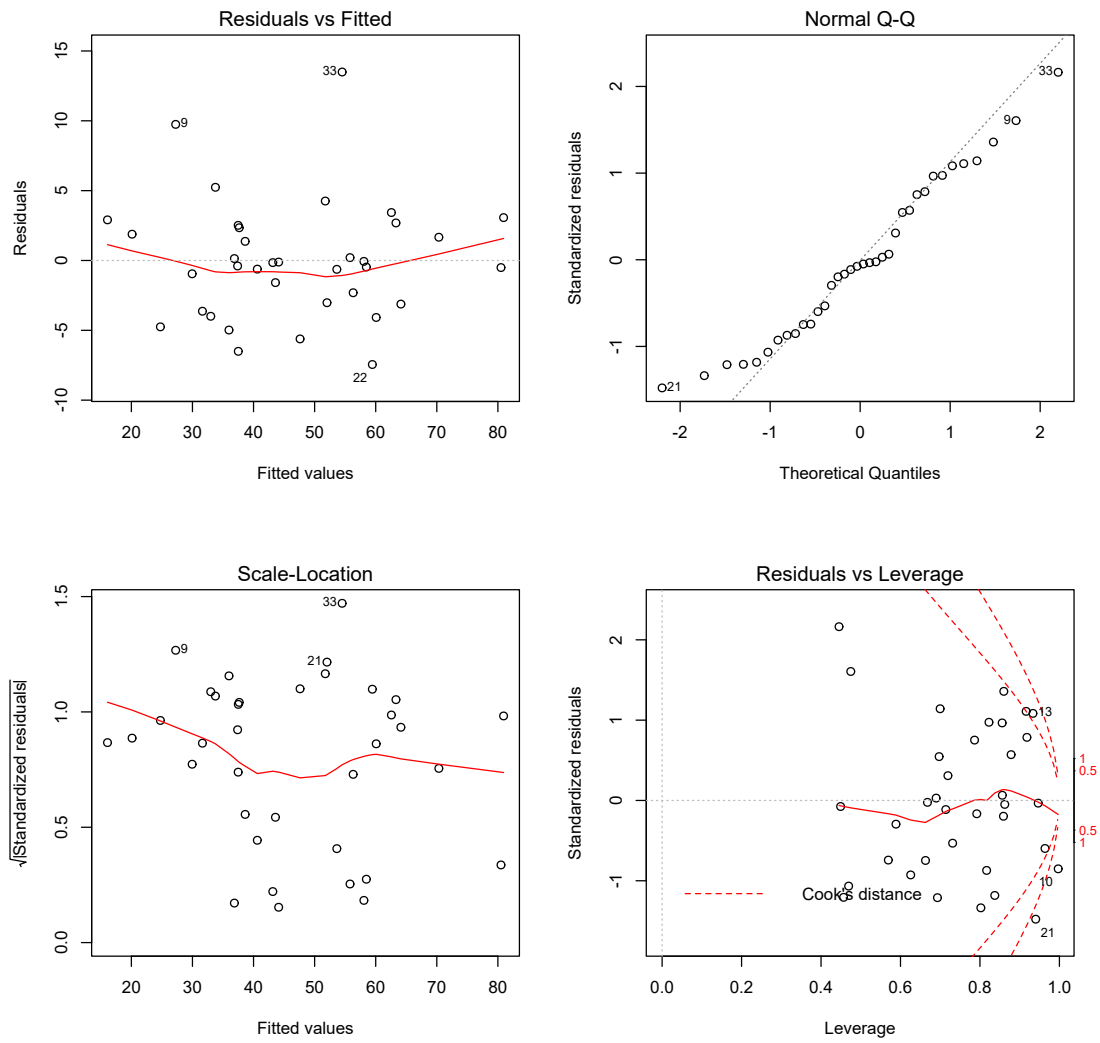


Figure D.4: Diagnostic plot for PR2 - Female.

Variable	PR3	PR3 - Male	PR3 - Female
Constant	-70.449***	-212.068***	-35.719**
Po.Ar%	5.895***	6.354***	4.553***
$On\eta_{IT}$	1.261***		
It_H	-0.215***	-0.736***	
It_E		2.493***	
$It_{C_{IT}}$		6.361***	
On_H			-0.352**
$It_{\eta_{IT}}$		3.236***	3.447***
It_{HV}	0.763***	0.541**	
MM		-5.492**	
CP		1,620.061***	
CI		74.408***	
CC		-206.486**	
CL030	4.151**	5.646***	

Table D.3: Comparison between models created with BIC selection for the entire sample and split between male and female (*: $p < 0.05$; **: $p < 0.01$; ***: $p < 0.001$).

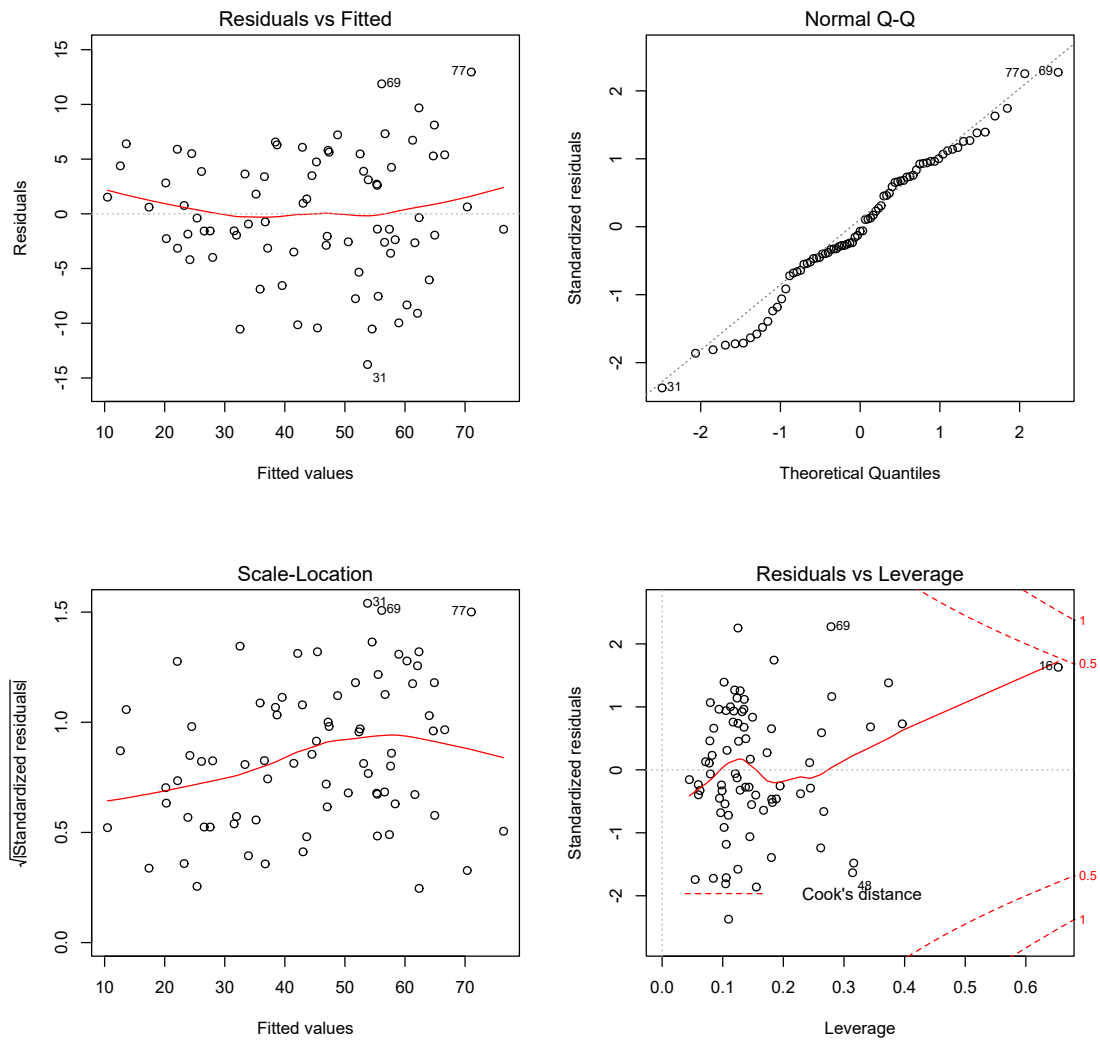


Figure D.5: Diagnostic plot for PR3 - Male.

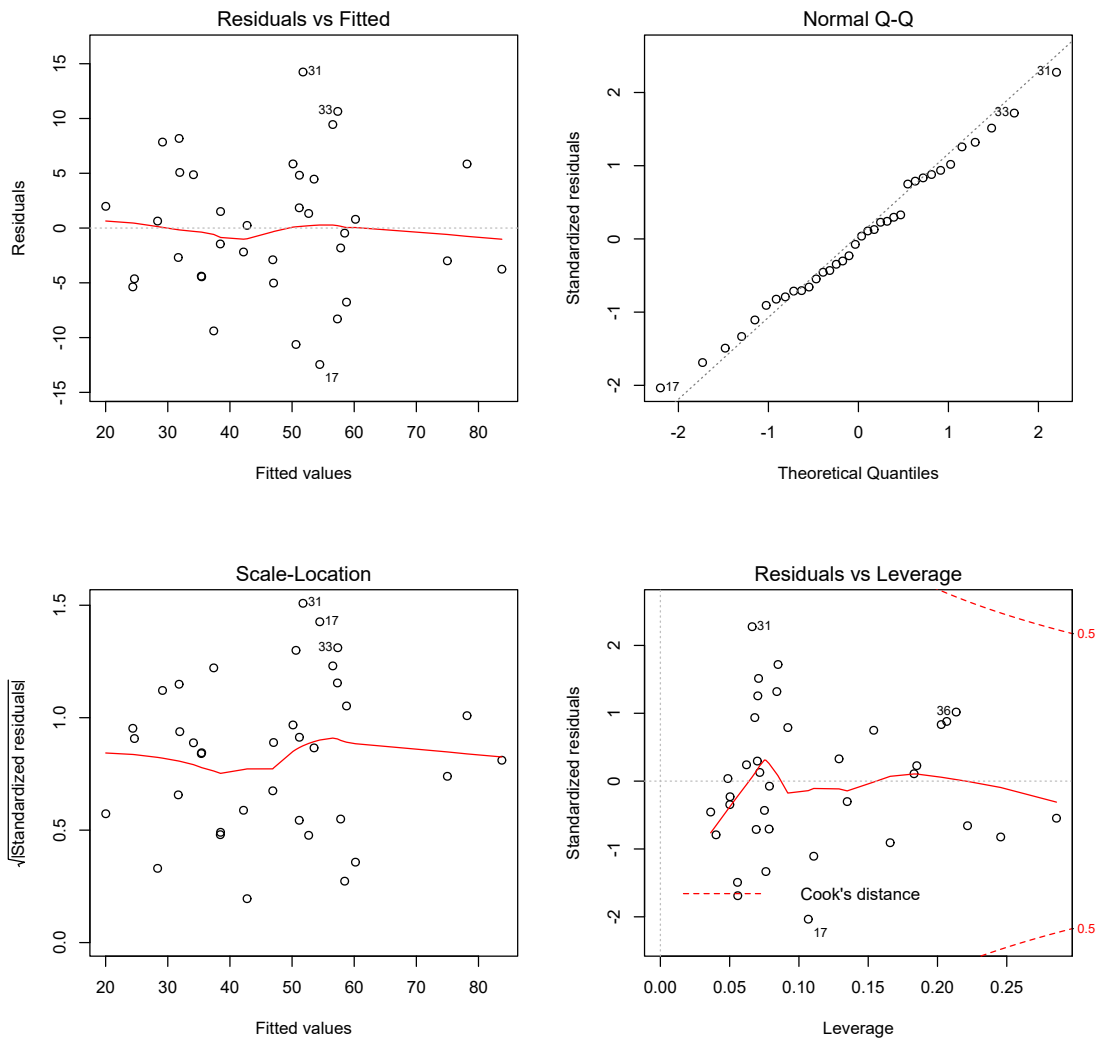


Figure D.6: *Diagnostic plot for PR3 - Female.*

APPENDIX E

SAMPLE DEMOGRAPHICS

Table E.1: *Demographics and cause of death for the entire sample and predicted age for the stepwise based models (GSW: gunshot wound).*

Code	Cause of death	Sex	Age	PR1	PR2	PR3
Rb30	Suicide by poisoning	Female	19	16.77	16.78	19.03
Rb10	self-poisoning	Female	20	23.06	24.8	20.69
Rb107	Traffic accident	Female	22	17.34	19.55	23.8
Rb9	Hit by lightening	Female	28	31.17	31.34	32.01
Rb6	Gunshot wound	Female	29	32.04	32.97	28.83
Rb97	Gunshot wound	Female	29	28.88	27.38	30.67
Rb18	Hanging	Female	31	39.47	38.87	35.18
Rb43	Drowning	Female	31	35.16	34.57	34.05
Rb13	self-poisoning	Female	37	27.36	28.83	25.13
Rb20	self-poisoning	Female	37	38.63	39.88	34.34
Rb36	Fall from Height	Female	37	29.06	31.2	31.92
Rb92	Sudden death	Female	39	31.81	32.58	36.13
Rb19	Fall from height	Female	40	40.2	35.83	38.23
Rb74	Asphyxia	Female	40	44.45	44.51	40.38
Rb88	Self-poisoning	Female	40	38.94	38.01	37.01
Rb108	Traffic accident	Female	40	41.51	39.38	39.35
Rb52	Self-poisoning	Female	42	50.97	52.25	51.41
Rb80	Self-poisoning	Female	42	52.72	51.52	51.13
Rb11	Fall from height	Female	43	39.52	38.49	36.89
Rb28	Burned	Female	44	46.51	45.14	44.51
Rb2	sudden death	Female	49	51.01	51.55	53.72
Rb72	Cerebral Trauma, Fall	Female	52	58.63	56.69	56.9
Rb67	Asphyxia	Female	53	54.16	55.44	54.12
Rb102	Sudden death	Female	54	48.93	47.6	48.45
Rb37	Sudden death	Female	56	62.1	62.54	53.9
Rb62	Multiorganic Disfunction	Female	56	54.38	54.83	57.49
Rb90	Sudden death	Female	56	59.85	58.91	51.4
Rb66	Self-poisoning	Female	58	57.31	57.45	60.47

Rb99	Traffic accident	Female	58	52.58	50.83	59.09
Rb83	Acute Miocardial Infraction	Female	61	61.38	63.84	61.68
Rb49	Acute Miocardial Infraction	Female	66	47.93	46.02	44.16
Rb60	Acute Miocardial Infraction	Female	66	56.77	55.87	55.02
Rb78	Haemorrhagic Shock, Car Accident	Female	68	52.18	52.64	52.86
Rb65	Acute Miocardial Infraction	Female	72	71.79	71.51	70.08
Rb77	Acute Miocardial Infraction	Female	80	80.03	78.78	78.98
Rb64	Haemorrhagic Shock	Female	84	82.27	79.9	81.93
Rb21	Traffic accident-car	Male	12	13.07	15.18	17.18
Rb41	Drowning	Male	17	12.17	12.72	15.1
Rb40	Falling from height, Trauma	Male	18	15.08	15.62	17.25
Rb42	Traffic accident-car	Male	18	17.88	16.57	18.18
Rb3	traffic accident	Male	19	26.62	25.98	26.31
Rb27	GSW	Male	20	24.24	22.76	24.82
Rb109	Asphyxia	Male	20	18.62	20.72	21.75
Rb68	Cerebral Trauma, Car Accident	Male	22	24.13	23.28	23.74
Rb73	Cerebral Trauma, Car Accident	Male	22	33.49	31.99	33.65
Rb15	Sudden death	Male	23	22.68	23.27	22.06
Rb5	Craniocerebral trauma-traffic accident	Male	24	26.14	25.94	26.22
Rb7	Occupational accident	Male	24	27.77	27.67	27.79
Rb17	Traffic accident-car	Male	25	25.6	23.65	26.85
Rb57	Infectious Disease	Male	25	30.33	30.21	31.07
Rb39	self-poisoning	Male	26	29.09	28.71	27.76
Rb105	Traffic accident	Male	28	24.13	22.04	11.64
Rb70	Haemorrhagic Shock, Fall	Male	29	31.77	32.64	35.63
Rb24	Self-poisoning	Male	30	25.14	25.23	27.46
Rb46	Traffic accident-car	Male	30	32.41	33.12	31.91
Rb95	Gunshot wound	Male	30	24.34	23.86	29.64
Rb96	Mechanical asphyxia	Male	30	27.84	27.76	28.67
Rb85	Acute Miocardial Infraction	Male	32	44.45	43.94	44.06
Rb1	Gunshot wound	Male	33	41.66	40.04	46.58
Rb25	Traffic accident-car	Male	33	32.56	31.15	30.61
Rb34	Traffic accident-car	Male	34	38.75	39.75	42.6
Rb58	Asphyxia	Male	35	45.91	45.64	45.64
Rb35	Traffic accident-car	Male	36	33.96	35.03	32.6
Rb26	GSW	Male	37	33.99	35.17	35.08

Rb54	Cerebral Contusion	Male	37	36.45	37.86	42.1
Rb93	Traffic accident	Male	38	42.6	45.6	46.84
Rb50	Overdose	Male	40	53.54	54.59	52.73
Rb106	Traffic accident	Male	40	35.03	37.14	39.05
Rb12	Traffic accident-car	Male	44	48.56	51.06	49.96
Rb16	Calcium oxide death (quicklime)	Male	44	58.65	57.71	58.42
Rb22	GSW	Male	44	41.13	39.26	38.12
Rb94	Asphyxia	Male	44	47.14	48.56	53.39
Rb8	traffic accident-car	Male	45	43.28	42.74	39.56
Rb44	Traffic accident-car	Male	45	46.47	47.56	45.59
Rb87	Acute Miocardial Infraction	Male	45	41.3	39.1	40.69
Rb101	Self-poisoning	Male	45	48.83	48.82	51.98
Rb111	Asphyxia	Male	47	51.96	49.79	50.23
Rb55	Acute Miocardial Infraction	Male	48	46.35	44.97	49.39
Rb100	Asphyxia	Male	48	51.37	53.24	50.54
Rb112	Myocardial infarction	Male	48	56.85	58.46	61.69
Rb4	Sudden death-cardiac infarction	Male	49	43.37	44.18	50.63
Rb48	Cerebral Contusion	Male	49	55.41	55.92	56.91
Rb32	Sudden Death	Male	50	44.38	45.06	42.37
Rb113	Sudden death	Male	52	58.83	60.11	65.02
Rb33	Sudden Death	Male	53	59.36	57.04	54.37
Rb45	Sudden death	Male	53	44.31	43.11	44.9
Rb89	Ventricular Rupture	Male	53	46.12	46.65	47.93
Rb38	Traffic accident-car	Male	54	53.66	55.04	53.24
Rb75	Acute Miocardial Infraction	Male	54	58.01	57.6	52.07
Rb82	Stabbing	Male	54	52.57	51.51	52.26
Rb23	Self-poisoning	Male	56	48.35	50.32	50.88
Rb76	Haemorrhagic Shock, Fall	Male	56	54.85	55.99	56.89
Rb86	Acute Miocardial Infraction	Male	56	58.39	59.41	58.7
Rb79	Self-poisoning	Male	57	55.22	54.95	52.43
Rb98	Sudden death	Male	57	57.25	57.56	58.34
Rb14	Hanging	Male	58	52.38	52.05	49.96
Rb31	Sudden Death	Male	58	51.58	51.29	50.56
Rb47	Self-poisoning	Male	58	55.46	56	57.48
Rb103	Sudden death	Male	58	58.31	60.52	63.24
Rb29	Traffic accident-car	Male	59	61.46	60.77	58.6

Rb56	Acute Miocardial Infraction	Male	62	65.75	68.57	69.23
Rb110	Sudden death	Male	62	60.2	60.62	54.56
Rb71	Self-poisoning	Male	63	60.63	60.72	58.8
Rb84	Overdose	Male	64	53.91	53.74	51.77
Rb61	Vertebral Trauma	Male	68	62.19	60.1	59.44
Rb104	Gunshot wound	Male	68	69.42	67.32	68.96
Rb81	Cerebral Haemorrhage, Car Accident	Male	70	64.22	65.01	61.52
Rb53	Cerebral Hemorrhage	Male	71	68.49	67.67	66.69
Rb51	Cerebral Trauma, Car Accident	Male	72	68.12	68.25	67.55
Rb69	Acute Miocardial Infraction	Male	72	67.52	69.3	69.95
Rb59	Acute Miocardial Infraction	Male	73	65.61	65.22	65.39
Rb63	Self-poisoning	Male	75	72.99	73.37	71.41
Rb91	Haemorrhagic Shock, Fall	Male	84	72.52	71.68	65.89